IL
NUOVO CIMENTO
ORGANO DELLA SOCIETÀ ITALIANA DI FISICA
SOTTO GLI AUSPICI DEL CONSIGLIO NAZIONALE DELLE RICERCHE

VOL. XIX. N. 2 *Serie decima* 16 Gennaio 1961

On the Viscosity of Liquids.

A. CARRELLI and F. PORRECA

Istituto di Fisica Sperimentale dell'Università - Napoli

(ricevuto il 1° Marzo 1960)

Summary. — In this work we show an experimental method allowing the determination of an imaginary part, if it exists, in the viscosity coefficient. The researches, which have been carried out by using a particular phasemeter, allowed us to measure actually this imaginary part, which in some liquids has a considerable value.

1. – Introduction.

If a lamina is vibrating with x as direction and with a frequency $\nu = \omega/2\pi$ in a liquid having density ϱ, the viscosity coefficient being μ (and therefore the kinematic viscosity coefficient is $\eta = \mu/\varrho$), a transversal viscosity wave shall spread in the liquid, having y as direction on a line at right angles to the plane of the mentioned lamina. The viscosity wave shall have wave surfaces parallel to the xz plane of the lamina (z is at right angles to the plane of the sheet).

If the vibration speed of the lamina is $u = a \cdot \exp[i(\omega t + \varepsilon)]$ the differential equation of the transversal vibrations propagating in the liquid, is the following [1]:

$$\frac{\partial u}{\partial t} = \eta \frac{\partial^2 u}{\partial y^2} .$$

But $\partial u/\partial t = i\omega u$ therefore $\partial^2 u/\partial y^2 = i\omega u/\eta$.

(1) H. LAMB: *Hydrodynamics* (New York, 1932), p. 619.

The general solution for this equation, if we consider $\beta = (\omega/2\eta)^{\frac{1}{2}}$, is supplied by

$$u_y = A \exp[(1+i)\beta y] + B \exp[-(1+i)\beta y] . \tag{1}$$

The value of the constants A and B depends on the limiting conditions. In the case in which the liquid extends towards the direction y, to a distance l from the oscillating lamina, and when the same liquid is in contact with both the surfaces of the lamina, considered as being indefinite, two conditions result:

a) for $y = 0$ the liquid has the same speed as the lamina, therefore $a = A + B$;

b) for $y = l$ the liquid has always a speed equal zero, and therefore it is possible to derive $A \exp[(1+i)\beta l] + B \exp[-(1+i)\beta l] = 0$.

By means of simple algebra we have

$$u_{y,t} = a \frac{\sinh(1+i)\beta(l-y)}{\sinh(1+i)\beta l} \cdot \exp[i(\omega t + \varepsilon)] . \tag{2}$$

Eq. (2) expresses the speed u in relation to y and to time t.

The force F, acting on the lamina's surface unit in contact with the liquid, is evidently

$$F = -\mu \left(\frac{\partial u}{\partial y}\right)_{y=0} .$$

Therefore from (2) we may derive

$$F = \mu(1+i)\beta a \coth(1+i)\beta l \cdot \exp[i(\omega t + \varepsilon)] .$$

From the definition of Z', which is the specific mechanical impedance, we have

$$Z' = \frac{F}{u} = \mu(1+i)\beta \coth(1+i)\beta l =$$

$$= \mu\beta \frac{\sinh 2\beta l + \sin 2\beta l}{\cosh 2\beta l - \cos 2\beta l} + i\mu\beta \frac{\sinh 2\beta l - \sin 2\beta l}{\cosh 2\beta l - \cos 2\beta l} .$$

If $2\beta l < 1$, leaving out terms starting from $2((2\beta l)^5/5!)$, we find the following expression for Z':

$$Z' = \frac{\mu}{l} + i\frac{\omega\varrho l}{3} . \tag{3'}$$

In view of our experimental conditions (see below) we have $l = 0.1$ cm, $\omega = 2\pi \cdot 50$ Hz therefore having $2\beta l < 1$ we have the condition $\mu > 6.28$ poises.

Supposing it is possible to measure Z' experimentally, from (3′) it is possible to find that for liquids having $\mu > 6.28$ we should obtain results from which it is possible to derive that the real part varies from liquid to liquid, whereas the imaginary part should be more or less constant, in view of the fact that, generally speaking, the density ϱ hardly varies.

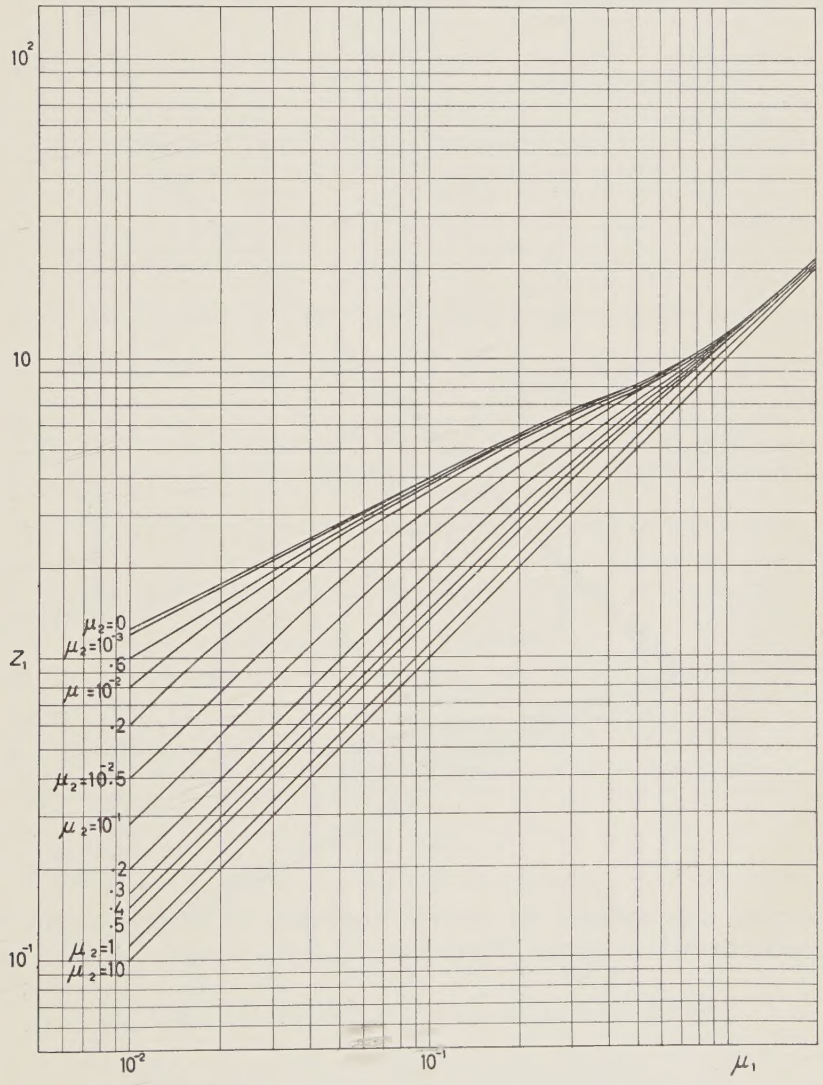

Fig. 1-*a*).

Instead, the experimental measurements of Z', obtained by a method which we shall describe later on, have shown interesting irregularities, in connection

with the various liquids, when compared to the above forecasts. In fact the coefficient of the imaginary part of Z' for certain substances is not only decidedly higher than $\omega\varrho l/3 \sim 10$ but also different for various liquids.

Then was considered the possibility of attributing a complex expression to the viscosity coefficient $\mu = \mu_1 + i\mu_2$ as many researchers have admittedly done recently in their studies on the liquid or semisolid states (2).

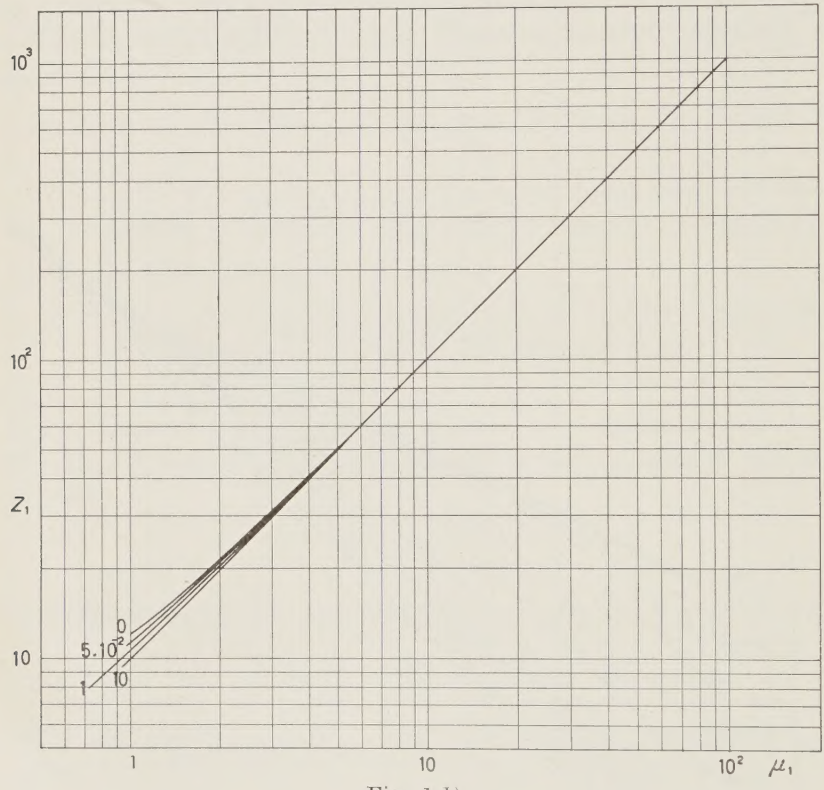

Fig. 1-*b*).

Following this position the generic expression of Z' (3) becomes rather complicated in view of the fact that in this case β is complex; indeed we have

$$Z' = Z_1 + iZ_2 = (\mu_1 + i\mu_2)(1 + i)\beta \coth (1 + i)\beta l ,$$

with

$$\beta = \frac{(\omega e)^{\frac{1}{2}}}{2}\left\{\left[\frac{(\mu_1^2 + \mu_2^2)^{\frac{1}{2}} + \mu_1}{\mu_1^2 + \mu_2^2}\right]^{\frac{1}{2}} - i\left[\frac{(\mu_1^2 + \mu_2^2)^{\frac{1}{2}} - \mu_1}{\mu_1^2 + \mu_2^2}\right]^{\frac{1}{2}}\right\} .$$

(2) T. H. F. HUETER and R. H. BOLT: *Sonics* (London, 1955); W. P. MASON: *Piezoelectric Crystals and their Application to Ultrasonics* (Amsterdam, 1950); J. FRENKEL: *Kinetic Theory of Liquids* (New York, 1955).

The « Istituto Nazionale per le Applicazioni del Calcolo » has had the courtesy to calculate the values Z_1 and Z_2 for pre-established values of μ_1 and μ_2. The curves shown in Fig. 1-*a*), *b*) and Fig. 2-*a*), *b*) give the values of Z_1 and Z_2 as function of μ_1 for various values of μ_2.

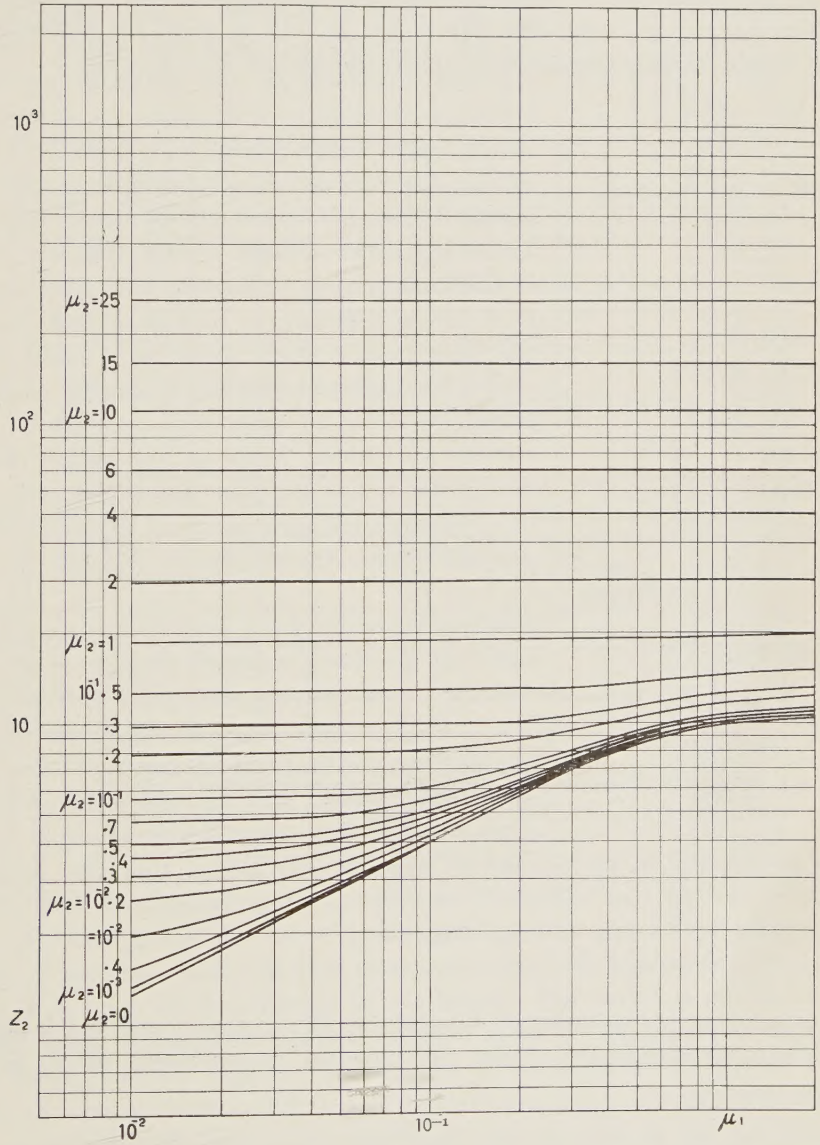

Fig. 2-*a*).

Once the values of Z_1 and Z_2 have been determined experimentally, it is possible by means of a graphic method to determine μ_1 and μ_2; in fact,

supposing that Z_1 and Z_2 are known, and considering Z_1 a constant, a curve is traced called μ_2, by means of the attached tables, as function of μ_1 relatively to those particular values for Z_1. Similarly, considering Z_2 constant, a second curve of μ_2 as function of μ_1 can be obtained. The co-ordinates of the point where eventually the two curves intersect each other on the plane (μ_2, μ_1) represent the values for μ_1 and μ_2 that are characteristic for the liquid having specific mechanical impedance $Z' = Z_1 + iZ_2$.

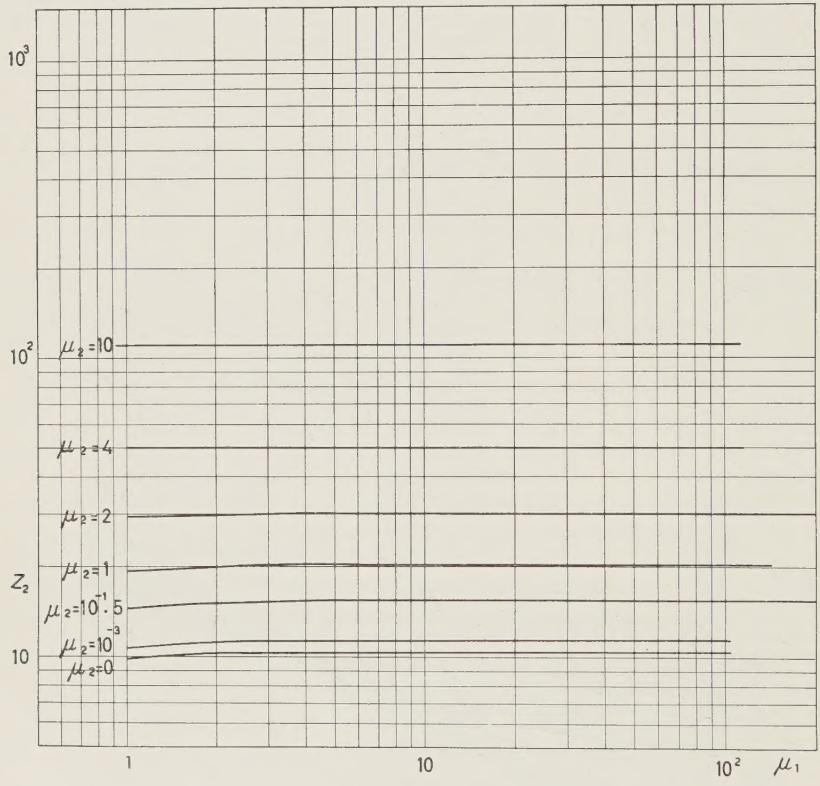

Fig. 2-*b*).

In conclusion the problem of determining the real part and the imaginary part of μ is reduced down to the experimental measurement of Z_1 and Z_2.

2. – Experimental device.

Mechanical part. – The experimental apparatus for the measurement of the mechanical impedance, generally speaking, is not very different from the one

built by FITZGERALD and FERRY ([3]) to compare the electric properties of gelatines and semisolid substances.

However it is much simpler and easier to build. The moving coil of an electrodynamic loudspeaker A (Fig. 3) (Geloso SP200) is rigidly connected to a light cylindrical stem L having 10 cm length, 0.5 cm diameter, and a thickness of $2 \cdot 10^{-2}$ cm. In the middle of this stem is fixed a cylinder C of 4 cm length, 4 cm diameter, 10^{-2} cm thickness. The cylinder may be immersed in a cylindrical container the base of which is a circular ring having a width of $2l = 0.2$ cm and as average diameter the diameter of the cylinder C. The end of the stem L carries another coil that can be placed within the radial magnetic field of a permanent magnet identical to the one called A so that a receiving device B is formed, which is identical to the transmitting one. The whole system is in perfect vertical axial symmetry. Particular care must be taken in having as little weight and as much rigidity as possible in the part oscillating with the coil A (stem, cylinder and coil B) in order that the dynamic conditions of the free A coil are not noticeably modified.

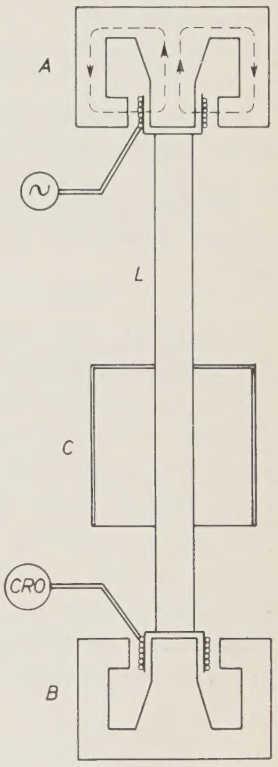

Fig. 3.

The magnet B is fixed, while the remaining part of the device may be displaced vertically inasmuch as it is fixed to a vertical arm that may slide continuously on a special fixed support.

In order to avoid the transmission of vibrations into the liquid, a separate base carries another support on which an arm is free to move along a vertical course. This arm carries the container in which there is the liquid under examination. The container is movable on horizontal and vertical planes by means of a mechanical device, so as to insure perfect parallelism between the cylinder C and the cylindrical sides of the container, for the whole path caused by the immersion of the cylinder in the liquid. The latter is another condition that must be carefully observed in order to make sure that the thickness l of the liquid does not vary, as the cylinder is immersed in the liquid.

The previously developed theory is referred to a plane and indefinite lamina. In the application the lamina is cylindrical. But in view of the fact that the length of the viscosity wave is comparatively great, the surface may be consi-

([3]) E. R. FITZGERALD and J. D. FERRY: *Journ. Colloid. Sci.*, **8**, 1 (1953).

dered as being practically plane. And bearing also in mind the remarkable mechanical action of the lamina, it may be considered indefinite which means that the force presented by the penetration of the lamina in the liquid is not taken into consideration.

Special graduations on the arms give the possibility of realizing the following conditions:

1) the coil B is situated symmetrically in the air gap of the magnet B;

2) in these conditions the cylinder C is in the air and its lower rim is barely lifted from the free surface of the liquid.

Starting from these positions, the amount according to which the container is lifted corresponds to the depth at which the cylinder is immersed in the liquid.

Calculation and measurement of the total impedance Z. – Let us now proceed with the calculation of the mechanical impedance Z_0 of the vibrating suspension, when the cylinder C vibrates in the air. Let $i_A = i_0 \exp[i\omega t]$ be the intensity of the alternating current fed into the coil A, having a length l_A placed in a magnetic field whose induction vector B_A is constant and at right angles with the turns of the coil. A force $F = B_A \cdot l_A \cdot i_A$ (F in dine, B_A in gauss, i_A in e.m.u.) acts on the coil. Consequently the system oscillates with an instantaneous velocity $v = v_0 \exp[i(\omega t - \varphi_0)]$ and at the terminals of the inducting coil, having a length l_B, placed in a magnetic field whose induction vector B_B is constant and at right angles with the wires, arises an alternating e.m.f., having the same frequency ω and a phase difference φ_0, given by

$$\Delta V_B = B_B \cdot l_B \cdot v = \Delta V_0 \cdot \exp[i(\omega t - \varphi_0)] \qquad (\Delta V_0 \text{ in } 10^{-8}\ \text{V}).$$

Hence the mechanical impedance in air is

$$Z_0 = \frac{F}{V} = B_A \cdot l_A \cdot B_B \cdot l_B \cdot \frac{i_A}{\Delta V_B} = K \frac{i_0}{\Delta V_0} \exp[i\varphi_0] .$$

If we wish to express i_0 in ampere and ΔV_0 in volt, provided the value of B in gauss remains unaltered, it is necessary to multiply the last quantity by 10^{-9} and then the expression of Z_0 (in C.G.S. absolute units) is given by

$$Z_0 = 10^{-9} K \frac{i_0}{\Delta V_0} \exp[i\varphi_0] . \quad i_0 \text{ in ampere; } \Delta V_0 \text{ in volt .}$$

Now, the variation ΔV_0 and φ_0 are measured (with i_0 constant equal $2.0 \cdot 10^{-4}$ A) when the cylinder is vibrating in a liquid.

Let ΔV and φ be the e.m.f. and the phase measured with the cylinder vibrating in a liquid, the total impedance of the system becomes

$$Z = 10^{-9} K \frac{i_0}{\Delta V} \exp[i\varphi]. \tag{4}$$

The variation in the impedance is evidently due to the action of the liquid on the cylinder.

The impedance Z_0 of the cylinder in air is also complex, and of $Z_0 = Z_0' + iZ_0''$ type. Now, supposing S is the surface of the cylinder immersed in the liquid and remembering that the latter is in contact with both sides of the cylinder, we may state [3] that the total impedance Z is

$$Z = Z_0 + 2SZ' = (Z_0' + 2SZ_1) + i(Z_0'' + 2SZ_2). \tag{4'}$$

By identically equalizing respectively the real parts and the coefficients of the imaginary parts of (4) and (4') we get the system

$$\left| \begin{array}{l} Z_0' + 2SZ_1 = 10^{-9} K \dfrac{i_0}{\Delta V} \cos\varphi, \\ Z_0'' + 2SZ_2 = 10^{-9} K \dfrac{i_0}{\Delta V} \sin\varphi. \end{array} \right. \tag{5}$$

From these we have the following functions ΔV and $\operatorname{tg}\varphi$ as functions of the cylindrical surface S in contact with the examined liquid:

$$\Delta V = \frac{10^{-9} K}{[(Z_0' + 2SZ_1)^2 + (Z_0'' + 2SZ_2)^2]^{\frac{1}{2}}}; \qquad \operatorname{tg}\varphi = \frac{Z_0'' + 2SZ_2}{Z_0' + 2SZ_1}.$$

ΔV is therefore a decreasing function of S. As to the variation of φ with S by deriving $\operatorname{tg}\varphi$ we have

$$\frac{\mathrm{d}}{\mathrm{d}S}(\operatorname{tg}\varphi) = \frac{2(Z_2 Z_0' - Z_1 Z_0'')}{(Z_0' + 2SZ_1)^2},$$

hence if $Z_2 = 0$, then φ decreases with S; if

$$Z_2 > 0 \qquad \text{and} \qquad Z_2 Z_0' > Z_1 Z_0''$$

then φ increases with S.

ΔV and φ were determined when S changes from 6.6 cm^2 (the cylinder being immersed in the liquid to a depth of $h = 0.5$ cm) to 33 cm^2 ($h = 2.5$ cm).

The values of ΔV and φ for $h < 0.5$ are not considered, so as not to take into account the rather complex effect of the first contact forces and of the adhesion ones between cylinder and liquid, that when $h \cong 0$ ($S \cong 0$) are evidently preponderant on the surface forces which only the exposed theory takes into account (*).

We must now discuss the determination of Z_1 and Z_2 which appear in the system (5). This is possible when, for a certain liquid ΔV, μ and S are experimentally known and if Z_0', Z_0'' and K are already known. Now we may say for $S \to 0$

$$(5') \qquad \begin{cases} Z_0' = 10^{-9} K i_0 \left(\dfrac{\cos\varphi}{\Delta V}\right)_{S\to 0}, \\ Z_0'' = 10^{-9} K i_0 \left(\dfrac{\sin\varphi}{\Delta V}\right)_{S\to 0}, \end{cases}$$

and the values of Z_0' and Z_0'' may therefore be calculated extrapolating for $S \to 0$ the experimental curves of ΔV and φ.

In order to determine the value of $K = B_A \cdot B_B l_A \cdot l_B$ (gauss per cm)^2 when l_A and l_B are known, the value of B was measured in the air gap of the radial fields of the magnets A and B by means of a coil built in such a way that it reacted only to the variations of flow due to the radial field whose lines of force are linked to the lateral surface of the coil, and did not react to the flow variations due to the vertical field linked to the section of the coil, which evidently appear as being equal and opposite (Fig. 4) (**).

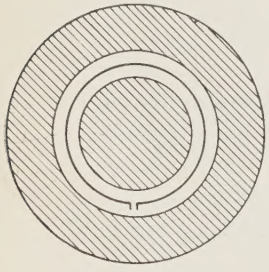

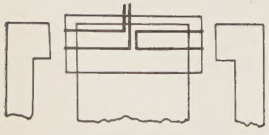

Fig. 4.

With our magnets we had $B_A = (8500 \pm 150)$ G and $B_B = (9350 \pm 175)$ G.

When K is known, from (5) and (5') the following explicit expressions are derived and they give the possibility of rapidly calculating Z_1 and Z_2

$$(6) \qquad \begin{cases} Z_1 = \dfrac{10^{-9} K i_0}{2S}\left[\dfrac{\cos\varphi}{\Delta V} - \left(\dfrac{\cos\varphi}{\Delta V}\right)_{S\to 0}\right], \\ Z_2 = \dfrac{10^{-9} K i_0}{2S}\left[\dfrac{\sin\varphi}{\Delta V} - \left(\dfrac{\sin\varphi}{\Delta V}\right)_{S\to 0}\right]. \end{cases}$$

One of the fundamental points of the work is experimentally set by the

(*) We believe that useful notions might be furnished on the surface pressure and tension by the variation of ΔV and φ obtained exploring with $h \simeq 0$.

(**) The solidity of this method for the measurement of B has been confirmed by an exchange of useful information with the Research and Consulting Office of Geloso S.p.A. whom we hereby wish to thank and credit.

fact that the values of Z_1 and Z_2 calculated according to the previous system, for the values of S itself, vary very slightly for a given liquid, involving as they do a relative error that generally speaking is not over 10%.

Electric circuits. – The electric circuits of the apparatus consist in a generator producing sinusoidal alternating voltage (Philips GM 2308) feeding the coil A that has a resistance $2 \cong 3$ ohm through which flows a current having an intensity $i = 20 \cdot 10^{-3}$ A. In series with coil A there is a purely ohmic resistance R (Fig. 5) at the terminals of which the ohmic drop is in phase with the intensity of the current i_A.

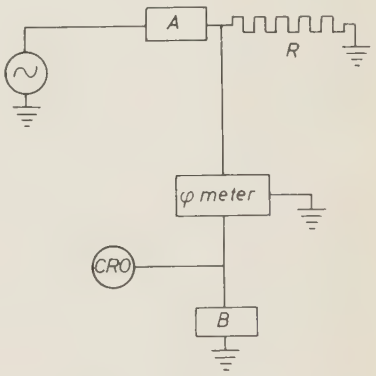

Fig. 5.

If the mechanical impedance Z is complex, there is a difference in phase between the e.m.f. induced at the terminals of coil B and the current in coil A. This e.m.f. is measured with an oscillograph. To measure the phase angle between the induced voltage ΔV_B and the intensity of the current i_A (or voltage at the terminals of R) a Vecchiacchi type phasemeter was used, capable of measuring the phase between two sinusoidal 50 Hz voltages.

The principle on which the measuring is based lays in the determination of the ratio $\Delta t/T$ between the interval of time Δt (between the change over passing by zero of the two sinusoidal voltages under comparison) and their period T. The two voltages, before being directly compared, are duly amplified by means of two absolutely identical channels, they are also brought to the same amplitude, filtered in order to eliminate eventual harmonics and transformed into symmetrical rectangular signals having fronts that correspond perfectly to the passages by zero of the original sinusoids.

Pulses are generated to correspond to these fronts and they are forwarded respectively to the two plates of a bistable multivibrator. They cause a rectangular signal the duration of which, in regards to the period T, is therefore a linear function of the dephasing. The measuring of the phase is performed by means of a bridge system to one arm of which the average value of the rectangular signal is applied while in the other one there is a direct current that by means of a linear potentiometric system can be reduced to zero. The terminals of the potentiometer are set in such a way that they correspond respectively to zero and 360 degrees of dephasing. The position of the potentiometer's slider, when the bridge is balanced, gives a direct reading that corresponds to the degree of the dephasing.

The amplitude of the two sinusoidal signals, the dephasing of which we are measuring, must not go beyond 10^{-1} V and must not be less than $2 \cdot 10^{-3}$ V. It is advisable to feed the filaments with direct current in order to avoid harmful interference with the voltages to be compared.

3. – Results.

In Fig. 6 and 7 are shown a few tipical curves, ΔV versus S and φ versus S.

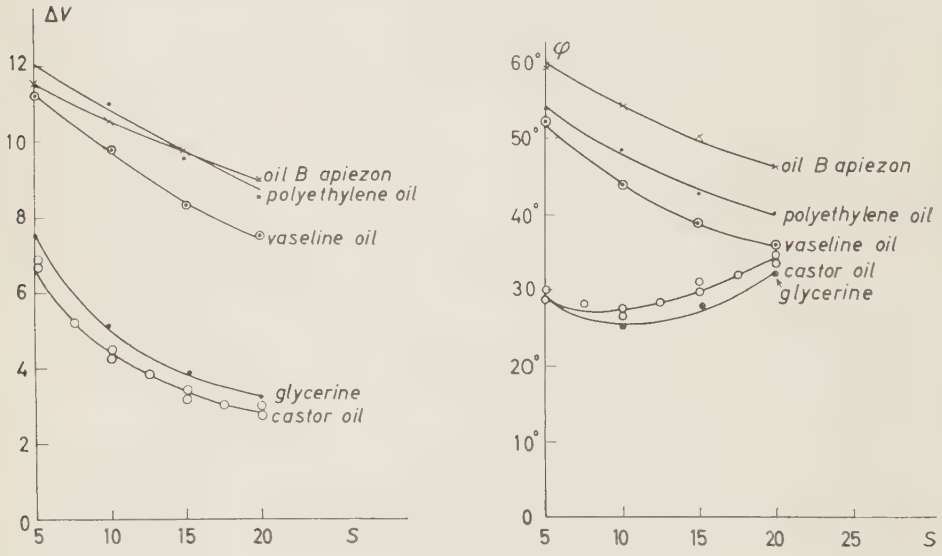

Fig. 6.

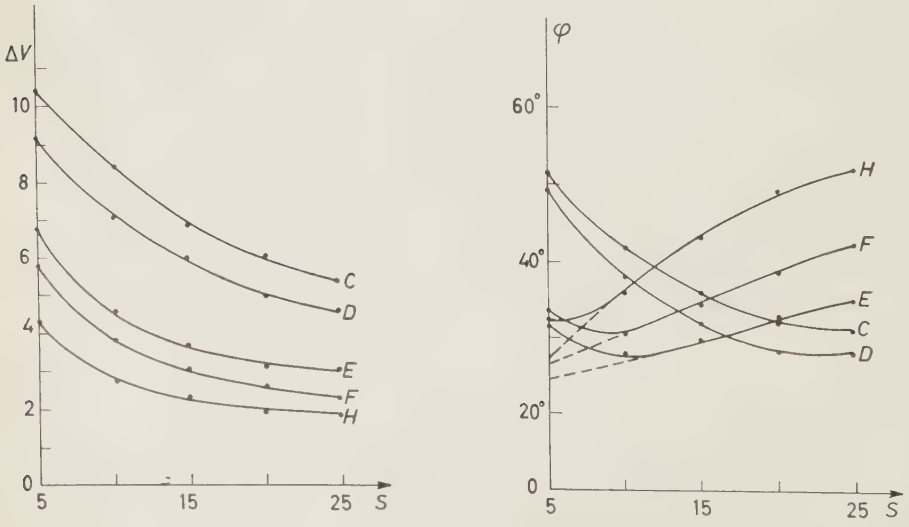

Fig. 7.

Table I shows the values of μ_1, μ_2 and the values of μ_{ost} giving the viscosity coefficient measured by means of the Ostwald viscosimeter or by means of other instruments set on the same principle.

TABLE I. – *Values in C.G.S. system at* (26 ± 2) °C.

	μ_{ost}	μ_1	μ_2
Apiezon Oil B	1.5 ± 0.1	1.6 ± 0.2	10^{-3}
Polyethylene Glycol	1.6 ± 0.1	1.5 ± 0.3	10^{-3}
Vaseline Oil	2.1 ± 0.1	2.2 ± 0.2	10^{-4}
Tylose in Water	2.5 ± 0.2	3.0 ± 0.3	$(1 \pm 0.5) \cdot 10^{-2}$
Mobiloil Sample (C)	3.2 ± 0.2	4.0 ± 0.4	10^{-3}
Mobiloil Sample (D)	4.4 ± 0.4	5.0 ± 0.4	10^{-3}
Glycerine	7.5 ± 0.5	8.2 ± 1	1.5 ± 0.5
Mobiloil Sample (E)	9.8 ± 0.5	9.5 ± 1.5	2.0 ± 0.4
Castor Oil	$(1.05 \pm 0.05) \cdot 10$	$(1.00 \pm 0.15) \cdot 10$	2.6 ± 0.5
Mobiloil Sample (F)	$(1.25 \pm 0.05) \cdot 10$	$(1.05 \pm 0.10) \cdot 10$	7.0 ± 1
Mobilube SAE 140	$(2.00 \pm 0.10) \cdot 10$	$(1.20 \pm 0.10) \cdot 10$	$(1.90 \pm 0.20) \cdot 10$
Mobiloil Sample (H)	$(2.46 \pm 0.15) \cdot 10$	$(1.50 \pm 0.15) \cdot 10$	$(1.20 \pm 0.15) \cdot 10$

From their perusal the following conclusions may be drawn:

1) the theoretical relation $Z_1 = \mu_1 / l$, (in our case $Z_1 = 10 \cdot \mu_1$), was confirmed very well by experimental methods with $1.5 \leqslant \mu_{ost} \leqslant 10$ poise in the sense that μ_1 appears to be equal to μ_{ost} (relative error $5 \cong 10\,\%$);

2) it appears that $\mu_{cst} > \mu_1$ if $\mu_{cst} > 10$ (compare the data relative to sample *F* and sample *H* of Mobiloil and Mobilube SAE 140);

3) for very viscous liquids $\mu_{ost} > 10$ it is possible to obtain a value for μ_2.

The table shows the values obtained for μ_1 and μ_2 in connection with 12 liquids that were the object of these preliminary measurements.

The work is in progress with the aim of considering the influence of the temperature and the frequency on μ_1 and μ_2.

* * *

The phasometer was designed, built and tested by the Technical Department of the Italian Radio and Television System in the Turin laboratories. We hereby wish to thank the Director of the said Department, Ing. LA ROSA.

RIASSUNTO

In questo lavoro viene esposto un metodo sperimentale che permette di determinare una componente immaginaria, se esistente, nel coefficiente di viscosità. La ricerca, che è stata condotta mediante l'impiego di un particolare fasometro, ha permesso effettivamente di misurare questa componente immaginaria, la quale in qualche liquido presenta un notevole valore.

Mesure de la section efficace totale π^+-p et π^--p de 400 MeV à 1.5 GeV.

J. C. Brisson, J. F. Detoeuf, P. Falk-Vairant, L. Van Rossum and G. Valladas

Service de Physique Corpusculaire à Haute Energie, C.E.N. - Saclay

(ricevuto il 22 Giugno 1960)

Summary. — Measurement of the total cross sections for π^+-p and π^--p by attenuation in liquid hydrogen of a beam whose energy was known to $\pm 1\%$ and with a total $\Delta P/P$ of $\pm 1.8\%$. The energies and values for the cross sections at the maxima are

$$\pi^-: \; T_{\pi_{lab}} = (605 \pm 6)\ \text{MeV}, \qquad \sigma_{tot} = (45.8 \pm 1.8)\ \text{mb},$$
$$T_{\pi_{lab}} = (890 \pm 9)\ \text{MeV}, \qquad \sigma_{t.t} = (58.0 \pm 1.8)\ \text{mb},$$
$$\pi^+: \; T_{\pi_{lab}} = (1330 \pm 30)\ \text{MeV}, \qquad \sigma_{t.t} = (38.0 \pm 2.0)\ \text{mb}.$$

Compilation of results concerning the elastic and inelastic cross sections obtained by other experimental techniques in the neighborhood of the second and third resonances of π^-. Discussion of the second and third resonances.

1. – Introduction.

Les sections efficaces totales d'absorption π^+-p et π^--p au dessus de la première résonance $\frac{3}{2}\,\frac{3}{2}$ ont été mesurées antérieurement par Cool *et al.* [1], Lindenbaum *et al.* [2], et plus récemment par Burrowes *et al.* [3], et Longo *et al.* [4].

[1] R. Cool, O. Piccioni et D. Clark: *Phys. Rev.*, **103**, 1082 (1956).

[2] S. J. Lindenbaum et L. C. L. Yuan: *Phys. Rev.*, **111**, 1380 (1958).

[3] H. C. Burrowes, D. O. Caldwell, D. H. Frisch, D. A. Hill., D. M. Ritson et R. A. Schluter: *Phys. Rev. Lett.*, **2**, 117 (1959).

[4] M. J. Longo, J. A. Helland, W. N. Hess, B. J. Moyer et V. Perez-Mendez: *Phys. Rev. Lett.*, **3**, 568 (1959).

L'existence probable de nouveaux isobares (5) donnait un nouvel intérêt à la connaissance précise de ces sections efficaces. En particulier il était nécessaire de préciser l'énergie des maxima observés aux environs de 600 et 800 MeV (3) dans la section efficace π^--p et de 1400 MeV dans la section efficace π^+-p.

Nous avons refait des mesures d'absorption dans l'hydrogène liquide à l'aide de faisceaux de π^+ d'énergie connue à $\pm 1\%$ et couvrant une bande d'impulsion de largeur relative égale à $\pm 1.8\%$.

L'expérience a été réalisée auprès du Synchrotron à protons de Saclay (*).

2. – Dispositif expérimental.

Nous avons utilisé deux faisceaux secondaires représentés dans les Fig. 1 et 2.

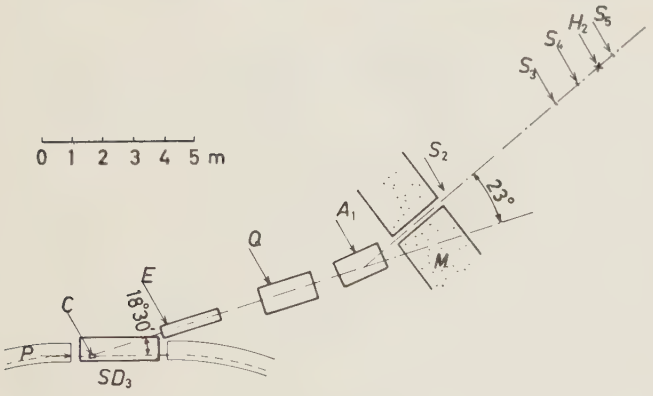

Fig. 1. – Faisceau no. 1. SD_3: 3e section droite; P: protons de 2.6 GeV, intensité environ $2 \cdot 10^{10}$/cycle; C: cible de carbone; E: écran magnétique; Q: quadrupôle à trois lentilles $\Phi = 15$ cm; A_1: aimant en C; M: mur de protection; H_2: cible à hydrogène; S_2, S_3, S_4, S_5: compteurs à scintillations.

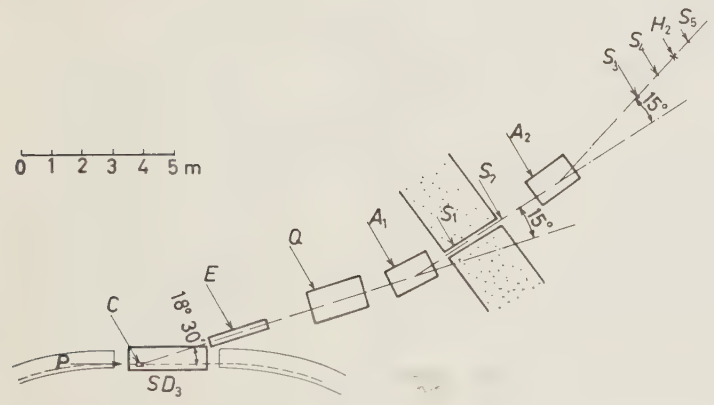

Fig. 2. – Faisceau no. 2. Voir légende Fig. 1; C: cible de cuivre; A_2: aimant en C; S_1: compteur à scintillations.

(5) R. R. Wilson: *Phys. Rev.*, **110**, 1212 (1958).

(*) Des résultats partiels de cette expérience commencée avec la collaboration de L. C. L. Yuan, ont été publiés dans une lettre à la *Phys. Rev.* (6).

(6) J. C. Brisson, J. F. Detoeuf, P. Falk-Vairant, L. Van Rossum, G. Valladas et L. C. L. Yuan: *Phys. Rev. Lett.*, **3**, 561 (1959).

Le premier faisceau a été utilisé pour des mesures de 400 MeV/c à 1200 MeV/c; la cible à l'intérieur de la machine était un parallèlépipède de carbone de 10 cm de long, de 3 cm de haut et 1.5 cm de large. Pour réduire la diffusion multiple aux basses énergies, un boudin d'hélium était placé le long du faisceau.

Le deuxième faisceau a été utilisé pour les mesures de 900 MeV/c à 1600 MeV/c, avec une cible de cuivre de $(10 \times 1.5 \times 1.5)$ cm.

L'intensité des π analysés était de l'ordre de 200 π^+ et 100 π^- pour 10^{10} protons dans la machine.

La cible à hydrogène, de longueur utile égale à 40 cm, représentée dans la Fig. 3, a été décrite ailleurs (7). Une cible témoin, identique à la première, permettait de mesurer l'effet cible vide et de surveiller le bon fonctionnement de l'appareillage électronique.

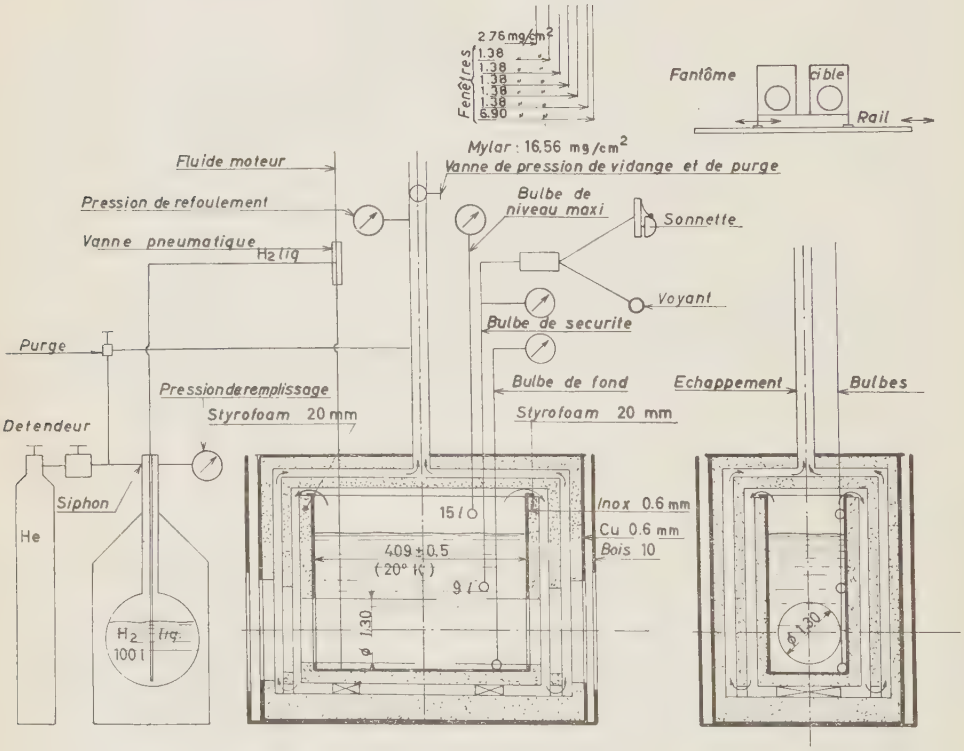

Fig. 3. – Cible à hydrogène liquide.

La direction des π à l'entrée de la cible est définie à $\pm 0.5°$ par un télescope de 3 ou 4 scintillateurs. Le dernier scintillateur du télescope, S_1, est

(7) P. PRUGNE, M. MARQUET et M. BOUGON: *Onde El.*, **39**, 612 (1959).

placé à 47 cm du centre de la cible; il a un diamètre de 6 cm; son épaisseur (3 mm) a été choisie assez petite pour diminuer l'effet d'absorption sans hydrogène (effet cible vide).

La cible est vue sous un angle de 6° par un scintillateur S_5 de 15 cm de diamètre placé à 72 cm du centre.

Dans le Tableau I nous donnons les caractéristiques des compteurs utilisés.

TABLEAU I. – *Disposition et caractéristiques des compteurs.*

Dénomination du compteur	Distance à la cible (m)	Dimensions des scintillateurs (cm)		Observation
		diamètre	épaisseur	
S_2	— 6.42	12	0.8	
S_3	— 1.47	6	0.6	faisceau
S_4	— 0.47	6	0.3	no. 1
S_5	+ 0.72	15	1	
S_1	— 9.77	12	1.2	
S_2	— 7.65	12	1.2	faisceau
S_3	— 1.47	6	0.6	no. 2
S_4	— 0.47	6	0.3	
S_5	+ 0.72	15	1	

Le schéma de principe de l'appareillage électronique est donné dans la Fig. 4.

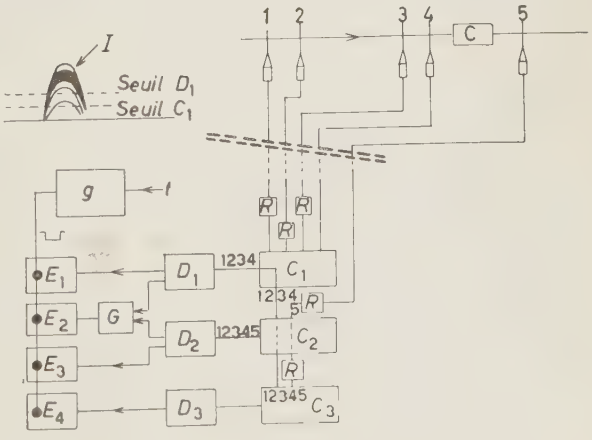

Fig. 4. – Appareillage électronique. C: cible; R: boîtes à retard; C_1, C_2, C_3: circuits de coïncidence; D_1, D_2, D_3: discriminateurs; G: coïncidence lente; E_1, E_2, E_3: échelles rapides (0.1 μs); E_1: comptage des π incidents; E_2: comptage des π transmis; E_3: échelle de contrôle; E_4: échelle des coïncidences fortuites; t: top de la machine; g: générateur de porte; I: impulsion de coïncidence 1, 2, 3, 4.

Les scintillateurs du télescope détectant les π incidents sont connectés à un circuit de coïncidence (C_1). Ce circuit commande l'échelle rapide E_1 (temps de résolution: 0.1 μs).

Les π transmis sont mis en évidence par une première coïncidence rapide ($\tau = 10^{-8}$ s) entre les impulsions provenant de C_1 et du compteur final. Pour les compter on remet en coïncidence les impulsions fournies par les discriminateurs rapides D_1 et D_2 [8] dans un circuit de coïncidence supplémentaire G. Cette coïncidence à « tout ou rien » certifie que chaque particule comptée comme particule transmise est certainement comptée comme particule incidente.

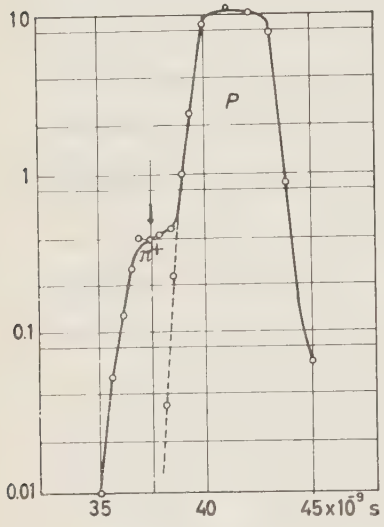

Fig. 5. – Séparation π^+-p à 1.6 GeV/c. En abscisse: retard entre les compteurs extrêmes. En ordonnée: taux de comptage du télescope (unité arbitraire).

Nous avons vérifié que le rendement du compteur 5 est supérieur à 0.999.

Le nombre d'interactions est donné par la différence $E_2 - E_1$.

Les coïncidences fortuites sont mesurées par C_3, circuit identique à C_2 mais qui reçoit le signal du compteur 5 avec un retard supplémentaire de $5 \cdot 10^{-8}$ s.

Dans la mesure des π^+ la séparation π-p était obtenue par temps de vol. Pour les mesures au dessus de 1 GeV un compteur supplémentaire (S_1) était placé au milieu du mur de protection de la machine.

La Fig. 5 montre la séparation π^+-p à 1.6 GeV/c.

Les échelles sont mises en marche électroniquement par un signal porte synchronisé sur la machine. La durée du faisceau était de l'ordre de 60 ms, obtenue par décroissance de l'amplitude H.F. de l'accélérateur.

3. – Tests de l'impulsion des faisceaux.

L'impulsion des π en fonction de l'intensité du courant dans l'aimant d'analyse a été déterminée par la méthode du fil pour six valeurs différentes du courant.

Dans le faisceau no. 1 nous avons constamment contrôlé la reproductibilité du champ magnétique en fonction du courant pour les deux polarités, à l'aide d'une jauge à effet Hall.

---

[8] J. Mey: *Rev. Sci. Instr.*, **30**, 282 (1959).

Un blindage magnétique à la sortie de la machine rend négligeable l'effet du champ de fuite, assurant la symétrie du faisceau pour les deux polarités. Dans le faisceau no. 1 l'énergie des particules a été mesurée directement par deux méthodes:

a) Parcours différentiel dans le cuivre, des protons à l'impulsion nominale de 800 MeV/c (Fig. 6), des π^+ à celle de 400 (Fig. 7) et 500 MeV/c et des π^- à 400 MeV/c.

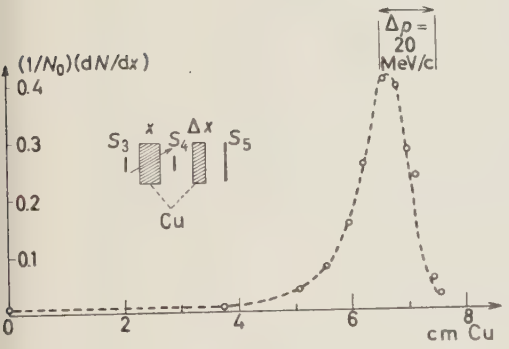

Fig. 6. – Courbe de parcours différentiel des protons de 800 MeV/c nominal. En abscisse: épaisseur x de cuivre en centimètres; en ordonnées: fraction $(1/N_0)\cdot(dN/dx)$ des particules s'arrêtant dans une tranche de cuivre d'épaisseur $\Delta x = 4$ mm.

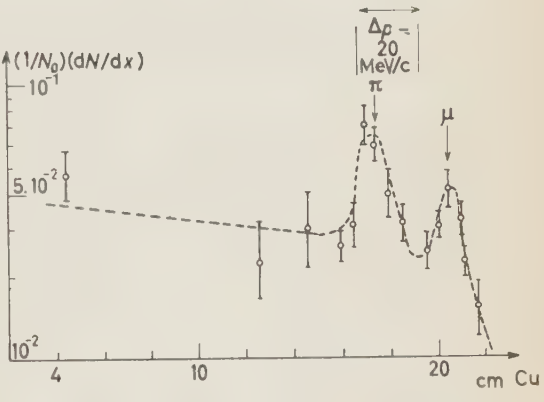

Fig. 7. – Courbe de parcours différentiel des π^+ de 400 MeV/c nominal. En abscisse: épaisseur x de cuivre en centimètres; en ordonnée: fraction $(1/N_0)\cdot(dN/dx)$ des particules disparaissant dans une tranche de cuivre d'épaisseur $\Delta x = 1$ cm.

b) Par la mesure du temps de vol des protons à l'impulsion nominale de 800 MeV/c (Fig. 8 et 9).

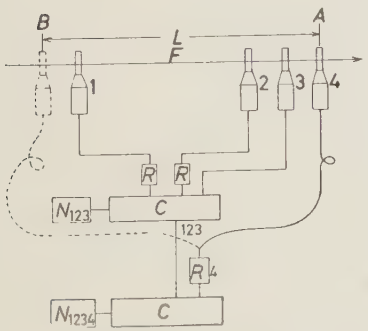

Fig. 8. – Mesure de l'impulsion par temps de vol. F: protons à l'impulsion nominale de 800 MeV/c; 1, 2, 3: télescope fixe; 4: compteur mobile, placé successivement en A et en B; N: circuits de comptage.

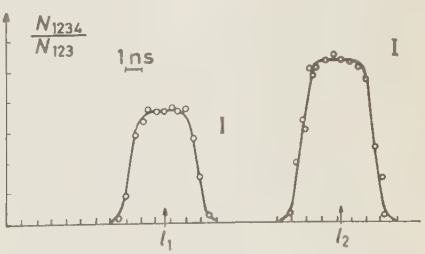

Fig. 9. – Mesure du temps de vol. $l_1 = 718.4$ cm; $l_2 = 1453.9$ cm; $l = l_2 - l_1 = (735.5 \pm 4)$ cm; $L = (697 \pm 1)$ cm; $\beta_{\text{câble}} = 0.675 \pm 0.003$. La relation $\beta_P/\beta_{\text{câble}} = L/l$ donne $\beta_P = 0.640 \pm 0.004$.

Dans ce cas, pour bien définir la direction des protons du faisceau on utilise le télescope $S_1S_2S_3$.

Un compteur indépendant S_4 est placé successivement dans les positions A et B.

Pour connaître l'instant moyen de passage des protons dans S_4, on mesure la courbe de retard de S_4 par rapport à $C_1 = S_1S_2S_3$.

La fig. 9 montre les courbes de coïncidence obtenues pour les deux positions A et B. On a porté en ordonnées le nombre de coïncidences $N_{1,2,3,4}$ rapporté au nombre $N_{1,2,3}$ du télescope, et en abscisses le retard dans S_4. Le barycentre de ces courbes, qui correspond au temps moyen, est défini à $\pm 10^{-10}$ s.

Soit l la différence des temps (exprimée en longueur de câble coaxial) et L la distance entre les positions A et B. On a $\beta_P/\beta_{\text{câble}} = L/l$.

Pour éliminer toute erreur systématique, $\beta_{\text{câble}}$ est mesurée avec le même dispositif en répétant la mesure avec les π dont la vitesse est suffisamment bien connue.

La valeur obtenue compte tenu de la perte d'énergie dans les scintillateurs est de (790 ± 10) MeV/c.

Le Tableau II montre pour le faisceau no. 1 que les différentes mesures effectuées sont en accord à $\pm 1\%$ avec celles du fil, corrigées de la perte d'énergie dans les scintillateurs et dans l'air.

TABLEAU II. – *Résumé sur les mesures de l'impulsion du faisceau no. 1.*

Date	Particules	Méthode	Parcours moyen total équivalent cuivre (cm)	$\bar{P}$ mesuré (erreur probable)	P prédit par le fil	$\dfrac{\bar{P}_{\text{mesuré}} - \bar{P}_{\text{fil}}}{\bar{P}_{\text{fil}}} \cdot 100$
13-3-60	π^+	parcours dans le cuivre	161.04	400($\pm$1.8 %)	403.5	-0.9 ± 1.8
15-5-60	π^+	»	233.19	513($\pm$1.8 %)	505	$+1.6 \pm 1.8$
17-7-60	π^+	»	163.68	402($\pm$1.2 %)	403	-0.25 ± 1.2
17-7-60	π^-	»	169.75	407($\pm$1.2 %)	403	-1.0 ± 1.2
11-3-60	p	»	72.92	802($\pm$1.2 %)	800	$+0.3 \pm 1.2$
28-4-60	p	»	72.38	800($\pm$0.8 %)	800	0 ± 0.8
15-6-60	p	(*)	73.33	805($\pm$1 %)	798	-0.9 ± 1.0
15-6-60	p	temps de vol	—	790($\pm$1.25%)	798	-1.0 ± 1.25

(*) Les mesures de parcours dans le cuivre ont été réalisées suivant le schéma de la Fig. 6 à l'exception de la mesure du 15÷6 dans laquelle la fin de parcours des protons a été déterminée au moyen d'émulsions.

Nous avons adopté pour valeur de l'impulsion, celle donnée par la méthode du fil.

Dans le faisceau no. 2 nous n'avons utilisé que la méthode du fil. Les mesures de la section efficace, faites dans les deux faisceaux, au voisinage du

troisième maximum, constituent un contrôle de l'étalonnage en impulsion de ce faisceau.

4. – Résultats.

Dans le Tableau III nous donnons les résultats des mesures des sections efficaces totales pour les π^+ et dans le Tableau IV ceux pour les π^- (*).

TABLEAU III. – *Section efficace totale* π^+-p.

$T_{\pi_{lab}}$ (MeV)	N.bre de mesures	Corrections				Erreurs			σ_{tot} (mb)
		contamination $(\mu+e)/\pi$%	géométrique (mb) élast.	géométrique (mb) inél.	autres (mb)	statistiques (mb)	contamination (mb)	autres (mb)	
376	2 (*)	30.7	0.75	0	0.5	0.76	1.2	0.8	40.39 ± 1.62
469	2 (*)	20.5	0.51	0.04	0.5	0.56	0.7	0.6	23.47 ± 1.08
567	2 (*)	17.0	0.29	0.10	0.5	0.42	0.5	0.5	17.26 ± 0.82
626	1 (*)	13.0	0.19	0.16	0.5	0.40	0.45	0.4	15.11 ± 0.72
664	2 (*)	11.7	0.16	0.18	0.5	0.39	0.37	0.4	14.75 ± 0.67
770	2 (*)	9.3	0.18	0.24	0.5	0.39	0.49	0.5	19.44 ± 0.80
818	1 (*)	8.5	0.22	0.27	0.5	0.34	0.53	0.5	21.40 ± 0.81
838	1 (*)	8.2	0.24	0.28	0.5	0.34	0.57	0.5	22.49 ± 0.83
863	2 (*)	8.1	0.28	0.30	0.45	0.44	0.55	0.5	21.88 ± 0.86
816	1 (**)	8.6	0.22	0.27	0.5	0.42	0.36	0.3	23.43 ± 0.61
866	2 (**)	7.7	0.28	0.30	0.44	0.41	0.46	0.4	23.37 ± 0.68
915	1 (**)	7.0	0.35	0.34	0.40	0.46	0.45	0.5	23.12 ± 0.74
965	2 (**)	6.3	0.44	0.36	0.35	0.45	0.48	0.5	23.80 ± 0.78
1014	1 (**)	5.6	0.60	0.40	0.34	0.45	0.51	0.6	25.85 ± 0.84
1064	1 (**)	5.1	0.76	0.44	0.32	0.46	0.54	0.7	26.78 ± 0.94
1114	1 (**)	4.5	0.95	0.45	0.28	0.58	0.55	0.8	27.51 ± 1.07
1164	1 (**)	4.2	1.12	0.50	0.29	0.55	0.62	1.0	30.65 ± 1.19
1213	1 (**)	3.7	1.42	0.53	0.37	0.60	0.71	1.1	35.27 ± 1.37
1263	1 (**)	3.4	1.63	0.56	0.47	0.62	0.73	1.3	36.64 ± 1.56
1288	2 (**)	3.3	1.70	0.57	0.30	0.5	0.76	1.3	37.37 ± 1.45
1313	3 (**)	3.1	1.79	0.59	0.29	0.37	0.74	1.3	38.07 ± 1.47
1338	2 (**)	3.1	1.88	0.61	0.26	0.55	0.75	1.4	37.65 ± 1.54
1363	2 (**)	2.9	1.95	0.63	0.23	0.55	0.72	1.4	36.16 ± 1.56
1412	3 (**)	2.9	2.03	0.66	0.19	0.48	0.74	1.5	36.53 ± 1.60
1462	2 (**)	2.6	2.00	0.70	0.10	0.51	0.68	1.5	34.10 ± 1.59

(*) Mesures dans le faisceau no. 1.
(**) Mesures dans le faisceau no. 2.

(*) Dans la publication [6] des résultats partiels, une erreur de l'ordre de 1% a été commise sur l'énergie des π^-, et les corrections géométriques avaient été calculées différemment d'après le travail de STERNHEIMER [9].

[9] R. M. STERNHEIMER: *Phys. Rev.*, **101**, 384 (1956).

TABLEAU IV. – *Section efficace totale* π^--p.

$T_{\pi_{lab}}$ (MeV)	N.bre de mesures	Corrections				Erreurs			σ_{tot} (mb)
		contamination ($\mu+e/\pi$%)	géométrique (mb)		autres (mb)	statistiques (mb)	contamination (mb)	autres (mb)	
			élast.	inél.					
373	2 (*)	35	0.12	0.24	0.50	0.9	0.9	0.5	28.81 ± 1.4
426	1 (*)	28	0.15	0.24	0.50	1.0	0.9	0.5	29.44 ± 1.4
468	2 (*)	25	0.20	0.26	0.50	0.64	0.9	0.5	29.96 ± 1.2
518	2 (*)	20	0.33	0.30	0.50	0.55	1.0	0.5	34.98 ± 1.3
567	2 (*)	18	0.53	0.33	0.50	1.27	1.3	0.5	44.82 ± 1.9
591	1 (*)	17	0.62	0.35	0.50	0.82	1.4	0.6	45.07 ± 1.7
604	1 (*)	16	0.63	0.36	0.50	1.15	1.4	0.6	45.74 ± 1.8
616	1 (*)	16	0.62	0.37	0.50	0.84	1.4	0.6	45.29 ± 1.7
643	1 (*)	15	0.53	0.40	0.50	1.57	1.3	0.7	44.47 ± 2.2
665	2 (*)	14	0.50	0.42	0.50	0.63	1.0	0.7	39.16 ± 1.4
719	2 (*)	12	0.50	0.50	0.50	0.86	0.9	0.8	34.90 ± 1.5
749	1 (*)	12	0.62	0.55	0.50	0.94	0.9	0.9	37.43 ± 1.6
769	1 (*)	10	0.80	0.58	0.50	1.48	0.9	0.9	37.38 ± 2.0
819	1 (*)	10	1.30	0.60	0.50	0.99	1.2	1.0	48.20 ± 1.9
840	1 (*)	9.5	1.67	0.56	0.50	1.17	1.4	1.1	55.13 ± 2.1
868	1 (*)	9.5	1.90	0.52	0.50	1.56	1.5	1.1	59.22 ± 2.4
890	1 (*)	9.5	2.05	0.48	0.50	1.26	1.4	1.2	58.46 ± 2.2
918	1 (*)	9.0	2.00	0.48	0.50	1.35	1.6	1.2	55.02 ± 2.4
943	1 (*)	9.0	1.86	0.51	0.50	1.72	1.5	1.3	50.67 ± 2.6
972	1 (*)	8.5	1.75	0.53	0.50	1.15	1.3	1.3	44.84 ± 2.2
1014	2 (*)	8.0	1.50	0.58	0.50	0.95	1.2	1.3	39.54 ± 2.0
1076	2 (*)	8.0	1.30	0.63	0.50	0.96	1.1	1.3	35.77 ± 2.0
1150	2 (*)	7.5	1.25	0.67	0.50	1.17	1.1	1.2	35.52 ± 2.0
797	1 (**)	10.5	1.00	0.60	0.50	0.69	0.80	0.8	40.20 ± 1.22
816	1 (**)	10.1	1.17	0.60	0.50	0.86	0.92	0.9	46.37 ± 1.50
836	1 (**)	9.8	1.46	0.57	0.50	0.72	0.96	1.1	48.13 ± 1.50
856	1 (**)	9.6	1.78	0.52	0.50	0.78	1.06	1.2	53.32 ± 1.72
866	1 (**)	9.3	1.88	0.51	0.50	0.90	1.08	1.2	54.20 ± 1.79
886	1 (**)	8.9	2.04	0.48	0.50	0.80	1.13	1.3	56.76 ± 1.84
915	1 (**)	8.4	2.02	0.48	0.50	0.74	1.10	1.3	55.17 ± 1.79
945	1 (**)	7.9	1.90	0.52	0.50	0.57	0.96	1.3	48.82 ± 1.63
965	2 (**)	7.6	1.79	0.53	0.50	0.74	1.12	1.3	45.70 ± 1.62
985	1 (**)	7.3	1.70	0.55	0.50	0.74	0.82	1.2	41.52 ± 1.53
1064	2 (**)	6.2	1.32	0.62	0.50	0.50	0.92	1.0	36.66 ± 1.30
1164	1 (**)	4.9	1.29	0.69	0.50	0.74	0.85	1.0	34.45 ± 1.32
1263	1 (**)	3.9	1.48	0.76	0.50	0.76	0.85	1.0	35.72 ± 1.35
1363	1 (**)	3.3	1.56	0.83	0.50	0.80	0.95	1.1	33.48 ± 1.41
1462	1 (**)	2.7	1.61	0.90	0.50	0.86	1.05	1.2	31.81 ± 1.50

(*) Mesures dans le faisceau no. 1.
(**) Mesures dans le faisceau no. 2.

La colonne 1 donne l'énergie des π dans le laboratoire compte tenu de la perte d'énergie des particules dans les différents matériaux traversés.

La colonne 2 indique le nombre de mesures indépendantes faites à l'énergie indiquée.

La section efficace d'absorption brute est donnée par l'expression

$$\sigma = -\frac{1}{L\,d\,N}\log\left(1-\frac{(\alpha_p-\alpha_v)(1+\beta_F)}{1-\alpha_v}\right), \tag{1}$$

où N = nombre d'Avogadro $= 6.02\cdot 10^{23}$

d = densité H_2 liquide $= 0.070\,6$ g/cm^2

L = longueur de la cible $= (40.9 \pm 0.2)$ cm

$\alpha_p = \dfrac{E_1 - E_2}{E_1} = \dfrac{\text{nombre de particules diffusées}}{\text{nombre de particules incidentes}}$ pour la cible pleine,

α_v = idem pour la cible vide

$\beta_F = \dfrac{E_4}{E_1} = \dfrac{\text{nombre de coïncidences fortuites}}{\text{nombre de particules incidentes}}$.

Au premier ordre du développement, l'expression (1) s'écrit:

$$\sigma = \frac{1}{NLd}(\alpha_p - \alpha_v)\left(1+\frac{\alpha_p+\alpha_v}{2}+\beta_F\right).$$

Les coïncidences fortuites β_F, toujours inférieures à 1.1 % étaient pratiquement égales dans les mesures faites avec cible pleine et cible vide. Dans les calculs nous avons pris la moyenne entre les deux mesures.

L'effet cible vide α_v était faible. Dans toutes les mesures le rapport α_v/α_p est resté inférieur à 0.15.

5. – Corrections.

Pour obtenir la section efficace totale vraie, nous avons effecté les corrections suivantes:

a) Pollution du faisceau en mésons μ *et électrons.* Cette pollution a été mesurée à l'aide d'un compteur Čerenkov à gaz.

La Fig. 10 représente une des mesures effectuées à 800 MeV/c dans le faisceau n. 2. Le gaz dans le compteur était du CO_2.

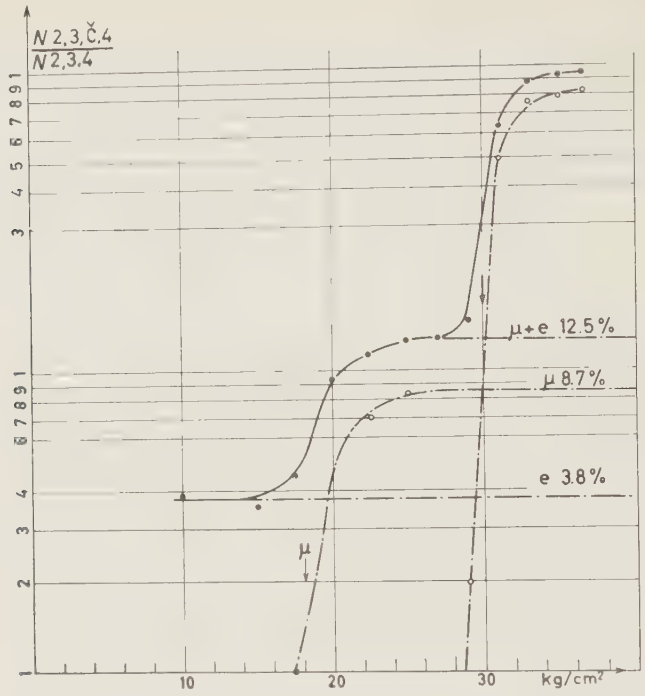

Fig. 10. – Mesure de la contamination $\pi^- + e^-$. Impulsion des π^-: 800 MeV/c. Le compteur Čerenkov à gaz (CO_2) était situé à la place de la cible à hydrogène, entre les compteurs 3 et 4. Les points noirs sont les résultats expérimentaux. Les courbes en traits interrompus représentent les contributions des diverses composantes du faisceau en supposant que chacune doit être voisine de l'intégrale d'une gaussienne.

Les Fig. 11 et 12 représentent la pollution en fonction de l'énergie du faisceau incident, y compris la contribution des μ provenant de la désintégration des π

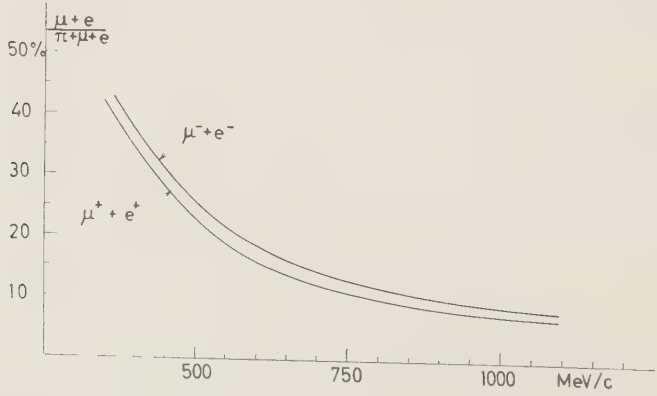

Fig. 11. – Pollution $(\mu+e)/(\pi+\mu+e)$ du faisceau no. 1.

après l'aimant analyseur. La majorité de ces mésons μ n'est pas discernable par cette méthode mais peut être calculée. La correction de pollution est donnée dans la colonne 3 et l'erreur estimée sur la section efficace provenant de l'imprécision de cette correction, dans la colonne 8.

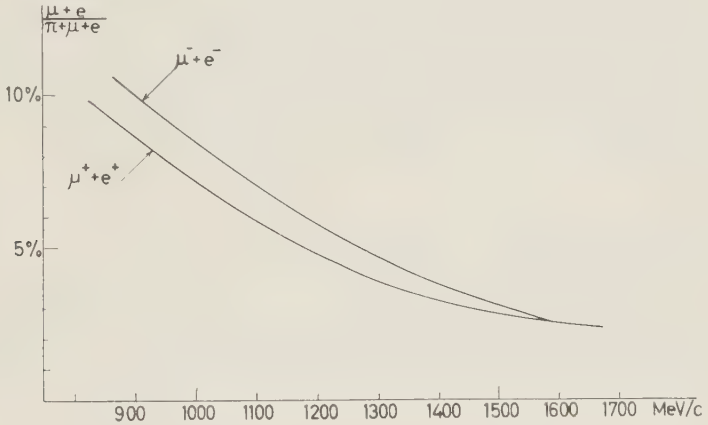

Fig. 12. – Pollution $(\mu+e)/(\pi+\mu+e)$ du faisceau no. 2.

b) *Correction géométrique.* Cette correction, qui tient compte de la diffusion vers l'avant, a pour expression:

$$\Delta\sigma = \pi\langle\theta^2\rangle\left[\left(\frac{dN}{d\Omega}\right)_{\text{inél}} + \left(\frac{dN}{d\Omega}\right)_{\text{él}}\right],$$

où $\pi\ \theta^2 \cong 0.035$ stéradian, est l'angle solide moyen sous lequel la cible est vue par le dernier compteur.

$(dN/d\Omega)_{\text{inél}}$ est la section efficace différentielle de production de particules chargées, dans les processus inélastiques. Pour les π^-, nous avons estimé cette section efficace d'après les résultats expérimentaux (cf. Tableau V).

La correction pour les π^+ a été calculée en supposant une certaine similitude entre les interactions inélastiques des π^+ et des π^- et en utilisant la section efficace totale élastique à 1.1 GeV ([10]). La section efficace inélastique pour cette énergie a été déterminée par différence entre les valeurs des sections efficaces totale et élastique.

$(dN/d\Omega)_{\text{él}}$ comprend à la fois les π diffusés élastiquement vers l'avant et les protons de recul correspondant aux π diffusés vers l'arrière. La section efficace vers l'avant a été calculée d'après le travail de J. W. Cronin ([11]).

Ces corrections géométriques, qui pourront être modifiées par l'apport de nouveaux résultats expérimentaux, sont données dans les colonnes 4 et 5.

([10]) L. O. Roellig and D. A. Glaser: *Phys. Rev.*, **116**, 1001 (1959).
([11]) J. W. Cronin: preprint Palmer Physical Laboratory (Princeton, N. J.).

c) Autres corrections. Nous avons tenu compte d'autres corrections mineures telles que:

— Contribution des interactions dans l'air de la cible vide.

— Pour les π^+, effet des coïncidences fortuites dues aux protons. Dans les mesures à haute énergie, 3% environ des particules incidentes comptées provenaient des coïncidences fortuites entre une particule traversant les deux premiers compteurs S_1S_2 et un proton du faisceau traversant le compteur S_3 et la cible. La section efficace mesurée a donc été corrigée de 0.03 fois la différence des sections efficaces respectives des π^+ et des protons aux énergies correspondantes.

6. – Discussion des résultats.

Dans les Fig. 13 et 14 nous donnons en traits pleins nos résultats et en pointillé les résultats récents de Berkeley ([1,12]). Pour les π^- nous avons aussi fait figurer les mesures à basse énergie de PONTECORVO *et al.* ([13]).

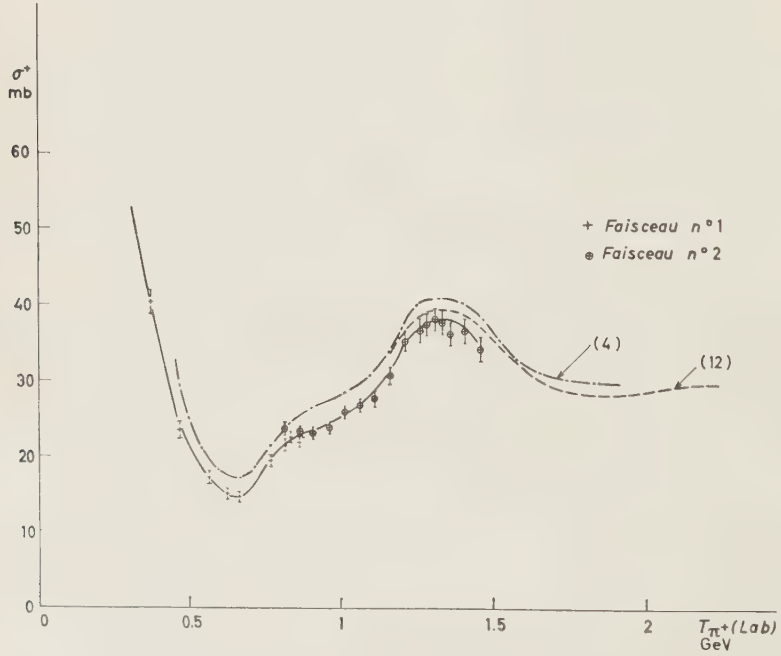

Fig. 13. – Section efficace totale π^+-p. En trait plein: résultats de Saclay; en trait pointillé: résultats de Berkeley ([4,12]).

([12]) T. J. DEVLIN, B. C. BARISH, W. N. HESS, V. PEREZ MENDEZ et J. SOLOMON: *Phys. Rev. Lett.*, **4**, 242 (1960).

([13]) B. PONTECORVO: *Kiev Report* (1959).

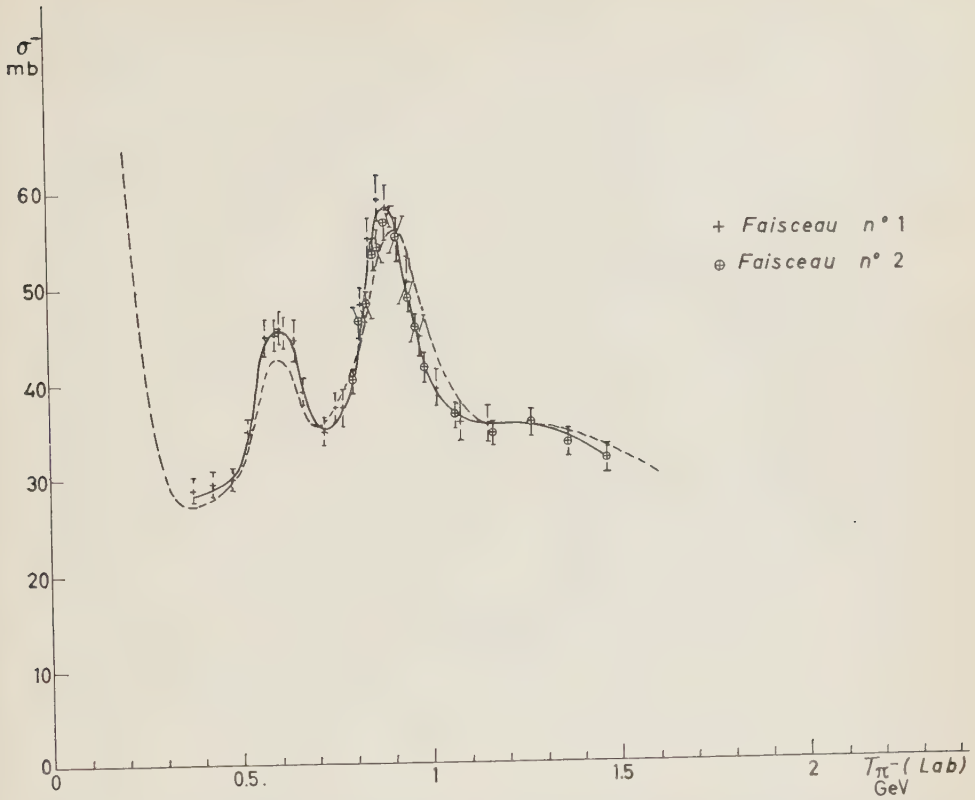

Fig. 14. – Section efficace totale π^--p. En trait plein: résultats de Saclay; en pointillé: en dessous de 400 MeV: résultats de Pontecorvo *et al.* [13], en dessus de 400 MeV: résultats de Berkeley [12].

L'erreur indiquée représente l'erreur totale.

La Fig. 15 représente la section efficace pour l'état de spin isotopique $T=\frac{1}{2}$

$$\tfrac{2}{3}\,\sigma_{(T=\frac{1}{2})} = \left[\sigma(\pi^-\mathrm{p}) - \tfrac{1}{3}\,\sigma(\pi^+\mathrm{p})\right].$$

Ces figures conduisent aux constatations suivantes:

a) Pour les π^- l'énergie et les section efficaces correspondant aux maxima sont, d'après nos mesures:

1^{er} maximum: $T_\pi = (605 \pm 6)$ MeV $\quad \sigma_{t.t} = (45.8 \pm 1.8)$ mb

$2^{\mathrm{ème}}$ maximum:

Faisceau 1 $\quad T_\pi = (890 \pm 9)$ MeV $\quad \sigma_{t.t} = (59.0 \pm 2\ \ )$ mb

Faisceau 2 $\quad T_\pi = (890 \pm 9)$ MeV $\quad \sigma_{t.t} = (56.8 \pm 1.8)$ mb

Nous retiendrons pour le deuxième maximum les valeurs

$$T_\pi = (890 \pm 9) \text{ MeV} \qquad \sigma_{tot} = (58.0 \pm 1.8) \text{ mb} .$$

Ces valeurs sont en accord avec les mesures citées [12].

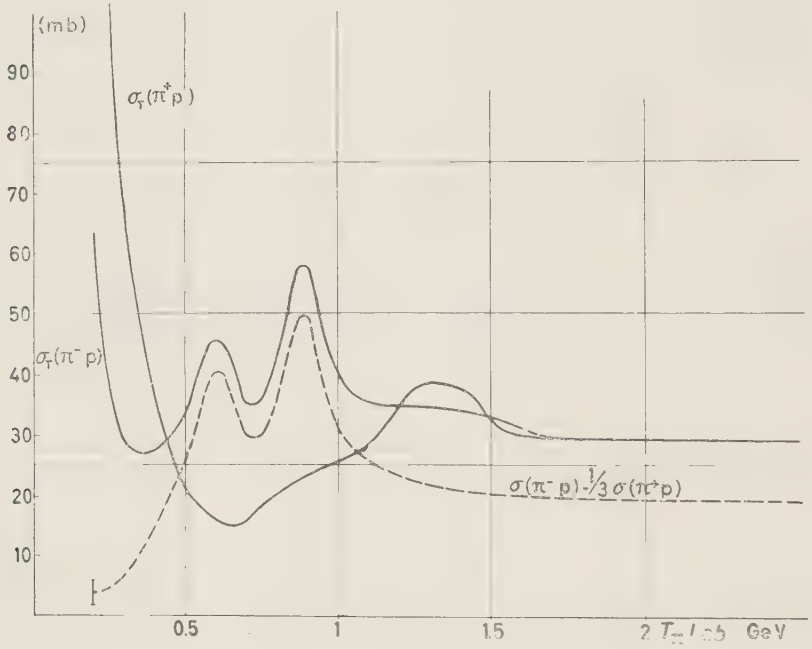

Fig. 15. – Section efficace pour l'état de spin isotopique $T=\frac{1}{2}$: $\frac{2}{3}\sigma_{(T=\frac{1}{2})} = \left[\sigma(\pi^-\text{-p}) - \frac{1}{3}\,\sigma(\pi^+\text{-p})\right]$.

b) L'énergie du premier maximum exprimé dans le centre de masse

$$E^* - m_p = (573 \pm 15) \text{ MeV} ,$$

concorde avec la valeur obtenue dans les expériences de photoproduction, soit $E^* - m_p = 570$ MeV [5].

c) Pour les π^+ la courbe de la Fig. 15 a été tracée en ne tenant compte que des erreurs statistiques: nous pensons que les erreurs dues à l'incertitude sur la pollution ne peuvent changer la forme de la courbe (*).

(*) *Note ajoutée à la correction.* – Des mesures récentes de la section efficace totale π^+-p, réalisées à Saclay, ont exclu, entre 600 MeV et 1 000 MeV, la possibilité d'une structure plus prononcée que celle indiquée par la courbe de la Fig. 13.

La discussion de l'origine des maxima observés exige la connaissance des sections efficaces totales élastiques et inélastiques ainsi que des distributions angulaires.

Il nous a paru intéressant de réunir les résultats des expériences de diffusion π^- au dessus de 460 MeV dans le Tableau V.

Il est possible que certains résultats aient été omis dans ce tableau par manque d'information.

Dans beaucoup de cas, les sections efficaces partielles étaient déduites, dans les travaux originaux, de la section efficace totale obtenue par Cool *et al.* [1], par multiplication du rapport de branchement de la voie correspondante. Ces valeurs sont reportées sur la même ligne que l'énergie. Sur la ligne du dessous nous avons indiqué les valeurs recalculées avec nos valeurs de la section efficace totale.

Pour le point à 915 MeV obtenu dans une expérience utilisant une chambre à propane nous avons normalisé la section efficace élastique totale pour obtenir une valeur de la section efficace vers l'avant égale à la valeur minimum théorique déduite par le théorème optique. On peut montrer [9,11] que la contribution à la section efficace différentielle vers l'avant de la partie réelle de l'amplitude de diffusion ne représente que quelques pourcents.

On dépend ainsi, pour la valeur minimum de la section efficace élastique, de l'extrapolation vers l'avant.

Dans l'étude du groupe de Bologne (réf. [7]) du Tableau V) cette extrapolation est faite en ajustant sur la distribution angulaire expérimentale un polynôme de la forme $\Sigma a_n \cos^n \theta$.

Nous avons pris la valeur extrapolée correspondant à la distribution en $\cos^6 \theta$ qui semble exprimer de façon satisfaisante les résultats (*).

Les résultats expérimentaux figurant dans le Tableau V sont reportés:

— dans la Fig. 16 pour les processus élastiques,

— dans la Fig. 17 pour les processus inélastiques chargés,

— dans la Fig. 18 pour les processus neutres.

On remarque que la section efficace élastique présente deux maximums importants aux mêmes énergies que la section efficace totale alors que la section inélastique chargée ne semble pas avoir ce comportement.

En supposant que les maximums observés sont dûs à des états résonants dans l'état $T = \frac{1}{2}$ pour lesquels un déphasage particulier δ_{Jl} passe par 90°,

(*) Pour ne pas dépendre de ce genre d'extrapolation, il serait nécessaire de connaître les rapports de branchement des différentes voies inélastiques chargés, neutres et élastiques. Une nouvelle expérience avec une chambre à bulles à hydrogène est souhaitable.

TABLEAU V. – *Mesure de diffusion* π^--p.

Energie (MeV)	Distribution en énergie	$(\sigma_{inél})_t$ (second. chargés) (mb)	$(\sigma_{neutres})_t$ (mb)	$(\sigma_{él})_t$ (mb)	σ_{total} (mb)	Observations	Nombre d'événements	Méthode	No. de réf.	Références
1	2	3	4	5	6	7	8	9	10	11
460	±10%	5.8±1	9.2±1.5	13.5±1	28.5 (*) 30 ±1.2 (***)	—	465	BP	(1)	CRITTENDEN *et al.*: *Phys. Rev. Lett.*, **2**, 121 (1959).
600	±10%	11.8±1.5 14.5	6.3±1 7.7	19 ±2 23.3	37.1 (*) 45.5±1.8 (***)	Val. recalculées	390	BP	(2)	CRITTENDEN *et al.*: *Phys. Rev. Lett.*, **2**, 121 (1959).
610	±1.6%	—	—	20 ±3	—	Normalisé sur valeur théoriq. de $(d\sigma/d\Omega)$ 0°	300	BH	(3)	GAILLARD *et al.*: *Compt. Rend. Ac. Sci.*, **249**, 1497 (1959).
770	±10%	13.3±1.5	7.2±1	16.6±2	37.1 (*) 37.4±2 (***)	—	500	BP	(4)	CRITTENDEN *et al.*: *Phys. Rev. Lett.*, **2**, 121 (1959).
800	—	23.3±2 18	9 ±1 7	21 ±2 16	53.3 41 ±2 (***)	Val. recalculées	~600	BH	(5)	MCCORMICK *et al.*: *Congrès CERN* (1958); UCRL-8302.
900	≈±6%	17.5±3 21.6	10 ±3 12.5	18.6±3 23	46 (*) 57 ±2 (***)	Val. recalculées	130	Em	(6)	WALKER *et al.*: *Phys. Rev.*, **104**, 526 (1956).
915	± 1%	—	—	19.8 $25\ \{^{+3}_{-2}$	—	Normalisé sur valeur théoriq. de $(d\sigma/d\Omega)$ 0°.	1421	BP	(7)	BERGIA *et al.*: *Nuovo Cimento*, **15**, 551 (1960).
950	± 2%	17.3±1.4 18.8	8.7±0.9 9.5	19.1±1.6 20.8	45 (*) 49 ±2 (***)	Val. recalculées	1200	BH	(8)	ERWIN *et al.*: *Phys. Rev.*, **109**, 1364 (1958).
960	±10%	18.2±3	8 ±5	20 ±3	46 (*)		320	DH	(9)	WALKER *et al.*: *Phys. Rev.*,

										Cimento, **14**, 211 (1959).
1 010	± 3%	19.8±3 16.8	6.4±1 5.4	22 ±3 18.6	48.2±3 41 ±2	Val. recalculées	600	BH	(11)	DERADO *et al.*: *Ann. d. Phys.*, **4**, 103 (1959).
1 300	± 1%			10 ±1		Normalisé sur valeur théoriq. de (dσ/dΩ) 0°.	850	BP	(12)	CHRETIEN *et al.*: *Phys. Rev.*, **108**, 383 (1957).
1 370	±10%	20 ±2		10 ±1	34 ±3 (*)	Neutres non mesurés.	500	DH	(13)	EISBERG *et al.*: *Phys. Rev.*, **97**, 797 (1955).
1 500	± 4%	16.6±3	9 ±2	9 ±1.5	34 ±3 (*)		193	Em	(14)	WALKER *et al.*: *Phys. Rev.*, **98**, 1416 (1955).
1 710	±10%	20 ±3		11 ±2		Neutres non mesurés.	200	DH	(15)	WHITTEN *et al.*: *Phys. Rev.*, **111**, 1676 (1958).
4 500	—	22.5±4	2 ±0.5	4.5±1	29 (**)		128	Em	(16)	WALKER *et al.*: *Phys. Rev.*, **108**, 872 (1957).
5 000	±15%	16.5±4 20.5	1.3±0.5	4.7±1 6	22.5	Val. corrigées [cf. (16)]	137	DH	(17)	MAENCHEN *et al.*: *Phys. Rev.*, **108**, 850 (1957).

LÉGENDE:

Colonne 1: Energie cinétique des π incidents dans le laboratoire.
2: Etalement en énergie du faisceau utilisé.
3: Section efficace totale des processus inélastiques donnant des secondaires chargés (y compris particules étranges).
4: Section efficace totale des processus donnant des particules neutres.
5: Section efficace totale élastique.
6: Section efficace totale obtenue ou utilisée dans le travail.
8: Nombre d'événements obtenus dans l'expérience.
9: Méthode utilisée: BP, chambre à bulles à propane; BH, chambre à bulles à hydrogène; DH, chambre à diffusion à hydrogène; Em, émulsion.

(*) σ_t obtenue par COOL *et al.*: *Phys. Rev.*, **103**, 1082 (1956).
(**) σ_t obtenue par WIKNER: UCRL-3639; BANDTEL *et al.*: *Phys. Rev.*, **99**, 673 (1955).
(***) σ_t obtenue dans ce travail, utilisée pour recalculer les sections efficaces partielles.

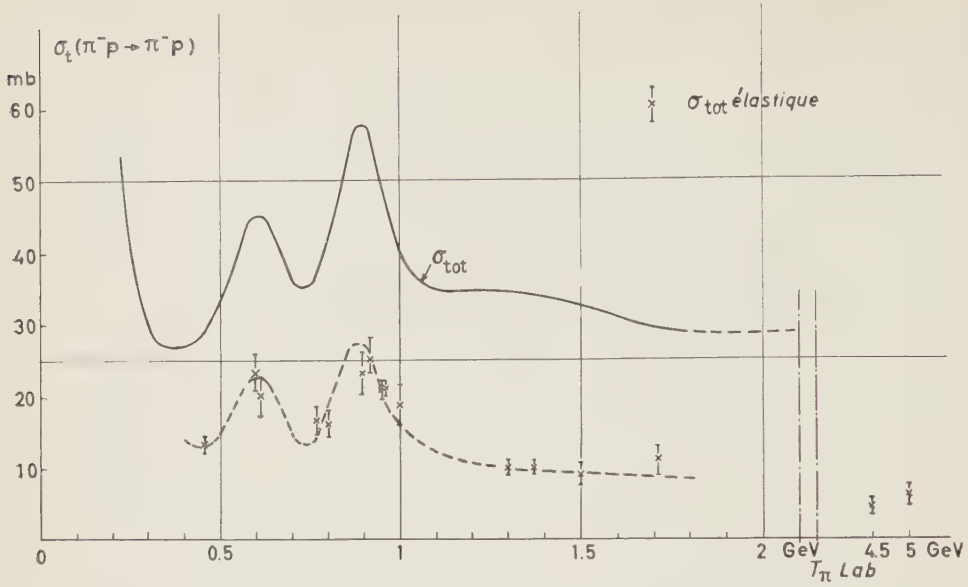

Fig. 16. – Section efficace totale des processus élastiques.

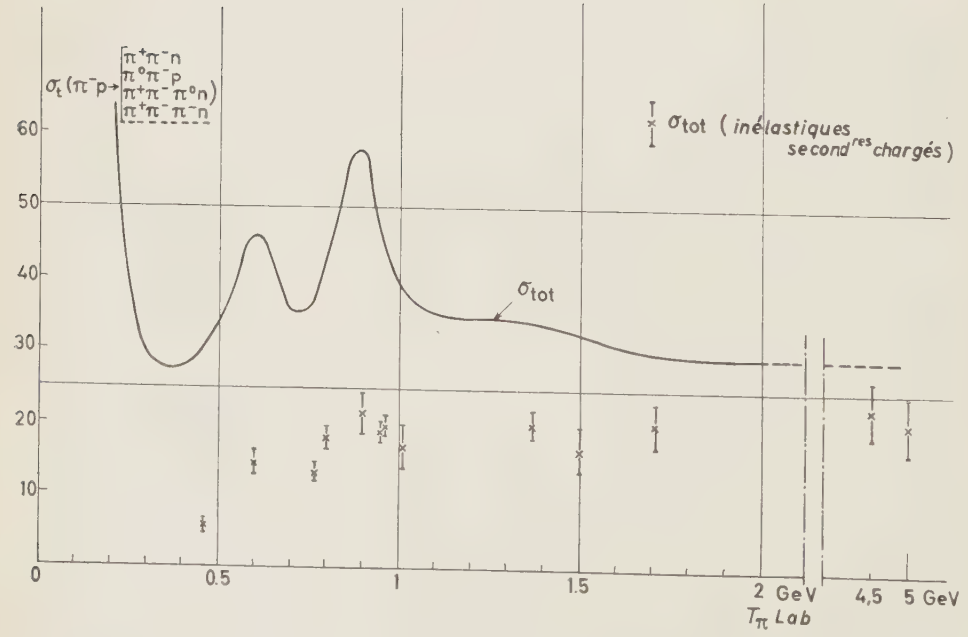

Fig. 17. – Section efficace totale des processus inélastiques chargés.

nous pouvons calculer les valeurs maximums de la section efficace totale correspondant à une valeur donnée de J.

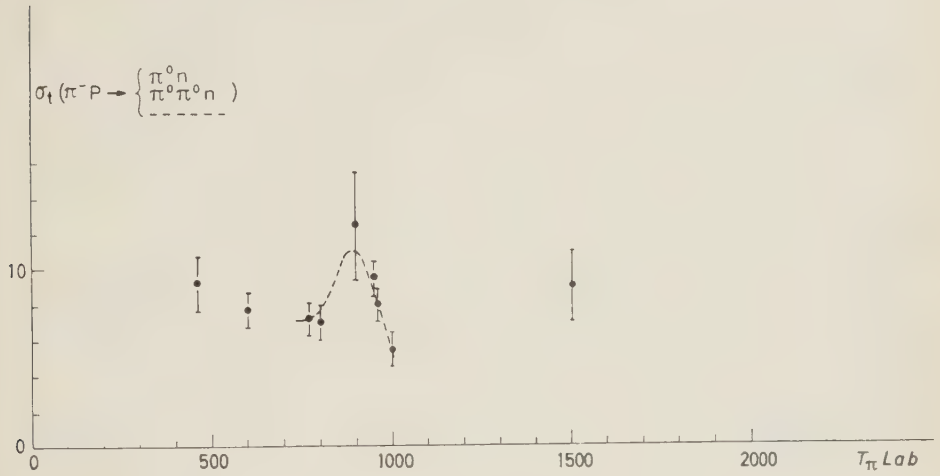

Fig. 18. – Section efficace totale des processus neutress.

Ces valeurs sont données dans le Tableau VI.

TABLEAU VI. – *Contribution maximum à la section efficace totale* π^--p *d'un état résonnant de* $T=\frac{1}{2}$ *et* J *donné.*

Energie $T_{\pi_{lab}}$ (MeV)	$\lambda\!\!\!^{-}$ (10^{-13} cm)	$r/\lambda\!\!\!^{-}$	$\pi\lambda\!\!\!^{-2}$ (mb)	$\sigma_{t.t}$ maximum pour $J=$ $\frac{1}{2}$ (mb)	$\frac{3}{2}$ (mb)	$\frac{5}{2}$ (mb)	$\frac{7}{2}$ (mb)	$\frac{9}{2}$ (mb)
605	0.435	2.53	5.95	15.9	31.8	47.6	63.5	—
890	0.347	3.17	3.8	10.1	20.3	30.2	40.3	50.4

LÉGENDE:

$$(\sigma_{\text{tot rés}})_{\max} = \tfrac{8}{3}\,\pi\lambda\!\!\!^{-2}\,(J+\tfrac{1}{2})\,.$$

Dans la 3ème colonne, on a reporté la valeur maximum du paramètre d'impact en unité $\lambda\!\!\!^{-}$ calculée avec $r = 1.1\cdot10^{-13}$ cm, déduit du scattering de diffraction obtenu à 1.3 GeV [réf. (12), Tableau V].

7. – Discussion du maximum à 890 MeV.

A ce maximum les sections efficaces partielles sont les suivantes:

$$\sigma_{t.t} \cong 58 \text{ mb} ; \quad \sigma_{\text{él}} \cong 27 \text{ mb} ; \quad \sigma_{\text{inel. chargés}} \cong 21 \text{ mb} ; \quad \sigma_{\text{neutres}} \cong 10 \text{ mb} .$$

Pour estimer la valeur de la section efficace totale provenant de l'état résonnant, on peut soustraire arbitrairement un fond continu non résonnant qui ne devrait pas être très différent de la valeur à 1.5 GeV (*).

On obtient ainsi une section efficace totale pour l'état résonnant, égale à 30 mb (Fig. 15).

Pour essayer de déterminer le moment angulaire responsable de cette résonance, nous pouvons remarquer que:

1) La résonance ne peut se faire dans l'état $J=\frac{1}{2}$ où $J=\frac{3}{2}$ seul, car la valeur expérimentale de $\sigma_{tot}=30$ mb est supérieure aux valeurs maximums calculées pour ces états.

2) La valeur $J=\frac{9}{2}$ parait exclue du fait que la distribution angulaire obtenue par le groupe de Bologne (réf. (7), Tableau V) semble être bien représentée par un polynôme en $\cos^6\theta$, alors que la valeur $\frac{9}{2}$ exigerait un polynôme en $\cos^8\theta$.

D'autre part, une résonance dans l'état $J=\frac{9}{2}$ où plus correspondrait à un moment orbital $l>4$ ce qui est peu vraisemblable lorsqu'on considère le paramètre d'impact. (cf. Tableau VI).

Les deux valeurs possibles sont donc $J=\frac{5}{2}$ et $J=\frac{7}{2}$.

Dans la Fig. 19 on a représenté les sections efficaces en fonction du facteur

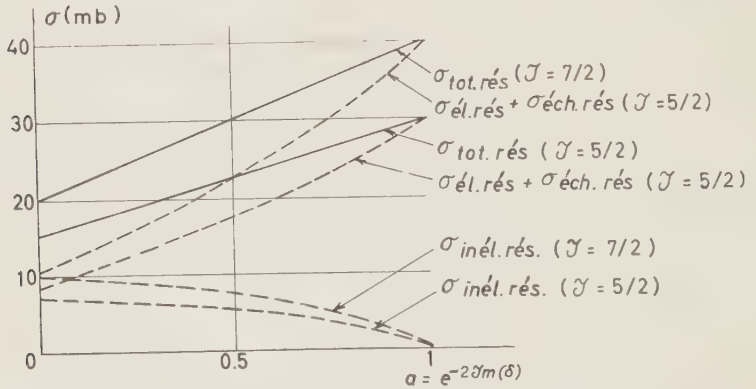

Fig. 19. – Contribution à la section efficace totale π^--p de la résonance de l'une des ondes partielles $J=\frac{5}{2}$ et $J=\frac{7}{2}$. Les sections efficaces sont données en fonction de Im (δ). On suppose Re $(\delta)=90°$. On a les relations

(1) $$\sigma_{\text{tot rés}}=\tfrac{2}{3}\cdot 2\pi\lambda^2(J+\tfrac{1}{2})(1+\exp[-2\,\text{Im}\,(\delta)])\,,$$

(2) $$(\sigma_{\text{él}}+\sigma_{\text{éch. de charges}})_{\text{rés}}=\tfrac{2}{3}\pi\lambda^2(J+\tfrac{1}{2})(1+\exp[-2\,\text{Im}\,(\delta)])^2\,,$$

$$\sigma_{\text{tot rés}}=\sigma_{\text{él rés}}+\sigma_{\text{éch. de charges rés}}+\sigma_{\text{inél. rés}}\,.$$

(*) On commet peut-être une erreur par excès, ce fond continu pouvant diminuer vers les basses énergies; mais cette erreur est en partie compensée par l'effet de la queue de la résonance de 605 MeV, dont nous n'avons pas tenu compte dans la soustraction.

d'absorption $a = \exp[-2\,\mathrm{Im}\,\delta]$ (où $\mathrm{Im}\,\delta$ désigne la partie imaginaire du déphasage δ_{Jl}). Si l'on admet pour la section efficace totale résonnante la valeur expérimentale de 30 mb, on constate que pour la valeur $J=\frac{5}{2}$ la contribution de la résonance à la section efficace inélastique est petite, alors que pour $J=\frac{7}{2}$ elle est égale à 7.5 mb.

Or, les Fig. 17 et 18 montrent que la section efficace inélastique ne subit pas d'augmentation de l'ordre de grandeur de 7 mb au passage de la résonance (*).

Ces constatations suggèrent que le J résonnant égale $\frac{5}{2}$ et que, par conséquent, cette résonance est un processus principalement élastique, en considérant comme processus élastiques les réactions (π^--p $\rightarrow$ π^--p) et (π^--p $\rightarrow$ π_0-n).

L'étude de la distribution angulaire à 915 MeV (Fig. 20) est également compatible avec la valeur $J=\frac{5}{2}$ et semble montrer une contribution importante des ondes D et F. En effet, il est nécessaire d'admettre un grand terme de spin-flip provenant de l'onde F pour rendre compte du maximum de la distribution angulaire à $\cos\theta = -0.75$ et, d'autre part, de supposer une forte influence de l'onde D pour expliquer la forme de la distribution angulaire vers l'avant (réf. 7 et 8, Tableau V).

La Fig. 20 représente les distributions angulaires au voisinage de la ré-

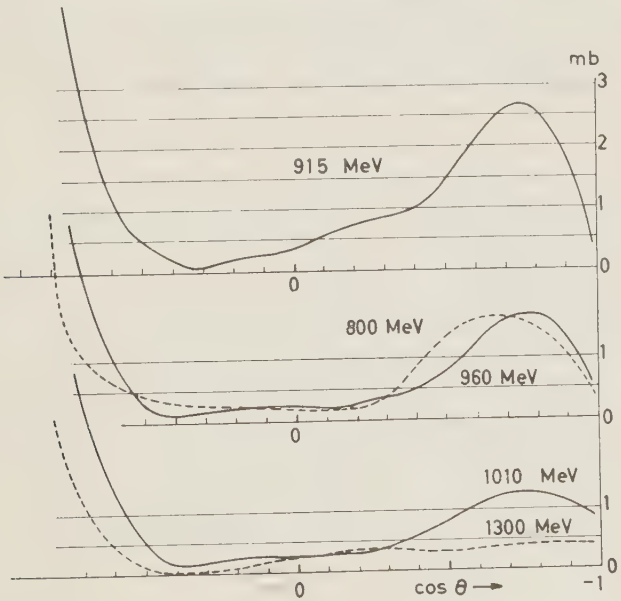

Fig. 20. – Distributions angulaires π^--p au voisinage de la 3e résonance. Pour les références, cf. Tableau V.

(*) Du fait que la section efficace neutre est de l'ordre de 10 mb et qu'elle doit inclure une forte proportion d'échange de charge, il est peu vraisemblable que la section efficace inélastique neutre contribue pour une grande part à cette variation.

sonance. Elle montre que le pic à $\cos\theta = -0.75$ passe par un maximum à l'énergie de la résonance.

Ce fait suggère alors que l'onde qui résonne, est l'onde $F\ \frac{5}{2}$.

Ceci serait en accord avec les interprétations préliminaires tirées de la photoproduction [14,18].

8. – Discussion du maximum à 605 MeV.

Les Fig. 16 et 17 suggèrent pour cette résonance un comportement des sections efficaces élastiques et inélastiques analogue à celui discuté pour la résonance à 890 MeV.

La valeur de la section efficace totale au maximum ($\sigma = (45.8 \pm 1.8)$ mb) est compatible avec l'existence d'un état résonnant de moment angulaire $J = \frac{3}{2}$ et de spin isotopique $T = \frac{1}{2}$ dont l'existence a été déduite des expériences de photoproduction [14]. PEIERLS a émis l'hypothèse que la parité orbitale des cet état était positive et que l'onde résonnante était donc $D\ \frac{3}{2}$.

L'analyse en déphasage de la distribution angulaire de la diffusion élastique π^--p à 600 MeV [15] ainsi que la mesure de la polarisation du proton de recul dans la réaction $\gamma + p \to \pi_0 + p$ [16] sont compatibles avec cette interprétation.

Cependant, des arguments récents montrent qu'on ne peut exclure de manière définitive l'état $P\ \frac{3}{2}$ [17].

* * *

Nous tenons à remercier Monsieur le Prof. A. BERTHELOT pour l'intérêt constant qu'il a montré au cours de ce travail, ainsi que Monsieur R. OMNÈS, du Service de Physique Mathématique, pour les nombreuses et fructueuses discussions que nous avons eues avec lui.

Nos remerciements vont également à L. C. L. YUAN, de Brookhaven, pour sa participation à l'expérience, ainsi qu'au Prof. G. PUPPI et à R. WALOSCHEK pour la discussion de l'expérience du groupe de Bologne.

Enfin nous remercions MM. R. LÉVY-MANDEL, P. STICKEL et F. PENET, ainsi que leurs collaborateurs du Département de Saturne pour l'aide apportée auprès de la machine; MM. P. PRUGNE, M. BOUGON et J. TICHIT, du groupe des Techniques Nucléaires, pour la construction et le fonctionnement de la

[14] R. F. PEIERLS: UCRL-8847; *Phys. Rev. Lett.*, **1**, 174 (1958).
[15] W. D. WALKER *et al.*: *Phys. Rev.*, **118**, 1612 (1960).
[16] P. C. SREIN: *Phys. Rev. Lett.*, **2**, 473 (1959).
[17] L. F. LANDOVITZ et L. MARSHALL: *Phys. Rev. Lett.*, **3**, 190 (1959).
[18] F. P. DIXON et R. L. WALKER: *Phys. Rev. Lett.*, **1**, 458 (1958).

cible à hydrogène; le Laboratoire de Physique Atomique du Collège de France pour la réalisation du compteur Čerenkov à gaz. Enfin nous remercions vivement MM. P. Autones, S. Bréhin, P. Roos et J. Thibaud, du groupe Electronique, qui ont réalisé l'ensemble de l'appareillage.

RIASSUNTO (*)

Misure della sezione d'urto totale per π^+-p e π^--p per assorbimento in idrogeno liquido con un fascio di energia nota entro $\pm 1\%$ e con un $\Delta P/P$ totale di $\pm 1.8\%$. Le energie ed i valori delle sezioni d'urto ai massimi sono

$$\pi^-: \quad T_{\pi_{lab}} = (605 \pm 6)\ \text{MeV}, \qquad \sigma_{tot} = (45.8 \pm 1.8)\ \text{mb},$$
$$T_{\pi_{lab}} = (890 \pm 9)\ \text{MeV}, \qquad \sigma_{tot} = (58.0 \pm 1.8)\ \text{mb},$$
$$\pi^+: \quad T_{\pi_{lab}} = (1330 \pm 30)\ \text{MeV}, \qquad \sigma_{tot} = (38.0 \pm 2.0)\ \text{mb}.$$

Compilazione dei risultati relativi alle sezioni d'urto elastiche ed anelastiche ottenuti con altre tecniche sperimentali nella prossimità della seconda e della terza risonanza del π^-. Discussione della seconda e della terza risonanza.

(*) *Traduzione a cura della Redazione.*

IL NUOVO CIMENTO Vol. XIX, N. 2 16 Gennaio 1961

Nuclear Magnetic Relaxation in Colloidal Solutions.

G. Bonera, L. Chiodi, G. Lanzi and A. Rigamonti

Istituto di Fisica dell'Università - Pavia

(ricevuto il 28 Giugno 1960)

Summary. — Nuclear relaxation times T_1 and T_2 have been measured for solutions of isinglass and silica gel in water. Furthermore we have researched the presence of more than one longitudinal relaxation times in these solutions. Thus some informations about the lifetime of water molecules in the absorbed phases are obtained.

1. – Introduction.

Zimmermann and Brittin [1], Kamiyoshi [2] and Winkler [3] have recently studied the behaviour of very small quantities of adsorbed water on silica gel or alumina regarding nuclear relaxation. Generally for adsorbed water these authors have found values of T_1 and T_2 several times less than those of ordinary water. Particularly Zimmerman and Brittin have observed in very small quantities of water adsorbed on silica gel two transversal relaxation times, which can be attributed to the existence of more than one layer of adsorbed water; in these conditions an appreciable difference can be observed only between the relaxation times relative to the first monomolecular layer and those relative to other layers.

The purpose of this work is to study the behaviour of some colloidal solutions regarding nuclear relaxation. The systems we have investigated are solutions in water of organic gelatins (isinglass) and silica gel.

(1) J. R. Zimmerman and W. E. Brittin: *Journ. Phys. Chem.*, **61**, 1328 (1957).
(2) M. K. Hamiyoshi: *Journ. Phys. Rad.*, **20**, 60 (1959).
(3) H. Winkler: *Arch. des Sci.*, **12**, fasc. spéc., 161 (1959).

The system we have studied are different from those investigated by other authors being constituted of solutions in water in which water is always in remarkable quantities. In fact in our systems the weight concentration of gel is never greater than 45%. Consequently the relaxation times we have measured are much greater than those measured by ZIMMERMAN amd BRITTIN. Thus we can obtain some informations about the lifetime of water molecules in the adsorbed phases.

The methods we have used in the measurement of relaxation times T_1 and T_2 have been already described ([4,5]). Furthermore we have searched for the presence of more than one longitudinal relaxation times with an already described experimental technique ([6]).

2. – Experimental results.

For solutions in water of isinglass at 18 °C the law with which the longitudinal component of the nuclear magnetization reaches the equilibrium value turns out to be, within experimental errors, exponential as far as concentrations about 20%. For greater concentrations of isinglass we could observe a deviation of this law from the exponential form; such deviation is already remarkable for concentrations of 30% (see Fig. 1).

The values of T_1 and T_2 we obtained for concentrations of isinglass under 20% are plotted in Fig. 2.

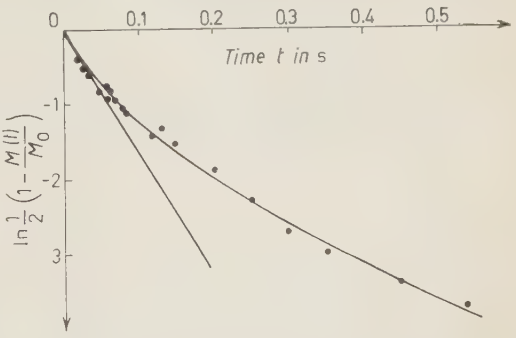

Fig. 1. – $\ln \frac{1}{2}(1 - M(t)/M_0)$ versus t for a water solution of isinglass whose concentration is 30%.

For silica gel solutions we have searched the for possible presence of more than one longitudinal relaxation time only in the range of concentrations between 25% and 45%. In this range experimental results point out that, within experimental errors, only a longitudinal relaxation time is present.

([4]) G. CHIAROTTI, G. CRISTIANI, L. GIULOTTO and G. LANZI: *Nuovo Cimento*, **12**, 519 (1954).

([5]) G. BONERA, L. CHIODI, L. GIULOTTO and G. LANZI: *Nuovo Cimento*, **14**, 119 (1959).

([6]) G. BONERA, L. CHIODI, G. LANZI and A. RIGAMONTI: *Nuovo Cimento*, **17**, 198 (1960).

Nuclear magnetization for concentrations above 45% varies too rapidly in order that an accurate research of its variation law can be performed with our experimental device. It is yet probable that even in the case of silica gel solutions with rather strong concentrations, more than one relaxation time be present.

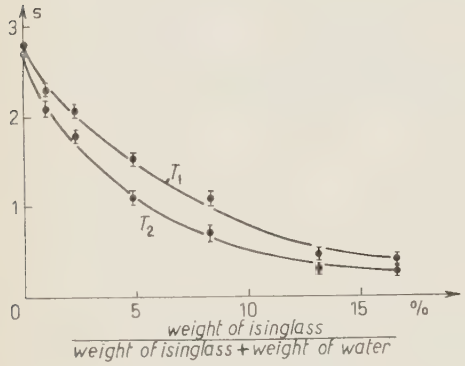

Fig. 2. – T_1 and T_2 versus concentration of isinglass.

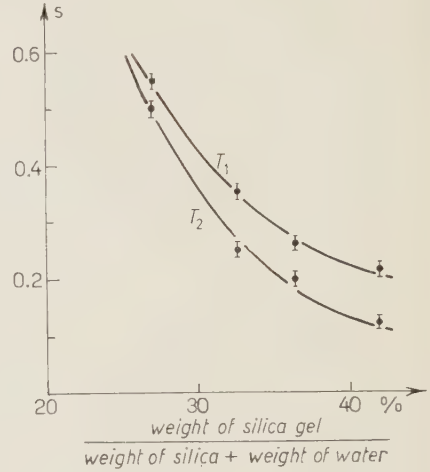

Fig. 3. – T_1 and T_2 versus concentration of silica gel.

In Fig. 3 we have plotted the results we have obtained for relaxation times in water solutions of silica gel at 18 °C at concentrations between 25% and 45%.

3. – Discussion.

In order to explain the behaviour of colloidal solutions regarding nuclear magnetic relaxation we must think that water molecules may be more or less strictly bound to the particles of colloid. We can therefore consider these solutions as multiphase systems; every phase has a different law for the variation with time of the local magnetic field. In such systems the i-th phase, which corresponds to a particular layer of water molecules, is characterized by a longitudinal relaxation time T_{1i} and a transversal relaxation time T_{2i}. Because the water molecules jump continually from phase to phase the longitudinal and transversal relaxation time of a water proton will be random variable taking on the values T_{1i} and T_{2i}.

Let μ be the part of the nuclear magnetization due to a single proton; we suppose that the longitudinal and transversal components of μ vary with continuity. If we consider *e.g.* the longitudinal component and if μ_0 is the

equilibrium value of the magnetization due to a single proton we may write

$$\mu_0 - \mu_z(t) = (\mu_0 - \mu_z(0)) \exp\left[-\int_0^t \frac{\mathrm{d}t}{T_1(t)}\right].$$

If the lifetime of a proton in every phase is small compared with t, then $1/T_1(t)$ is a function of time which fluctuates very rapidly. The value of the integral is then equal to the mean value of this function time t. Let $1/T_1$ be the mean value of the function $1/T_1(t)$, then

$$\frac{1}{T_1} = \sum_i \frac{P_i}{T_{1i}}, \tag{1}$$

P_i being the fraction of protons present in the i-th phase.

We can conclude that when the exchange is very rapid with respect to t then the law for the relaxation of the longitudinal component of nuclear magnetization is still exponential and the longitudinal relaxation time we measure is given by (1), *i.e.* $1/T_1$ is the weighted average of the reciprocals of the relaxation times in the various phases (*). This means that if we find an exponential variation of the nuclear magnetization in a multiphase system then the exchange is rapid with respect to t, *i.e.* practically respect to the relaxation time we measure. For the case of transverse relaxation time, if the exchange is rapid we have in the same way

$$\frac{1}{T_2} = \sum_i \frac{P_i}{T_{2i}}.$$

It is now possible, from the examination of our experimental results to give a more extensive interpretation of nuclear magnetic relaxation in solutions of isinglass in water at various concentrations. Because the concentration of the isinglass is relatively small and because the signals due to the particles in suspension are wide and therefore of little amplitude, the values we have found for T_1 and T_2 can be practically attributed to the water protons and not to those of the isinglass.

As shown in Fig. 2 both T_1 and T_2 are smaller than the nuclear relaxation times of pure water and decrease with the increase of concentration. These results could be foreseen; in fact when the concentration increases then the population of the phases in which the water molecules are more strictly bound

(*) Zimmerman and Brittin [1] obtain the same results studying multiphase systems with the stochastic theory of Kubo.

increases and therefore in (1) and (2) the statistical weight of the smallest relaxation times increases.

We want then to point out that the values of T_2 are less than those of T_1 and that the ratio T_1/T_2 increases with concentration. This can be explained assuming that there are phases in which the water molecules are so strictly bound that their correlation time is large enough to cause T_2 to be less than T_1; furthermore the statistical weight of these phases increases with concentration and consequently we can expect a corresponding increase of the ratio T_1/T_2.

For the case of silica gel we can conclude that in the range of concentrations we have investigated, the condition of rapid exchange between water molecules is verified. Also for these solutions we find that T_1 and T_2 decrease with the increase of the concentration of gel and that the ratio T_1/T_2 increases with concentration.

* * *

The authors are indebted to Professor L. GIULOTTO for his assistence and for his very useful suggestions.

The authors also wish to express their gratefulness to the Consiglio Nazionale delle Ricerche, for its grant, and to the Office, Chief of Research and Development, U.S. Department of Army, who has sponsored in part this work through its European Office.

RIASSUNTO

Sono stati misurati i tempi di rilassamento nucleare T_1 e T_2 per soluzioni in acqua di colla di pesce e gel di silice. È stata inoltre ricercata la presenza di più tempi di rilassamento longitudinali in queste soluzioni. Si sono così ottenute alcune informazioni sui tempi di vita delle molecole d'acqua nelle fasi adsorbite.

Nuclear Potential for the K^+-Meson.

T. G. Lim and S. J. Bosgra

Natuurkundig Laboratorium, Universiteit van Amsterdam - Amsterdam

(ricevuto il 18 Luglio 1960)

Summary. — The data of K^+-mesons elastically scattered by complex nuclei in G-5 nuclear emulsion have been analyzed. Only small angles in the energy region of (40÷80) MeV were considered. The phase shift optical model analysis has been applied, using the W.K.B.J. approximation for the evaluation of phase shifts. The calculations are based on the assumption that the elastic nuclear scattering potential may be approximated by a real square model. The magnitude is estimated to be (21±5) MeV, if in the relation of the nuclear radius $R = r_0 A^{\frac{1}{3}}$, $r_0 = 1.2 \cdot 10^{-13}$ cm, and it is (17±5) MeV, if $r_0 = 1.4 \cdot 10^{-13}$ cm.

1. – Introduction.

The experimental data analysed in this paper are obtained from the same sample of K^+-meson tracks, mentioned in the previous report [1]. We only analysed the elastic scattering data of K^+-mesons which are elastically deflected at small angles, in the energy region of (40 ÷ 80) MeV. In the small angle region we namely expect the interference between the Coulomb and the nuclear scattering to be strong.

For the nuclear potential, instead of a complex model with an edge which gradually drops off, we adopt a real square model in all our computations of the cross-sections. Some reasons for the use of this model have been given earlier [2]. A computation of the transparency of nuclear matter with respect to K^+-mesons shows that this quantity is rather high in the energy region considered (Sect. 2).

[1] T. G. Lim and P. G. van Breemen: *Nuovo Cimento*, **17**, 887 (1960).
[2] T. G. Lim and J. P. van der Linden: *Nuovo Cimento*, **11**, 67 (1959).

The elastic scattering in the small angle region is described by the scattering potential V_{sc}. This potential consists of a real square model nuclear potential, V_n, superposed on the Coulomb potential V_C. The Coulomb potential is assumed to be due to a homogeneous charge distribution. The nuclear radius, R, is assumed to satisfy the relation $R = r_0 A^{\frac{1}{3}}$. We further assume that the magnitude of V_n, *i.e.* V, does not depend on the nuclear mass. Thus we have:

$$(1.1) \qquad \begin{cases} V_{sc} = V + \dfrac{Ze^2}{2R}\left(3 - \left(\dfrac{r}{R}\right)^2\right), & \text{for } r \leqslant R, \\ V_{sc} = \dfrac{Ze^2}{r}, & \text{for } r > R. \end{cases}$$

2. – Transparency of the nuclei.

The relation between the transparency t of nuclear matter to the mean free path of inelastic scattering λ_i is given by (2.1) [3],

$$(2.1) \qquad t = \frac{\lambda_i^2}{2R^2}\left\{1 - \left(1 + \frac{2R}{\lambda_i}\right)\exp\left[-\frac{2R}{\lambda_i}\right]\right\},$$

with: $\lambda_i = 4\pi R^3/3A\bar{\sigma}$, where R is the nuclear radius which satisfies the relation $R = r_0 A^{\frac{1}{3}}$ (A: mass number);

$\bar{\sigma}$: weighted average of the collision cross-section of the impinging particle with the nucleon (*). In our specific case, where we consider K^+-meson scattering, $\bar{\sigma}$ means the weighted average of the K^+-meson-nucleon collision cross-section.

By substituting an experimental value of $\bar{\sigma}$ in (2.1), and computing thus the value of t, we may obtain an idea of the transparency of the emulsion nuclei with respect to the K^+-meson (in the energy region concerned). For $\bar{\sigma} \approx 4$ mb, a typical experimental value for the K^+-meson kinetic energy region of (40 ÷ 120) MeV [4], we find that the average value of the transparency of C, Ag, Br, and O is ~ 0.8. This result gives an indication that the nuclear matter is very transparent with respect to K^+-mesons.

[3] B. Rossi: *High Energy Particles* (New York, 1952), p. 360.

(*) $\bar{\sigma} = (Z\sigma_p + (A - Z)\sigma_n)/A$, with Z: number of protons; A: mass number; $\sigma_p(\sigma_n)$: cross section of the collision with protons (neutrons).

[4] B. Bhowmik, D. Evans, S. Nilsson, D. J. Prowse, F. Anderson, D. Keefe, A. Kernan and J. Losty: *Nuovo Cimento*, **6**, 440 (1958).

3. – Computation.

The differential cross-sections for the elastic scattering have been computed by the method of partial waves, and the phase shifts have been evaluated in the W.K.B.J. approximation ([5,6]). For the computation of the theoretical differential cross-sections we used the ARMAC electronic computer of the Mathematisch Centrum of Amsterdam. The correctness of the program has been carefully checked at many stages of the computation ([7]).

For the determination of the sign of V, as well as the magnitude of it, we analysed the elastic scattering data of the energy region of (40÷80) MeV. The experimental points are then compared with the theoretical values, computed for $E_K = 60$ MeV.

4. – Sign of V.

To decide on the sign of V, two types of the resultant $(d\sigma/d\omega) = f(\vartheta)$ curves have been computed. In one type, the constructive interference between the Coulomb and the nuclear scattering amplitude is considered, while in the other type we consider the destructive interference between the two scattering amplitudes.

The resultant curves are obtained by the superposition of four component-curves: $(d\sigma/d\omega)_i = f_i(\vartheta)$, with $i =$ Ag, Br, C, O. A closer study of the component curves gives us an insight how the resultant curve is built up.
In Fig. 1 and 2 these component curves are shown. They have been computed in the centre of mass system for the following parameters: E_K (kinetic energy of the K⁺-meson): 60 MeV, $r_0 = 1.2 \cdot 10^{-13}$ cm, $V = -10$ MeV (Fig. 1), and $V = +20$ MeV (Fig. 2). The negative value of V corresponds to an attractive nuclear potential (destructive interference), and the positive value of V corresponds to a repulsive one (constructive interference).

The resultant curves $(d\sigma/d\omega) = f(\vartheta)$ are obtained from the relation

$$(d\sigma/d\omega) = \sum \alpha_i (d\sigma/d\omega)_i \,, \tag{4.1}$$

where α is the relative frequency of the element. $\sum \alpha_i = 1$. From Fig. 1 and 2 we see that the resultant curves (Fig. 3) reflect the general behaviour

([5]) G. COSTA and G. PATERGNANI: *Nuovo Cimento*, 5, 448 (1957).
([6]) P. M. MORSE and H. FESHBACH (New York, 1953), p. 1011.
([7]) T. G. LIM: *Thesis* (Amsterdam).

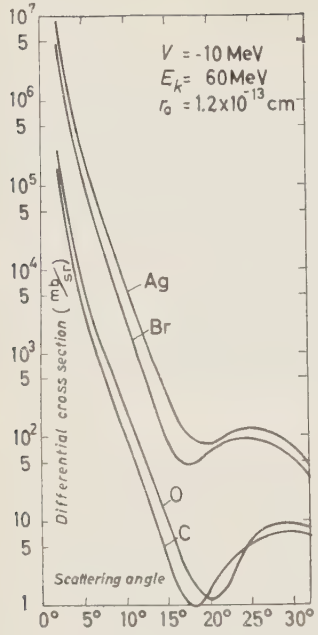

Fig. 1. – $(d\sigma/d\omega)_i = f_i(\vartheta)$; i = Ag, Br, C, O. $E_K = 60$ MeV, $r_0 = 1.2 \cdot 10^{-13}$ cm, $V = -10$ MeV. Destructive interference.

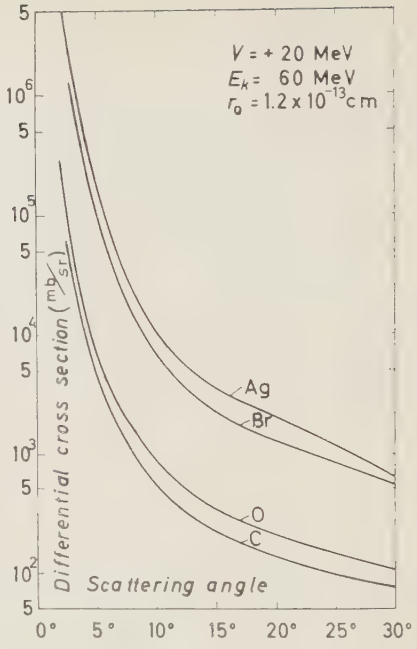

Fig. 2. – $(d\sigma/d\omega)_i = f_i(\vartheta)$; i = Ag, Br, C, O. $E_K = 60$ MeV, $r_0 = 1.2 \cdot 10^{-13}$ cm, $V = +20$ MeV. Constructive interference.

of the component curves in the angle region of interest.

As far as the sign is concerned, from Fig. 3 we deduce that the experimental points follow the curve computed for the repulsive nuclear potential rather than that of the attractive potential. This was also indicated when using the Born approximation (1).

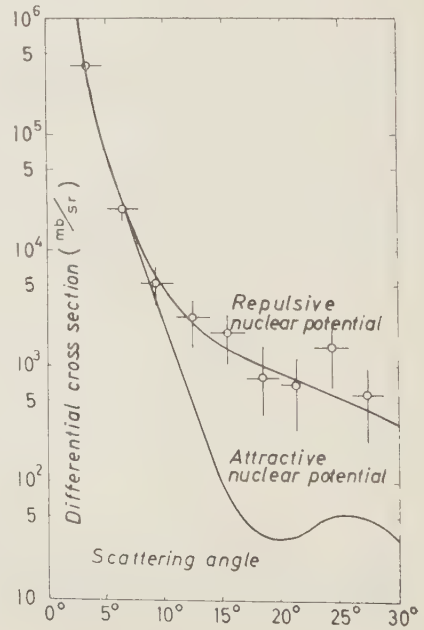

Fig. 3. – $(d\sigma/d\omega) = \sum \alpha_i (d\sigma/d\omega)_i$. $V = -10$ MeV, $V = +20$ MeV.

5. – Value of V.

To illustrate how the resultant curves $(d\sigma/d\omega) = f(\vartheta)$ vary with the parameter V $(V > 0)$, in Fig. 4 we draw the resultant curves for some values of V, viz. $V = 10$, 15 and 20 MeV. The kinetic energy $E_K = 60$ MeV, and $r_0 = 1.2 \cdot 10^{-13}$ cm. The computations have been done for the centre of mass system.

The twisting character of the bunch of curves show resemblance with the curves, as computed by MELKANOFF *et al.* [8]. These authors used a more complicated model for the nuclear potential and examined a higher kinetic energy region $(E_K = (100 \div 150)$ MeV). The best fit value of V to the experimental results is obtained by minimizing the expression

$$(5.1) \quad \sum_i d_i^2 = \sum_i \left\{ \frac{(d\sigma/d\omega)_{\text{exp},i} - (d\sigma/d\omega)_{\text{th},i}}{\Delta(d\sigma/d\omega)_{\text{exp},i}} \right\}^2,$$

where $(d\sigma/d\omega)_{\text{exp}}$ is the average experimental differential cross-section, $(d\sigma/d\omega)_{\text{th}}$ is the average theoretical differential cross-section, obtained by the rule of Simpson, computed for each interval $(i - 1\frac{1}{2}^\circ, i + 1\frac{1}{2}^\circ)$, and $\Delta(d\sigma/d\omega)_{\text{exp}}$ is the experimental standard deviation.

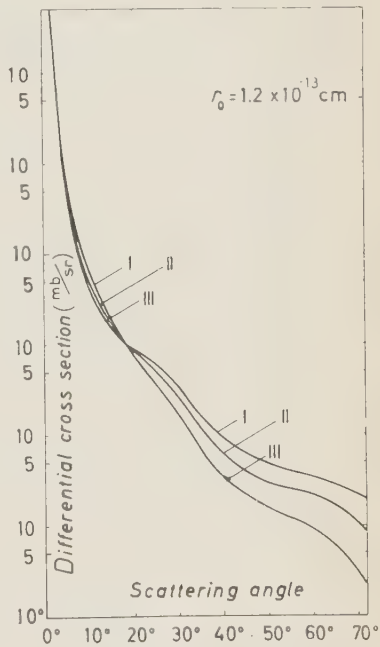

Fig. 4. – $(d\sigma/d\omega) - f(\vartheta)$ curves for the c.m. system. $V = 10$, 15, and 20 MeV, for the curves I, II, and III respectively. $E_K = 60$ MeV, $r_0 = 1.2 \cdot 10^{-13}$ cm.

$\sum_i d_i^2$ has been calculated for several values of V with $E_K = 60$ MeV, using $r_0 = 1.2 \cdot 10^{-13}$ cm in one set of computations, and using $r_0 = 1.4 \cdot 10^{-13}$ cm in another set of computations (see ref. [2]). The best fit of the theoretical curve to the experimental data is found by determining the minimum value of $\sum_i d_i^2$, obtained by interpolation.

We then find $V = (21 \pm 5)$ MeV, for $r_0 = 1.2 \cdot 10^{-13}$ cm. For $r_0 = 1.4 \cdot 10^{-13}$ cm. this minimum value is shifted to a lower value of V, viz. (17 ± 5) MeV. This value is in good agreement with that found by HOANG *et al.* [9]. The errors given are estimated from the statistical spread of the experimental

[8] M. A. MELKANOFF, O. R. PRICE, D. H. STORK and H. K. TICHO: *Phys. Rev.*, **113**, 1303 (1959).

[9] T. F. HOANG, M. F. KAPLON and R. CESTER: *Phys. Rev.*, **107**, 1698 (1957).

cross-sections, and coincide reasonably with the values as computed according to the convention adopted by MELKANOFF *et al.* ([8]). These values of V lie within the range of values found by various groups of investigators using nuclear emulsion, and who examined the K^--meson scattering up to a kinetic energy of ~ 150 MeV ([4,5,8-14]).

* * *

This work is part of the Research Program of the Stichting voor Fundamenteel Onderzoek der Materie (Fundamental Research on Matter, F.O.M.), financially supported by the Netherlands Foundation for Pure Scientific Research (Z.W.O.).

The authors want to express their gratitude to Professor G. W. RATHENAU for his stimulating interest and critical discussions at various stages of the investigation. For the facility of using the ARMAC electronic computer many thanks are due to Professor A. VAN WIJNGAARDEN and his staff in the computing department of the Mathematisch Centrum of Amsterdam. Mrs. W. QUIRING and J. A. ZONNEVELD are thanked for their help in preparing the necessary program. We also want to thank Mrs. A. G. TENNER and F. ARTMANN for their criticisms.

([10]) N. N. BISWAS, L. CECCARELLI-FABRICHESI, M. CECCARELLI, K. GOTTSTEIN, N. C. VARSHNEYA and P. WALOSCHEK: *Nuovo Cimento*, **5**, 123 (1957).

([11]) G. COCCONI, G. PUPPI, G. QUARENI and A. STANGHELLINI: *Nuovo Cimento*, **5**, 172 (1957).

([12]) M. BALDO CEOLIN, M. CRESTI, N. DALLAPORTA, M. GRILLI, L. GUERRIERO, M. MERLIN, G. A. SALANDIN and G. ZAGO: *Nuovo Cimento*, **5**, 402 (1957).

([13]) C. MARCHI, G. QUARENI, A. VIGNUDELLI, G. DASCOLA and S. MORA: *Nuovo Cimento*, **5**, 1790 (1957).

([14]) G. IGO, D. G. RAVENHALL, J. J. TIEMANN, W. W. CHUPP, G. GOLDHABER, S. GOLDHABER, J. E. LANNUTTI and R. M. THALER: *Phys. Rev.*, **109**, 2133 (1958).

RIASSUNTO (*)

Si sono analizzati i dati sui mesoni K^+ in scattering elastico su nuclei complessi in emulsioni nucleari G-5. Si sono considerati solo piccoli angoli nel campo di energie $(40 \div 80)$ MeV. Si è applicata l'analisi degli spostamenti di fase del modello ottico, usando l'approssimazione di W.K.B.J. per la valutazione degli spostamenti di fase. I calcoli sono basati sull'ipotesi che il potenziale di scattering nucleare elastico può essere approssimato con un modello quadrato reale. Si stima che la grandezza sia (21 ± 5) MeV, se nella relazione del raggio nucleare si ha $R = r_0 A^{\frac{1}{3}}$, $r_0 = 1.2 \cdot 10^{-13}$ cm, e (17 ± 5) MeV, se $r_0 = 1.4 \cdot 10^{-13}$ cm.

(*) *Traduzione a cura della Redazione.*

IL NUOVO CIMENTO Vol. XIX, N. 2 16 Gennaio 1961

Scattering of μ-Mesons.

R. L. Sen Gupta, S. Ghosh, A. Acharya, M. M. Biswas and K. K. Roy

Physical Laboratory, Presidence College - Calcutta

(ricevuto il 9 Agosto 1960)

Summary. — The scattering of μ-mesons is investigated by means of a rectangular cloud chamber with copper and lead plates placed alternately inside the chamber. μ-mesons after traversing thick layers of iron and lead absorber placed above and below the chamber are made to stop in 7.6 cm of iron layer by an anticoincidence method. The momenta of the scattered μ-mesons are thus well-defined in the region of $(1.18 \pm .05)$ GeV/c. The observed angular distribution coincides with the point-charge model of the nucleus given by Molière in the case of lead, and in the case of copper the distribution is just above the Molière curve.

1. – Introduction.

For the last few years various theoretical and experimental investigations about μ-meson-nucleon interactions have greatly contributed in determining the nuclear structure and its charge distribution. Several experiments [1-5] involving measurements of scattering of high-energy cosmic ray μ-mesons of different momentum ranges through finite thicknesses of matter have shown that there exists an anomalously large excess of scattering of μ-mesons compared to the expected value, calculated on the basis of the « solid » nucleus theory.

The above observations, however, are in contradiction to the fact that μ-mesons are very weakly coupled to the nucleons. The weak coupling of μ-me-

[1] W. L. Whittemore and R. P. Shutt: *Phys. Rev.*, **88**, 1312 (1952).
[2] E. P. George, J. L. Redding and P. T. Trent: *Proc. Phys. Soc.*, A **66**, 533 (1953).
[3] B. Leontic and A. W. Wolfendale: *Phil. Mag.*, **44**, 1101 (1953).
[4] I. B. McDiarmid: *Phil. Mag.*, **45**, 933 (1954); **46**, 177 (1955).
[5] M. L. T. Kannangara and G. S. Srikantia: *Phil. Mag.*, **44**, 1091 (1953).

sons with nucleons is proved by the existence of μ-mesons at a great depth underground and the absence of direct production of single μ-mesons in accelerator experiments in the laboratory. The electromagnetic character of the μ-meson as « heavy electron » is also established ([6]).

Again HOFSTADTER *et al.* ([7,8]), PIDD, HAMMER and RAKA ([9]) as well as FITCH and RAINWATER ([10]), COOPER and HENLY ([11]) as to their μ-mesonic X-ray experiments, interpreted the results of their experiments on high energy electron scattering in terms of electromagnetic interactions of singly charged particles with finite extension of the nucleus of smaller radius than the value previously accepted. This smaller value of nuclear radius alone is not sufficient to explain the « anomalous » component of the above-mentioned μ-meson scattering experiments, indicating clearly a contradiction between the theories ([12,13]) and the experimental facts.

There has also appeared recently a contradiction between groups of investigators in their experimental findings about the « anomalous » scattering. AMALDI and FIDECARO ([14]) in their experiment on μ-meson scattering in lead and iron observed no « anomalous » scattering. Recently FUKUI, KITAMURA and WATASE ([15]) have reported that in their experiment with delayed coincidence their experimental results do not support the existence of anomalous scattering in the energy region near 1 GeV.

In μ-meson scattering experiments in which comparison between the observed distribution of scattering angles and the expected distribution based on the theories ([12,13]) of electromagnetic scattering is made, beam contamination by nuclear-reacting particles such as π-mesons, protons etc., should be avoided. Again, since the electromagnetic scattering is very sensitive to the energy of the particles scattered, the energy of the particles recorded for analysis must be well defined. So μ-meson scattering experiments with direct measurement of the energy of the particles and with a mono-energetic beam are expected to yield more accurate and reliable results than those making in-

([6]) T. COFFIN, R. L. GARWIN, S. PENMAN, L. M. LEDERMAN and A. M. SACHS: *Phys. Rev.*, **109**, 973 (1958).

([7]) R. HOFSTADTER, H. R. FETCHER and J. A. MCINTYRE: *Phys. Rev.*, **91**, 422 (1953).

([8]) R. HOFSTADTER, H. R. FETCHER and J. A. MCINTYRE: *Phys. Rev.*, **92**, 978 (1953).

([9]) R. W. PIDD, C. L. HAMMER and E. C. RAKA: *Phys. Rev.*, **92**, 436 (1953).

([10]) V. L. FITCH and J. RAINWATER: *Phys. Rev.*, **92**, 789 (1953).

([11]) L. N. COOPER and E. M. HENLY: *Phys. Rev.*, **91**, 480 (1953); **92**, 801 (1953).

([12]) G. MOLIÈRE: *Zeits. f. Naturf.*, **2***a*, 133 (1947); **3***a*, 78 (1948).

([13]) S. OLBERT: *Phys. Rev.*, **87**, 319 (1952).

([14]) E. AMALDI and G. FIDECARO: *Nuovo Cimento*, **7**, 535 (1950).

([15]) S. FUKUI, T. KITAMURA and Y. WATASE: *Phys. Rev.*, **113**, 315 (1959).

direct measurement of the energy of the particles having a spectral distribution of momentum.

In consideration of the above facts we have carried out the present experiment with particular attention to the estimation of the energy of the μ-meson beam, the momentum of the incident beam being (1.18 ± .05) GeV/c.

2. – Experimental arrangement.

The cloud chamber used for the present experiment contains three lead plates and four copper plates, each of thickness 1.27 cm, the lead and copper plates being placed alternately inside it. The effective volume of the chamber is 14 in.×14 in.×5 in. The chamber is triggered by a μ-meson stopped in a layer of iron of thickness 7.6 cm by an arrangement of fourfold coincidence and twofold anticoincidence counter trays as shown schematically in Fig. 1. The use of the twofold anticoincidence is found to avoid completely any possible uncertainty in the stopping of the μ-mesons, which fact has been checked from time to time during the progress of the experiment. An iron absorber 1 m thick is placed above the chamber in order to absorb highly nuclear-interacting components of the incident cosmic-ray beam. Before the μ-meson is stopped it has to traverse an absorber of 43 cm of lead and 38 cm of iron below the chamber, so that the μ-meson has a momentum above 1130 MeV/c. The stopping layer of 7.6 cm of iron is placed between the lowermost coincidence counter tray (C_4) and anticoincidence counter trays, and the mesons recorded in the experiment have momenta lying between 1130 MeV/c and 1230 MeV/c.

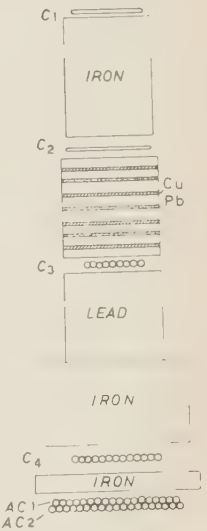

Fig. 1. – Schematic diagram for experimental arrangement.

The maximum angle of acceptance from the centre of the top of the chamber is 12° in the experiment. Measurements of scattering angles are made for the central five plates (3 lead plates and 2 copper plates), the extreme ones being excluded due to distortions of the tracks in the uppermost and the lowermost compartments. Angles are measured by means of a microscope provided with a rotating stage having graduations reading up to .05°.

3. – Results and discussions.

In this experiment 702 traversals in lead plates and 550 traversals in copper plates have been analysed under the conditions stated in the previous section.

In order to calculate the « noise-level » scattering high-energy coincidence tracks (coincidence between 2nd, 3rd and 4th counter trays) have been selected at random. A histogram is plotted with r.m.s. angles of scattering against number of the particles. From the peak value in the distribution of the r.m.s. angles the value of the « noise-level » scattering is calculated by the usual method (1) from the relation

$$\theta^2_{n(\text{most probable})} \approx [(n-1)/n]\sigma^2$$

the notations carrying usual significances. The « noise-level » scattering is found to be 0.808 degree, the values of θ_n and n being 0.7 degree and 5 respectively.

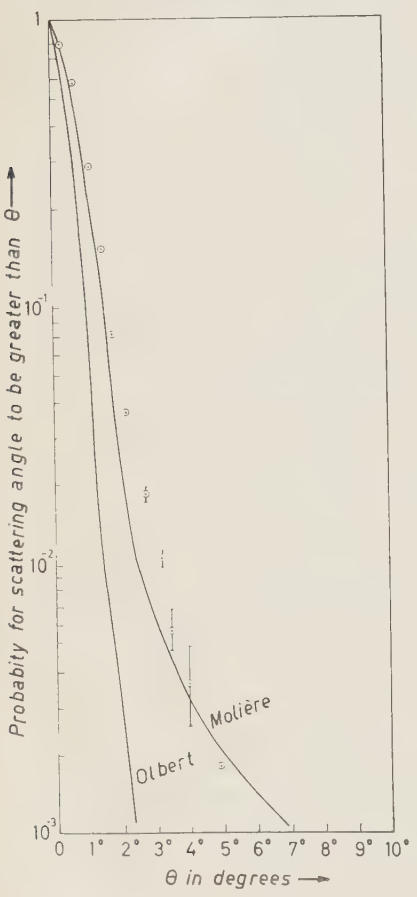

Fig. 2. – Integral scattering distribution for copper.

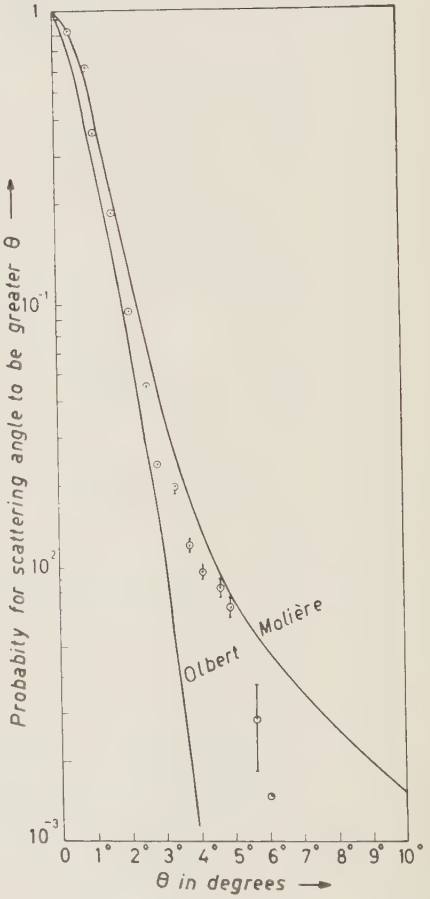

Fig. 3. – Integral scattering distribution for lead.

The distributions of the observed angles of scattering in lead and copper plates are compared with the theoretical expected distributions based on Molière's « point » nucleus and Olbert's « solid » nucleus theories.

The differential distribution $f_M(p\theta)$ for Molière's theory has been corrected for the « noise-level » scattering incurred in the experiment in order to compare directly between the expected and observed distributions. However, the above correction is not applied in the case of Olbert's, the observed distribution being much above Olbert's distribution. The corrected Molière distribution is of the form

$$g_M(p\vartheta_0)\,\mathrm{d}(p\theta_0) = \frac{\mathrm{d}\,(p\vartheta_0)}{(2\pi)^{\frac{1}{2}}\,\sigma}\int_{-\infty}^{+\infty} f_M(p\theta)\,\exp\left|-\frac{[\,(p\theta_0)^2-(p\vartheta)^2\,]}{2\sigma^2}\right|\mathrm{d}(p\theta)\,.$$

The integral distributions of scattering angles were then calculated from the above differential distributions and plotted in Fig. 2 and 3 for copper and lead respectively. The curves show comparison between the observed distributions and the distributions calculated following Molière's and Olbert's theories. The experimental points are plotted by dots with statistical fluctuations.

For both the materials (lead and copper) our results indicate that the observed distributions are reasonably in agreement with that of Molière, at least up to 5°. This fact indicates that the scattering of μ-mesons having an average momentum of 1.18 GeV/c follows Molière's theory of Coulomb scattering for « point » nuclei.

* * *

This work was jointly supported financially by the Government of West Bengal and the Ministry of Scientific Research and Cultural Affairs, Government of India.

RIASSUNTO (*)

Si è analizzato lo scattering dei mesoni μ con una camera a nebbia rettangolare con piastre di rame e piombo poste alternate nell'interno della camera. I mesoni μ dopo aver attraversato grossi spessori di assorbitori di ferro e piombo posti sopra e sotto la camera vengono arrestati in uno spessore di ferro di 7.6 cm col metodo della anticoincidenza. Le quantità di moto dei mesoni μ di scattering sono così ben definite e comprese nella regione di $(1.18 \pm .05)$ GeV/c. La distribuzione angolare osservata nel caso del piombo coincide con il modello a carica puntiforme del nucleo dato da Molière, mentre nel caso del rame la distribuzione è appena al di sopra della curva di Molière.

(*) *Traduzione a cura della Redazione.*

IL NUOVO CIMENTO Vol. XIX, N. 2 16 Gennaio 1961

Bremsstrahlung Spectrum of the 1000 MeV Electronsynchrotron at Frascati.

G. Diambrini

C.N.R.N., Laboratori Nazionali - Frascati

A. S. Figuera (*), B. Rispoli (**) and A. Serra

C.N.R.N., Divisione Elettronica - Roma

(ricevuto il 26 Agosto 1960)

Summary. — The final results of some measurements on angular distribution and on Bremsstrahlung spectrum of the γ-ray beam of the Frascati electronsynchrotron are given. The experimental results of angular distribution for thick target fit with Schiff's theoretical angular distribution. We find, on the contrary, a difference between theory and experiments for thin target and this can be explained by multiple crosses through the target of the accelerated electrons. For the spectrum shape, comparing the experimental results with Bethe and Heitler's theory, we have that for thin target the experimental points are in fair agreement with the theoretical previsions while for thick target we find a difference in the high energy range and we see that this difference can be explained by many different reasons.

1. – Introduction.

In this paper definite results [1] about the bremsstrahlung spectrum of the 1000 MeV Frascati electronsynchrotron by using different targets and collimators are given.

(*) At present: Physics Department, University of Maryland.

(**) Comitato Nazionale per le Ricerche Nucleari and Istituto di Fisica dell'Università di Roma.

(1) The first results were given in *Nuovo Cimento*, **15**, 500 (1960).

The subject of this experiment is to give a contribution to the understanding of the electronsynchrotron beam production mechanism, and to get useful results for research in photoproduction when using photons of an energy near to the upper limit of the spectrum.

Because the spectrum shape of the γ-ray beam depends essentially on the effective target thickness, on the collimation, on the energetic distribution of primary electrons and on possible multiple crossings through the target, it is necessary to determine the effective thickness of the targets in use, and the transmission factors of the collimators. So the angular distribution of the beam intensity for two different thicknesses of target are studied and the results, shown in Section 2, are compared with the theoretical angular distribution.

The experimental apparatus used for the bremsstrahlung spectrum measurements has been described in Section 3.

In Section 4 are given the spectra obtained by using 0.13 and 0.013 r.l. target thickness and, for each one of these, two collimators with acceptance angles of 3.6 and 0.75 mrad respectively.

In order that this paper may be useful to those wishing to measure spectrum with other similar accelerators there are some mathematical explanations in the Appendix.

2. – Beam angular distribution.

The experimental arrangement for the beam angular distribution measurement is shown in Fig. 1, where:

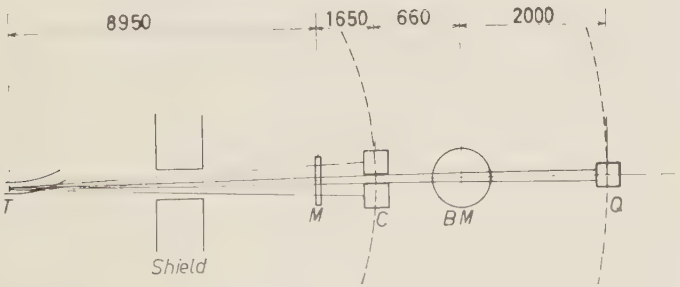

Fig. 1. – Experimental arrangement for angular distribution measurements. (Distances are given in millimeters).

T is the electronsynchrotron tantalum target;

M is an ionization chamber with thin aluminium walls and with electrodes of total thickness of $4.3 \cdot 10^{-4}$ r.l.;

C is a lead collimator (collimators with hole diameters of 5 mm and 2 mm corresponding to angular openings 0.47 and 0.19 mrad respectively, were used);

BM is a « sweep » magnet in the gap of which there is a field of about 15 kG able to sweep aside all charged particles travelling with the beam;

Q is a total absorption chamber of the type described by WILSON [2].

The distance of 2 m between BM and Q ensures that any charged particles travelling with the beam and being deflected by BM, will not impinge upon the chamber Q and affect the ionization measurements. The collimator C and the chamber Q are placed on movable bases which can be moved azimuthally about the centre T.

The chamber M, crossed by the whole beam, has been used in order to be able to refer to the same charge m, the measurements taken at several angles. Charges q collected in Q by the beam portion crossing C, and charges m collected in M, are measured by integrators connected to ionization chambers.

The angular distribution of beam intensity defined by

$$I(\theta) = \frac{q(\theta)}{m},$$

is obtained by moving the collimator C and the chamber Q about the centre T at an angle θ. By following this method, measurements in steps of 0.5 mrad were made with tantalum targets of 0.5 and 0.05 mm in thickness respectively equal to 0.13 and 0.013 r.l. Each measurement has been repeated at least four times.

The measurements with 0.13 r.l. target were made with a 5 mm hole collimator C, *i.e.* with a 0.47 mrad angular opening and by taking as charge unity $m = 1.2 \cdot 10^{-6}$ C.

The experimental results are shown in Fig. 2 together with the theoretical angular distribution, computed by using Schiff's formula [3]

$$\frac{I(\theta)}{I_0} = \frac{Ei(-\theta^2/2\beta x)}{\ln 2\beta x E^2 - C},$$

where Ei is the exponential integral function [4], β is a function depending on the energy E (expressed in units of mc^2) of the electrons striking the target

[2] R. R. WILSON: *Nucl. Instr.*, **1**, 101 (1957).
[3] L. I. SCHIFF: *Phys. Rev.*, **70**, 87 (1946).
[4] E. JANKE and F. EMDE: *Tables of Functions* (New York, 1945).

and on the target material and thickness x (expressed in cm), $C = 0.5772$ is the Euler constant.

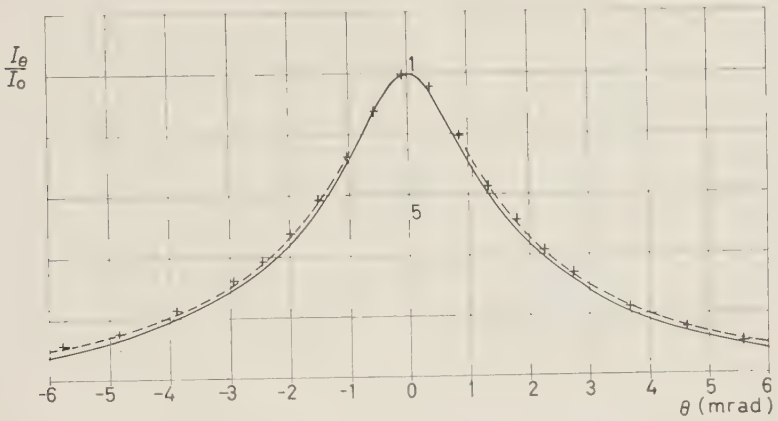

Fig. 2. – Angular distribution. —— Schiff theoretical angular distribution for 0.13 r.l. target; – – – Schiff theoretical angular distribution for 0.156 r.l. target; + experimental points for 0.13 r.l. target.

The continuous curve refers to the 0.5 mm (0.13 r.l.) thick target while the dashed curve was calculated for the 0.6 mm (0.156 r.l.) thick target to take into account that the target is inclined at approxymately 30° to the direction of the electron beam, making the effective target thickness 0.6 mm. So it was confirmed that the thickness contributing to the radiation is in effect the true thickness.

The 0.013 r.l. target measurements were made by using a collimator C having a 2 mm diameter hole *i.e.* a 0.19 mrad angular opening, taking as charge unity $m = 4 \cdot 10^{-7}$ C. The experimental results are shown in Fig. 3 together with the Schiff theoretical distribution, calculated for a 0.05 mm (0.013 r.l.) target thick-

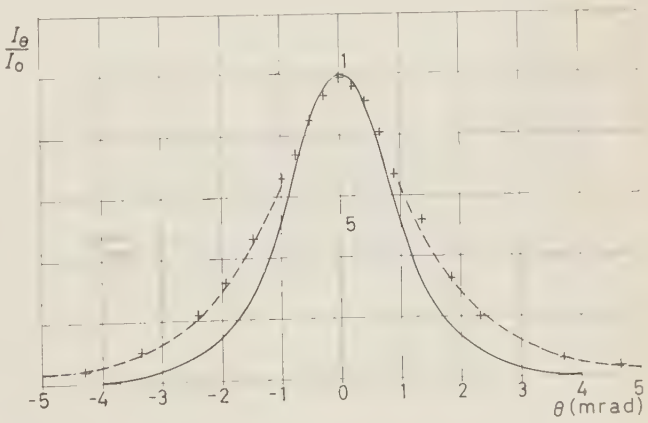

Fig. 3. – Angular distribution. —— Schiff theoretical angular distribution for 0.013 r.l. target; – – – Schiff theoretical angular distribution for 0.039 r.l. target; + experimental points for 0.013 r.l. target.

ness as shown by the continuous curve. It can be seen that there is a discrepancy between theoretical curve and experimental results which fit the theoretical distribution (dashed curve) calculated for a 0.15 mm (0.039 r.l.) target thickness.

It can be deduced then that the target has an effective thickness, contributing to the radiation, greater than the actual thickness.

This phenomenon can be explained qualitatively (5) by examining the effect of multiple crossings of electrons through the target. In fact if we consider only the ionization energy losses, about 100 keV, for each crossing of the target, and as the width of the target is 4.5 mm, electrons can only cross the target three times before attaining a new orbital equilibrium.

This gives the same effect as electrons crossing once a target of three times the actual target thickness.

3. – Experimental apparatus used for the bremsstrahlung spectrum measurements.

The experimental arrangement for the bremsstrahlung spectrum determination is shown in Fig. 4 where:

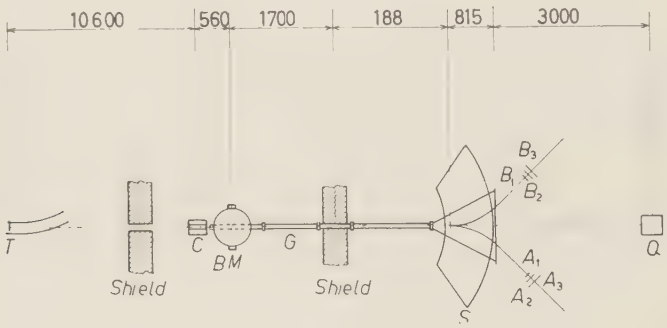

Fig. 4. – Experimental arrangement for bremsstrahlung spectrum measurements. (Distances are given in millimeters).

T is the tantalum target (with a thickness: $s_1 = 0.13$ or $s_2 = 0.013$ r.l.) of the electronsynchrotron;

C is a lead collimator 30 cm in lenght. Two collimators were used, one having a central hole diameter of 38 mm giving an accepted angle of 3.6 mrad, and the other having a central hole diameter of 8 mm, giving an acceptance angle of 0.75 mrad;

(5) A correct quantitative explanation requires the study of very low energy photon losses.

BM is the « sweep » magnet, in the gap of which there is a field of 15 kG;

G is a tube evacuated to a pressure of 0.03 mm Hg which is connected at one end to the chamber of the spectrometer;

S is an electron pair spectrometer ([6]);

R is the spectrometer radiator, made of an aluminium disc 6 cm in diameter and $1.08 \cdot 10^{-3}$ r.l. thick;

Q is a monitor formed by a total absorption quantameter ([2]);

A_1, A_2, A_3 and B_1, B_2, B_3 are two scintillation counter telescopes placed so that they can detect only the symmetric pairs of electrons.

The beam, collimated by C, enters the tube G after being « cleaned » by the sweep magnet, then it is completely absorbed by the monitor Q after crossing the radiator R in which the electron pairs are produced.

The input of the vacuum tube G and the output end of the vacuum chamber of the spectrometer are sealed with 0.2 mm thick mylar foil.

The counter telescopes detect the symmetric pairs having an energy E function of field B in the spectrometer gap. The energy K of the γ-ray producing pair is given by $K = 2E$ neglecting the rest mass of the two electrons.

The energy selection is obtained by changing the magnetic field value in the spectrometer gap from 0.5 to 10.5 kG. In this manner the two counter telescopes, that are in a fixed position, can detect the electron symmetric pairs in the energy range from 25 MeV to 525 MeV. So it is possible to examine the full spectrum of γ-rays.

In order to determine the position of the telescopes, the electron trajectories were determined by means of an electronic computer and controlled experimentally by the floating wire technique.

The spectrometer magnet current supply had a stability of $\pm$ 0.1 per cent. The electron trajectories were determined with a precision of $\pm$ 0.3 per cent The spectrometer is previously calibrated by determining the behaviour of the field intensity as function of the magnet current. For any value of the magnetic field there is a determined electron energy for the electrons crossing the two telescopes. So it is possible to express the electron energy as a function of the magnet current.

The current is measured with a precision of 0.1 per cent by a comparison method using a precision potentiometer and a standard cell.

As the width of the first counter of each telescope is 18 mm, by the spectrometer optics ([6]) the percentage interval of the energy accepted by the telescopes $\Delta E / E = 2.7$ per cent is obtained. The successive counter dimensions of each

([6]) G. Bologna, G. Diambrini, A. S. Figuera, U. Pellegrini, B. Rispoli, A. Serra and R. Toschi: Internal note no. 17 of Laboratori Nazionali di Frascati (Sept. 28, 1959) to be published in *Nucl. Instr. and Methods*.

telescope were increased in order to avoid counting losses due to the electron scattering. The first scintillator height is 54 mm. All the scintillators are of 1 mm plastic.

Fig. 5 shows the block diagram of the electronic apparatus used for the bremsstrahlung spectrum measurements.

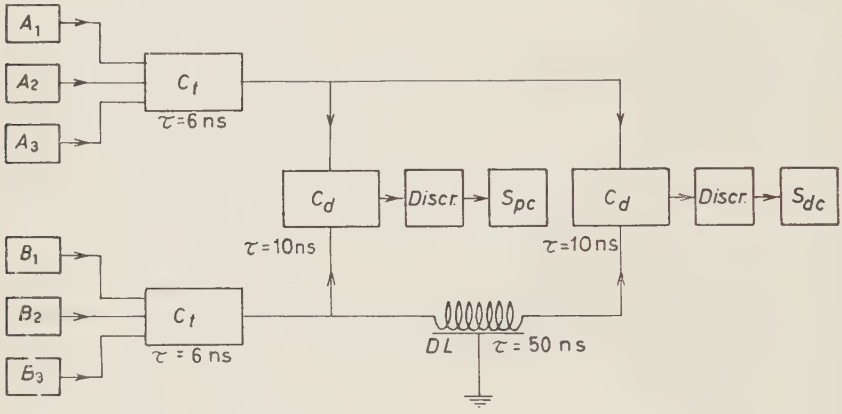

Fig. 5. – Electronics block diagram.

The photomultiplier anodes of the three counters of each telescope are connected to a three-fold coincidence circuit C_t with a resolution time of $\tau = 6$ ns. The outputs of the two three-fold coincidences C_t go to two two-fold coincidence circuits C_d with $\tau = 10$ ns directly to the first, and to the second through a delay DL of 50 ns.

The two-fold coincidences are followed by a discriminator and a scaler. It is possible to record simultaneously the prompt S_{pc} and delayed coincidence S_{dc}.

Knowing the delayed coincidence it is possible to calculate true coincidences due to symmetric pairs produced in the aluminium radiator by making the difference $S = S_{pc} - S_{dc} - B$, where $B = B_p - B_d$ is the difference between the prompt and delayed coincidences when the spectrometer radiator R is removed.

Measurements of the difference S as a function of the electron energy were made by varying the magnet current and by referring each measurement to the same charge $q = 3 \cdot 10^{-6}$ C collected in the monitor Q which corresponds to about $1.4 \cdot 10^{10}$ equivalent quanta crossing the radiator R. The measurements for each energy were repeated several times in order to have a statistical error of less than 1 per cent.

This was possible without prolonging the measurement time in view of the electronsynchrotron's high beam intensity. Even when a collimator of 0.75 mrad

is used an average intensity of $6 \cdot 10^9$ equivalent quanta per minute is obtained after the collimator.

The γ-beam intensity was maintained, during the measurement, at a level (below the maximum in the case of a 3.6 mrad collimator) so that also for the low energy range of the spectrum, the ratio $\eta = S_{dc}/S$ was less than 5 per cent. In fact because of the high resolution power of the coincidence circuits the maximum contribution to chance coincidences is given by the coincidences due to two asymmetric pairs, each one of these having an electron of energy equal to E.

The ratio between spurious coincidences and true coincidences is given by

$$\eta = 8\tau \frac{Y}{T}\left(1 - \frac{E}{K_{max}}\right)^2,$$

where τ is the resolution time of the coincidence circuit, T is the length of the pulse of the electrosynchrotron γ-ray beam, K_{max} is the maximum energy of photons, E is the electron energy and

$$Y = \Phi_{tot} s N_e \frac{A \varrho X}{P},$$

where: Φ_{tot} is total cross section for the production of pairs; s is the thickness in r.l. of the electronsynchrotron target; N_e is the number of primary electrons striking the target; A is the Avogadro number; ϱ is the density (g/cm^3) of the spectrometer radiator; X is the spectrometer radiator thickness (cm); P is the spectrometer radiator atomic weight.

Then it can be seen that η is maximum when the energy is low and it is directly proportional to the intensity $N_e s/T$ of the γ-ray beam.

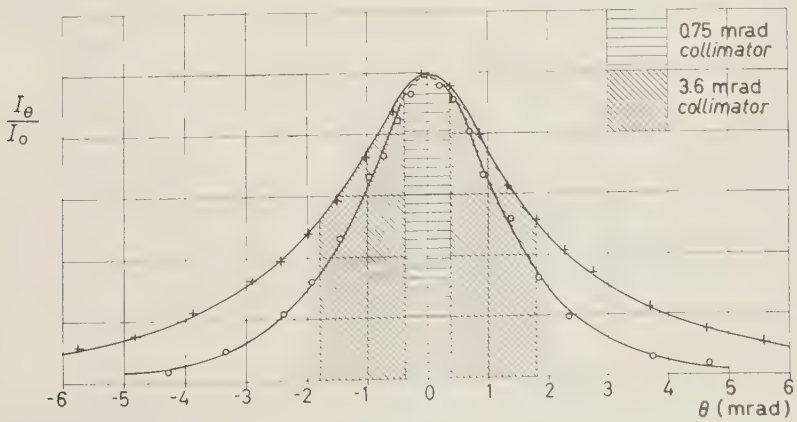

Fig. 6. – Diagram of the transmission factors of the collimators.

The 8 mm collimator (angular opening 0.75 mrad) has a transmission factor of 1.3 per cent and 3.2 per cent using respectively 0.13 and 0.013 r.l. targets.

The 38 mm collimator (angular opening 3.6 mrad) has transmission factors of 20 per cent with the 0.13 target and of 42.5 per cent with the 0.013 r.l. target.

The transmission factors defined by the ratio between the transmitted intensity and the incident intensity were calculated by the experimental angular distributions shown in Fig. 6.

4. – Experimental results of the bremsstrahlung spectrum measurements.

Let us define now the function « intensity of the bremsstrahlung » $I(u)$ given by

$$I(u) = KN(K)\frac{q^* E_0}{q}, \tag{1}$$

where $u = K/E_0$, $E_0 = 1000$ MeV maximum energy of primary electrons and $N(K)$ is the number of photons having energy $K = uE_0$.

Monitor Q gives an integral information of the energy transmitted by the beam by collecting the electric charge

$$q = q^* \int_0^{E_0} K N(K)\,\mathrm{d}K ,$$

corresponding to q/q^* MeV of irradiated energy, $q^* = 2.07 \cdot 10^{-19}$ C/MeV being a characteristic constant of the instrument.

The number $S = S_{pc} - S_{dc} - B$ of symmetric pairs of electrons is given by

$$S = N(K)\Delta K r \left[\sigma_p\left(K, \frac{1}{2}\right) + \sigma_t\left(K, \frac{1}{2}\right)\right]\frac{\Delta E}{K} ,$$

where: $\sigma_p(K, \frac{1}{2})$ and $\sigma_t(K, \frac{1}{2})$ are respectively the cross-sections of the production of symmetric pairs in the field of the nucleus corrected for the Born approximation ([7,8]) and in the field of the electron ([9]); r is the number of atoms per cm² of spectrometer radiator; $\Delta E = \Delta K/2$ is the energy spread of electrons accepted by the scintillators.

([7]) H. Bethe and W. Heitler: *Proc. Roy. Soc.*, A **146**, 83 (1934).
([8]) H. Davies, H. A. Bethe and L. C. Maximon: *Phys. Rev.*, **93**, 788 (1934).
([9]) J. A. Wheeler and W. E. Lamb: *Phys. Rev.*, **55**, 858 (1939); **101**, 1836 (1956).

From the expressions (1) and (2) we can obtain

$$I(u) = \frac{2q^* E_0}{rq} \frac{S}{[\sigma_p(K, \tfrac{1}{2}) + \sigma_t(K, \tfrac{1}{2})](\Delta K/K)^2}.$$

Particularly for two selected energies $K = K_0$ and $K = K_n$ we have

$$\frac{\Delta K_0}{K_0} = \frac{\Delta K_n}{K_n}, \qquad q_0 = q_n, \qquad q_0^* = q_n^*.$$

so that

$$\frac{I_n}{I_0} = \frac{S_n}{S_0} \frac{\sigma_p(K_0, \tfrac{1}{2}) + \sigma_t(K_0, \tfrac{1}{2})}{\sigma_p(K_n, \tfrac{1}{2}) + \sigma_t(K_n, \tfrac{1}{2})}.$$

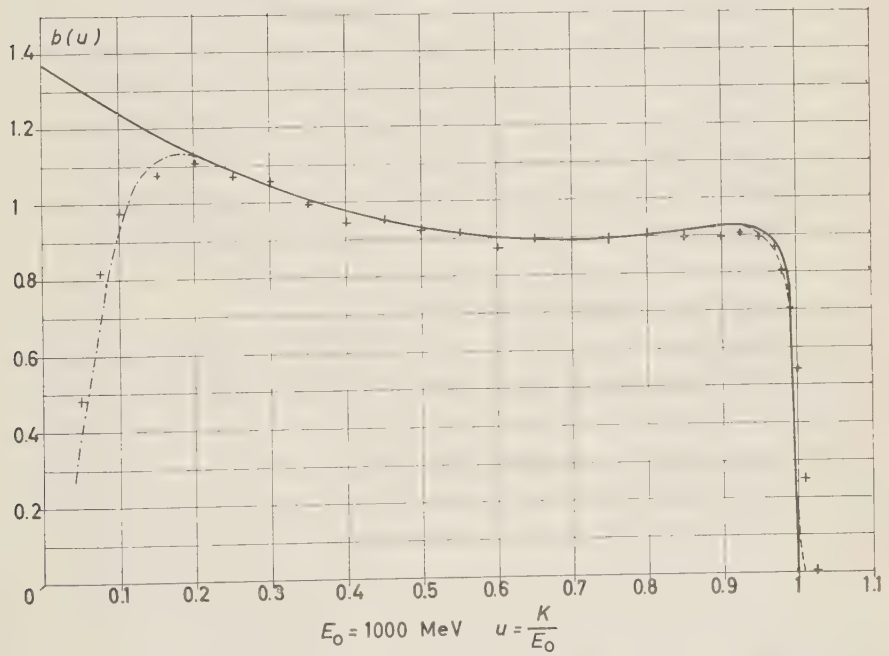

Fig. 7. Bremsstrahlung spectrum of 0.013 r.l. target and 0.75 mrad collimator. Theoretical (BETHE and SALPETER); - - - - theoretical, corrected for the scattering in the radiator and for the vertical dimension of the scintillators; — theoretical, corrected for the resolution function of the detecting apparatus.

In Fig. 7, 8, 9 are shown the experimental results of the ratio I_n/I_0 with the statistical error (less than 1 per cent) as function of $u = K/E_0$, by assuming $K_0 = 700$ MeV. These experimental results were compared with the theo-

retical behaviour (continuous curve) given by the expression:

$$b(u) = \frac{K(\sigma_n + \sigma_{el})}{\int_0^1 K(\sigma_n + \sigma_{el})\,\mathrm{d}u},$$

which is the value of the intensity of the bremsstrahlung normalized at the unit area. In this expression σ_n and σ_{el} are respectively the cross-sections for bremsstrahlung in the field of the nucleus corrected for the Born approximation ([7,10]) and in the field of the electron ([9]).

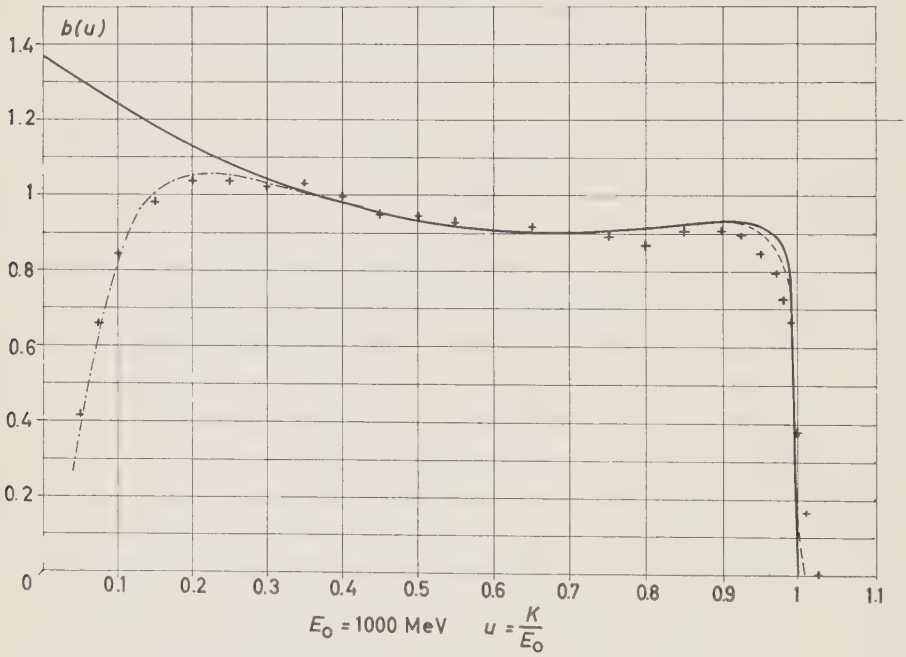

Fig. 8. – Bremsstrahlung spectrum of 0.013 r.l. target and 3.6 mrad collimator. —— Theoretical (BETHE and SALPETER); –·–·– theoretical, corrected for the scattering in the radiator and for the vertical dimension of the scintillators; – – – theoretical, corrected for the resolution function of the detecting apparatus.

The dashed curve that departs from the continuous curve in the low energy range of photons was obtained by subtracting from the theoretical curve the counting losses due to the scattering of electrons in the radiator and to the vertical dimension of the scintillators (see Appendix).

([10]) H. OLSEN: *Phys. Rev.*, **99**, 1335 (1955).

The dashed curve shown in the range of the high energy spectrum, is obtained by averaging the theoretical curve on the triangular resolution of the detecting apparatus.

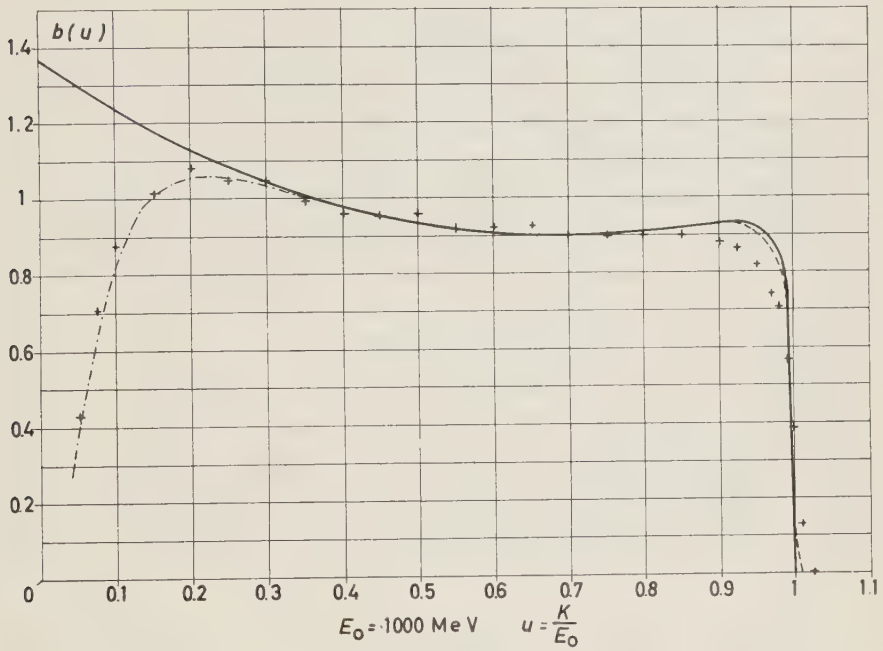

Fig. 9. – Bremsstrahlung spectrum of 0.13 r.l. target and 3.6 mrad collimator. —— Theoretical (BETHE and SALPETER); –·–·– theoretical, corrected for the scattering in the radiator and for the vertical dimension of the scintillators; –·–·– theoretical, corrected for the resolution function of the detecting apparatus.

One can see how the experimental results fit within the limits of 2 per cent with the theoretical curve in Fig. 7 corresponding to the 0.013 r.l. target and to a collimator with a transmission factor of 3.2 per cent while they do not fit when a collimator with a transmission factor of 42.5 per cent is used (Fig. 8), and they move even further away when a 0.13 r.l. target with a collimator transmission factor of 20 per cent are used (Fig. 9). Another series of measurements made with a 0.13 target and a transmission factor of 1.3 per cent (not shown) are equal (within the experimental tolerance) to the results shown in Fig. 9.

This discrepancy in the high energies range is principally due to:

a) the electrons crossing target may irradiate a high energy photon after irradiating one ore more of very low energy because of the target thickness;

b) the effects of collimation together with scattering in the target;

c) the energy fluctuations of the electrons striking the target.

The effect of the target thickness can easily be seen by comparing the experimental results, for $u > 0.8$ shown in Fig. 7 and 8 at the thin target with results of Fig. 9 at the thick target.

For the collimator effects, it can be said that if the beam is collimated there are no accepted large angle photons generated which are generally obtained by electrons that penetrate more deeply before irradiating (the natural emission angle of photons is ~ 0.5 mrad). In fact by the examination of the data obtained using the same thin target but different collimators, it is possible to see (Fig. 7 and 8) that there is a loss of high energy photons using collimators with larger acceptance angles; however this effect is negligible below a certain value of the acceptance angle of the collimator because of the shape of the function I_0/I_0 shown in Fig. 6.

The effect of point *c*) contributes less than the others to the deformation of the spectrum.

In conclusion we can see from Fig. 7 that the energy spread of electron-synchrontron electrons produces deviations in the high energy range of the spectrum less than 2 per cent.

Appendix

Calculation for determining the counting losses due to vertical deviation scattering of electrons in the radiator of the spectrometer.

If we consider a projection in a vertical plane passing through the axis of the γ-ray beam, the angular distribution of the electrons which have crossed a radiator of thickness δ is:

$$P(\theta)\,\mathrm{d}\theta = \frac{1}{\sqrt{2\pi}\theta_M} \exp\left[-\frac{1}{2}\left(\frac{\theta}{\theta_M}\right)^2\right]\mathrm{d}\theta\,.$$

where $\theta_M(16\,E)\sqrt{\delta}$ and $P(\theta)\,\mathrm{d}\theta$ is the probability that the direction of an electron is between θ and $\theta + \mathrm{d}\theta$.

The probability for a positive electron to be generated in $\mathrm{d}\theta^+$ and for negative electron in $\mathrm{d}\theta^-$ simultaneously is then:

$$P(\theta^+, \theta^-)\,\mathrm{d}\theta^+\,\mathrm{d}\theta^- = \frac{1}{2\pi\theta_M^+\theta_M^-} \exp\left[-\frac{1}{2}\left(\frac{\theta^+}{\theta_M^+}\right)^2\right] \exp\left[-\frac{1}{2}\left(\frac{\theta^-}{\theta_M^-}\right)^2\right]\mathrm{d}\theta^+\,\mathrm{d}\theta^-,$$

If the electrons of a pair are detected by two detectors $2\,h$ in height placed at a distance s from the radiator (measured along the trajectory), we can write

the probability $I(\delta, z)$ of detecting an electron pair that has been generated at a point of vertical co-ordinate z (the origin of the co-ordinate is at the center of the radiator) and has passed through a thickness δ as:

$$I(\delta, z) = \frac{1}{2\pi\theta_M^+\theta_M^-}\int_{\theta_1^+}^{\theta_2^+}\exp\left[-\frac{1}{2}\left(\frac{\theta^+}{\theta_M^+}\right)^2\right]\mathrm{d}\theta\int_{\theta_1^-}^{\theta_2^-}\exp\left[-\frac{1}{2}\left(\frac{\theta^-}{\theta_M^-}\right)^2\right]\mathrm{d}\theta\ ,$$

θ_1^+, θ_1^-, θ_2^+, θ_2^- are the limit angles (functions of h and z) accepted by the detectors for electron pairs generated at a point of the radiator of co-ordinate z.

For the probability of detecting an electron pair emitted from an arbitrary point between 0 and z_0, which has to pass through the thickness δ of the radiator, we have:

$$W(\delta) = \frac{\int_0^{z_0} N(z)\, I(\delta, z)\,\mathrm{d}z}{\int_0^{z_0} N(z)\,\mathrm{d}z}\ . \tag{A.1}$$

where $N(z)$ is the probability that the pairs are generated at the height z.

We consider $N(z) = \text{const}$ because in the first approximation the intensity distribution of the γ-ray beam on the radiator surface is constant. Let us neglect successive integration on the thickness, because of the assumption that all electrons do pass through the thickness $\delta_0/2$ (in our case we have $\delta_0 = 1.08\cdot10^{-3}$ r.l.).

By these simplifications we may express the relation (A.1) by:

$$W\left(\frac{\delta_0}{2}\right) = \frac{1}{z_0}\int_0^{z_0} I\left(\frac{\delta_0}{2}, z\right)\mathrm{d}z\ .$$

We can resolve graphically this integral.

Considering the symmetric pairs only we have

$$E^+ = E^- = E; \qquad \theta_M^+ = \theta_M^- = \theta_M = \frac{16}{E}\sqrt{\frac{\delta_0}{2}}; \qquad \frac{\theta^+}{\theta_M^+} = \frac{\theta^-}{\theta_M^-} = t\ ,$$

$$\theta_1^- = \theta_1^+ = \theta_1; \qquad \theta_2^- = \theta_2^+ = \theta_2; \qquad x_1 = \frac{\theta_1}{\theta_M}; \qquad x_2 = \frac{\theta_2}{\theta_M}\ .$$

Then:

$$I\left(\frac{\delta_0}{2}, z\right) = \frac{1}{\sqrt{2\pi}}\int_{x_1}^{x_2}\exp\left[-\frac{t^2}{2}\right]\mathrm{d}t\ ,$$

that is a tabulated integral.

Integrating the equation by KERST and SERBER ([11]), we can obtain the expression of the limit angles as a function of the z co-ordinate and of height $2h$ of the detectors ([6]). We have:

$$\theta_{1,2} = \frac{1}{V_{12}} [\pm h - V_{11} z] .$$

In this equation V_{11} is the linear vertical enlargement, that is the ratio between the arrival height at the detector and the departure height from the radiator of an electron which has at the beginning a zero angle with the spectrometer axis. The quantity V_{12} is the ratio between the arrival height at the detector and the departure angle at the radiator projected on the vertical plane passing through the spectrometer axis, of an electron that leaves the centre of the radiator.

The quantities V_{11}, V_{12} were determined by using the floating wire technique. We obtain the values:

$$\theta_{1,2} = [\pm 11.61 - 0.30 \cdot z] \text{ mrad} .$$

Then for each value of z we have the two integration limits for the integral: $I(\delta_0/2, z)$.

([11]) D. W. KERST and R. SERBER: *Phys. Rev.*, **60**, 53 (1941).

RIASSUNTO

Vengono dati i risultati finali di una serie di misure sulla distribuzione angolare e sullo spettro di bremsstrahlung dell'elettrosincrotrone di Frascati. I risultati sperimentali di distribuzione angolare per un convertitore spesso coincidono con la distribuzione teorica di Schiff mentre per un convertitore sottile si ha una discrepanza che può essere spiegata come effetto di attraversamenti multipli del convertitore del sincrotrone da parte degli elettroni accelerati. Per la forma dello spettro, dal confronto dei dati sperimentali con l'andamento previsto da Bethe e Heitler si ha che per convertitore sottile l'andamento sperimentale coincide abbastanza bene con l'andamento teorico mentre con convertitore spesso si nota una discrepanza nella regione ad alta energia, discrepanza che si vede può essere dovuta a diverse cause.

IL NUOVO CIMENTO Vol. XIX, N. 2 16 Gennaio 1961

Direct Pair Production by High Energy Muons (*).

J. F. Gaebler, W. E. Hazen and A. Z. Hendel

The University of Michigan - Ann Arbor, Mich.

(ricevuto il 27 Agosto 1960)

Summary. — A multiplate cloud chamber was operated 1 032 *ft* underground to study electromagnetic interactions of fast cosmic ray muons. 222 electron showers were observed. A histogram was obtained for transferred energies from 30 to 3 000 MeV. The showers are primarily due to direct pair production and knock-on processes. The results indicate that there is agreement with knock-on theory but that the direct pair production cross section is about $\frac{1}{2}$ that predicted by the Murota-Ueda-Tanaka theory.

1. – Introduction.

When a charged particle passes through matter, electron showers are produced by three types of electromagnetic interactions: the knock-on process, bremsstrahlung, and direct pair production. The first two are believed to be well understood since there is good agreement between theory and experimental results. As for pair production, recent theoretical papers [1,2] have eliminated some of the earlier disagreement between theories. Most of the experiments on direct pair production have been made with electron primaries in nuclear emulsions. Muon primaries have several advantages: For electron primaries, bremsstrahlung is the dominant process and bremsstrahlung followed by con-

(*) Assisted by a grant from the Horace H. Rackham School of Graduate Studies of The University of Michigan and the joint program of the Office of Naval Research and the Atomic Energy Commission.

(1) M. M. Block, D. T. King and W. W. Wada: *Phys. Rev.*, **96**, 1627 (1954).

(2) T. Murota, A. Ueda and H. Tanaka: *Progr. Theor. Phys.*, **16**, 482 (1956).

version of the photon cannot easily be distinguished from a direct pair. For muon primaries this difficulty does not exist since bramsstrahlung is negligible. For high energy muons, pair production also dominates knock-on processes. Furthermore, some of the approximations introduced in the theory of direct pair production are believed to be better justified for muon primaries, which are therefore well suited to compare theory and experiment. ROE and OZAKI [3] have done the only experiment with muon primaries in a cloud chamber. Their paper gives an excellent recent review of both pair-production theory and experiments.

In the present experiment, electron showers produced by the high-energy muon component of cosmic rays underground were observed and interpreted in terms of electromagnetic interactions of muons.

2. – Experiment.

A cloud chamber with a sensitive volume of $(25 \times 80 \times 60)$ cm was set up in a salt mine 1032 ft. below the surface of the ground. The chamber contained twelve 1/8 in. lead plates, each with two .02 in. aluminum plates for better light reflection. It was triggered by coincidence of Geiger-Muller counter trays above and below the chamber. Thus most of the pictures show single energetic particles traversing the chamber. The pictures were scanned for electron showers produced by these particles.

In order to be taken into account, a picture had to contain one penetrating particle, distinctly visible in all 13 intervals in both stereoscopic views. Pictures with more than one penetrating particle entering the chamber were discarded, as it was assumed that these particles were produced in a nuclear interaction and were therefore not muons. However, a particle entering the chamber accompanied by what appeared to be a low-energy knock-on electron produced in the roof of the chamber was allowed. Pictures in which the penetrating particle missed the defining counters were also discarded. 2329 pictures were thus selected. Showers of three or more tracks produced in one of the first 8 plates were recorded as events. There were 222 such events. The number of tracks of each event in each interval between plates was recorded. Tracks at an angle larger than 60° with the primary were not recorded, nor were apparently « reflected » (back scattered) electrons. Sometimes the number of tracks had to be estimated from ionization, especially in dense showers and in the first intervals of an energetic shower, where the opening angle is too small for a clear separation of the tracks. As approximately 10 % of the pictures have events, some pictures should contain 2 or more

[3] B. P. ROE and S. OZAKI: *Phys. Rev.*, **116**, 1022 (1959).

events. Only one such double event was recognized, since two showers will sometimes not be clearly separated. It was therefore necessary to make the following correction: To the number of events of a given number N of tracks, we add a correction for unresolved coincidence of a shower of N tracks with another shower and we subtract the expected coincidences of 2 smaller showers that add up to N tracks. This correction increases the number of events by 5 %.

3. – Energy of the showers.

In order to compare the results with theory it is necessary to find the number of events as a function of the energy of the showers. This will be done in two steps: 1) an energy will be associated with each event, and 2) the number of events in a chosen energy interval will be determined.

Wilson's Monte Carlo calculations [4] provide a good estimate of the average number of tracks produced by a shower of given energy in a cloud chamber. To apply Wilson's curves the following features were taken into account.

a) Although we reject showers starting in the bottom four plates, about 30 % of the showers are not completely contained in the chamber, part of their energy being dissipated below the last visible interval. Wilson's shower curves were then cut-off at the last interval.

b) The number of tracks is only given in Wilson's paper for photon-initiated showers and for electron-initiated showers. Part of our showers are produced by knock-on electrons, others by electron pairs, but for any particular shower there is no unambiguous distinction between the two processes. However, most knock-on showers have only one track below the first plate whereas most pair showers have two or more tracks (see Section 5). This was taken into account and the effect of the remaining uncertainty is small. A further distinction was made between photon-initiated showers and those produced by direct pairs: at higher energies, theory [1,2] predicts a less equal division of energy between the two electrons for direct pairs than for photons.

c) The energy is a function of the amount of material traversed per plate. This was calculated to be the thickness of the plate plus 10 % to account for inclined electron tracks.

Since an energy has now been assigned to each shower, we can construct a histogram of the number of events *vs.* assigned energies. However, there is not a unique correspondence between number of tracks and energy. In order

[4] R. R. Wilson: *Phys. Rev.*, **86**, 261 (1952).

to find the corresponding correction, the distribution of track numbers *vs.* energy was found from a sheaf of Wilson's history graphs ([5]). This distribution is symmetrical, it varies little with energy, and it can be approximated by a Gaussian distribution with an average standard deviation of 21 %. This deviation folded into the shower energy spectrum leads to a correction of −2%.

Logarithmic energy intervals of $E_0 \pm 21$ % were chosen for the display of the data in order to facilitate visualization of possible uncertainties. Fig. 1 gives the histogram of the number of showers *vs.* energy of the shower. The error flags are standard deviations of the statistical uncertainties. The theoretical curves in Fig. 1 will be discussed in the next paragraph.

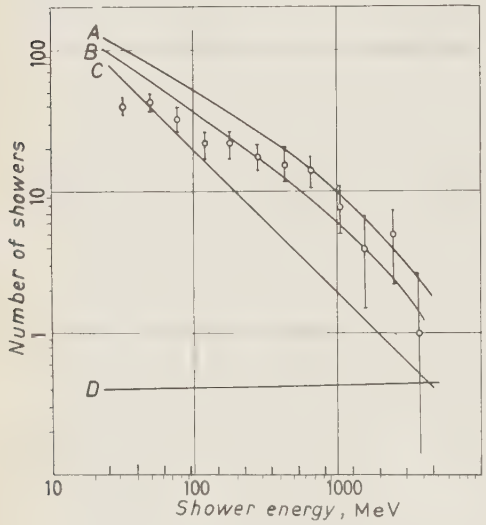

Fig. 1. – Number of showers *vs.* shower energy. Observed and predicted numbers of showers are compared for logarithmic energy intervals indicated by the vertical lines at the bottom of the figure. *A*, total predicted number of events; *C*, predicted number of knock-on events; *D*, predicted number of bremsstrahlung events; *B*, total predicted number of events, assuming only ½ the Murota cross-section for direct pair production as used in curve *A*. The error flags on the experimental points are statistical standard deviations.

4. – Theory.

Equations for both bremsstrahlung and knock-on probabilities are given in Rossi's book ([6]). These probabilities are largely independent of the energy of the primary. Murota *et al.* ([2,7]) derived an equation for the direct pair production cross-section and Roe ([8]) evaluated and integrated this equation. Since this cross-section is a function of the energy of the primary, it is necessary to take into account the energy spectrum of the muons in our experiment. This spectrum was calculated from depth-intensity measurements for depths

([5]) R. R. Wilson: private communication.
([6]) B. Rossi: *High Energy Particles* (New York, 1952).
([7]) T. Murota and A. Ueda: *Progr. Theor. Phys.*, **16**, 497 (1957).
([8]) B. P. Roe: *Thesis* (Cornell University, 1959).

greater than that of the mine and the corresponding range-energy relation. BARRETT *et al.* (9) measured the muon intensity at a depth of 1574 m.w.e. Their paper also summarizes depth-intensity data and furthermore gives an approximate equation for range *vs.* energy for fast mesons. The resulting integral energy spectrum for the present experiment is given in Fig. 2. With this spectrum folded into Murota's theory, the expected number of pairs in chosen logarithmic energy intervals was calculated (*).

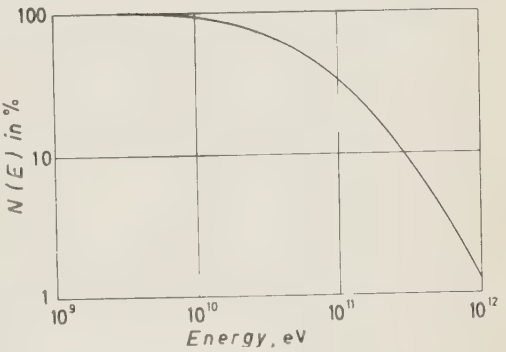

Fig. 2. – Integral energy spectrum at 860 m w.e. below the top of the atmosphere. Calculated from intensity-depth data and range-energy relations.

Fig. 1 shows the calculated number of pairs, knock-on and bremsstrahlung events as a function of the shower energy. Curve *A* gives the total number of events, curve *C* and *D*, predicted knock-on and bremsstrahlung events, respectively. It can also be seen from this figure that pair production should be the dominant process at our energies.

The following correction is included in Fig. 1. Inclined tracks traverse more material and also have a larger average energy. HAZEN and RANDALL (10) measured the angular distribution of muons at the site of the present experiment. This distribution folded into the geometry of our apparatus increases the expected cross-section by about 6 %.

5. – Results.

Fig. 1 shows that the experimental results are consistently below the expected values. In order to find out whether the discrepancy is due to knock-on events or pairs (or both) we consider the number of tracks below the plate in which a shower originates. Wilson's charts were used to estimate the probability of one track below the first plate or two or more tracks. The results are given in Table I.

(9) P. H. BARRETT, L. M. BOLLINGER, G. COCCONI, Y. EISENBERG and K. GREISEN: *Rev. Mod. Phys.*, **24**, 133 (1952).

(*) The same predicted number of pairs would be produced by monoenergetic muon primaries of about 80 GeV This energy varies slightly with the energy of the pairs. It is 70 GeV for 100 MeV pair energy and 90 GeV at 1000 MeV.

(10) W. E. HAZEN and C. A. RANDALL: *Nuovo Cimento*, **8**, 878 (1958).

TABLE I.

Shower energy	MeV	50	100	200	300
Pairs with only 1 track below 1st plate	%	38±9	24±7	4±3	8±4
Single electrons with 2 or more tracks	%	0	8±4	—	4±3

For the knock-on process, there is almost always only one track in the first interval. The thickness of our plates is ~ 0.6 radiation lengths and the probability of multiplication of an electron is small for all energies considered. Low energy pairs, on the other hand, sometimes lose one electron within the first plate. Taking into account the probabilities of Table I, the numbers of predicted showers starting with one track and two or more tracks were calculated and are compared with experimental data in Fig. 3. Fig. 3*a* depends almost entirely on the number of knock-on events and there is agreement with predicted values. Fig. 3*b* shows that the number of showers with two or more tracks below the first plate is considerably smaller than predicted. If we assume that the calcu-

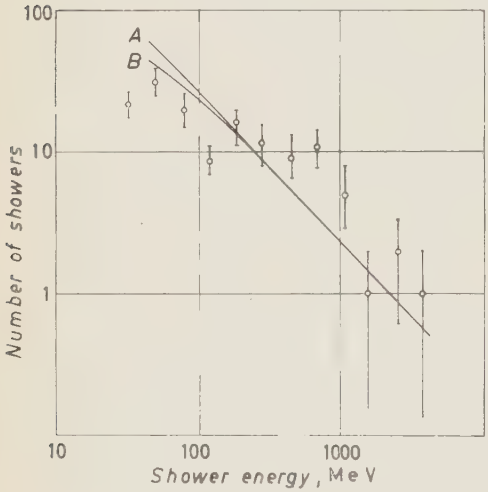

Fig. 3*a*. – Number of showers with one track below the first plate *vs.* shower energy. Curve *A* was calculated from pair production and knock-on theories and from Wilson's charts. Curve *B* was calculated assuming that the number of direct pairs is ½ that predicted. The error flags on the experimental points are statistical standard devations.

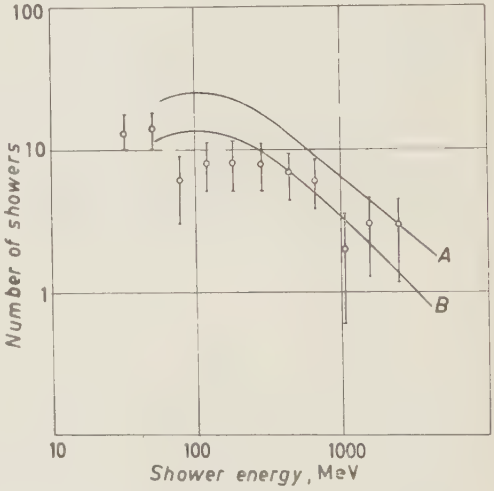

Fig. 3*b*. – Number of showers with two or more tracks below the first plate *vs.* shower energy. Curve *A* was calculated from pair production and knock-on theories and from Wilson's charts. Curve *B* was calculated assuming that the number of direct pairs is ½ that predicted.

lated number of knock-on events agrees with our data and that the number of direct pairs is at all energies $\frac{1}{2}$ that predicted, we get good agreement with experimental data both for the total number of events (curve B in Fig. 1) and for the number of tracks below the first plate (curves B in Fig. 3*a* and *b*).

ROE and OZAKI [3] find a similar ratio between observed and predicted numbers of direct pairs.

6. – Discussion of results.

It is necessary to examine and evaluate systematic errors before we can draw any conclusions. In scanning, there are several possible sources of error. Let us first consider the number of events. We have already taken into account the effect of two or more unresolved showers in the same picture. The relative number of events might be overestimated if a shower produced in the chamber could trigger the counters when the primary would not. However, the 2 to 3 inches of lead between the chamber and the lower counter all but eliminate this possibility. Since it is not always possible to identify unambiguously the origin of a shower, some showers that originate above the first plate might have been included and some showers produced in the last plates might not have been included. The opposite is also possible, as for instance when a shower originates in plate 9 and should therefore not be counted, but is accepted due to a coincident knock-on electron below the 8-th plate. An analysis of the data shows however that the effect of this uncertainty is negligible. The number of events might also be influenced by the criterion for accepting a picture. If the primary track was not distinctly visible in one of the intervals, the picture was discarded. However, a shower might mask the primary track and the picture would then be accepted because of the event. To evaluate this bias, the number of events in discarded pictures was counted. As it is approximately 10 % of the discarded pictures, a proportion equal to that in accepted events, no significant bias was found. Systematic errors in the number of events are therefore considered negligible in comparison with the statistical errors shown in Fig. 1.

We next examine the energy of a shower. It is determined from the number of associated tracks. Some tracks might be outside the illuminated region of the cloud chamber. Others might be far from the rest of the shower tracks and therefore considered as background. On the other hand, some background tracks might be mistaken for shower tracks. There are, however, very few background tracks. This is due to the unusually low radioactivity of the salt, to the fact that little radioactive contamination is brought into the mine, and to the natural shielding from cosmic rays provided by the location deep under-

ground. Errors in the observed number of shower tracks are therefore also believed to be small.

It is more difficult to estimate errors introduced by the application of Wilson's curves to find the energy histogram. The distribution of energies that correspond to a given number of tracks has an average standard deviation of 21% for a single event (see Section 3). The statistical uncertainty in the energy of the experimental points in Fig. 1 depends on the number of events per chosen interval. The resulting average statistical error in the abscissae is about 5%. H. THOM (as quoted in reference (6)) has analyzed electron showers of 950 MeV in a cloud chamber, which suggest that the energy of the showers is about 10% larger than predicted by the application of Wilson's curves. It seems therefore safe to assume that a possible systematic error in the energy of a shower is smaller than 20 %.

There are also several sources of possible systematic errors in the theoretical curve *A* that is compared in Fig. 1 with the experimental results.

a) The modified Bhabha's theory (1) predicts cross-sections which differ by as much as a factor of 2 from Murota's theory (2,7). However, the main difference between these theories is in the formalism and Murota's approach includes terms neglected in other theories. Therefore only Murota's results were used. It is, however, important to mention that Bhabha's modified theory would disagree even more with our data, since it predicts smaller cross-sections than Murota's theory at high transferred energies and larger cross-sections at low energies. Murota's theory was used with the following choice of arbitrary parameters: $\alpha = 2$, $a = 3mc^2/\varepsilon$. Other reasonable combinations of parameters yield cross-sections that are up to 10% larger. A comparison between different theories and between parameters is given in Roe's thesis (8).

b) The energy spectrum used is based on depth-intensity measurements and on the range-energy relation given by BARRETT *et al.* (9) (see Section 4). This relation was found by an estimate of the different forms of energy loss. Of these, neither nuclear energy losses of μ-mesons are yet well known nor are pair production losses. There is, however, no circular argument involved as pair production losses have little influence. GEORGE (11) arrives at a slightly different range-energy relation than BARRETT *et al.* (9). An analysis of these sources indicates a possible systematic error of about $\pm 15\%$ in our « theoretical » curve.

Even if we assume that the theoretical points in Fig. 1 are 15 % below the given curve *A* and that furthermore the shower energies have been underestimated by 20 %, agreement with theory cannot be obtained below 350 MeV.

(11) E. P. GEORGE: *Progress in Cosmic Ray Physics* (Amsterdam, 1952).

Above 350 MeV either of the two corrections would give good agreement. It is therefore reasonable to assume that the observed number of direct pairs is about $\frac{1}{2}$ that predicted (curve B in Fig. 1). At higher energies, the experimental points tend to be above curve B. However, it should be kept in mind that for electromagnetic interactions with large momentum transfers, quantum electrodynamics is suspected to yield unsatisfactory results ([12]). Both knock-on and pair production cross-sections might be larger for interactions at small distances ([13]). More data at higher energies would therefore be interesting.

([12]) S. DRELL: *Ann. of Phys.*, **4**, 75 (1958).
([13]) R. F. DEERY: *Thesis* (University of Washington, 1960).

RIASSUNTO (*)

Per studiare le interazioni elettromagnetiche dei muoni veloci dei raggi cosmici si è fatta funzionare una camera a nebbia a molte piastre a 1032 ft. sotto terra. Si è ottenuto un istogramma per le energie trasferite da 30 a 3000 MeV. Gli sciami sono principalmente dovuti a produzione diretta di coppie e a processi di « knock-on ». I risultati indicano che vi è concordanza con la teoria del « knock-on » mentre la sezione d'urto della produzione diretta di coppie è circa $\frac{1}{2}$ di quella predetta della teoria di Murota-Ueda-Tanaka.

(*) *Traduzione a cura della Redazione.*

Electromagnetic Scattering of Hyperons (*).

M. J. Englefield (**) and B. Margolis

Department of Physics and Astronomy, The Ohio State University - Columbus, Ohio

(ricevuto il 30 Agosto 1960)

Summary. — The interaction between the magnetic moment of a neutral hyperon and the charge of a nucleus causes large polarizations in small-angle scattering. The feasibility of using the effect to measure the magnetic moment is considered.

The value of the magnetic moment of the Λ^0 is of great interest, and recently Goldhaber [1] has proposed a method for its determination. The purpose of this note is to bring to attention the possibility of determining the magnetic moment by measurement of asymmetries in small angle scattering. At the present time the method proposed here is experimentally more difficult than Goldhaber's method, but affords, in principle, an independent determination of this important quantity.

According to Schwinger [2], the electromagnetic interaction between a neutral spin $\frac{1}{2}$ particle and a target nucleus of charge Ze has a polarizing power

$$P = \frac{2\gamma \cdot \mathrm{Im}\, f(\theta) \cdot \cot \theta/2}{|f(\theta)|^2 + \gamma^2 \cot^2 \theta/2}, \tag{1}$$

where $f(\theta)$ is the amplitude of the wave scattered by specifically nuclear forces, and

$$\gamma = \frac{1}{2}\mu \cdot \frac{\hbar}{Mc} \cdot \frac{Ze^2}{\hbar c}. \tag{2}$$

We take M and μ to be the mass and magnetic moment (in units of $e\hbar/2Mc$) of the Λ^0, which is believed [3] to have spin $\frac{1}{2}$.

(*) Supported in part by the National Science Foundation and in part by the U. S. Atomic Energy Commission.

(**) Present address: Department of Physics, Iowa State University of Science and Technology, Ames, Iowa.

(1) M. Goldhaber: *Phys. Rev.*, **101**, 1828 (1956).

(2) J. Schwinger: *Phys. Rev.*, **73**, 407 (1948).

(3) F. S. Crawford, M. Cresti, M. L. Good, M. L. Stevenson and H. K. Ticho: *Phys. Rev. Lett.*, **2**, 114 (1959).

The hyperons from the reaction

$$\pi^- + p \rightarrow \Lambda^0 + K^0 \tag{3}$$

are polarized perpendicularly to the production plane [4]. The polarization (1) will therefore produce a left-right asymmetry in a subsequent scattering. If the hyperons are produced 100% polarized, then this asymmetry will be $P(\theta)$ for scattering through center-of-mass angle θ in the production plane. Λ^0-p elastic scattering has been observed [5] in a liquid hydrogen bubble chamber, and the possibility therefore arises of using the above asymmetry to estimate μ.

Assuming that the Λ^0-p nuclear scattering only involves S-waves, for $\theta \geqslant 1^0$ (1) is well approximated by $P = 2\gamma k \cot\theta/2$, where $\hbar k$ is the relative momentum. If the laboratory energy of the incident hyperon is 50 MeV, $P = 11.6\,\mu$ % at 1°, and depends inversely on the angle. The resulting asymmetries are not likely to be observable.

A larger effect, however, would be obtained by scattering from heavier nuclei, owing to the factor Z in (2), and it may be profitable to use a xenon bubble chamber. The S-wave assumption is now invalid, but the polarization may be estimated [2] by approximating the nuclear scattering by that from a hard sphere in the high energy limit. The radius of the sphere is taken from the formula $R = 1.5 \cdot A^{\frac{1}{3}} \cdot 10^{-13}$ cm, when the model gives fair agreement with the cross-section of Xe for neutron scattering at the energies considered. The model is probably poor, but is as good as any other in the absence of information on the Λ^0-Xe cross-section. On this basis, we obtain the following values for the polarization (1) at small angles:

E \ θ	$\frac{1}{2}$	1	2	4	6	8	10
5	82.1	48.9	25.7	13.1 μ	8.7 μ	6.5 μ	5.2 μ
	100	82.1	48.9				
9	67.7	37.6	19.5 μ	9.7 μ	6.5 μ	4.9 μ	3.9 μ
	97.1	67.7					
16	53.8	28.6	14.6 μ	7.3 μ	4.9 μ	3.6 μ	
	87.1	53.8					
25	44.3	23.0	11.7 μ	5.8 μ	3.9 μ		
	76.7	44.3					
49	32.5	16.6 μ	8.3 μ	4.1 μ			
	60.1						

[4] F. S. Crawford jr., M. Cresti, M. L. Good, K. Gottstein, E. M. Lyman, F. T. Solmitz, M. L. Stevenson and H. K. Ticho: *Phys. Rev.*, **108**, 1102 (1957).

[5] F. S. Crawford jr., M. Cresti, M. L. Good, T. F. Solmitz, M. L. Stevenson and H. K. Ticho: *Phys. Rev. Lett.*, **2**, 174 (1959).

E is the laboratory energy in MeV, and θ is the center-of-mass angle in degrees. The polarizations are given in per cent. Where two polarizations are given, the upper is for $\mu = 1$, the lower for $\mu = 2$. A blank means the angle is sufficiently large for the electromagnetic scattering to be reduced owing to the finite extent of the nucleus ([2]).

At the lower energies, these effects are sufficiently large to give hope of their observation, although many difficulties are apparent. For example, the recoil Xe nucleus is no doubt extremely difficult to detect when the scattering angle is so small. Thus Goldhaber's suggestion ([1]) is more likely to be realized in the near future.

RIASSUNTO (*)

L'interazione fra il momento magnetico di un iperone e la carica di un nucleo causa forti polarizzazioni negli scattering a piccoli angoli. Si esamina la possibilità di usare questo effetto per misurare il momento magnetico.

(*) *Traduzione a cura della Redazione.*

IL NUOVO CIMENTO Vol. XIX, N. 2 16 Gennaio 1961

On the Axioms of Quantum Field Theory.

W. Weidlich

Institut für Theoretische Physik der Freien Universität - Berlin

(ricevuto il 1° Settembre 1960)

Zusammenfassung. — Ein Satz von Axiomen für die Quantenfeldtheorie wird diskutiert, der in einigen Punkten von dem Lehmann-Symanzik-Zimmermannschen abweicht, jedoch ebenfalls Lorentzinvarianz, Asymptotenbedingung und Kausalität enthält. Ausgangspunkt ist die nichtrelativistische kanonische Feldtheorie, welche in bestimmter Weise auf den relativistischen Fall übertragen wird. Wegen des Haagschen Theorems muß dabei der Begriff des lokalen, kausalen Feldes verallgemeinert werden.

Introduction.

In order to avoid the difficulties arising from explicit use of field equations, quantum field theory mainly has been developed in the last years by evaluating a number of axioms ([1,2]) which are supposed to describe adequately the fundamental properties of elementary-particle systems: α) relativistic invariance, β) existence of asymptotically free particles resp. fields before and after interaction, γ) causality of the interaction.

In particular it was possible to derive dispersion relations ([3]) and general representations for certain matrix elements ([1,5]). But the existence of nontrivial examples, satisfying all axioms and leading to an S-matrix $\neq 1$, has

---

([1]) H. Lehmann, K. Symanzik and W. Zimmermann: *Nuovo Cimento*, **1**, 205 (1955); **6**, 319 (1957).

([2]) A. S. Wightman: *Some Math. Probl. of Relat. Quantum Theory* (1957), unpublished manuscript.

([3]) For instance: H. Lehmann: *Nuovo Cimento*, **10**, 579 (1958).

([4]) H. Lehmann: *Nuovo Cimento*, **11**, 342 (1954).

([5]) F. J. Dyson: *Phys. Rev.*, **110**, 1460 (1958).

not yet been proved. So it may be worth-while to discuss an alternative set of axioms which also contain the essentials of conditions α), β), γ) and for which it may be easier to construct models. We begin with the non-relativistic case and consider canonical systems of interacting fields with an asymptotic condition. The transition to the relativistic case will meet with some difficulties in connection with the Theorem of Haag ([6,7]).

So it will be necessary to abandon the usual « totally local » interacting fields and to define « σ-local » field operators having more complicated transformation properties under the Lorentz-group. Nevertheless the theory will be explicitly Lorentz-invariant in the usual sense (confr. (2.17) for instance) and it will be possible to give conditions for macroscopic causality.

1. – Non-relativistic case.

We start with the following assumptions:

a) The physical system is described by field operators

$$\{\overline{\psi}_M(\mathfrak{r}, t);\ \overline{\pi}_N(\mathfrak{r}, t)\} \equiv \overline{\chi}_s(\mathfrak{r}, t)$$

satisfying canonical commutation relations:

$$\text{(1.1)} \qquad \begin{cases} [\overline{\psi}_M(\mathfrak{r}_1, t);\ \overline{\psi}_N(\mathfrak{r}_2, t)] = [\overline{\pi}_M(\mathfrak{r}_1, t);\ \overline{\pi}_N(\mathfrak{r}_2, t)] = 0\ , \\ [\overline{\psi}_M(\mathfrak{r}_1, t);\ \overline{\pi}_N(\mathfrak{r}_2, t)] = i\,\delta_{MN}\,\delta(\mathfrak{r}_1 - \mathfrak{r}_2)\ . \end{cases}$$

All $\overline{\chi}_s(\mathfrak{r}, t)$ for a fixed t form a complete system of operators with the usual representation in the Hilbertspace $\mathfrak{H}$ known from the theory of free fields.

b) In $\mathfrak{H}$ an unitary representation of the group

$$\mathfrak{G} = \mathfrak{R} \times \mathfrak{T}$$

($\mathfrak{R}$ = inhomogeneous rotation group; $\mathfrak{T}$ = time translation group) is given with infinitesimal transformations $M_{nm} = -M_{mn}$; P_m; H ($m, n = 1, 2, 3$), acting on $\overline{\chi}_s(\mathfrak{r}, t)$ by

$$\text{(1.2)} \qquad \exp\left[i(\mathfrak{k}\cdot\mathfrak{a} + H\tau)\right]\overline{\chi}_s(\mathfrak{r}, t)\exp\left[-i(\mathfrak{k}\cdot\mathfrak{a} + H\tau)\right] = \overline{\chi}_s(\mathfrak{r} + \mathfrak{a};\ t + \tau)$$

([6]) R. Haag: *Dan. Mat. Fys. Medd.*, **29**, no. 12 (1955).
([7]) D. Hall and A. S. Wightmann: *Dan. Mat. Fys. Medd.*, **31**, no. 5 (1957).

and

$$U(D)\,\overline{\chi}_M(\mathfrak{x}, t)\,U(D) = D^{-1}_{MN}\,\overline{\chi}_N(D\mathfrak{x}; t)$$

for $D =$ rotation.

c) $\mathfrak{H}$ and the representation of $\mathfrak{G}$ being such, that «free» canonical operators $\chi_s(\mathfrak{x}, t)$ exist, besides the $\overline{\chi}_s(\mathfrak{x}, t)$ which

1) also satisfy *a*), *b*) and are represented in $\mathfrak{H}$ equivalently to the $\overline{\chi}_s(\mathfrak{x}, t)$,

2) are «free» in the sense, that M_{nm}, P_m, H, expressed by $\chi_s(\mathfrak{x}, t)$ have the form well-known from the theory of free fields.

Clearly with $\chi_s(\mathfrak{x}, t)$ also $\chi'_s(\mathfrak{x}, t) = U\chi_s(\mathfrak{x}, t)U^{-1}$ is free, if $[U(G); U] = 0$ for all $G \in \mathfrak{G}$.

d) Among the $\chi_s(\mathfrak{x}, t)$ there are two systems $\chi^{\text{in}}_s(\mathfrak{x}, t)$; $\chi^{\text{out}}_s(\mathfrak{x}, t)$, such that

$$\overline{\chi}_s(\mathfrak{x}, t) \to \chi^{\text{out}}_{\text{in}\,s}(\mathfrak{x}, t) \qquad \text{for } t \to \pm\infty. \tag{1.3}$$

The kind of convergence will be specified later on.

We now give some simple consequences of the axioms *a*) ... *d*).

Taking arbitrary free operators $\chi_s(\mathfrak{x}, t)$, we have from $(c; 1)$ the existence of an unitary $V(t)$ connecting χ and $\overline{\chi}$:

$$\overline{\chi}_M(\mathfrak{x}, t) = V(t)\,\chi_M(\mathfrak{x}, t)V^{-1}(t)\,. \tag{1.4}$$

Using (1.2) for both $\overline{\chi}_M$ and χ_M we first conclude:

$$[U(R); V(t)] = 0 \qquad \text{for all } R \in \mathfrak{R}. \tag{1.5}$$

Proof: With $\overline{U}(R) = V(t)U(R)V^{-1}(t)$ we easily get from (1.2); (1.4):

$$[\overline{U}^{-1}(R)U(R);\ \overline{\chi}_M(\mathfrak{x}, t)] = 0\,,$$

hence

$$U(R) = \lambda(R)\overline{U}(R)\,; \qquad |\lambda(R)| = 1 \tag{$*$}$$

as the $\chi_M(\mathfrak{x}, t)$ are complete; because of $(*)$ the $\lambda(R)$ give an unitary one-dimensional repr. of $\mathfrak{R}$; as there only exists the identical one, $\lambda(R) = 1$.

This completes the proof.

From the rest of (1.2) we get:

$$V(t) = \exp[iHt]V(0)\exp[-iHt]\,, \tag{1.6}$$

$V(t)$ can always be expressed as a functional of $\bar{\chi}_M(\mathrm{r}, t)$ or of $\chi_M(\mathrm{r}, t)$: $V(t) \equiv \equiv V[\chi_M(t)]$. From (1.4) and $V(t) = V(t)V[\chi_M(t)]V^{-1}(t)$ we have

$$V[\chi_M(t)] = V[\bar{\chi}_M(t)] , \tag{1.7}$$

saying that the functional form of $V(t)$ in the $\chi_M(\mathrm{r}, t)$'s is the same as in the $\bar{\chi}_M(\mathrm{r}, t)$'s.

Instead of choosing the Hamiltonian $H\{\bar{\chi}_M(t)\}$ at the outset of a theory we may as well consider $V[\chi_M(t)]$ as the quantity given primarily. Then, in principle, for each operator $A = A[\chi_M(t)]$ its form $A\{\bar{\chi}_M(t)\}$ in $\bar{\chi}_M(\mathrm{r}, t)$ is known:

$$A\{\bar{\chi}_M(t)\} \equiv V^{-1}(t)V(t)A[\chi_M(t)]V^{-1}(t)V(t) = V^{-1}[\bar{\chi}_M(t)]A[\bar{\chi}_M(t)]V[\bar{\chi}_M(t)] . \tag{1.8}$$

Thus the Hamiltonian, being « free » if written in the $\chi_M(\mathrm{r}, t)$'s, may have a complicated form written in the $\bar{\chi}_M(\mathrm{r}, t)$'s. To compare our formulation with the conventional one we introduce fields

$$\chi^0_M(\mathrm{r}, t) = V(0)\chi_M(\mathrm{r}, t)V^{-1}(0) , \tag{1.9}$$

being equal $\bar{\chi}_M(\mathrm{r}, t)$ for $t = 0$, but satisfying the equation of motion:

$$\dot{\chi}^0_M(\mathrm{r}, t) = i[H_0; \chi^0_M(\mathrm{r}, t)] . \tag{1.10}$$

with $H_0 = V(0)HV^{-1}(0)$.

The two Hamiltonians H, H_0 for $\bar{\chi}_M(\mathrm{r}, t)$, $\chi^0_M(\mathrm{r}, t)$ of course have the same spectrum. We now consider the operator

$$W(t) = \exp[iH_0t] \exp[-iHt] = V(0)V^+(t) , \tag{1.11}$$

with respect to (1.6): (1.10).

In simple quantum-mechanical cases of potential scattering the strong convergence of the corresponding $W(t)$ to Moller operators $\Omega_\pm$ can be proved (8). Therefore we postulate for $V(t)$ analogously:

$$V(t)V^+(0) \Rightarrow \Omega_\pm \quad \text{or} \quad V(t) \Rightarrow \Omega_\pm V(0) \equiv U_\pm \quad \text{for } t \to \pm\infty \tag{1.12}$$

in the sense of strong convergence. In our case (no bound states) $\Omega_\pm$ and $U_\pm$ then are unitary. (It would be of no use postulating weak convergence $V(t) \to U_\pm$ only, as $(\varphi_1, [V(t) - U_\pm]\varphi_2) \to 0$ for all fixed $\varphi_1, \varphi_2 \in \mathfrak{H}$ and $\|\varphi\| = \|V(t)\varphi\| = \|U_\pm\varphi\|$ automatically involve $\|(V(t) - U_\pm)\varphi\| \to 0$ for all $\varphi \in \mathfrak{H}$.)

(8) W. Brenig and R. Haag: *Fortschr. d. Phys.*, **7**, 183 (1959).

If $U_{\pm}$ exists by condition (1.12), it fulfills

$$[U(G): U_{\pm}] = 0 \qquad \text{for all } G \in \mathfrak{G}. \tag{1.13}$$

Proof: $[U(R): \Omega_{\pm} V(0)] = 0$ is trivial by (1.5) and definition of $\Omega_{\pm}$: $[H: U_{\pm}] = 0$ results from $H\Omega_{\pm} = \Omega_{\pm} H_0$: $H_0 V(0) = V(0) H$.

We shall now give the precise formulation of axiom *d*):

Let $\chi^{in}(x)$ be a solution of the free Heisenberg equations; then the scalar product $(f_a^M, \chi^{in}) = \chi^{in}$ will be a time-independent operator and we have the convergence:

$$(f_a^M: \overline{\chi}_M) \equiv \overline{\chi}^a(t) = V(t) \chi^a V^{-1}(t) \Rightarrow U_{\pm} \chi^a U_{\pm}^{-1} \equiv \chi^a_{out} \tag{1.4'}$$

$$\text{for } t \to \pm \infty\colon \ \chi_M^{in/out}(\mathbf{x}, t) = U_{\pm} \chi_M(\mathbf{x}, t) U_{\pm}^{-1}.$$

The S-matrix, defined by

$$\chi^a_{in} = S \chi^a_{out} S^{-1}, \tag{1.14}$$

will have the form:

$$S = U_- U_+^{\dagger} = \Omega_- V(0) V^{\dagger}(0) \Omega_+^{\dagger} = \Omega_- \Omega_+^{\dagger}; \tag{1.15}$$

of course: $[U(G): S] = 0$ for all $G \in \mathfrak{G}$.

We still have to investigate the meaning of (1.12) for V. Assuming the existence of $\Omega_{\pm}$ (for the moment we shall write it in the form (1.15), to get relation (1.25) for the matrix elements of $V(0)$; afterwards the convergence (1.12) has to be verified.

Let us first introduce eigenvectors $\Phi_{E,\alpha}$: $\Psi_{E,\alpha}$ of H_0 resp. H:

$$H_0 \Phi_{E,\alpha} = E \Phi_{E,\alpha}\colon \quad H \Psi_{E,\alpha} = E \Psi_{E,\alpha} \qquad (\alpha \text{ additional parameters}) \tag{1.16}$$

where to each $\Phi_{E,\alpha}$ belongs one

$$\Psi_{E,\alpha} = V^{\dagger}(0) \Phi_{E,\alpha} \tag{1.17}$$

and vice versa.

On the other hand the eigenvectors $\Psi_{E,\alpha}^{\pm}$ of H, related to $\Phi_{E,\alpha}$ by

$$\Psi_{E,\alpha}^{\pm}(t) \Rightarrow \Phi_{E,\alpha}(t) \qquad \text{for } t \to \pm \infty,$$

where

$$\dot{\Psi}^{\pm}_{E,\alpha}(t) = \frac{1}{i} H \Psi^{\pm}_{E,\alpha}(t); \qquad \dot{\Phi}_{E,\alpha}(t) = \frac{1}{i} H_0 \Phi_{E,\alpha}(t);$$

$$\Psi^{\pm}_{E,\alpha}(0) \equiv \Psi^{\pm}_{E,\alpha}; \qquad \Phi_{E,\alpha}(0) \equiv \Phi_{E,\alpha}$$

are given by

$$\Psi^{\mp}_{E,\alpha} = \Omega_{\pm} \Phi_{E,\alpha} = \Phi_{E,\alpha} + \frac{1}{E - H \mp i\varepsilon} Q \Phi_{E,\alpha} . \tag{1.18}$$

with $Q = H - H_0$.

The so defined $\Omega_{\pm}$ must agree with (1.12), if the limit exists [9]. As $\Psi^{-}_{E,\alpha} = \Omega_{+} V(0) \Psi_{E,\alpha}$ ($U_{+} \Psi_{E,\alpha}$ and $\Psi_{E,\alpha}$ belong to the same eigenvalue E of H, there must be

$$(\Phi_{E'\beta} | V(0) \Omega_{\pm} | \Phi_{E,\alpha}) = (\Psi_{E'\beta} | U_{\pm} | \Psi_{E\alpha}) = \delta(E' - E)(\delta_{\beta\alpha} + u_{\pm}(E'\beta; E\alpha)) . \tag{1.19}$$

Writing now the matrix elements of $V(0) = 1 + Y$ in the form

$$(\Phi_{E'\alpha'} | V(0) | \Phi_{E\alpha}) = (\Psi_{E'\alpha'} | V(0) | \Psi_{E\alpha}) = \delta(E' - E)\delta_{\alpha'\alpha} + v(E'\alpha'; E\alpha) \tag{1.20}$$

and regarding

$$\frac{1}{E - H \pm i\varepsilon} = V^{+}(0) \frac{1}{E - H_0 \pm i\varepsilon} V(0) ,$$

we obtain

$$V(0) \Omega_{\pm} \Phi_{E,\alpha} = \Phi_{E,\alpha} + \left(Y + \frac{1}{E - H_0 \mp i\varepsilon} [H_0; Y] \right) \Phi_{E,\alpha} = \tag{1.21}$$

$$\Phi_{E,\alpha} + \sum_{E'\alpha'} \left\{ v(E'\alpha'; E\alpha) + \frac{1}{E - E' \mp i\varepsilon} (E' - E) v(E'\alpha'; E\alpha) \right\} \Phi_{E'\alpha'} .$$

If $v(E'\alpha'; E\alpha)$ is regular for $(E' - E) \to 0$, (1.21) reduces to $V(0)\Omega_{\pm} \Phi_{E,\alpha} = \Phi_{E,\alpha}$ or $V(0)\Omega_{\pm} = 1$ and $U_{\pm} = 1$; $S = 1$. The simplest form of $v(E'\alpha'; E\alpha)$ to avoid this trivial case is

$$v(E'\alpha'; E\alpha) = \frac{1}{E' - E - i\eta} v_{+}(E'\alpha'; E\alpha) - \frac{1}{E' - E + i\eta} v_{-}(E'\alpha'; E\alpha) , \tag{1.22}$$

where $v_{\pm}(E'\alpha'; E\alpha)$ are regular at $E' = E$, and satisfy the unitarity conditions

[9] M. GELL-MANN and M. L. GOLDBERGER: *Phys. Rev.*, **91**, 398 (1953).

for $V(0)$. Going to the limit $\eta \to 0$; $\varepsilon \to 0$ and using the well known formulas

$$(1.23)\qquad \begin{cases} \lim_{\varepsilon \to 0} \dfrac{1}{E' - E \pm i\varepsilon} = P \dfrac{1}{E' - E} \mp i\pi\delta(E' - E); \\ (E' - E)\,\delta(E' - E) = 0; \qquad (E' - E) P \dfrac{1}{E' - E} = 1, \end{cases}$$

we get

$$(1.21')\qquad V(0)\Omega_{\pm}\Phi_{E,\alpha} = \Phi_{E,\alpha} + \sum_{E',\alpha'} 2\pi i\,\delta(E' - E)\, v_{\pm}(E'\alpha'; E\alpha)\Phi_{E'\alpha'}$$

or by comparison with (1.19):

$$(1.24)\qquad u_{\pm}(E\beta; E\alpha) = 2\pi i\, v_{\pm}(E\beta; E\alpha).$$

Thus the matrix elements of $V(0)$ diagonal in the energy are connected with those of $U_{\pm}$ and S in a simple way, while the non-diagonal elements of $V(0)$ are necessary to give the whole time-development of the theory. For these (1.6) and (1.20) imply:

$$(1.25)\qquad (\Psi_{E'\alpha'}, V(t)\Psi_{E\alpha}) = \delta(E' - E)\,\delta_{\alpha'\alpha} + \frac{\exp[i(E' - E)t]}{E' - E - i\eta} v_{+}(E'\alpha'; E\alpha) - \frac{\exp[i(E' - E)t]}{E' - E + i\eta} v_{-}(E'\alpha'; E\alpha).$$

Taking normalized states instead of $\Psi_{E,\alpha}$ and using

$$(1.26)\qquad \begin{cases} \lim_{t \to +\infty} \dfrac{\exp[i\omega t]}{\omega - i\eta} = -\lim_{t \to -\infty} \dfrac{\exp[i\omega t]}{\omega + i\eta} = 2\pi i\,\delta(\omega); \\ \lim_{t \to -\infty} \dfrac{\exp[i\omega t]}{\omega - i\eta} = \lim_{t \to +\infty} \dfrac{\exp[i\omega t]}{\omega + i\eta} = 0, \end{cases}$$

we verify $V(t) \to U_{\pm}$ for $t \to \pm\infty$, involving $V(t) \Rightarrow U_{\pm}$, as $V(t)$, $U_{\pm}$ are unitary. For applications it will be more convenient, to put $V(t) = \exp[iT(t)]$; $T(t) = T^{\dagger}(t)$. Then $V(t) \Rightarrow \exp[iT_{\pm}]$ is true at least, if $T(t) \Rightarrow T_{\pm}$.

2. – Relativistic theory.

Section **1** should be considered as a preparation for the relativistic case. To facilitate the transition to the latter, we need some notations and definitions at the beginning.

Let us consider all space-time co-ordinate systems Σ generated from one

Σ_0 by applying any element L of the inhomogeneous Lorentz group $\mathfrak{L}$. (As usual all L are referred to an arbitrary, but fixed system Σ_0)

Σ is said to belong to the σ-plane $\sigma = \sigma(\Sigma)$, if the equation of $\sigma(\Sigma)$ in Σ is: $t = 0$. $\mathfrak{R}(\sigma) \subset \mathfrak{L}$ be the subgroup of all Lorentz transformations $L(\sigma)$ leaving σ invariant: $L(\sigma) \cdot \sigma = \sigma$. Clearly two pairs of co-ordinate-systems (Σ_1, Σ_2) and (Σ_1', Σ_2') are in equivalent relative situations, if $\Sigma_1' = L'\Sigma_1$; $\Sigma_2' = L'\Sigma_2$; $L' \in \mathfrak{L}$. Usually the arguments x, k, ... of operators refer to a fixed system Σ_0. As it will be convenient to change the frame of reference, we write it down explicitly from now on. Thus, the usual field operators $\varphi_M(x)$ will now be written $\varphi_M(\Sigma_0 | x)$. Going to $L\Sigma_0$, they satisfy

$$(2.1)\qquad \begin{cases} \varphi_N(\Sigma_0 | x) = \lambda^S_N(L)\varphi_S(L\Sigma_0 | L^{-1}x) \\ \text{particularly for scalar fields:} \\ A(\Sigma_0 | x) = A(L\Sigma_0 | L^{-1}x) \quad \text{or} \quad A(\Sigma_0 | Lx) = A(L\Sigma_0 | x)\ . \end{cases}$$

If an unitary representation of $\mathfrak{L}$ is given, $U(L)$ act on $\varphi_M(\Sigma_0 | x)$ by

$$(2.2)\qquad U(L)\varphi_M(\Sigma_0 | x)\, U^{-1}(L) = \lambda^N_M(L^{-1})\varphi_N(\Sigma_0 | Lx) = \varphi_M(L\Sigma_0 | x)$$

using (2.1).

More generally, (2.2) implies

$$(2.2')\qquad U(L)\, B(\Sigma_0 | \xi)\, U^{-1}(L) = B(L\Sigma_0 | \xi)$$

for any functional $B(\Sigma_0 | \xi)$ of the $\varphi_M(\Sigma_0 | x)$ with arguments ξ referring to Σ_0.

Considering operators $\varphi_M(\Sigma | x)$ with $x \in \sigma$ we often use Σ belonging to σ; in Σ is $x = (\mathfrak{x}, 0)$.

Definition: A system of operators $\psi_M(\Sigma | \mathfrak{x})$ given on $\sigma(\Sigma)$ is said to be σ-local if it satisfies

$$(2.3)\qquad U(L(\sigma))\, \psi_M(\Sigma | \mathfrak{x})\, U^{-1}(L(\sigma)) = D^N_M(D^{-1})\, \psi_N(\Sigma | D\mathfrak{x} + \mathfrak{a})\ ,$$

where $L(\sigma) = (D, \mathfrak{a})$ in Σ and unitary $U(L)$ are presumed to exist, and

$$(2.4)\qquad [\psi_M(\Sigma | \mathfrak{x});\ \psi_N(\Sigma | \mathfrak{x}')] = 0 \qquad \text{for } \mathfrak{x}' \neq \mathfrak{x}.$$

A σ-local system $\chi_M(\Sigma | \mathfrak{x})$ is called canonical, if it fulfills the canonical commutation relations (1.1). If a σ-local system for $\sigma(\Sigma)$ is given, we get such systems for any $\sigma' = \sigma(L'\Sigma)$ by defining

$$(2.5)\qquad \psi_M(L'\Sigma | \mathfrak{x}) = U(L')\, \psi_M(\Sigma | \mathfrak{x})\, U^{-1}(L')\ .$$

If it is possible to associate fields $\varphi_M(\Sigma_0|x)$ to the family of σ-local systems $\psi_M(\Sigma|\mathfrak{x})$, such that (2.1) is valid for $\varphi_M(\Sigma_0|x)$ and $\psi_M(\Sigma|\mathfrak{x}) = \varphi_M(\Sigma|\mathfrak{x}, 0)$, we call the family totally local.

Clearly fields, which satisfy (2.1), (2.2) and causal commutation relations $[\varphi_M(\Sigma|\mathfrak{x}, 0); \varphi_N(\Sigma|\mathfrak{x}', 0)] = 0$ for all Σ and $\mathfrak{x} \neq \mathfrak{x}'$, always generate a totally local family of $\psi_M(\Sigma|\mathfrak{x})$. But not every family of σ-local operators is totally local. A well known counter-example for the case of a free scalar field are the operators $e^\dagger(\Sigma_0|\mathfrak{x})$, $e(\Sigma_0|\mathfrak{x})$ creating and annihilating localized states on $\sigma(\Sigma_0)$ in the sense of NEWTON and WIGNER [10]. They are defined by:

$$e(\Sigma_0|\mathfrak{x}) = \frac{1}{(2\pi)^{\frac{3}{2}}} \int k_0^{\frac{1}{2}} \exp[i\mathfrak{k}\cdot\mathfrak{x}]\, a(\Sigma_0|k)\, \mathrm{d}m(k) \quad \text{and herm. conj.}, \tag{2.6}$$

where

$$\mathrm{d}m(k) = \frac{\mathrm{d}^3k}{k_0}; \qquad k_0 = +\sqrt{m^2 + k^2};$$

$$[a(\Sigma_0|k),\, a^\dagger(\Sigma_0|k')] = k_0\, \delta(\mathfrak{k} - \mathfrak{k}'); \qquad [e(\Sigma_0|\mathfrak{x});\, e^\dagger(\Sigma_0|\mathfrak{x}')] = \delta(\mathfrak{x} - \mathfrak{x}').$$

Their transformation-properties result from that of $a(\Sigma_0|k)$:

$$\begin{cases} U(L)\, a(\Sigma_0|k)\, U^{-1}(L) = a(L\Sigma_0|k) = a(\Sigma_0|Lk) & \text{for homogeneous } L \in \mathfrak{L}, \\ U(\Lambda)\, a(\Sigma_0|k)\, U^{-1}(\Lambda) = a(\Lambda\Sigma_0|k) = \exp[-i\Lambda_\nu k^\nu]\, a(\Sigma_0|k) & \\ \qquad\qquad\qquad\qquad\qquad\qquad\qquad\qquad\qquad\qquad \text{for translations } \Lambda \in \mathfrak{L}. & \end{cases} \tag{2.7}$$

and especially imply $e(\Sigma_0|0) \neq e(L\Sigma_0|0)$ for $L \neq L(\sigma(\Sigma_0))$, even if L leaves invariant the origin of Σ_0. Hence, $e(\Sigma_0|0)$ depends not only on the world point $(0, 0)$ in Σ_0 or $L\Sigma_0$, but also on $\sigma(\Sigma_0)$ or $\sigma(L\Sigma_0)$, to which it belongs. Physically this is clear: $e^\dagger(\Sigma_0|\mathfrak{x})$ creates a localized state $\Phi_{\mathfrak{x}}^{\Sigma_0}$ on $\sigma(\Sigma_0)$ at point $\mathfrak{x}$, composed of waves of different momentum. Seen from an observer in $\Sigma' = L'\Sigma_0$ moving relative to Σ_0, $\Phi_{\mathfrak{x}}^{\Sigma_0}$ is no longer strictly localized because of (2.7), resp. localization in this sense is no Lorentz-invariant conception. The question now arises, if σ-local families of operators, being more general than local, causal fields, may be applied to describe causally interacting systems. In this connection we recall the theorem of Haag [6], stated in the form of Hall and Wightman [7].

Two canonical fields $q_j(\Sigma_0, x)$, $\pi_j(\Sigma_0, x)$; $j = 1, 2$ (corresponding to totally local operator families) agree in all their vacuum-expectation values up to the

[10] T. D. NEWTON and E. P. WIGNER: *Rev. Mod. Phys.*, **21**, 400 (1949).

fourth order at least, if they have equivalent representations on $\sigma(\Sigma_0)$, resp. if

$$V\varphi_1(\Sigma_0|\mathfrak{x},0)V^{-1}=\varphi_2(\Sigma_0|\mathfrak{x},0)\ ;\qquad V\pi_1(\Sigma_0|\mathfrak{x},0)V^{-1}=\pi_2(\Sigma_0|\mathfrak{x},0)\ .$$

To avoid such agreement between interpolating fields and « free » asymptotic fields we may consider

α) field theories with local, causal interpolating fields, which are non-canonical or, if canonical, have representations in $\mathfrak{H}$ inequivalent to that of the asymptotic fields, or, abandoning these fields corresponding to totally local operator families:

β) field theories with interpolating σ-local operator families, which even may be canonical and have representations equivalent to that of the asymptotic « free » fields.

While the axioms and consequences of case α) have been formulated by Lehmann, Symanzik, Zimmermann [1] and other authors, we shall try here to do so for the second case.

Axioms for β).

a) An Hilbert space $\mathfrak{H}$ exists, in which an unitary representation of the inhomogeneous Lorentz group $\mathfrak{L}$ is given, furthermore « free » canonical fields $\chi_M(\Sigma_0|x)=\{\varphi_M(\Sigma_0|x),\ \pi_N(\Sigma_0|x)\}$ satisfying (2.1), (2.2) and the canonical commutation rules

$$[\varphi_M(\Sigma|\mathfrak{x},0);\pi_N(\Sigma\ \mathfrak{x}',0)]=i\,\delta_{MN}\delta(\mathfrak{x}'-\mathfrak{x})\ ,\ \ldots \qquad \text{for all } \Sigma,$$

forming a complete operator system on every $\sigma(\Sigma)$ and free in the sense, that the infinitesimal transformations P_ν, $M_{\nu\mu}=-M_{\mu\nu}$ $(\mu,\nu=0\ldots3)$ of $\mathfrak{L}$ have the free form if expressed by $\chi_M(\Sigma_0|x)$.

b) The operators $\overline{\chi}_M(\Sigma|\mathfrak{x})$, which are to describe the interacting physical system, constitute a σ-local canonical operator family equivalent to $\chi_M(\Sigma|\mathfrak{x},0)$ on every $\sigma(\Sigma)$. So an unitary $V(\sigma)$ exists for $\sigma(\Sigma)$, connecting χ and $\overline{\chi}$:

$$\overline{\chi}_M(\Sigma|\mathfrak{x})=V(\tau)\,\chi_M(\Sigma|\mathfrak{x},0)\,V^{-1}(\sigma)\ . \tag{2.8}$$

Formulas (2.3) for $\overline{\chi}_M(\Sigma|\mathfrak{x})$ and (2.2) for $\chi_M(\Sigma|\mathfrak{x},0)$ immediately imply (as in the non-relativistic case (1.5))

$$[U(L(\sigma));\ V(\sigma)]=0 \qquad \text{for all } L(\sigma)\in\mathfrak{R}(\sigma). \tag{2.9}$$

As the vacuum Φ_0 is the only state in $\mathfrak{H}$ invariant under all Lorentz trans-

formations and the one particle states must behave like free ones, we require

$$V(\sigma)\Phi_0 = \Phi_0\,; \qquad V(\sigma)\Phi_1 = \Phi_1 \tag{2.10}$$

for all $V(\sigma)$ and all free one particle states Φ_1.

c) We have to restate explicitly the meaning of relativistic invariance for a quantum field theory:

1) No system Σ is physically preferred to any other; only the relative situation of two systems Σ_1, $\Sigma_2 = L\Sigma_1$ is relevant for statements of the theory.

2) The transformation properties of certain quantities like total energy-momentum and energy-momentum of single incoming and outgoing particles are known from experiment. These conditions are warranted by the following postulates: $\overline{Q}(\Sigma|\xi)$ be an observable assigned to a measurement on Σ at $t = 0$, and $\Phi_\alpha^\Sigma \in \mathfrak{H}$ the state found thereby (arguments ξ, α refer to Σ); then the observable $\overline{Q}(L\Sigma|\xi)$ and state $\overline{\Phi}_\alpha^{L\Sigma}$, assigned to the corresponding measurement on $L\Sigma$ are given by

$$\overline{Q}(L\Sigma|\xi) = U(L)\overline{Q}(\Sigma|\xi)U^{-1}(L)\,; \qquad \overline{\Phi}_\alpha^{L\Sigma} = U(L)\overline{\Phi}_\alpha^{\Sigma}\,. \tag{2.11}$$

As (2.5) is valid for $\overline{\chi}_M(\Sigma|\mathfrak{x})$ and $\chi_M(\Sigma|\mathfrak{x}, 0)$ as well, $\overline{Q}(L\Sigma|\xi)$ has the same form written in $\overline{\chi}_M(L\Sigma|\mathfrak{x})$ resp. $\chi_M(L\Sigma|\mathfrak{x}, 0)$ as $Q(\Sigma|\xi)$ written in $\overline{\chi}_M(\Sigma|\mathfrak{x})$ resp. $\chi_M(\Sigma|\mathfrak{x}, 0)$. Furthermore, (2.5) and (2.8) imply

$$V(L\cdot\sigma) = U(L)V(\sigma)U^{-1}(L)\,. \tag{2.12}$$

This is compatible with (2.9) because of

$$U(L')U(L(\sigma)(U^{-1}(L') = U(L(L'\sigma))\,.$$

The expectation value of $\overline{Q}(\Sigma_2|\xi)$ in $\overline{\Phi}_\beta^{\Sigma_1}$ now only depends on the relative situation of Σ_2, Σ_1:

$$(\overline{\Phi}_\beta^{\Sigma_1}|\overline{Q}(\Sigma_2|\xi)|\overline{\Phi}_\beta^{\Sigma_1}) = (\overline{\Phi}_\beta^{\Sigma_1'}|\overline{Q}(\Sigma_2'|\xi)|\overline{\Phi}_\beta^{\Sigma_1'}) \tag{2.13}$$

by (2.11), if

$$\Sigma_j' = L'\Sigma_j \qquad (j = 1, 2).$$

To satisfy condition 2), we need

d) Asymptotic condition:

$$V(\sigma) \to U(\quad) \qquad \text{for } \sigma \to \infty, \tag{2.14}$$

where $U_\pm$ is unitary and satisfies:

$$[U(L);\ U_\pm] = 0 \qquad \text{for all } L \in \mathfrak{L}. \tag{2.15}$$

(As in the non-relativistic case weak convergence of $V(\sigma)$ to $U_\pm$ involves strong one.)

This implies

$$\bar{\chi}_M(\Sigma|\mathfrak{x}) \Rightarrow U_\pm \chi_M(\Sigma|\mathfrak{x}) U_\pm^{-1} \equiv \overset{\text{out}}{\chi}{}^{\text{in}}_M(\Sigma|\mathfrak{x}) \qquad \text{for } \sigma(\Sigma) \to \pm\infty, \tag{2.16}$$

where $\overset{\text{out}}{\chi}{}^{\text{in}}_M(\Sigma|\mathfrak{x})$ belong to the « free » fields $\overset{\text{out}}{\chi}{}^{\text{in}}_M(\Sigma_0|x) = U_\pm \chi_M(\Sigma_0|x) U_\pm^{-1}$. (The particles belonging to the asymptotic $\overset{\text{out}}{\chi}{}^{\text{in}}_M(\Sigma_0|x)$ have of course to be considered as « dressed ».)

Since it can be proved on the other side (*), that only weak convergence of local, causal fields to « free » asymptotic fields is possible; the σ-local $\bar{\chi}(\Sigma|\mathfrak{x})$ cannot be a totally local operator family belonging to a local, causal field $\bar{\chi}(\Sigma_0|x)$; in other words, a non-trivial $V(\sigma)$ cannot satisfy the necessary and sufficient condition for $\bar{\chi}(\Sigma|\mathfrak{x})$ to be totally local:

$$V(\sigma_1[x])\,\chi_M(\Sigma_0|x)V^{-1}(\sigma_1[x]) = V(\sigma_2[x])\,\chi_M(\Sigma_0|x)V^{-1}(\sigma_2[x]),$$

where the $\sigma_j[x]$ are arbitrary σ-planes containing the point x. The S-matrix, defined as in (1.14), is given by

$$S = U_- U_+^\dagger \quad \text{clearly: } [U(L);\ S] = 0 \qquad \text{for all } L \in \mathfrak{L}. \tag{2.17}$$

For causality the next conditions for $V(\sigma)$ will be decisive.

e) Quasilocality of $V(\sigma)$:

In the following we shall make the assumption, that a « local » observable $\bar{Q}(\Sigma|\mathfrak{x})$ composed only of $\bar{\chi}_M(\Sigma|\mathfrak{x}')$; $\mathfrak{x}' \approx \mathfrak{x}$ is assigned to a measurement « at the point $(\mathfrak{x}, 0)$ » in Σ. Instead of $\bar{\chi}_M(\Sigma|\mathfrak{x})$ we may consider the Newton-Wigner operators $\bar{e}_N(\Sigma|\mathfrak{x})$, $\bar{e}_N^\dagger(\Sigma|\mathfrak{x})$ belonging to $\bar{\chi}_M(\Sigma|\mathfrak{x})$ as associated with measurements at $(\mathfrak{x}, 0)$ in Σ. Up to regions of order of Compton wavelength this turns out to be the same. For instance in the case of scalar field $A(\Sigma_0|x)$, using (2.6):

$$\bar{A}(\Sigma|\mathfrak{x}) = V(\sigma(\Sigma))\,A(\Sigma|\mathfrak{x}, 0)\,V^{-1}(\sigma(\Sigma)) = \tag{2.18}$$

$$= \sqrt{\frac{1}{2}} \int \left\{ \bar{e}(\Sigma|\mathfrak{x}')\,K(\mathfrak{x}' - \mathfrak{x}) + \bar{e}^\dagger(\Sigma|\mathfrak{x}')\,K^*(\mathfrak{x}' - \mathfrak{x}) \right\} \mathrm{d}^3\mathfrak{x}',$$

(*) I am indebted to Dr. Doebner for pointing out this to me.

with

$$m = 1; \qquad K(\mathfrak{x}'-\mathfrak{x}) = \frac{1}{|\mathfrak{x}'-\mathfrak{x}|^{5/4}} H^{(1)}_{5/4}(i|\mathfrak{x}'-\mathfrak{x}|); \qquad H^{(1)}_{5/4} = \text{Hankel function},$$

and

$$\bar{e}(\Sigma|\mathfrak{x}') = V(\sigma(\Sigma))\, e(\Sigma, \mathfrak{x}')\, V^{-1}(\sigma(\Sigma)) .$$

The quasilocality of $V(\sigma)$ now means, roughly spoken, that

$$\bar{\chi}_M(\Sigma|\mathfrak{x}) = V(\sigma(\Sigma))\, \chi_M(\Sigma|\mathfrak{x}, 0)\, V^{-1}(\sigma(\Sigma))$$

if expressed by $\chi_M(\Sigma|\mathfrak{x}', 0)$, essentially only contains $\chi_M(\Sigma|\mathfrak{x}', 0)$ with $|\mathfrak{x}'-\mathfrak{x}| \leqslant$ Compton wave-length of the particles considered. To give a more exact formulation, we consider normalizable states $\Phi^\Sigma(\mathfrak{v})$ created from vacuum Φ_0 by repeated application of « free » Newton-Wigner operators $e^\dagger_N(\Sigma|\mathfrak{x})$ with $r \in \mathfrak{v}$ and taking linear combinations. Then $V(\sigma(\Sigma))$ is called quasi-local, if

$$\text{maximum of } \frac{(\Phi^\Sigma_1(\mathfrak{v}_1)|\, V(\sigma(\Sigma))\,|\Phi^\Sigma_2(\mathfrak{v}_2))}{\|\Phi^\Sigma_1(\mathfrak{v}_1)\| \cdot \|\Phi^\Sigma_2(\mathfrak{v}_2)\|} \ll 1 , \tag{2.19}$$

as soon as the distance $d(\mathfrak{v}_1; \mathfrak{v}_2)$ of the space-regions $\mathfrak{v}_1$, $\mathfrak{v}_2$ considerably exceeds the Compton wave-length λ. $V(\sigma(\Sigma))$ being quasi-local, $V(\sigma(\Sigma'))$ for any $\Sigma' = L'\Sigma$ is quasi-local too, as $V(\sigma(\Sigma'))$ is composed of $e_N(\Sigma'|\mathfrak{x})$, $e^\dagger_N(\Sigma'|\mathfrak{x})$ resp. $\chi_M(\Sigma'|\mathfrak{x}, 0)$ in the same way as $V(\sigma(\Sigma))$ of $e_N(\Sigma|\mathfrak{x})$, $e^\dagger_N(\Sigma|\mathfrak{x})$ resp. $\chi_M(\Sigma|\mathfrak{x}, 0)$.

Condition *e*) has important consequences.

1) In principle we are able to discuss observables beyond the scope of pure *S*-matrix theory. So we may interpret for instance the well defined energy-momentum tensor $T_{\nu\mu}(\Sigma_0, x)$ of the free $\chi_M(\Sigma_0|x)$ as belonging to the interacting system, after having expressed $T_{\nu\mu}(\Sigma|\mathfrak{x}, 0)$ by interacting-operators $\bar{\chi}_M(\Sigma, \mathfrak{x})$ on the σ-plane $\sigma(\Sigma)$ taken into account (in analogy to (1.8)). The interpretation is possible, as $\int_{\mathfrak{v}} T_{\nu 0}(\Sigma\ \mathfrak{x}, 0)\, \mathrm{d}^3\mathfrak{x}$ except for negligible contributions only consists of $\bar{\chi}_M(\Sigma|\mathfrak{x}')$ with $\mathfrak{x}' \in \mathfrak{v}$ because of *e*).

2) By « macroscopic causality » we understand the following concept: Let us consider states $\bar{\Phi}^\Sigma(\mathfrak{v})$, which describe a system of interacting particles confined to the region $\mathfrak{v}$ on $\sigma(\Sigma)$. $\bar{\Phi}^\Sigma(\mathfrak{v}) = V(\sigma(\Sigma))\, \Phi^\Sigma(\mathfrak{v})$ with the « free » $\Phi^\Sigma(\mathfrak{v})$ as introduced above. The system will now develop causally in time (time co-ordinate refers to Σ), if

$$(\bar{\Phi}^{\Sigma_1}(\mathfrak{v}_1);\ \bar{\Phi}^{\Sigma_2}(\mathfrak{v}_2)) \approx 0 \tag{2.20}$$

where Σ_2 arises from Σ_1 by time translation, and $\mathfrak{v}_2 \subset \sigma(\Sigma_2)$ lies outside the light cone spreading from $\mathfrak{v}_1 \subset \sigma(\Sigma_1)$.

It can be proved easily for our interaction, that (2.20) is satisfied except for regions $\mathfrak{v}_2$ of order of Compton wavelength immediately near the light cone of $\mathfrak{v}_1$. The proof consists of tyree steps. First we express the operators creating $\bar{\Phi}^{\Sigma_1}(\mathfrak{v}_1)$ from Φ_0 by the free $\chi_M(\Sigma_1|\mathfrak{x})$, where mainly $\mathfrak{x} \in \mathfrak{v}_1$, using condition c); secondly $\chi_M(\Sigma_1|\mathfrak{x})$ can be expanded in the well known manner in $\chi_M(\Sigma_2|\mathfrak{x}')$, $\mathfrak{x}' \in \sigma(\Sigma_2)$ within the light cone of $\mathfrak{x} \in \sigma(\Sigma_1)$; at last we re-express $\chi_M(\Sigma_2\,\mathfrak{x}')$ by $\bar{\chi}_M(\Sigma_2\,\mathfrak{x}'')$ or $\bar{e}_M(\Sigma_2\,\mathfrak{x}'')$, using c) again. This behaviour seems to differ from that of non-local theories of the Kristensen-Møller type [11] discussed some years ago, for which it was proved by Stückelberg and Wanders [12], that also macroscopically acausal effects exist. The reason for this difference lies in the concept of locality, which in our case depends on the σ-plane, wherein observations are made.

As $V(\sigma) = \exp[iT(\sigma)]$ introduces the interaction and so may be regarded as the starting point of the theory, we ask for its simplest form satisfying all conditions and warranting an S-matrix $S \neq 1$. In analogy to the non-relativistic case we put (P_ν = total energy-momentum, α additional parameters)

$$(2.20)\qquad (\Phi^{\Sigma_0}_{P'_\nu\alpha'}|\,T(\sigma_0)\,|\,\Phi^{\Sigma_0}_{P_\nu\alpha}) = \\ = \frac{\delta(\mathfrak{p}'-\mathfrak{p})}{P'_0-P_0-i\varepsilon}\,\tau_+(P'_\nu\alpha';\,P_\nu\alpha) - \frac{\delta(\mathfrak{p}'-\mathfrak{p})}{P'_0-P_0+i\varepsilon}\,\tau_-(P'_\nu\alpha';\,P_\nu\alpha)\,.$$

If we write $U(L)\Phi^{\Sigma_0}_{P_\nu\alpha} = \Phi^{L\Sigma_0}_{P_\nu\alpha} = \Phi^{\Sigma_0}_{L[P_\nu\alpha]}$, the following conditions have to be fulfilled by $\tau_\pm(P'_\nu\alpha';\,P_\nu\alpha)$:

$$(2.21)\qquad \tau_\pm(L[P'_\nu\alpha'];\,L[P_\nu,\alpha]) = \tau_\pm(P'_\nu\alpha';\,P_\nu\alpha) \qquad \text{for } L = L(\sigma_0)$$

corresponding to (2.9). Furthermore, $\tau_-(P'_\nu\alpha';\,P_\nu\alpha)$ must be regular at $P'_0 = P_0$ and such, that $T(\sigma) \Rightarrow T_\pm$ for $\sigma \to \pm\infty$ (including $V(\sigma) \Rightarrow U_\pm = \exp[iT_\pm]$), where

$$(2.22)\qquad (\Phi^{\Sigma_0}_{P'_\nu\alpha'}|\,T_\pm\,|\,\Phi^{\Sigma_0}_{P_\nu\alpha}) = 2\pi i\,\delta^4(P'-P)\,\tau_\pm(P'_\nu\alpha';\,P_\nu\alpha)$$

and $\tau_\pm(L[P'_\nu\alpha'];\,L[P_\nu,\alpha]) = \tau_\pm(P'_\nu\alpha';\,P_\nu\alpha)$ for all $L \in \mathfrak{L}$ and $P'_\nu = P_\nu$, corresponding to (2.15).

If we express $T(\sigma_0)$ in the momentum creation and annihilation operators

[11] P. Kristensen and C. Møller: *Dan. Mat. Fys. Medd.*, **27**, no. 7 (1952).
[12] E. C. G. Stueckelberg and G. Wanders: *Helv. Phys. Acta*, **27**, 667 (1954).

$a_M(\Sigma_0|k)$ of the «free» fields $\chi_M(\Sigma_0|x)$, it will consists of terms of the form:

$$\int a^{\dagger}_{M_i}(\Sigma_0|k_i)\ldots a^{\dagger}_{M_1}(\Sigma_0|k_1)\cdot \tag{2.23}$$

$$\cdot\frac{\delta\left(\sum_1^i \mathfrak{k}-\sum_1^j \mathfrak{k}'\right)}{\sum_1^j k_0-\sum_1^j k'_0\pm i\varepsilon}\,\vartheta^{M_1\ldots N_j}_{\mp}(k_1\ldots k'_j)\,a_{N_1}(\Sigma_0|k'_1)\ldots a_{N}(\Sigma_0|k'_j)\,\mathrm{d}m_1\ldots\mathrm{d}m'_j\,.$$

with $\mathrm{d}m=\mathrm{d}^3k/k_0$. (2.21), (2.22) are carried over to $\vartheta^{M_1\ldots N_j}_{\mp}(k_1\ldots k'_j)$ and on the right side at least two annihilation operators must appear to satisfy (2.10). $T(\sigma)$ given, the question of quasilocality can be decided in principle. We have to express (2.23) by the Newton-Wigner operators $e_M(\Sigma_0,\mathfrak{x})$, $e^{\dagger}_M(\Sigma_0\,\mathfrak{x}')$ belonging to the «free» fields $\chi_M(\Sigma_0|x)$ and try to verify (2.19). It will be easy to regard additional conservation laws for the interacting system: If in $\mathfrak{H}$ a representation of $\mathfrak{L}\times\mathfrak{G}$ is given and the interaction has to be invariant under the transformations of $\mathfrak{G}$, it suffices to choose $V(\sigma)$ so, that

$$[V(\sigma);\ U(G)]=0 \qquad \text{for all } G\in\mathfrak{G}. \tag{2.24}$$

* * *

I should like to thank Professor Ludwig, Dr. Doebner and Dr. Berendt for their interest and many valuable discussions. Mr. Rosenthal I thank for revising the manuscript.

RIASSUNTO (*)

Si discute un gruppo di assiomi per la teoria quantistica dei campi che in alcuni punti differiscono da quelli di Lehmann-Symanzik-Zimmermann, pur presentando anch'essi l'invarianza rispetto alle trasformazioni di Lorentz, la condizione asintotica e la causalità. Punto di partenza è la teoria canonica dei campi non relativistica che viene riportata in modo determinato al caso relativistico. Per il teorema di Haag è necessario per far ciò generalizzare il concetto del campo causale locale.

(*) *Traduzione a cura della Redazione.*

IL NUOVO CIMENTO Vol. XIX, N. 2 16 Gennaio 1961

Theoretical Calculation of the Solar Diurnal Variation of the Cosmic Ray Intensity (*).

K. NAGASHIMA (**), V. R. POTNIS (***) and M. A. POMERANTZ

Bartol Research Foundation of the Franklin Institute - Swarthmore, Penn.

(ricevuto il 12 Settembre 1960)

Summary. — By formulating an expression for the anisotropy of the primary cosmic ray intensity, the expected solar diurnal variation of the intensity of the nucleonic component of the cosmic radiation at sea level is calculated at various geomagnetic latitudes and longitudes for the following cases: (*a*) the anisotropy is produced outside the terrestrial magnetic field (extra-terrestrial origin), and (*b*) the anisotropy is produced inside the terrestrial magnetic field (terrestrial origin). In this calculation, the orientational difference between the earth's rotational and the geomagnetic dipole axes is considered. The present expression for the anisotropy, Δf, contains three parameters, m, n and P_i. The parameter, m, determines the rigidity dependence of Δf in the expression, $\Delta f \propto P^{-m}$. The parameter, n, determines the directional dependence of Δf in momentum space with respect to the plane parallel to the geomagnetic or geographic equator in the expression $\Delta f \propto (\cos\theta)^n$, where θ is the angle between the plane and the direction mentioned above. P_i is a definite value of rigidity, for rigidities smaller than which Δf is zero. This expression for the anisotropy could easily be utilized in terms of any description of the model of production of the anisotropy by the appropriate choice of these three parameters. It is also possible to determine the most suitable values of these parameters by the comparison of the calculated and observed diurnal variations. The geographic local time of the maximum intensity shows a geomagnetic longitudinal dependence for both terrestrial and extra-terrestrial origins. On the other hand, the amplitude shows a longitudinal dependence at latitudes higher than 50°, only for the extra-terrestrial origin. At latitudes lower than 50°, there is no significant difference between the diurnal variations expected from the terrestrial and extra-terrestrial origins. The altitude correction factors of the diurnal variation of the nucleonic component are obtained. These factors are nearly independent of the geomagnetic longitude of the observational station.

(*) This work was supported in part by the National Science Foundation and the Office of Naval Research.

(**) On leave of absence from the Department of Physics, Nagoya University, Japan.

(***) Pre-ent address: Lashkar (M.P.), India.

1. – Introduction.

It has been suggested by ELLIOT and DOLBEAR (1) that the acceleration and deceleration mechanism of the solar stream, proposed by ALFVÉN (2) to explain the cosmic ray origin and Forbush type decrease, causes the solar diurnal variation of cosmic ray intensity (extra-terrestrial origin). Subsequently, more detailed theoretical investigations of the diurnal variation were made by several authors: ALFVÉN (3), BRUNBERG and DATTNER (4), DORMAN and FEINBERG (5), DORMAN (6) and one of the present authors (7). Taking into account the solar general magnetic dipole field, BRUNBERG and DATTNER (4) calculated the anisotropy of cosmic ray intensity produced by the solar stream. DORMAN (6) and one of the present authors (7) studied the anisotropy caused by an ordered magnetic field frozen in the solar stream, and calculated the diurnal variation in the earth's atmosphere expected from the anisotropy.

These calculations of the diurnal variation in the atmosphere were made by neglecting the orientational difference between the earth's rotational and the geomagnetic dipole axes. In the geomagnetic co-ordinates system, the asymptotic orbit of a negatively-charged particle ejected vertically from the earth is defined by its geomagnetic latitude, A_N (northward positive), and the eastward rotational angle, Ψ_E, of its meridian plane from the one including the observational station, S, (cf. Fig. 1*a*). These quantities are independent of the geomagnetic longitude of the observational station. If we translate A_N and Ψ_E from the geomagnetic to the geographic co-ordinate system, then these translated quantities depend on geomagnetic longitude, even at the same geomagnetic latitude. Thus, if the direction of the maximum anisotropy lies in the geographic meridian plane, the amplitude and the geographic local time of the maximum intensity would be different at different stations which are located at the same geomagnetic latitude but at different longitudes. Hence, the orientational difference between the magnetic and the rotational axes should be taken into account in the calculation of the diurnal variation.

The expression for the anisotropy used here contains three parameters, and could easily be utilized in terms of any theory of the origin of the anisotropy

(1) H. ELLIOT and D. W. DOLBEAR: *Journ. of Atmos. Terr. Phys.*, **1**, 205 (1951).
(2) H. ALFVÉN: *Phys. Rev.*, **75**, 1732 (1949); *Cosmical Electrodynamics* (Oxford, 1950).
(3) H ALFVÉN: *Tellus*, **6**, 232 (1954).
(4) E. A BRUNBERG and A. DATTNER: *Tellus*, **6**, 254 (1954).
(5) L. I. DORMAN and E. L. FEINBERG: *Memoria del V Congreso Internacional de radiacion cosmica*, Mexico, 1955, p. 393 (1958); *Suppl. Nuovo Cimento*, **8**, 379 (1958).
(6) L. I. DORMAN: *Cosmic Ray Variations* (Moscow, 1957).
(7) K. NAGASHIMA: *Memoria del V Congreso Internacional de Radiacion Cosmica*, Mexico, 1955, p. 349 (1958); *Journ. Geomag. Geoelectr.*, **7**, 51 (1955).

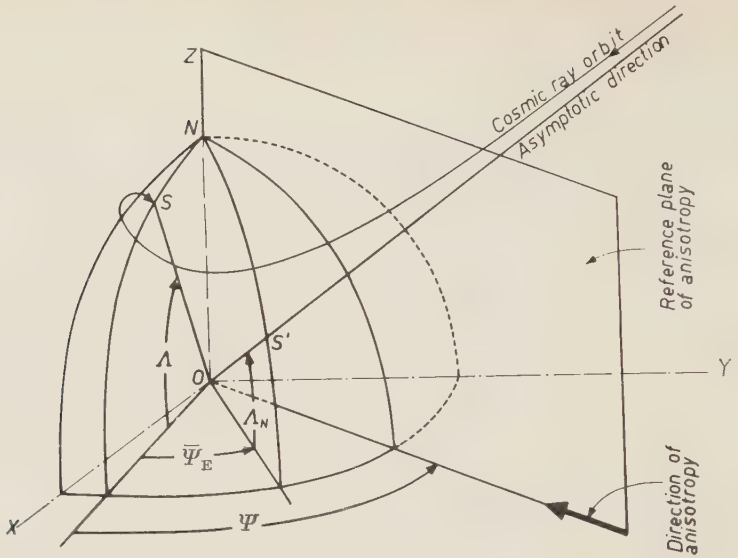

Fig. 1*a*. – Geomagnetic co-ordinates system in position space.

by the appropriate choice of these parameters. It is also possible to find the most suitable values of these parameters by the direct comparison between the observed and calculated diurnal variations. Calculations of the diurnal

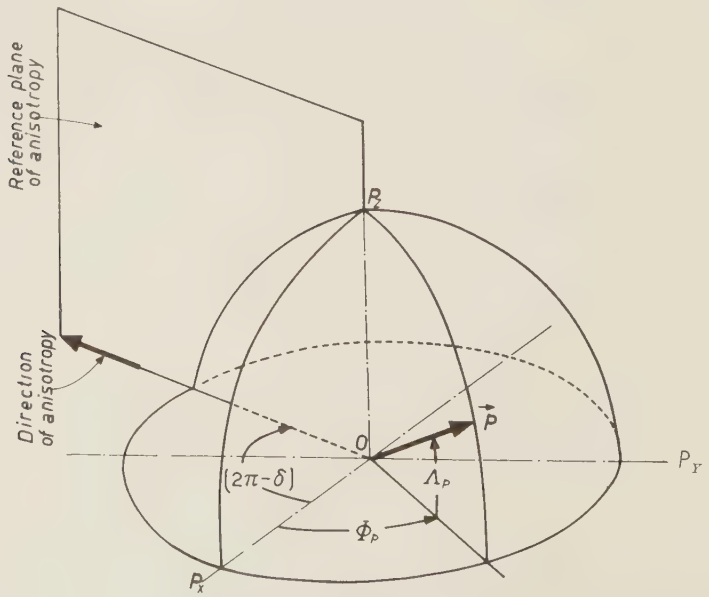

Fig. 1*b*. – Co-ordinates system in momentum space.

variation, in which the orientational difference of the magnetic and the rotational axes was considered, were made independently by MURAKAMI [8].

On the basis of directional measurements of the solar diurnal variation of μ-mesons at sea level, ELLIOT and ROTHWELL [9] suggested that the anisotropy might be produced by some modulation effect in the earth's magnetic field (terrestrial origin). Similar measurements were conducted by PARSONS and FENTON [10] and PARSONS [11] to compare the terrestrial and extra-terrestrial origin hypotheses, and there was no definite conclusion in favor of the former. Moreover, no theoretical basis for the terrestrial origin has been proposed thus far. Yet it was considered worthwhile for further comparison with experimental results to calculate the expected diurnal variations for this case, under the assumption that the direction of maximum anisotropy would lie in the geomagnetic meridian plane.

2. – Terrestrial origin.

Two different mechanisms might give rise to the diurnal variation in this case. The first is characterized by an anisotropic distribution of cosmic ray intensity in momentum space and a uniform distribution of the intensity in the position space; and the second by an isotropic distribution in momentum space and a non-uniform distribution of intensity in the position space. Only the former case will be discussed in this paper.

Let $f(p)\,\mathrm{d}p$ and $f_D(\boldsymbol{p})\,\mathrm{d}p$ be the directional differential momentum spectra of primary cosmic rays in the normal and disturbed states respectively, where f is independent of the direction of motion but f_D is not. To specify $\boldsymbol{p}$, we define the following co-ordinates: one axis (p_Z) parallel to the geomagnetic dipole axis, and the other two (p_X, p_Y) parallel to the geomagnetic equatorial plane, as shown in Fig. 1*b*. In this co-ordinate system, $\boldsymbol{p}$ can be expressed in terms of three quantities p, Λ_p and Φ_p (cf. Fig. 1*b*).

The deviation of the directional intensity in the disturbed state from that in the normal state is given by

$$\Delta f(p, \Lambda_p, \Phi_p) = f_D(\boldsymbol{p}) - f(p)\,, \tag{1}$$

In general, Δf can be expanded in spherical harmonics, as follows,

$$\Delta f = \sum_{n,\,m} \{A_{nm}(p)\cos(m\Phi_p) + B_{nm}(p)\sin(m\Phi_p)\} P_n^m(\cos\Lambda_p)\,, \tag{2}$$

---

(8) K. MURAKAMI: private communication.
(9) H. ELLIOT and P. ROTHWELL: *Phil. Mag.*, **1**, 669 (1956).
(10) N. R. PARSONS and A. G FENTON: *Suppl. Nuovo Cimento*, **8**, 313 (1958).
(11) N. R. PARSONS: *Austr. Journ. Phys.*, **10**, 462 (1957).

where A_{nm} and B_{nm} are functions of p, and P_n^m is the associated Legendre function of the 1st kind. For the computation of the diurnal variation, only the terms of $m = 1$ are required in the above equation. These terms can be written as follows,

$$\Delta f(p, \Lambda_p, \Phi_p) = g(p, \Lambda_p) \cos\{\Phi_p - \delta(p, \Lambda_p)\}, \tag{3}$$

where $\delta(p, \Lambda_p)$, the phase angle, is in general a function of p and Λ_p, but is here assumed for simplicity to be independent of these quantities. The direction $\Phi_p = \delta$ gives the maximum deviation of intensity at the same value of Λ_p and lies in a meridian plane through the p_z-axis. Hereafter this plane is referred to as the reference plane of anisotropy. The direction which is determined by the intersection between the reference plane of anisotropy and the plane of $\Lambda_p = 0$ is called the direction of anistropy, as shown in Fig. 1*b*. Finally, we choose the following formula for Δf to simplify the calculation of the diurnal variation:

$$\Delta f(p, \Lambda_p, \Phi_p) = \alpha_0 f(p)(p_0/p)^m (\cos\Lambda_p)^n \cos(\Phi_p - \delta), \tag{4}$$

where m and n are constant numbers and p_0 is a definite value of momentum. α_0 is the value of the ratio $\Delta f/f$ at $p = p_0$, $\Lambda_p = 0$ and $\Phi_p = \delta$. (Note that m and n in eq. (2) are different from those used in eq. (4) and all the subsequent equations.)

So far, we have represented Δf in terms of momentum, p, but hereafter for convenience, rigidity P will be used instead of p. It is assumed that all the cosmic rays of different charges (Z) have the same form of anisotropy as defined by eq. (4) depending only on their rigidity, P.

We introduce one more parameter, P_i, which restricts Δf as follows,

$$\begin{cases} \Delta f(P, \Lambda_p, \Phi_p) & \text{is given by eq. (4), if } P \geqslant P_i, \\ \Delta f(P, \Lambda_p, \Phi_p) & = 0, \quad \text{if } P < P_i. \end{cases} \tag{5}$$

By a proper choice of these three parameters m, n and P_i in eq. (4) and (5), it is possible to express easily the anisotropy expected from a particular theory.

If Ψ is the angle between the meridian plane including S and the reference plane of anisotropy, as shown in Fig. 1*a*, then the ratio of the excess intensity, ΔI, produced by the anisotropy of eq. (4) to the intensity, I, in the normal state at S is

$$D \equiv \Delta I/I = (\alpha_0/I) \sum_Z \int_{P_c}^{\infty} \eta_Z(P, x) f_Z(P, x)(P_0/P)^m (\cos\Lambda_N)^n \cos(\Psi - \Psi_E)\, dP, \tag{6}$$

where I at an atmospheric depth x g/cm^2 is given by

$$I = \sum_Z \int_{P_c}^{\infty} y_Z(P, x) f_Z(P) \, \mathrm{d}P \,. \tag{7}$$

In eq. (6) and (7), P_c is the magnetic cut-off rigidity at S, and $y_Z(P, x)$ and $f_Z(P)$ are the specific yield function at x and the differential rigidity spectrum of the primary cosmic radiation of atomic number Z, respectively.

In the case of terrestrial origin, the place where the anisotropy is produced is at a finite distance from the earth, therefore, strictly speaking, it is not correct to use the values of Φ_E and Λ_N for the asymptotic orbit as the quantities which determine the deflection angles of cosmic ray between the source and the earth. However, if it is assumed that the source is located in the earth's magnetic field far from the earth's surface, and most of the deflection experienced by a cosmic ray occurs between the source and the earth, we can use the values for the asymptotic orbit as an approximation.

Under these assumptions for the anisotropy and for the deflection angles, the diurnal variations expected from the terrestrial origin are the same as those from the extra-terrestrial origin in which the orientational difference of the earth's magnetic and rotational axes is neglected. Thus, by comparing the diurnal variations expected from the terrestrial origin with those from the extra-terrestrial origin discussed in the following section, it is possible to check the validity of neglecting the orientational difference, mentioned above.

Considering eq. (7), eq. (6) can be transformed as follows,

$$D = \alpha_0 A \cos\left(\Psi - \langle \Psi_E \rangle\right) , \tag{8}$$

where

$$A = \sqrt{C^2 + S^2}; \qquad \langle \Psi_E \rangle = \mathrm{tg}^{-1}(S/C) , \tag{9}$$

and

$$\begin{Bmatrix} C(m, n, P_i) \\ S(m, n, P_i) \end{Bmatrix} = I^{-1} \int_{P_c}^{\infty} \{\mathrm{d}I(P, x)/\mathrm{d}P\} (P_0/P)^m (\cos \Lambda_N)^n \begin{Bmatrix} \cos \Psi_E \\ \sin \Psi_E \end{Bmatrix} \mathrm{d}P \,. \tag{10}$$

As is seen in eq. (8), the maximum value of D occurs when the relative position of S with respect to the reference plane of anisotropy satisfies the condition $\Psi = \langle \Psi_E \rangle$, which is referred to as the average deflection angle of cosmic rays. $\langle \Psi_E \rangle$ has the following relation with the geomagnetic local time ([12])

([12]) A. G. McNish: *Terr. Mag.*, **41**, 37 (1936); S. Chapman and J. Bartels: *Geomagnetism* (Oxford, 1940), p. 646.

of the maximum intensity, T_{max},

$$\langle \Psi_E \rangle_{S_1} - \langle \Psi_E \rangle_{S_2} = 15\{T_{max}(S_2) - T_{max}(S_1)\}\,, \tag{11}$$

where S_1 and S_2 denote the two observational stations.

For the calculations of A and $\langle \Psi_E \rangle$, we adopt the values of Ψ_E and A_N obtained by BRUNBERG and DATTNER ([13]) for the high rigidity region, and by DWIGHT ([14]) and FIROR ([15]) for the low rigidity region. These are combined in Fig. 2*a* and 2*b*. For the function dI/dP, we use the values obtained by WEBBER and QUENBY ([16]).

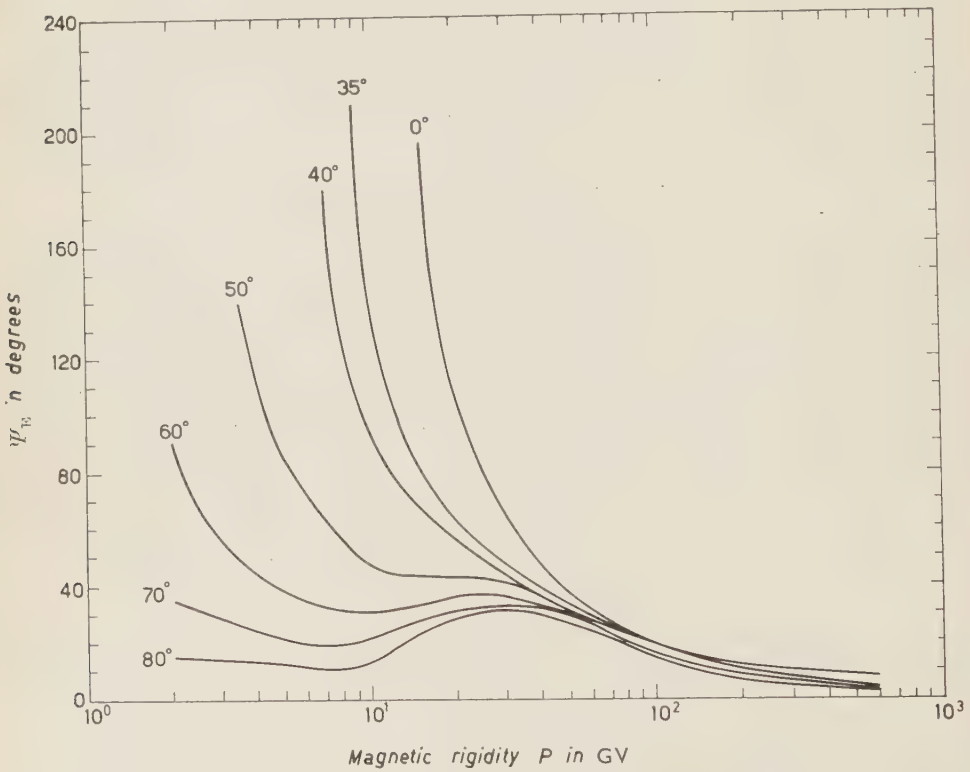

Fig. 2*a*. – Ψ_E of the asymptotic orbit of the cosmic ray for vertical incidence as a function of rigidity obtained by combining those in references ([13-15]). Geomagnetic latitude of the observational station is attached to each curve.

([13]) E. A. BRUNBERG and A. DATTNER: *Tellus*, **5**, 135, 269 (1953).
([14]) K. DWIGHT: *Phys. Rev.*, **78**, 40 (1950).
([15]) J. FIROR: *Phys. Rev.*, **94**, 1017 (1954).
([16]) W. R. WEBBER and J. J. QUENBY: *Phil. Mag.*, **4**, 654 (1959).

The calculations of A and $\langle \Psi_E \rangle$ for the nucleonic component at sea level were made for the following cases: $\Lambda = 0°$, 35°, 40°, 50°, 60°, 70°, 80°; $m = 0, 1, 2$; $n = 1, 2, 4$; and $P_i = 0, 5, 10$ (GV); where Λ is the geomagnetic latitude of the observational station. Three values for each of the parameters m, n and P_i were chosen to allow the interpolation or extrapolation of the diurnal variation in terms of these parameters.

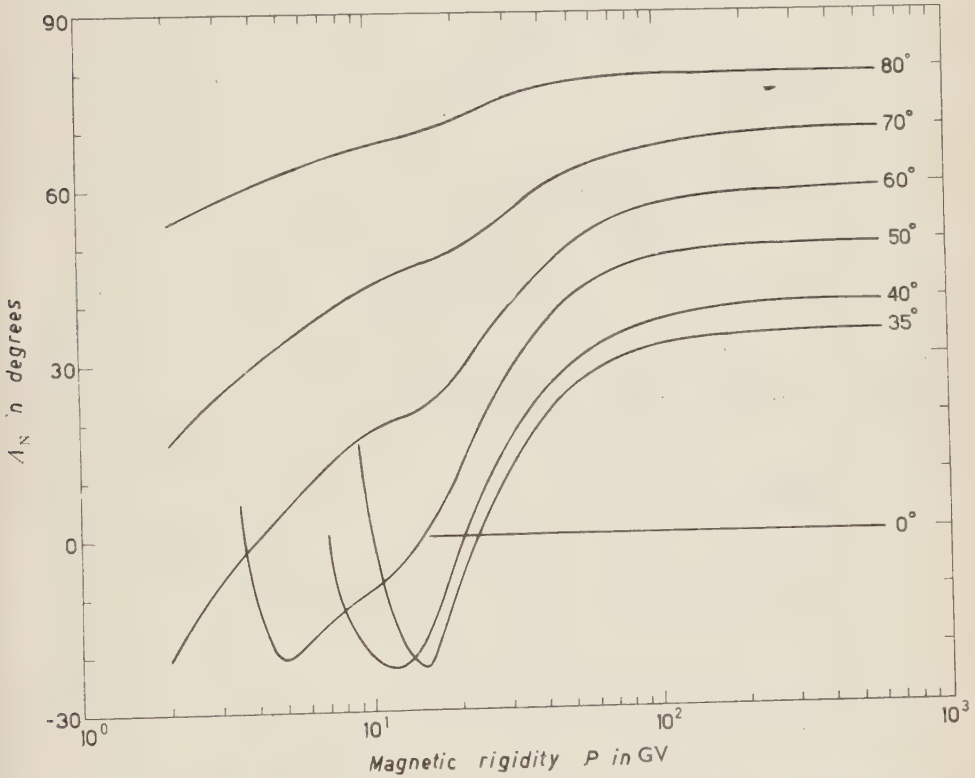

Fig. 2*b*. – A_N of the asymptotic orbit of the cosmic ray for vertical incidence as a function of rigidity obtained by combining those in references [13-15]. Geomagnetic latitude of the observational station is attached to each curve.

In these calculations, we adopted 10 GV for the value of P_0 and used the values of Ψ_E and A_N for $P = 600$ GV over the region $600 < P < \infty$. The effect of this rigidity interval upon the diurnal variation cannot be neglected for the small value of m. We neglected the integration of eq. (10) between $P_i < P < P_l$, where P_l is the lowest limit of rigidity for which values of Ψ_E and A_N are available (cf. Fig. 2). The errors introduced by this approximation will be estimated later.

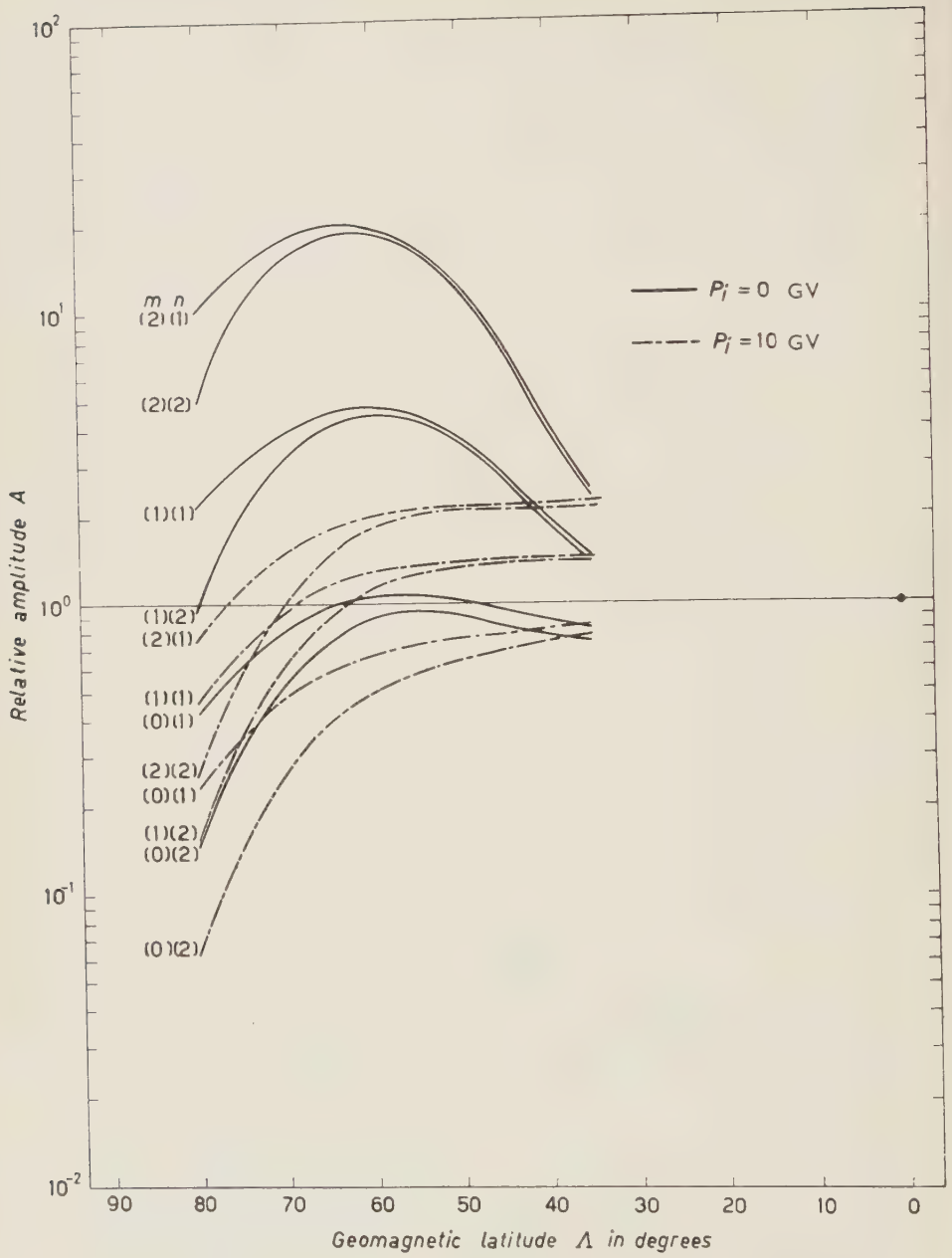

Fig. 3*a*. – Amplitude, A, normalized at the geomagnetic equator, as a function of the geomagnetic latitude, for the case of terrestrial origin. Three parameters m, n and P_i are shown in the figure.

In the rigidity region, $P_i \leqslant P \leqslant 600$ GV, the Newton-Cotes formula was employed for the integration (*) by choosing the subintervals, ΔP, as follows:

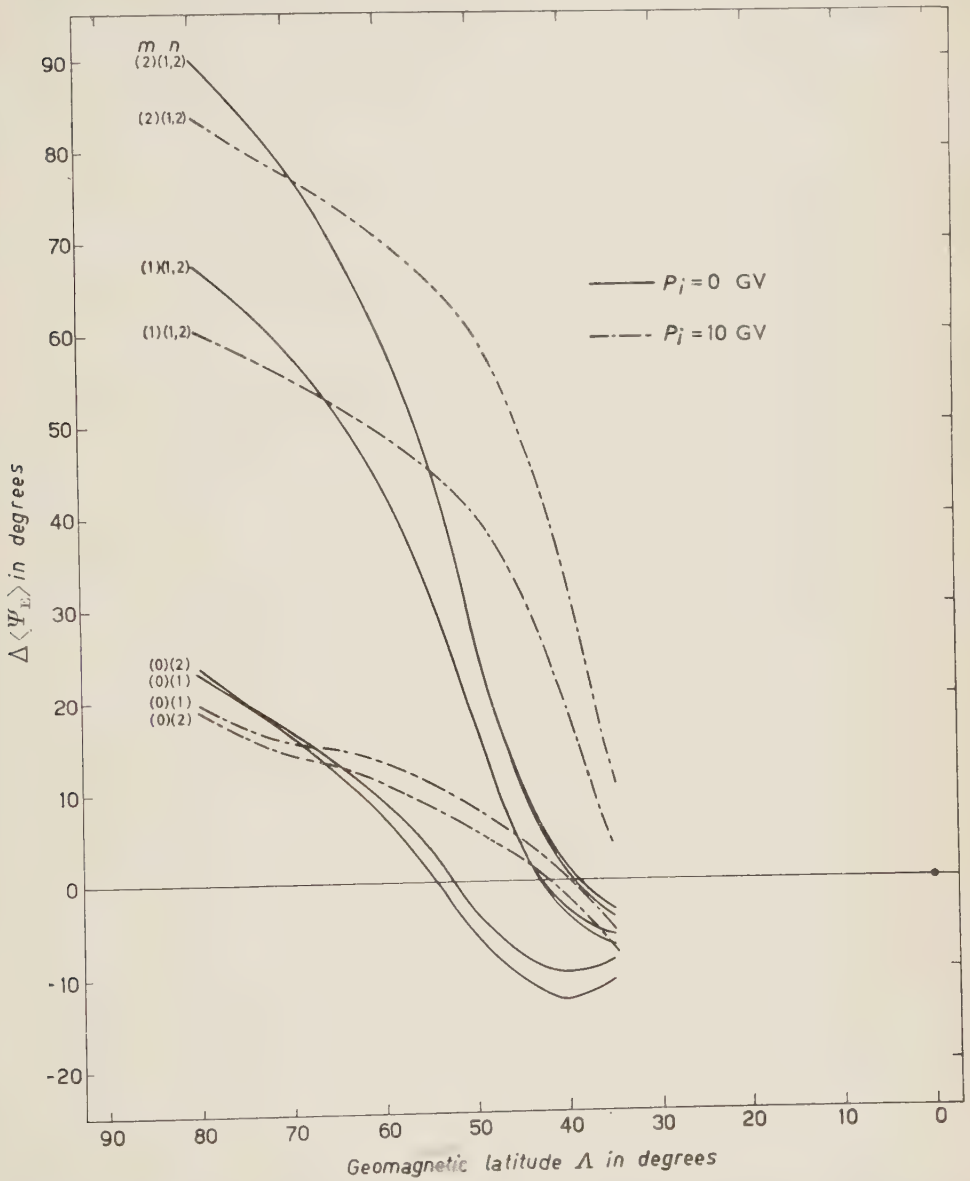

Fig. 3*b*. – $\Delta\langle\Psi_E\rangle = \langle\Psi_E\rangle_{\Lambda=0} - \langle\Psi_E\rangle_\Lambda$, as a function of the geomagnetic latitude, for the case of terrestrial origin. Three parameters m, n and P_i are shown in the figure.

(*) The integration was performed on UNIVAC no 1 of the Franklin Institute Computing Center.

TABLE Ia. – *Amplitude A and average deflection angle $\langle\Psi_E\rangle$, in degrees, for P_i=0 GV, based on the terrestrial origin.*

	G.M. Lat. Λ	m=0		m=1		m=2	
		A	$\langle\Psi_E\rangle$	A	$\langle\Psi_E\rangle$	A	$\langle\Psi_E\rangle$
	0	0.75	39	0.15	82	0.062	104
	35	0.62	48	0.23	88	0.16	107
	40	0.65	50	0.31	86	0.27	102
n=1	50	0.77	43	0.58	65	0.79	78
	60	0.79	30	0.73	38	1.23	43
	70	0.61	23	0.61	24	1.13	25
	80	0.31	16	0.33	14	0.63	13
	0	0.75	39	0.15	82	0.062	104
	35	0.57	50	0.22	89	0.15	108
	40	0.58	52	0.30	86	0.25	103
n=2	50	0.68	45	0.56	65	0.76	78
	60	0.66	32	0.69	38	1.21	43
	70	0.40	23	0.48	24	0.96	25
	80	0.11	16	0.15	14	0.30	13
	0	0.75	39	0.15	82	0.062	104
	35	0.48	55	0.21	90	0.14	109
	40	0.48	57	0.27	87	0.23	104
n=4	50	0.57	50	0.52	65	0.71	78
	60	0.52	34	0.64	39	1.16	44
	70	0.21	24	0.32	24	0.70	26
	80	0.017	14	0.030	13	0.073	14

TABLE Ib. – *Amplitude A and average deflection angle* $\langle \Psi_E \rangle$, *in degrees, for* $P_i = 5$ GV, *based on the terrestrial origin.*

	G.M. Lat. Λ	$m=0$		$m=1$		$m=2$	
		A	$\langle \Psi_E \rangle$	A	$\langle \Psi_E \rangle$	A	$\langle \Psi_E \rangle$
$n=1$	0	0.75	39	0.15	82	0.062	104
	35	0.62	48	0.23	88	0.16	107
	40	0.65	50	0.31	86	0.27	102
	50	0.75	39	0.49	54	0.54	61
	60	0.70	28	0.49	33	0.55	33
	70	0.53	22	0.38	22	0.44	21
	80	0.26	17	0.20	15	0.23	13
$n=2$	0	0.75	39	0.15	82	0.062	104
	35	0.57	50	0.22	89	0.15	108
	40	0.58	52	0.30	86	0.25	103
	50	0.66	42	0.47	54	0.52	60
	60	0.57	30	0.46	33	0.53	33
	70	0.33	23	0.28	22	0.34	21
	80	0.085	16	0.077	14	0.097	13
$n=4$	0	0.75	39	0.15	82	0.062	104
	35	0.48	55	0.21	90	0.14	109
	40	0.48	57	0.27	87	0.23	104
	50	0.54	45	0.44	55	0.49	60
	60	0.43	32	0.41	33	0.50	33
	70	0.15	23	0.15	21	0.20	20
	80	0.011	15	0.013	13	0.017	12

TABLE Ic. – *Amplitude A and average deflection angle* $\langle \Psi_E \rangle$, *in degrees, for* $P_i = 10$ GV, *based on the terrestrial origin.*

	G.M. Lat. Λ	$m=0$		$m=1$		$m=2$	
		A	$\langle \Psi_E \rangle$	A	$\langle \Psi_E \rangle$	A	$\langle \Psi_E \rangle$
	0	0.75	39	0.15	82	0.062	104
	35	0.64	45	0.23	78	0.14	92
	40	0.63	39	0.23	62	0.14	70
$n=1$	50	0.57	31	0·22	42	0.14	43
	60	0.50	26	0.20	32	0.12	33
	70	0.36	24	0.15	27	0.092	26
	80	0.18	20	0.072	22	0.047	20
	0	0.75	39	0.15	82	0.062	104
	35	0.59	47	0.22	79	0.14	92
	40	0.56	42	0.21	62	0.13	70
$n=2$	50	0.48	34	0.21	42	0.13	43
	60	0.37	28	0.17	33	0.11	33
	70	0.20	25	0.095	27	0.063	26
	80	0.048	20	0.024	21	0.016	20
	0	0.75	39	0.15	82	0.062	104
	35	0.50	51	0·20	80	0.13	93
	40	0.45	45	0.19	62	0.12	69
$n=4$	50	0.37	38	0.19	43	0.13	44
	60	0.24	31	0.14	33	0.10	32
	70	0.072	26	0.042	26	0.029	25
	80	0.0045	21	0.0028	20	0.0020	19

$\Delta P = 0.5$ GV for the rigidity region $P \leqslant 20$ GV; $\Delta P = 2$ for $20 \leqslant P \leqslant 30$; $\Delta P = 5$ for $30 \leqslant P \leqslant 60$; $\Delta P = 10$ for $60 \leqslant P \leqslant 100$; and $\Delta P = 100$ for $100 \leqslant P \leqslant 600$.

The results are given in Tables I*a*, I*b* and I*c*. For particular cases, the latitude dependence of A, normalized at the equator, and of $\Delta\langle\Psi_E\rangle = \langle\Psi_E\rangle_{A=0} - \langle\Psi_E\rangle_A$ are shown in Fig. 3*a* and 3*b*, respectively. Table II, which supplements Table I, provides the values of A and $\langle\Psi_E\rangle$ at the equator for $P_i = 20$, 30 GV, $m = 0, 1$ and any value of n. This allows the interpolation or extrapolation of A and $\langle\Psi_E\rangle$ in terms of P_i at the equator.

TABLE II. – *Amplitude, A, and average deflection angle, $\langle\Psi_E\rangle$, in degrees, at $A=0°$ for $P_i=20$ and 30 GV based on the terrestrial origin.*

m	$P_i = 20$ GV		$P_i = 30$ GV	
	A	$\langle\Psi_E\rangle$	A	$\langle\Psi_E\rangle$
0	0.65	38	0.55	27
1	0.13	59	0.079	38
2	0.041	71	0.016	45

3. – Extra-terrestrial origin.

We take the geographic co-ordinates as those of the position space and define new co-ordinates in momentum space, one axis (p_z) of which is parallel to the earth's rotational axis, and the other two (p_x, p_y) parallel to the geographic equatorial plane. In this co-ordinate system (p_x, p_y, p_z), momentum $\boldsymbol{p}$ is expressed in terms of three quantities ρ, λ_p and η_p. The definition of λ_p and η_p is similar to that of A_p and Φ_p for the terrestrial origin (cf. Fig. 1*b*).

Under the same assumption as in the case of terrestrial origin, we use the form for the anisotropy given by eq. (4) which is now referred to the new co-ordinates. Then the reference plane and the direction of anisotropy defined in the previous section are parallel to the earth's rotational axis and to the geographic equatorial plane, respectively.

However, for the case of the extra-terrestrial origin, the anisotropy is produced in the solar system, and thus could be represented by a simpler form in the heliographic co-ordinate system rather than in the geographic co-ordinate system defined above. If we use the form for the anisotropy given by eq. (4) which is now referred to the heliographic co-ordinates, the reference plane and the direction of anisotropy are parallel to the heliographic meridian plane and to the heliographic equatorial plane, respectively. However, as far as the diurnal variation is concerned, this form for the anisotropy defined in the heliographic co-ordinates is equivalent to the same form defined in the geo-

graphic co-ordinates. The only difference between these two forms appears in the difference of the values of α_0 and n. This will be discussed in the Appendix. Consequently, in the following, we use the form for the anisotropy given by eq. (4) which is defined in the geographic co-ordinates (p_x, p_y, p_z).

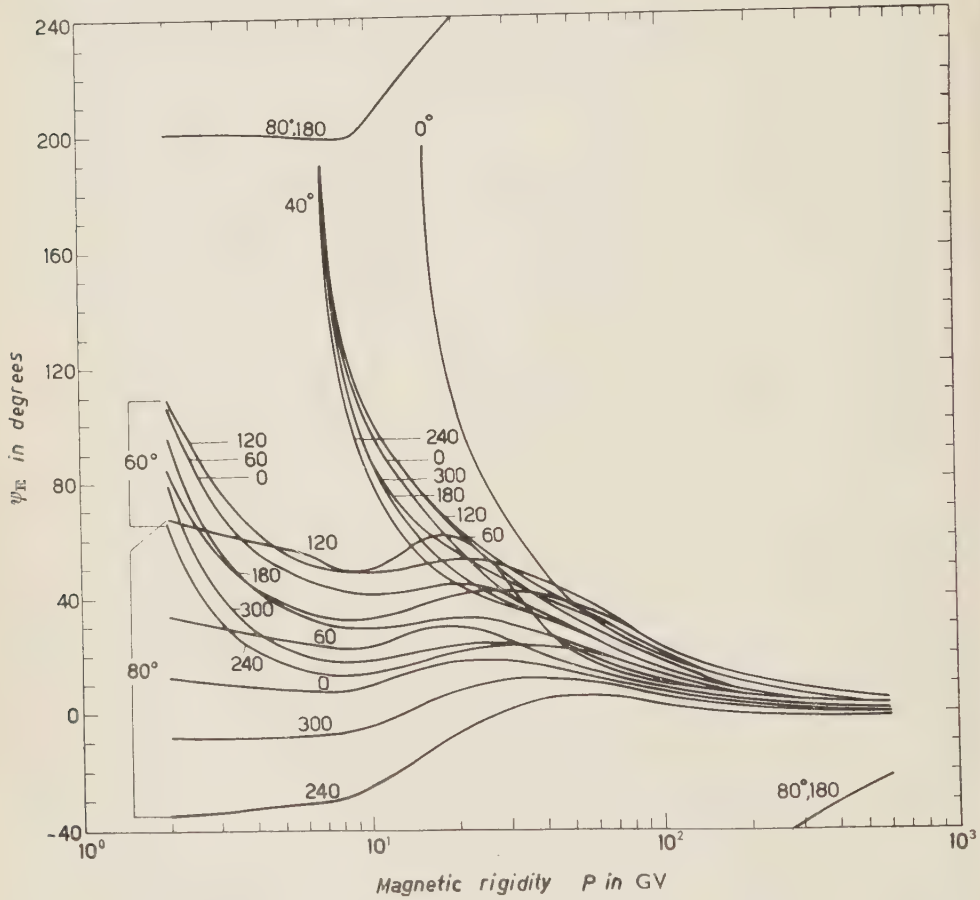

Fig. 4*a*. – ψ_E of the asymptotic orbit of the cosmic ray for vertical incidence as a function of rigidity. Geomagnetic latitude and longitude of the observational station are attached to each group of curves and on each curve, respectively.

In order to calculate the diurnal variation produced by this anisotropy, it is necessary to use the geographic representation (ψ_E, λ_N) of the asymptotic orbit. λ_N and ψ_E are the geographic latitude of the asymptotic orbit (measured northward positive), and the rotational angle of its geographic meridian plane with respect to the geographic meridian plane including the observation station, S (measured eastward positive). These are obtained by a transformation of Ψ_E and Λ_N from geomagnetic to geographic co-ordinates. In this trans-

formation, $\lambda = 78.5°$ N, and $\varphi = 291°$ E were used as the geographic position of the geomagnetic north pole. The results ([17]) are shown in Fig. 4*a*, 4*b*, 4*c* and 4*d*, in which we can see the geomagnetic longitudinal dependence of ψ_E and λ_N at the same geomagnetic latitude.

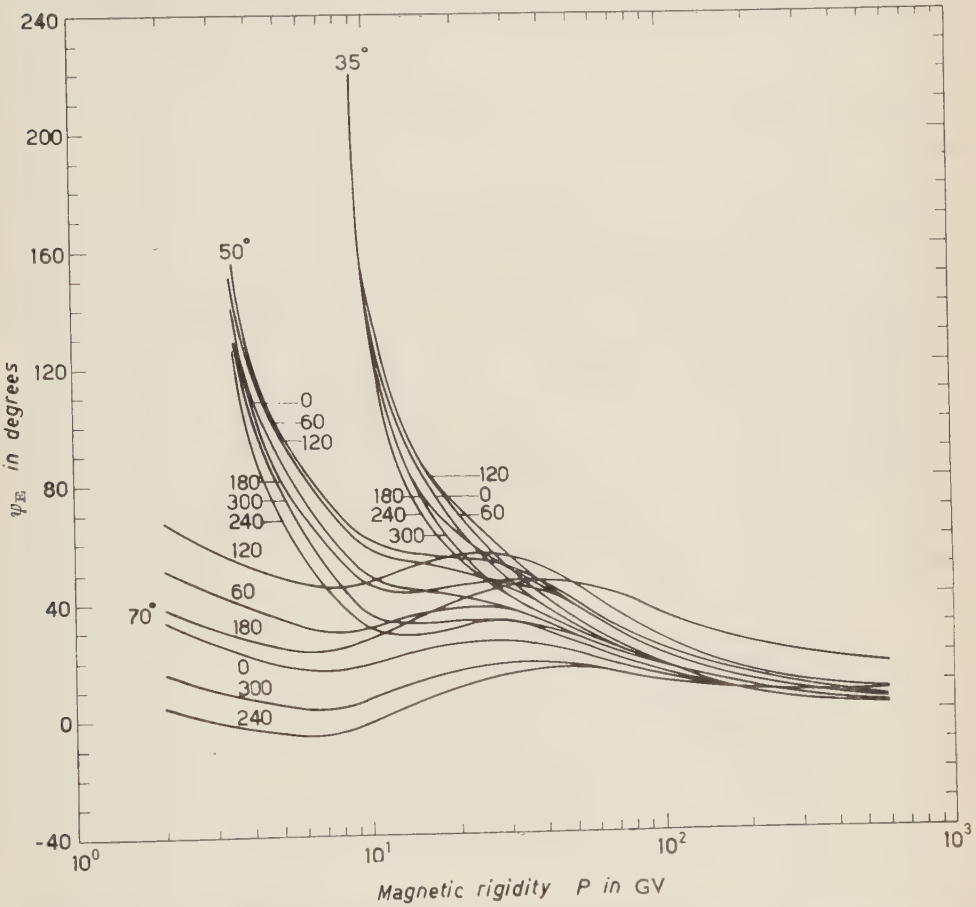

Fig. 4*b*. – ψ_E of the asymptotic orbit of the cosmic ray for vertical incidence as a function of rigidity. Geomagnetic latitude and longitude of the observational station are attached to each group of curves and on each curve, respectively.

Using the quantities defined above, we obtain the following equation representing the diurnal variation which is quite similar to eq. (8).

$$D = \alpha_0 a \cos(\psi - \langle \psi_E \rangle) , \tag{12}$$

([17]) The same results have been plotted in a different manner on the global diagram for specific stations by BRUNBERG. E. A. BRUNBERG: *Tellus*, **8**, 215 (1960).

where

$$a = \sqrt{c^2 + s^2}; \qquad \langle \psi_E \rangle = \mathrm{tg}^{-1}(s/c)\,, \tag{13}$$

and

$$\begin{Bmatrix} c(m, n, P_i) \\ s(m, n, P_i) \end{Bmatrix} = I^{-1} \int_{P_c}^{\infty} \{\mathrm{d}I(P, x)/\mathrm{d}P\}(10/P)^m (\cos \lambda_N)^n \begin{Bmatrix} \cos \psi_E \\ \sin \psi_E \end{Bmatrix} \mathrm{d}P\,. \tag{14}$$

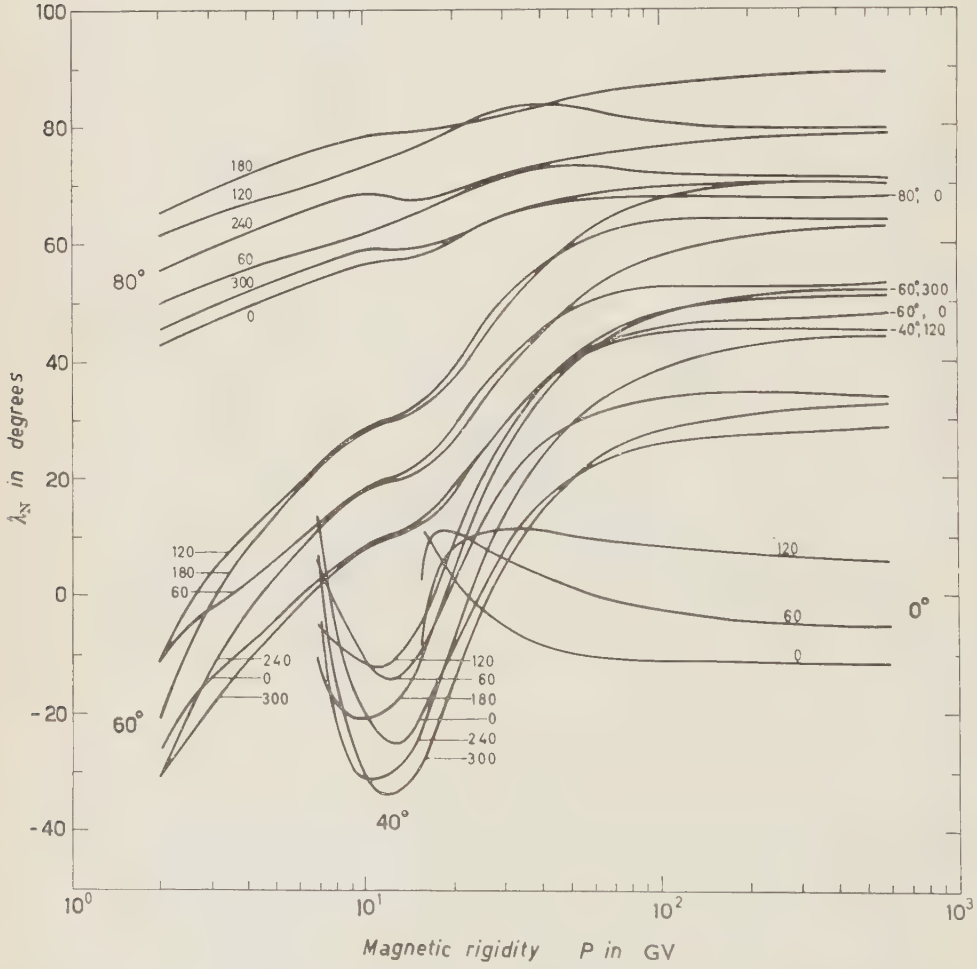

Fig. 4c. – λ_N of the asymptotic orbit of the cosmic ray for vertical incidence as a function of rigidity. Geomagnetic latitude and longitude of the observational station are attached to each group of curves and on each curve, respectively.

In eq. (12) ψ is an angle between the geographic meridian plane including S and the reference plane of anisotropy. ψ_E is the average deflection angle

of cosmic rays and has the following relation with the geographic local time of the maximum intensity of the diurnal variation, t_{max},

$$\langle \psi_E \rangle_{S_1} - \langle \psi_E \rangle_{S_2} = 15\{t_{max}(S_2) - t_{max}(S_1)\}\,, \tag{15}$$

where S_1 and S_2 denote the two observational stations. These defintions of ψ and $\langle \psi_E$ are similar to those of Ψ and $\langle \Psi_E$ for the terrestrial origin (cf. Fig. 1*a* and Section 2).

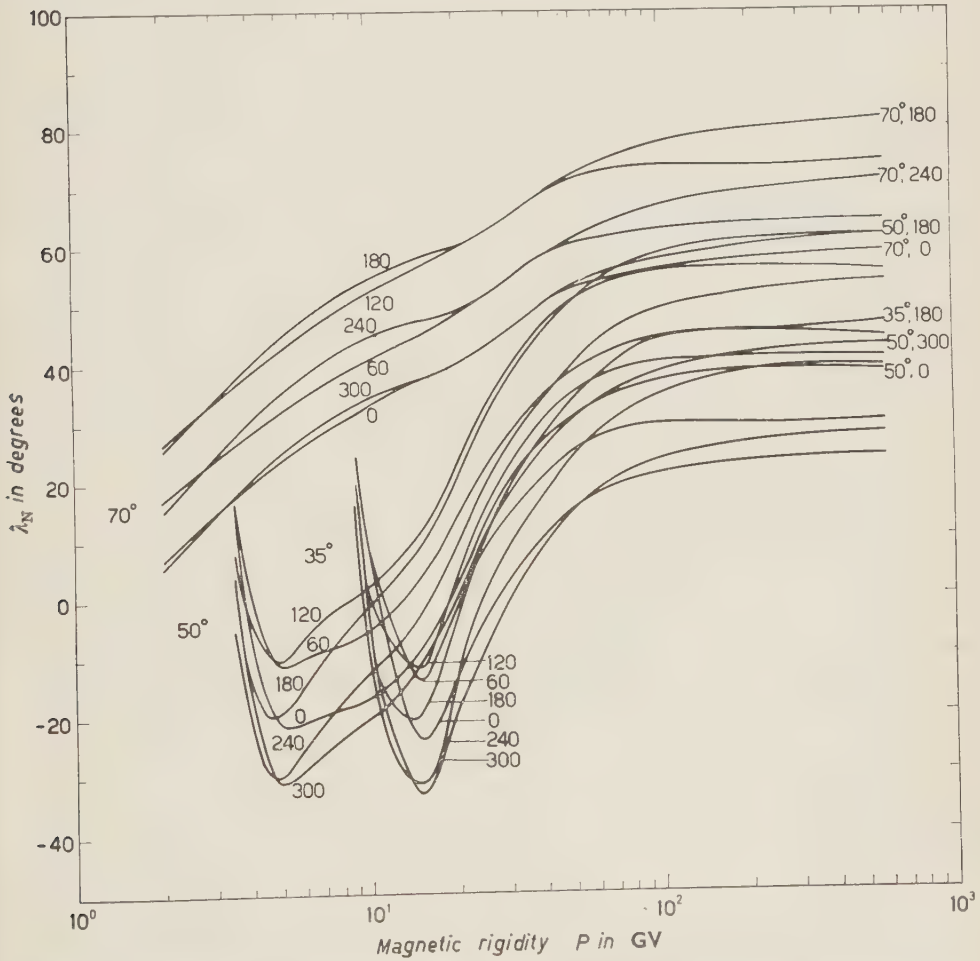

Fig. 4*d*. – λ_N of the asymptotic orbit of the cosmic ray for vertical incidence as a function of rigidity. Geomagnetic latitude and longitude of the observational station are attached to each group of curves and on each curve, respectively.

As mentioned in the previous section, owing to a finite distance between the earth and the source where the anisotropy is produced, the values of λ_N

and Ψ_E for the asymptotic orbit were used in eq. (6) as an approximation to express the deflection angle of a cosmic ray particle between the source and the earth. On the contrary, for the present case, the distance between the source and the earth can safely be assumed to be infinite, so eq. (12) holds exactly.

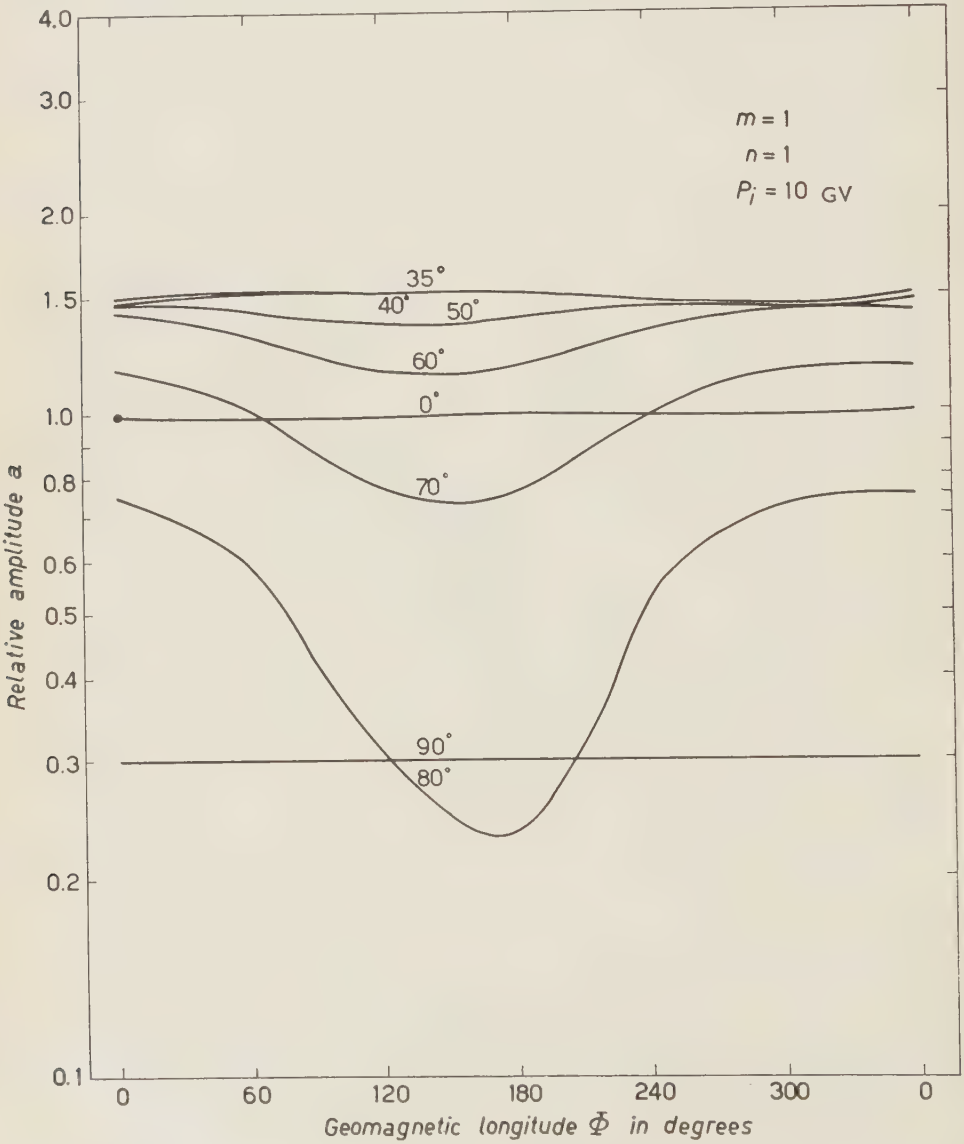

Fig. 5*a* – Amplitude, a, normalized at $\Lambda=0°$ and $\Phi=0°$, as a function of the geomagnetic longitude for $m=1$, $n=1$ and $P_i=10$ GV, based on the extra-terrestrial origin. Geomagnetic latitude of the observational station is attached on each curve.

Using the same approximations as in the previous section, the amplitude, a, and the average deflection angle, $\langle \psi_E \rangle$, for the nucleonic component at sea level were calculated for the following cases: $A = 0°$, $35°$, $40°$, $50°$, $60°$, $70°$,

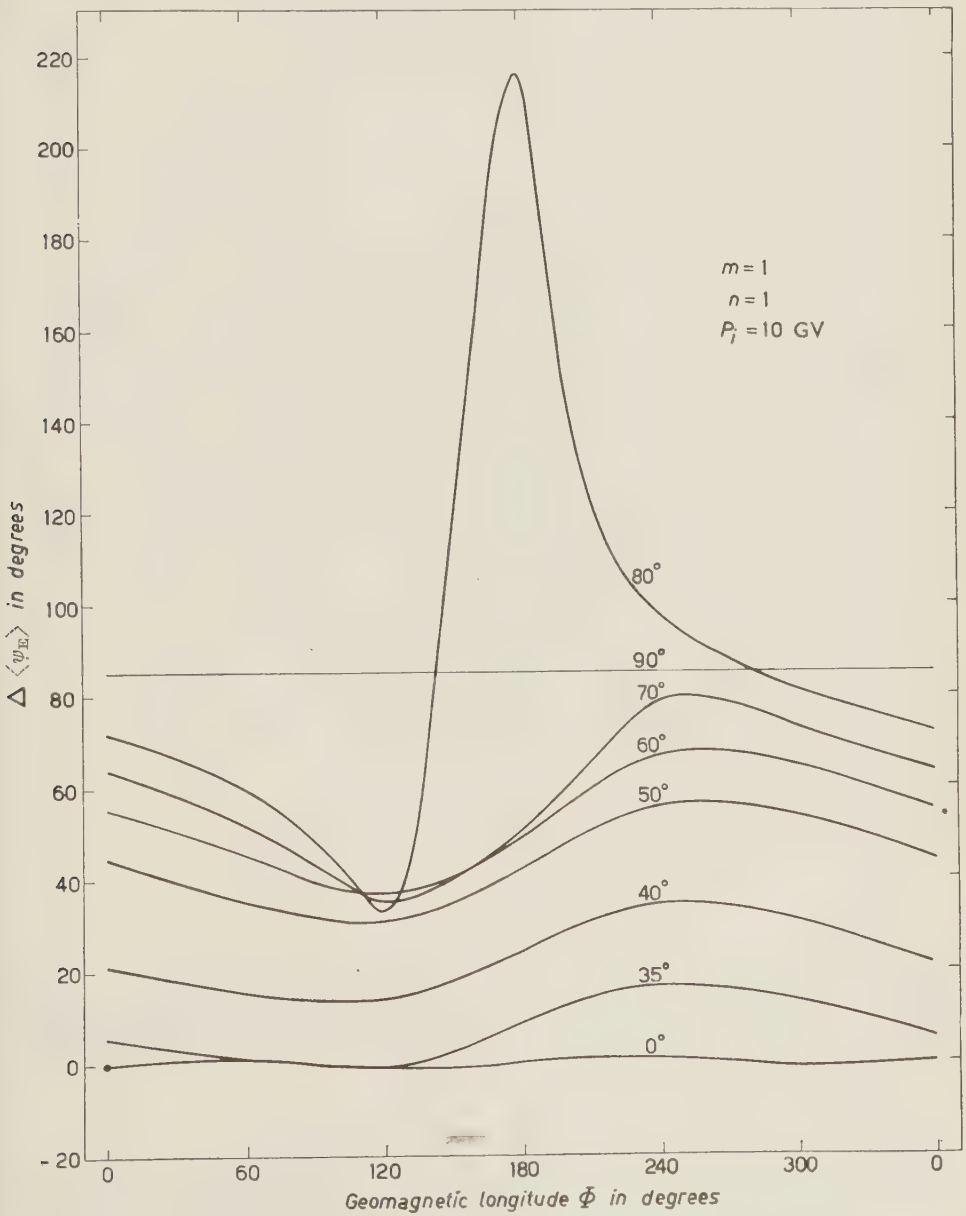

Fig. 5*b*. – $\Delta\langle\psi_E\rangle = \langle\psi_E\rangle_{A=0,\,\Phi=0} - \langle\psi_E\rangle_{A,\,\Phi}$, as a function of the geomagnetic longitude for $m=1$, $n=1$ and $P_i=10$ GV, based on the extra-terrestrial origin. Geomagnetic latitude of the observational station is attached on each curve.

80°, 90°; $\Phi = 0°$, 60°, 120°, 180°, 240°, 300°; $m = 0$, 1, 2; $n = 1$, 2, 4; and $P_i = 0$, 5, 10 (GV), where Λ and Φ are the geomagnetic latitude and longitude of the observational station, respectively. The results are given in Tables III*a*, *b*, *c*,

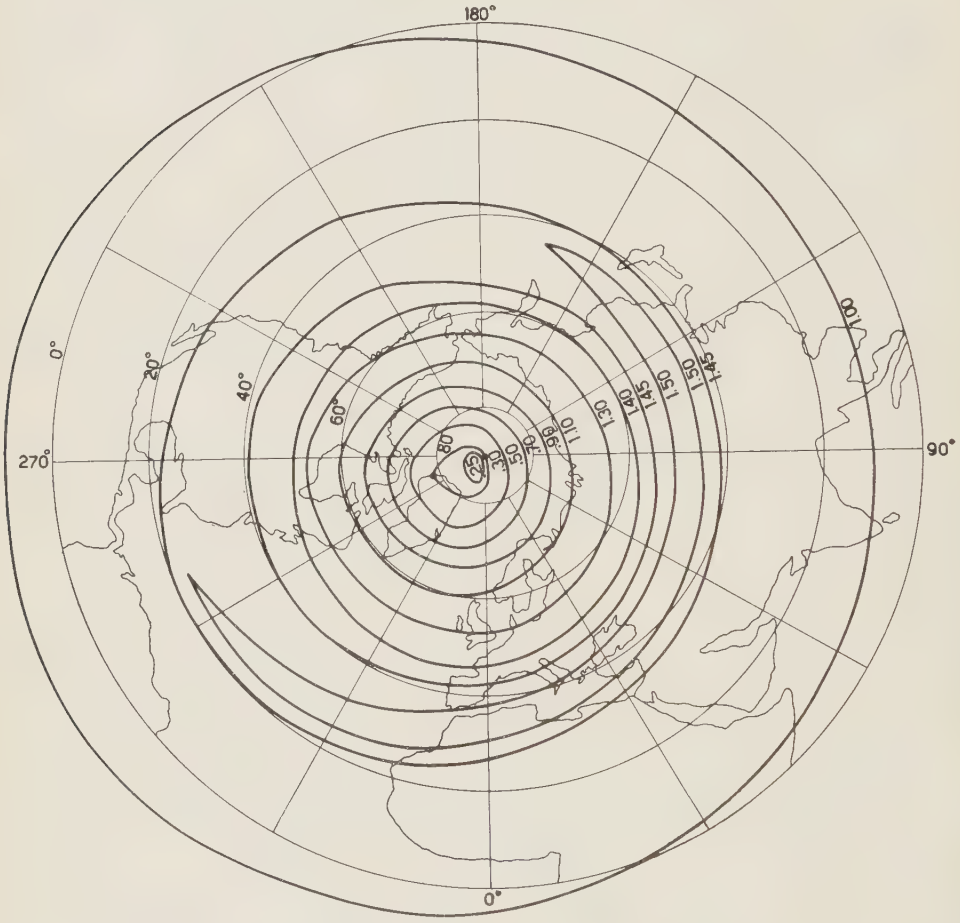

Fig. 6*a* – Distributon of the amplitude, *a*, normalized at $\Lambda = 0°$ and $\Phi = 0°$, on the geographic polar map for $m = 1$, $n = 1$, and $P_i = 10$ GV, based on the extra-terrestrial origin. Thick and thin lines represent contours of equal amplitude and geographic co-ordinates, respectively.

IV*a*, *b*, *c* and V*a*, *b*, *c*, which are limited to the northern hemisphere. The diurnal variation in the southern hemisphere at the geomagnetic latitude Λ_s and longitude Φ_s is equal to that in the northern hemisphere at $\Lambda = -\Lambda_s$ and $\Phi = \Phi_s \pm 180°$.

Table II computed for the terrestrial origin is applicable also in this case

as a supplement to Tables III, IV and V, because there are no differences between A and a and between $\langle \Psi_{E} \rangle$ and $\langle \psi_{E} \rangle$ at low latitudes (cf. Tables I, III, IV and V).

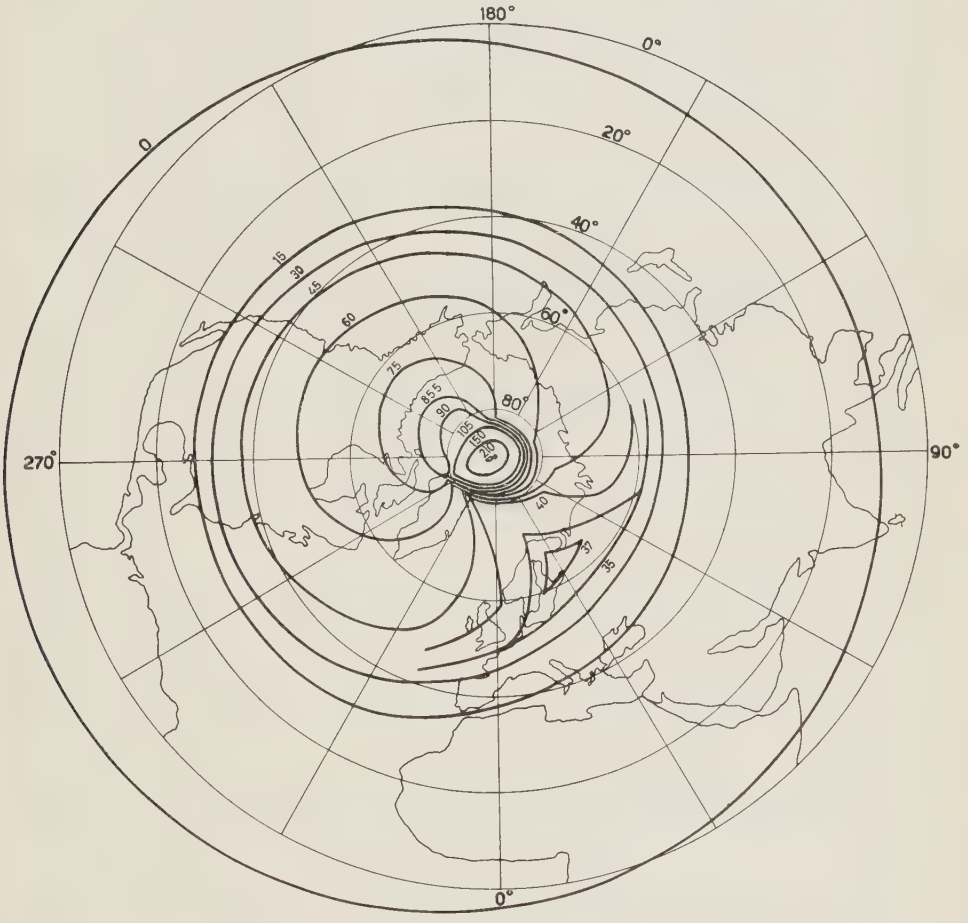

Fig. 6*b*. – Distributon of $\Delta\langle\psi_{E}\rangle = \langle\psi_{E}\rangle_{\Lambda=0,\,\Phi=0} - \langle\psi_{E}\rangle_{\Lambda,\,\Phi}$, on the geographic polar map for $m=1$, $n=1$ and $P_i=10$ GV, based on the extra-terrestrial origin. Thick and thin lines represent contours of equal value of $\Delta\langle\psi_{E}\rangle$, in degree and geographic co-ordinates, respectively.

As an example, the geomagnetic longitudinal dependence of amplitude a, normalized at $\Lambda = 0°$ and $\Phi = 0°$, and of $\Delta\langle\psi_{E}\rangle = \langle\psi_{E}\rangle_{\Lambda=0,\,\Phi=0} - \langle\psi_{E}\rangle_{\Lambda,\,\Phi}$ is shown in Fig. 5*a* and 5*b* respectively, for the case $m = 1$, $n = 1$ and $P_i = 10$ GV. The distributions of these normalized values on the geographic polar maps are shown in Fig. 6*a* and 6*b* for the same case.

TABLE III-*a*. – *Amplitude a, and average deflection angle,* $\langle\psi_E\rangle$, *in degrees, for* $P_i = 0$ GV *and* $m = 0$, *based on the extra-terrestrial origin.*

	G.M. Long. →	0		60		120		180		240		300	
	G.M. Lat. ↓	a	$\langle\psi_E\rangle$	a	$\langle\psi_E\rangle$	a	$\langle\psi_E\rangle$	a	$\langle\psi_E\rangle$	a	$\langle\psi_E\rangle$	a	$\langle\psi_E\rangle$
	0	0.75	41	0.76	39	0.74	40	0.75	41	0.76	39	0.75	40
	35	0.64	46	0.61	50	0.57	55	0.59	51	0.63	43	0.65	42
	40	0.66	48	0.63	53	0.60	58	0.62	53	0.66	42	0.67	43
$n=1$	50	0.80	41	0.76	49	0.71	55	0.73	46	0.78	33	0.81	34
	60	0.86	28	0.79	37	0.69	46	0.69	35	0.79	17	0.86	19
	70	0.74	19	0.65	29	0.49	45	0.46	31	0.61	4	0.73	10
	80	0.49	10	0.40	21	0.22	46	0.13	−140	0.32	−15	0.46	0
	90	0.20	0	0.20	0	0.20	0	0.20	0	0.20	0	0.20	0
	0	0.74	41	0.75	39	0.73	40	0.74	41	0.75	39	0.73	40
	35	0.61	47	0.57	52	0.51	60	0.51	56	0.56	45	0.60	43
	40	0.62	49	0.59	56	0.53	64	0.53	57	0.57	44	0.61	43
$n=2$	50	0.73	43	0.69	52	0.62	60	0.62	58	0.68	34	0.72	35
	60	0.77	29	0.67	40	0.54	50	0.54	37	0.67	18	0.77	20
	70	0.57	19	0.44	31	0.28	48	0.25	30	0.40	2	0.55	9
	80	0.25	10	0.17	22	0.059	49	0.031	−149	0.12	−18	0.22	0
	90	0.040	0	0.040	0	0.040	0	0.040	0	0.040	0	0.040	0
	0	0.72	41	0.75	39	0.71	40	0.72	41	0.75	39	0.71	40
	35	0.56	48	0.50	57	0.42	69	0.41	64	0.46	48	0.52	44
	40	0.55	51	0.51	62	0.44	73	0.42	64	0.45	47	0.51	44
$n=4$	50	0.62	46	0.59	58	0.52	66	0.52	54	0.55	36	0.59	36
	60	0.65	31	0.53	44	0.39	54	0.39	39	0.53	18	0.64	21
	70	0.37	20	0.24	33	0.11	50	0.098	29	0.20	0	0.35	9
	80	0.072	10	0.036	24	0.0059	55	0.0021	−156	0.017	−23	0.058	−2
	90	0.0016	0	0.0016	0	0.0016	0	0.0016	0	0.0016	0	0.0016	0

TABLE III-*b*. – *Amplitude a, and average deflection angle,* $\langle\psi_E\rangle$, *in degrees, for* P_i 0 GV *and* $m=1$, *based on the extra-terrestrial origin.*

	G.M. Long. →	0		60		120		180		240		300	
	G.M. Lat. ↓	a	$\langle\psi_E\rangle$	a	$\langle\psi_E\rangle$	a	$\langle\psi_E\rangle$	a	$\langle\psi_E\rangle$	a	$\langle\psi_E\rangle$	a	$\langle\psi_E\rangle$
$n=1$	0	0.15	86	0.15	84	0.15	86	0.15	86	0.15	84	0.15	86
	35	0.23	89	0.23	94	0.23	96	0.23	87	0.22	79	0.22	83
	40	0.31	88	0.32	93	0.32	94	0.31	83	0.30	74	0.29	80
	50	0.57	67	0.59	76	0.59	79	0.59	64	0.57	49	0.56	55
	60	0.75	38	0.73	50	0.69	58	0.70	41	0.74	21	0.75	26
	70	0.69	21	0.63	35	0.53	51	0.51	29	0.61	— 1	0.68	8
	80	0.46	10	0.39	26	0.25	56	0.19	—154	0.32	—27	0.44	4
	90	0.16	0	0.16	0	0.16	0	0.16	0	0.16	0	0.16	0
$n=2$	0	0.15	86	0.15	84	0.15	87	0.15	86	0.15	84	0.15	87
	35	0.22	89	0.23	95	0.22	98	0.22	88	0.21	80	0.21	83
	40	0.30	88	0.31	94	0.31	96	0.29	84	0.27	74	0.27	80
	50	0.55	67	0.58	76	0.57	80	0.56	64	0.53	49	0.51	55
	60	0.73	38	0.70	51	0.63	59	0.64	42	0.71	20	0.73	25
	70	0.61	21	0.51	36	0.37	51	0.35	28	0.48	1	0.60	8
	80	0.28	10	0.20	26	0.086	57	0.052	—156	0.14	—28	0.25	—5
	90	0.031	0	0.031	0	0.031	0	0.031	0	0.031	0	0.031	0
$n=4$	0	0.15	86	0.14	84	0.14	87	0.15	86	0.14	84	0.14	87
	35	0.21	89	0.22	96	0.21	100	0.20	90	0.18	80	0.18	84
	40	0.27	89	0.30	96	0.29	98	0.26	85	0.22	74	0.22	81
	50	0.50	67	0.55	77	0.55	80	0.53	64	0.47	48	0.44	54
	60	0.70	38	0.65	52	0.55	60	0.56	42	0.65	20	0.69	25
	70	0.48	21	0.35	36	0.19	52	0.18	28	0.31	— 2	0.47	8
	80	0.10	10	0.056	27	0.012	59	0.0047	—158	0.027	30	0.083	—6
	90	0.0012	0	0.0012	0	0.0012	0	0.0012	0	0.0012	0	0.0012	0

TABLE III-*c*. – *Amplitude a, and average deflection angle,* $\langle\psi_E\rangle$, *in degrees, for* $P_i = 0$ GV *and* $m = 2$, *based on the extra-terrestrial origin.*

	G.M. Long. →	0		60		120		180		240		300	
	G.M. Lat. ↓	a	$\langle\psi_E\rangle$	a	$\langle\psi_E\rangle$	a	$\langle\psi_E\rangle$	a	$\langle\psi_E\rangle$	a	$\langle\psi_E\rangle$	a	$\langle\psi_E\rangle$
	0	0.062	104	0.061	104	0.062	106	0.062	104	0.061	104	0.062	106
	35	0.16	108	0.16	113	0.16	114	0.15	105	0.15	98	0.15	103
	40	0.27	105	0.27	110	0.27	110	0.26	99	0.25	91	0.25	98
$n=1$	50	0.79	81	0.81	89	0.81	91	0.80	76	0.76	62	0.74	69
	60	1.27	46	1.27	58	1.24	66	1.25	46	1.28	25	1.26	31
	70	1.24	22	1.15	38	1.00	53	0.99	29	1.13	— 2	1.23	8
	80	0.89	10	0.74	28	0.50	59	0.40	—158	0.61	—31	0.81	—7
	90	0.27	0	0.27	0	0.27	0	0.27	0	0.27	0	0.27	0
	0	0.062	104	0.060	104	0.061	106	0.062	104	0.060	104	0.061	106
	35	0.15	108	0.15	113	0.16	115	0.15	106	0.14	99	0.14	104
	40	0.26	106	0.27	110	0.27	111	0.25	99	0.22	92	0.23	99
$n=2$	50	0.75	81	0.80	89	0.80	91	0.78	76	0.70	61	0.68	69
	60	1.25	45	1.25	59	1.18	66	1.20	47	1.24	25	1.23	31
	70	1.15	23	0.99	38	0.76	54	0.73	29	0.95	2	1.13	8
	80	0.55	10	0.41	28	0.19	60	0.12	—159	0.28	31	0.49	—7
	90	0.054	0	0.054	0	0.054	0	0.054	0	0.054	0	0.054	0
	0	0.061	104	0.059	103	0.060	106	0.061	104	0.059	103	0.060	106
	35	0.14	108	0.15	113	0.15	116	0.14	107	0.12	101	0.12	105
	40	0.24	107	0.26	111	0.26	112	0.22	99	0.18	94	0.19	102
$n=4$	50	0.68	81	0.78	89	0.79	92	0.73	75	0.60	61	0.56	70
	60	1.21	44	1.21	59	1.09	67	1.11	47	1.18	25	1.16	30
	70	0.99	23	0.75	39	0.46	55	0.43	30	0.69	— 1	0.96	8
	80	0.23	10	0.13	28	0.030	61	0.013	—159	0.063	—32	0.18	—7
	90	0.0021	0	0.0021	0	0.0021	0	0.0021	0	0.0021	0	0.0021	0

TABLE IV-*a*. – *Amplitude a, and average deflection angle,* $\langle\psi_E\rangle$, *in degrees, for* $P_i = 5$ GV *and* $m = 0$, *based on the extra-terrestrial origin.*

	G.M. Long. →	0		60		120		180		240		300	
	G.M. Lat. ↓	a	$\langle\psi_E\rangle$	a	$\langle\psi_E\rangle$	a	$\langle\psi_E\rangle$	a	$\langle\psi_E\rangle$	a	$\langle\psi_E\rangle$	a	$\langle\psi_E\rangle$
$n=1$	0	0.75	41	0.76	39	0.74	40	0.75	41	0.76	39	0.74	40
	35	0.64	46	0.61	50	0.57	55	0.59	51	0.63	43	0.65	42
	40	0.66	48	0.63	53	0.60	58	0.62	53	0.66	42	0.67	43
	50	0.78	37	0.74	45	0.68	51	0.70	43	0.76	29	0.78	30
	60	0.78	25	0.71	34	0.61	43	0.60	33	0.70	16	0.78	18
	70	0.65	18	0.56	28	0.41	43	0.39	31	0.53	5	0.64	10
	80	0.43	10	0.35	20	0.18	41	0.11	−134	0.28	−12	0.41	2
	90	0.18	0	0.18	0	0.18	0	0.18	0	0.18	0	0.18	0
$n=2$	0	0.74	41	0.75	39	0.73	40	0.74	41	0.75	39	0.73	40
	35	0.61	47	0.57	52	0.51	60	0.51	56	0.56	45	0.60	43
	40	0.62	49	0.59	56	0.53	64	0.53	57	0.57	44	0.61	43
	50	0.71	39	0.66	48	0.59	56	0.59	46	0.66	31	0.70	31
	60	0.69	26	0.59	36	0.46	46	0.45	35	0.58	16	0.68	18
	70	0.48	18	0.37	29	0.22	46	0.20	30	0.33	4	0.47	10
	80	0.21	10	0.14	21	0.044	45	0.021	−144	0.094	−15	0.19	1
	90	0.037	0	0.037	0	0.037	0	0.037	0	0.037	0	0.037	0
$n=4$	0	0.72	41	0.75	39	0.71	40	0.72	41	0.75	39	0.71	40
	35	0.56	48	0.50	57	0.42	69	0.41	64	0.46	48	0.52	44
	40	0.55	51	0.51	62	0.44	73	0.42	64	0.45	47	0.51	44
	50	0.60	41	0.56	53	0.48	61	0.49	49	0.53	33	0.57	33
	60	0.57	28	0.45	40	0.30	50	0.31	36	0.44	17	0.56	20
	70	0.29	19	0.18	31	0.074	47	0.063	28	0.15	2	0.27	9
	80	0.054	10	0.026	22	0.0034	50	0.0010	−152	0.012	−18	0.043	−1
	90	0.0015	0	0.0015	0	0.0015	0	0.0015	0	0.0015	0	0.0015	0

TABLE IV-*b*. – *Amplitude a, and average deflection angle,* $\langle\psi_E\rangle$, *in degrees, for* $P_i=5$ GV *and* $m=1$, *based on the extra-terrestrial origin.*

	G.M. Long. →	0		60		120		180		240		300	
	G.M. Lat. ↓	a	$\langle\psi_E\rangle$	a	$\langle\psi_E\rangle$	a	$\langle\psi_E\rangle$	a	$\langle\psi_E\rangle$	a	$\langle\psi_E\rangle$	a	$\langle\psi_E\rangle$
	0	0.15	86	0.15	84	0.15	86	0.15	86	0.15	84	0.15	86
	35	0.23	89	0.23	94	0.23	96	0.23	87	0.22	79	0.22	83
	40	0.31	88	0.32	93	0.32	94	0.31	83	0.30	74	0.29	80
$n=1$	50	0.48	56	0.49	65	0.49	68	0.49	54	0.49	39	0.47	44
	60	0.51	31	0.49	43	0.45	51	0.45	36	0.49	16	0.51	20
	70	0.44	19	0.39	32	0.32	48	0.31	28	0.37	0	0.43	7
	80	0.29	10	0.24	24	0.15	52	0.10	−150	0.20	−23	0.27	−3
	90	0.11	0	0.11	0	0.11	0	0.11	0	0.11	0	0.11	0
	0	0.15	86	0.15	84	0.15	87	0.15	86	0.15	84	0.15	87
	35	0.22	89	0.23	95	0.22	98	0.22	88	0.21	80	0.21	83
	40	0.30	88	0.31	94	0.31	96	0.29	84	0.27	74	0.27	80
$n=2$	50	0.46	56	0.48	65	0.47	69	0.47	54	0.46	39	0.44	44
	60	0.49	31	0.46	43	0.39	51	0.40	36	0.46	16	0.50	20
	70	0.37	19	0.30	32	0.20	47	0.19	27	0.27	1	0.36	7
	80	0.16	10	0.11	24	0.043	53	0.023	−153	0.076	−24	0.14	−3
	90	0.021	0	0.021	0	0.021	0	0.021	0	0.021	0	0.021	0
	0	0.15	86	0.14	84	0.14	87	0.15	86	0.14	84	0.14	87
	35	0.21	89	0.22	96	0.21	100	0.20	90	0.18	80	0.18	84
	40	0.27	89	0.30	96	0.29	98	0.26	85	0.22	74	0.22	81
$n=4$	50	0.42	56	0.46	66	0.45	70	0.44	55	0.41	38	0.37	43
	60	0.47	32	0.41	44	0.31	52	0.32	36	0.42	16	0.47	20
	70	0.27	19	0.18	32	0.085	47	0.072	26	0.15	2	0.25	7
	80	0.051	10	0.026	24	0.0043	53	0.0013	−156	0.012	−25	0.041	−4
	90	0.00083	0	0.00083	0	0.00083	0	0.00083	0	0.00083	0	0.00083	0

TABLE IV-c. – *Amplitude a, and average deflection angle, $\langle\psi_E\rangle$, in degrees, for $P_i=5$ GV and $m=2$, based on the extra-terrestrial origin.*

	G.M. Long. →	0		60		120		180		240		300	
	G.M. Lat. ↓	a	$\langle\psi_E\rangle$	a	$\langle\psi_E\rangle$	a	$\langle\psi_E\rangle$	a	$\langle\psi_E\rangle$	a	$\langle\psi_E\rangle$	a	$\langle\psi_E\rangle$
	0	0.062	104	0.061	104	0.062	106	0.062	104	0.061	104	0.062	106
	35	0.16	108	0.16	113	0.16	114	0.15	105	0.15	98	0.15	103
	40	0.27	105	0.27	110	0.27	110	0.26	99	0.25	91	0.25	98
$n=1$	50	0.53	63	0.55	72	0.56	74	0.55	59	0.53	44	0.51	51
	60	0.57	32	0.55	44	0.52	52	0.52	36	0.56	16	0.57	20
	70	0.50	18	0.45	32	0.38	47	0.36	26	0.43	3	0.49	6
	80	0.33	9	0.28	24	0.18	53	0.13	−156	0.23	−27	0.31	5
	90	0.12	0	0.12	0	0.12	0	0.12	0	0.12	0	0.12	0
	0	0.062	104	0.060	104	0.061	106	0.062	104	0.060	104	0.061	106
	35	0.15	108	0.15	113	0.16	115	0.15	106	0.14	99	0.14	104
	40	0.26	106	0.27	110	0.27	111	0.25	99	0.22	92	0.23	99
$n=2$	50	0.50	63	0.54	72	0.55	75	0.54	59	0.50	44	0.46	50
	60	0.56	32	0.53	44	0.47	52	0.48	36	0.54	16	0.56	20
	70	0.44	18	0.36	32	0.25	47	0.23	25	0.33	− 3	0.42	6
	80	0.19	9	0.14	24	0.057	53	0.031	−157	0.091	−27	0.17	− 5
	90	0.023	0	0.023	0	0.023	0	0.023	0	0.023	0	0.023	0
	0	0.061	104	0.059	103	0.060	106	0.061	104	0.059	103	0.060	106
	35	0.14	108	0.15	113	0.15	116	0.14	107	0.12	101	0.12	105
	40	0.24	107	0.26	111	0.26	112	0.22	99	0.18	94	0.19	102
$n=4$	50	0.45	63	0.53	72	0.54	75	0.51	59	0.44	43	0.38	49
	60	0.55	32	0.50	45	0.40	52	0.40	36	0.51	16	0.55	20
	70	0.33	18	0.23	32	0.12	47	0.097	25	0.19	4	0.31	5
	80	0.066	9	0.035	24	0.0062	54	0.0018	159	0.015	−28	0.051	− 6
	90	0.00091	0	0.00091	0	0.00091	0	0.00091	0	0.00091	0	0.00091	0

TABLE V-*a*. – *Amplitude a, and average deflection angle,* $\langle\psi_E\rangle$, *in degrees, for* $P_i = 10$ GV *and* $m = 0$, *based on the extra-terrestrial origin.*

	G.M. Long. →	0		60		120		180		240		300	
	G.M. Lat. ↓	a	$\langle\psi_E\rangle$	a	$\langle\psi_E\rangle$	a	$\langle\psi_E\rangle$	a	$\langle\psi_E\rangle$	a	$\langle\psi_E\rangle$	a	$\langle\psi_E\rangle$
	0	0.75	41	0.76	39	0.74	40	0.75	41	0.76	39	0.74	40
	35	0.66	43	0.63	48	0.60	52	0.61	48	0.65	40	0.67	40
	40	0.65	38	0.62	43	0.58	47	0.59	43	0.63	33	0.65	33
$n=1$	50	0.61	29	0.57	35	0.50	41	0.50	36	0.57	24	0.61	24
	60	0.57	22	0.51	30	0.42	39	0.41	33	0.50	16	0.57	17
	70	0.47	18	0.39	27	0.27	42	0.25	36	0.37	9	0.46	12
	80	0.31	11	0.24	18	0.12	34	0.064	−114	0.20	−5	0.29	5
	90	0.14	0	0.14	0	0.14	0	0.14	0	0.14	0	0.14	0
	0	0.74	41	0.75	39	0.73	40	0.74	41	0.75	39	0.73	40
	35	0.63	44	0.59	50	0.52	56	0.53	52	0.58	41	0.62	40
	40	0.61	38	0.56	45	0.50	52	0.50	46	0.55	35	0.59	33
$n=2$	50	0.55	30	0.49	38	0.40	45	0.40	39	0.48	26	0.54	25
	60	0.48	24	0.39	32	0.28	43	0.27	35	0.38	17	0.47	18
	70	0.32	19	0.23	28	0.12	46	0.11	36	0.21	8	0.31	12
	80	0.14	12	0.086	19	0.022	37	0.010	−124	0.062	−7	0.12	5
	90	0.028	0	0.028	0	0.028	0	0.028	0	0.028	0	0.028	0
	0	0.72	41	0.75	39	0.71	40	0.72	41	0.75	39	0.71	40
	35	0.58	45	0.52	54	0.43	65	0.42	59	0.47	44	0.54	40
	40	0.53	40	0.48	49	0.39	59	0.38	52	0.43	37	0.50	34
$n=4$	50	0.46	33	0.38	42	0.29	51	0.30	42	0.38	28	0.45	27
	60	0.36	27	0.26	36	0.15	46	0.15	37	0.25	18	0.36	20
	70	0.16	21	0.088	31	0.029	49	0.026	35	0.077	8	0.15	13
	80	0.028	12	0.012	21	0.00097	44	0.00031	−133	0.0066	−9	0.024	4
	90	0.0011	0	0.0011	0	0.0011	0	0.0011	0	0.0011	0	0.0011	0

TABLE V-*b*. – *Amplitude a, and average deflection angle,* $\langle \psi_E \rangle$, *in degrees, for* $P_i = 10$ GV *and* $m = 1$, *based on the extra-terrestrial origin.*

	G.M. Long. →	0		60		120		180		240		300	
	G.M. Lat. ↓	a	$\langle \psi_E \rangle$	a	$\langle \psi_E \rangle$	a	$\langle \psi_E \rangle$	a	$\langle \psi_E \rangle$	a	$\langle \psi_E \rangle$	a	$\langle \psi_E \rangle$
$n=1$	0	0.15	86	0.15	84	0.15	86	0.15	86	0.15	84	0.15	86
	35	0.23	80	0.23	85	0.23	86	0.23	77	0.22	69	0.22	73
	40	0.22	64	0.23	70	0.23	72	0.23	62	0.22	51	0.22	55
	50	0.22	41	0.22	50	0.21	54	0.21	44	0.22	30	0.22	32
	60	0.21	30	0.20	40	0.18	49	0.18	37	0.20	18	0.21	21
	70	0.17	22	0.15	34	0.12	50	0.11	35	0.15	6	0.17	12
	80	0.11	14	0.089	25	0.046	52	0.035	−130	0.078	−12	0.11	4
	90	0.045	0	0.045	0	0.045	0	0.045	0	0.045	0	0.045	0
$n=2$	0	0.15	86	0.15	84	0.15	87	0.15	86	0.15	84	0.15	87
	35	0.22	80	0.22	85	0.22	88	0.22	78	0.20	69	0.20	73
	40	0.21	64	0.22	71	0.22	73	0.21	62	0.20	51	0.20	54
	50	0.21	41	0.21	50	0.19	56	0.19	44	0.21	30	0.21	32
	60	0.20	30	0.17	41	0.14	50	0.14	37	0.18	18	0.20	21
	70	0.14	22	0.10	34	0.061	51	0.059	35	0.097	6	0.13	12
	80	0.056	14	0.036	26	0.010	53	0.0063	−134	0.028	−13	0.052	3
	90	0.0091	0	0.0091	0	0.0091	0	0.0091	0	0.0091	0	0.0091	0
$n=4$	0	0.15	86	0.14	84	0.14	87	0.15	86	0.14	84	0.14	87
	35	0.20	80	0.22	87	0.21	90	0.20	79	0.18	68	0.18	72
	40	0.19	63	0.21	72	0.20	75	0.19	63	0.17	50	0.16	52
	50	0.20	42	0.19	51	0.17	56	0.18	44	0.19	30	0.19	32
	60	0.18	30	0.14	41	0.092	50	0.095	36	0.14	18	0.18	21
	70	0.083	22	0.048	34	0.018	50	0.017	34	0.044	5	0.080	12
	80	0.014	14	0.0061	26	0.00060	54	0.00021	137	0.0036	−14	0.012	3
	90	0.00036	0	0.00036	0	0.00036	0	0.00036	0	0.00036	0	0.00036	0

TABLE V-c. – *Amplitude a, and average deflection angle, $\langle\psi_E\rangle$, in degrees, for $P_i = 10$ GV and $m = 2$, based on the extra-terrestrial origin.*

	G.M. Long. →	0		60		120		180		240		300	
	G.M. Lat. ↓	a	$\langle\psi_E\rangle$	a	$\langle\psi_E\rangle$	a	$\langle\psi_E\rangle$	a	$\langle\psi_E\rangle$	a	$\langle a_E\rangle$	a	$\langle\psi_E\rangle$
	0	0.062	104	0.061	104	0.062	106	0.062	104	0.061	104	0.062	106
	35	0.14	94	0.15	98	0.15	99	0.14	89	0.13	82	0.13	88
	40	0.14	73	0.14	79	0.14	79	0.14	68	0.13	58	0.13	64
$n=1$	50	0.13	44	0.14	53	0.13	57	0.13	44	0.14	30	0.13	33
	60	0.13	30	0.12	41	0.11	50	0.11	36	0.13	17	0.13	20
	70	0.11	22	0.096	34	0.075	50	0.073	33	0.093	5	0.11	11
	80	0.071	13	0.057	26	0.032	54	0.024	−137	0.049	−15	0.068	2
	90	0.027	0	0.027	0	0.027	0	0.027	0	0.027	0	0.027	0
	0	0.062	104	0.060	104	0.061	106	0.062	104	0.060	104	0.061	106
	35	0.14	94	0.14	99	0.14	100	0.14	90	0.12	82	0.12	88
	40	0.13	73	0.14	79	0.14	80	0.13	68	0.12	57	0.11	62
$n=2$	50	0.13	44	0.13	53	0.13	57	0.13	44	0.13	30	0.13	33
	60	0.13	30	0.11	42	0.094	50	0.095	36	0.12	17	0.13	20
	70	0.087	22	0.067	34	0.042	50	0.040	33	0.064	4	0.086	11
	80	0.037	13	0.024	26	0.0076	54	0.0044	−139	0.018	−16	0.034	2
	90	0.0055	0	0.0055	0	0.0055	0	0.0055	0	0.0055	0	0.0055	0
	0	0.061	104	0.059	103	0.060	106	0.061	104	0.059	103	0.060	106
	35	0.13	95	0.14	99	0.14	100	0.12	90	0.10	82	0.11	88
	40	0.11	72	0.13	79	0.13	80	0.12	68	0.099	56	0.091	60
$n=4$	50	0.12	44	0.13	53	0.12	57	0.12	44	0.13	30	0.12	33
	60	0.12	31	0.095	42	0.066	50	0.068	36	0.098	17	0.12	20
	70	0.056	21	0.034	34	0.013	50	0.012	32	0.030	4	0.054	11
	80	0.010	13	0.0044	26	0.00048	54	0.00015	−140	0.0024	−16	0.0085	1
	90	0.00022	0	0.00022	0	0.00022	0	0.00022	0	0.00022	0	0.00022	0

4. – Discussion and conclusion.

4·1. *Error estimation of the diurnal variation.* – As mentioned in the previous sections, we used the quadrature of Newton-Cotes formula for the integration of eq. (10) and (14) in the rigidity region $P_l \leqslant P \leqslant 600$ GV. The estimated errors introduced by this quadrature were 3% in amplitude and 1' in the average deflection angle at the equator for the case $m = 0$. From this estimation it could be inferred that the errors at other latitudes for various values of parameters are within about 4% in amplitude and 3° in the average deflection angle.

We neglected the integration of C (or c) and S (or s) given by eq. (10) (or eq. (14)) in the rigidity interval $P_c \leqslant P < P_l$. The values of P_c and P_l in GV are respectively 14.9 and 15.5 at $\Lambda = 0°$; 6.7 and 9.0 at $\Lambda = 35°$; 5.1 and 7.0 at $\Lambda = 40°$ and 2.5 and 3.5 at $\Lambda = 50°$. Then, for the case $P_i < P_l$, the results contain some errors which will be estimated as follows.

The diurnal variation produced by the anisotropy in the neglected rigidity interval is given by

$$\Delta D = \alpha_0 \Delta A \cos\left(\Psi - \langle \Delta \Psi_E \rangle\right) ; \tag{16}$$

where

$$\Delta A = \sqrt{(\Delta C)^2 + (\Delta S)^2}; \qquad \langle \Delta \Psi_E \rangle = \mathrm{tg}^{-1}(\Delta S / \Delta C) , \tag{17}$$

and

$$\begin{Bmatrix} \Delta C \\ \Delta S \end{Bmatrix} = I^{-1} \int_{P_c}^{P_l} \{ \mathrm{d}I(P, x)/\mathrm{d}P \} (10/P)^m (\cos \Lambda_N)^n \begin{Bmatrix} \cos \Psi_E \\ \sin \Psi_E \end{Bmatrix} \mathrm{d}P . \tag{18}$$

In the interval $P_c \leqslant P < P_l$, the function $\{\mathrm{d}I(P, x)/\mathrm{d}P\}(10/P)^m$ in eq. (18) can be replaced by an average value $\langle \{\mathrm{d}I(P, x)/\mathrm{d}P\}(10/P)^m \rangle$, and $(\cos \Lambda_N)^n$ can be approximated to unity since Λ_N tends to oscillate near the equator. Further, we assume the following representation of Ψ_E as a function of P in the interval $P_c \leqslant P < P_l$:

$$\Psi_E(P) = q(P - P_c)^{-1} + r , \tag{19}$$

Where q and r are constants which satisfy the boundary conditions at $P = P_l$:

$$\Psi_E = \Psi_E(P_l) \text{ and } \mathrm{d}\Psi_E/\mathrm{d}P = (\mathrm{d}\Psi_E/\mathrm{d}P)_{P=P_l},$$

and are given by

$$\begin{cases} q = -(P_l - P_c)^2 (\mathrm{d}\Psi_E/\mathrm{d}P)_{P=P_l} , \\ r = \Psi_E(P_l) + (P_l - P_c)(\mathrm{d}\Psi_E/\mathrm{d}P)_{P=P_l} . \end{cases} \tag{20}$$

Then, ΔC and ΔS can be integrated as follows:

$$\begin{Bmatrix}\Delta C\\ \Delta S\end{Bmatrix} = (q/I)\langle(\mathrm{d}I/\mathrm{d}P)(10/P)^m\rangle\left[y_i^{-1}\begin{Bmatrix}\cos(y_i+r)\\ \sin(y_i+r)\end{Bmatrix} + \right. \tag{21}$$

$$\left. + C_i(y_i)\begin{Bmatrix}\sin r\\ -\cos r\end{Bmatrix} - \{\pi/2 - S_i(y_i)\}\begin{Bmatrix}\cos r\\ \sin r\end{Bmatrix}\right],$$

where $y_i = \Psi_{\mathrm{E}}(P_i) - r$, and $S_i(y_i)$ and $C_i(y_i)$ are sine and cosine integrals. The calculated values of ΔA and $\langle\Delta\Psi_{\mathrm{E}}\rangle$ are listed in Table VI, for the case of terrestrial origin. At latitudes higher than 50°, the magnetic cut-off rigidity, P_c, should be replaced by $P \approx 2$ GV in view of the atmospheric cut-off, so $P_l - P_c = 0$ and then $\Delta D = 0$.

As is seen in Tables I and VI, the value of the ratio $\Delta A/A$ is about 0.03 for $m = 0$, but increases to about 0.1 and 0.2 for $m = 1$ and 2, respectively. Thus, the contribution of this rigidity interval to the diurnal variation can not be neglected in such latitudes, for large values of m. In these cases, it would be better to correct A and $\langle\Psi_{\mathrm{E}}\rangle$ by ΔA and $\langle\Delta\Psi_{\mathrm{E}}\rangle$, although the procedure for obtaining the correction terms is only approximate.

TABLE VI. – *Estimated values of the amplitude, ΔA, and the average deflection angle $\langle\Delta\Psi_{\mathrm{E}}\rangle$, of the diurnal variation produced by the anisotropy in the rigidity interval, $P_c \leqslant P < P_l$.*

m	$A=0°$		35°		45°		50°	
	ΔA	$\langle\Delta\Psi_{\mathrm{E}}\rangle$	ΔA	$\langle\Delta\Psi_{\mathrm{E}}\rangle$	ΔA	$\langle\Delta\Psi_{\mathrm{E}}\rangle$	ΔA	$\langle\Delta\Psi_{\mathrm{E}}\rangle$
0	0.013	225°	0.022	279°	0.032	237°	0.013	183°
1	0.0086		0.029		0.054		0.043	
2	0.0057		0.040		0.095		0.14	

In the case of the extra-terrestrial origin, the diurnal variation produced by the anisotropy in the neglected rigidity interval is given by

$$\Delta D = \alpha_0 \Delta a \cos(\psi - \langle\Delta\psi_{\mathrm{E}}\rangle)\,. \tag{22}$$

In eq. (22), Δa and $\langle\Delta\psi_{\mathrm{E}}\rangle$, defined by the equations similar to eq. (17) and (18), depend on the geomagnetic longitude of the observational station. However, these values can be replaced to a good approximation with the values of ΔA and $\langle\Delta\Psi_{\mathrm{E}}\rangle$ in Table VI which are independent of the geomagnetic longitude. Even in the worst case, the errors introduced by this substitution are about 30% in Δa and 15° in $\langle\Delta\psi_{\mathrm{E}}\rangle$.

4·2. *Altitude correction.* – In order to determine the altitude dependence, calculations of the diurnal variation of the nucleonic component for the atmospheric depth $x = 680$ g/cm² at several latitudes were performed for the case of the extra-terrestrial origin.

The diurnal variation itself depends on the geomagnetic longitude. However, the ratio of the amplitude, $R = a(x = 680)/a(x = 1030)$, and the difference of the average deflection angle, $\Delta\langle\psi_E\rangle_x = \langle\psi_E\rangle_{x=680} - \langle\psi_E\rangle_{x=1030}$, between two different altitudes at the same geomagnetic position for the same values of m, n and P_i do not show any strong geomagnetic longitudinal dependence. These are listed in Table VII. The indicated errors were obtained from the calculations at geomagnetic longitudes $\Phi = 0°$, 120° for latitude $\Lambda = 0°$; $\Phi = 60°$, 120°, 300° for $\Lambda = 50°$; and $\Phi = 120°$, 300° for $\Lambda = 60°$. These values represent altitude correction factors for the diurnal variation at any longitude. They also apply to the case of terrestrial origin.

As shown in Table VII, the value of R is larger or smaller than unity according to a particular choice of the values of m and P_i. Hence, the amplitude of the diurnal variation at high altitude could be smaller than that at sea level. On the other hand, the value of $\Delta\langle\psi_E\rangle_x$ is larger than or equal to zero. Hence, the geographic local time of the maximum intensity at high altitude is earlier than or equal to that at sea level.

TABLE VII. – *Ratio of the amplitude,* $R = a(x=680)/a(x=1030)$, *and difference of the average deflection angle,* $\Delta\langle\psi_E\rangle_x = \langle\psi_E\rangle_{x=680} - \langle\psi_E\rangle_{x=1030}$, *between two different altitudes,* $x = 680$ *and* 1030 g/cm² *(for* $n = 1$*).*

P_i (GV)	$m \rightarrow$ / $\Lambda \downarrow$	0		1		2	
		R	$\Delta\langle\psi_E\rangle_x$	R	$\Delta\langle\psi_E\rangle_x$	R	$\Delta\langle\psi_E\rangle_x$
0	0°	0.96	10°	1.24	1°	1.26	2°
	50°	0.99 ± 0.03	9° ± 1°	1.30 ± 0.01	7°	1.49	8° ± 1°
	60°	1.07 ± 0.03	4° ± 2°	1.46 ± 0.02	3°	1.73 ± 0.02	3°
5	0°	0.96	10°	1.24	1°	1.26	2°
	50°	0.95 ± 0.03	6° ± 1°	1.17 ± 0.02	3°	1.27	2°
	60°	0.96 ± 0.02	2° ± 2°	1.16 ± 0.01	0°	1.26 ± 0.01	0°
10	0°	0.96	10°	1.24	1°	1.26	2°
	50°	0.83 ± 0.02	4° ± 1°	0.98	0°	1.01	0°
	60°	0.83 ± 0.02	3° ± 1°	0.97	0°	1.00 ± 0.01	0°

4·3. *Comparison between A and a, and between* $\langle\Psi_E\rangle$ *and* $\langle\psi_E\rangle$. – At geomagnetic latitudes higher than 50°, the amplitude, a, for the extra-terrestrial origin depends on the geomagnetic longitude, in contrast with the amplitude, A, for the terrestrial origin (cf. Fig. 5*a* or Tables III, IV and V). On the

contrary, at latitudes lower than 50°, the values of the amplitude a are almost constant and nearly the same as those of A (cf. Tables I, III, IV and V).

For the case of the terrestrial origin, $\langle \Psi_E \rangle$ is constant at the same geomagnetic latitude, hence the geomagnetic local time of the maximum intensity, T_{max}, is also constant at the same latitude. If we transform T_{max} (Λ) to the geographic local time t^t_{max} (Λ, Φ) at the observational station (Λ, Φ), then t^t_{max} (Λ, Φ) shows the geomagnetic longitudinal dependence, which is similar to that of the geographic local time of maximum intensity, t^{et}_{max} (Λ, Φ), expected from the extra-terrestrial origin. In general, the relation between the geomagnetic and the geographic local times depends on the declination of the sun ([12]), and so equinox was chosen for the specification of the solar position in the present transformation.

The longitudinal dependence of t^t_{max} and t^{et}_{max} is shown in Fig. 7, where the

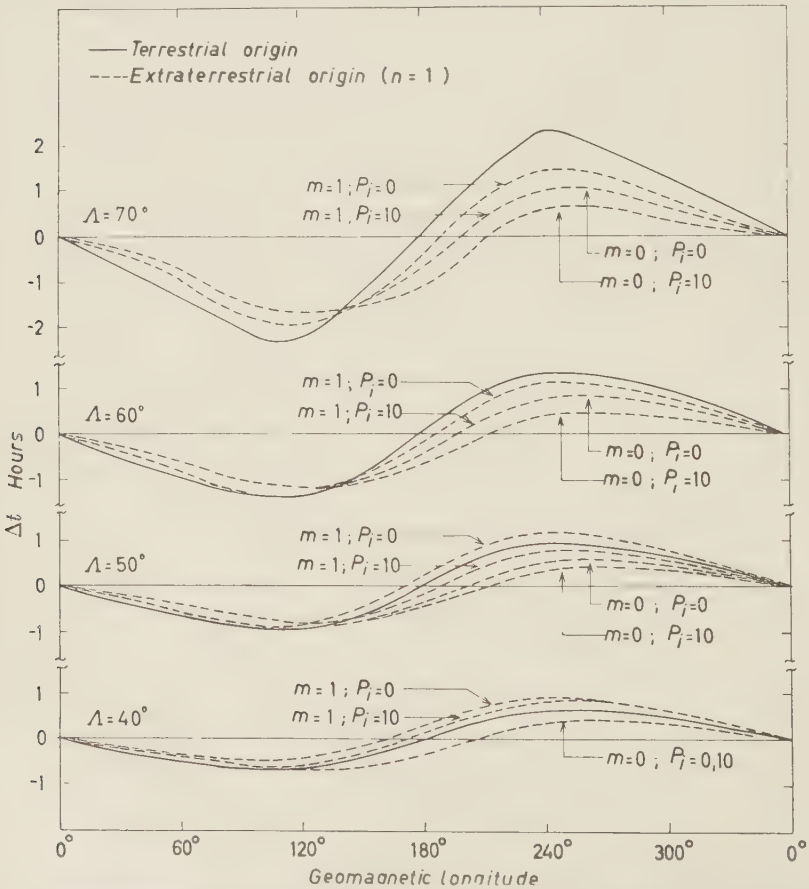

Fig. 7. – Geomagnetic longitude dependences of $\Delta t = t_{max}(\Lambda, \Phi) - t_{max}(\Lambda, 0)$, expected from the terrestrial (full line) and the extra-terrestrial (dashed line) origins, for several geomagnetic latitudes. Three parameters m, n and P_i are shown in the figure.

function Δt is defined by the following equation for both terrestrial and extra-terrestrial cases,

$$\Delta t = t_{\max}(\Lambda, \Phi) - t_{\max}(\Lambda, 0) \,. \tag{13}$$

As is seen in Fig. 7, the maximum difference between the values of $t^{et}_{\max}$ (Λ, Φ) or $t^{t}_{\max}$ (Λ, Φ) at the same latitude is more than one hour over the region of middle and high latitudes, irrespective of the particular choice of the values of m and P_i given in the figure. It must be remembered that Δt^e for the extra-terrestrial origin is a function of m, n and P_i, whereas Δt^t for the terrestrial origin is not, and is simply determined by the geometrical positions of the two stations.

At latitudes lower than 50°, there is no significant difference between Δt^t and Δt^{te}. Moreover, there is no marked difference between the values of $\langle \Psi_E \rangle_\Lambda$ and $\langle \psi_E \rangle_{\Lambda, \Phi = 0}$ at these latitudes, as is seen in the comparison between Table I and Table III, IV or V. Thus, $t^{et}_{\max}$ (Λ, Φ) is nearly the same as $t^{t}_{\max}$ (Λ, Φ) at these latitudes.

From the above comparisons between A and a, and between $\langle \Psi_E \rangle$ and $\langle \psi_E \rangle$, it can be concluded that the diurnal variations expected from the terrestrial and extra-terrestrial origins are the same at latitudes lower than 50 for small values of n, but are quite different from each other at latitudes higher than 50°.

This conclusion justifies neglecting the orientational difference between the earth's rotational and the geomagnetic dipole axes for the calculation of the diurnal variation based on the extra-terrestrial origin, but only for latitudes lower than 50°. If the values of $A(\Lambda)$ and $\langle \psi_E \rangle_\Lambda$ are known for these latitudes, the values of $a(\Lambda, \Phi)$ and $\langle \psi_E \rangle_{\Lambda, \Phi}$ can be obtained approximately by, the following equations,

$$\begin{cases} a(\Lambda, \Phi) \approx A(\Lambda) \,, \\ \langle \psi \rangle_{E\,\Lambda, \Phi} \approx \langle \Psi_E \rangle_\Lambda - 15\,\Delta t^t \,, \end{cases} \tag{24}$$

where Δt^t is given by eq. (23).

4·4. *Parameters m, n and* P_i. – The expression for the anisotropy, Δf, given by eq. (4) contains three parameters, m, n and P_i. The parameter, m, determines the rigidity dependence of Δf (*i.e.* $\Delta f \propto P^{-m}$). The parameter, n, determined the directional dependence of Δf with respect to the plane parallel to the geomagnetic or geographic equator (*i.e.* $\Delta f \propto (\cos \Lambda_p)^n$ or $\propto (\cos \lambda_p)^n$). P_i is a definite value of rigidity, for rigidities smaller than which Δf is zero. It is possible to determine the most suitable values of these parameters, by the comparison of the calculated and observed diurnal variations. The calculated diurnal variation depends strongly on the parameters, m and P_i, but

does not show any strong dependence on n except at high latitudes. This provides a simplification in the analysis of the diurnal variation.

The expression for the anisotropy could be easily utilized in terms of several earlier theories by the appropriate choice of these three parameters. For example, the anisotropy produced by the isotropic distribution of the cosmic ray intensity in the sun's rotational frame of reference, suggested by ALFVÉN [3], characterized by $m=0$, $n=1$, and $P_i=0$; the anisotropy produced by the ordered magnetic field frozen in the solar stream, proposed by DORMAN [6] and by one of the present authors [7], is approximately characterized by $m=1$, and $P_i \neq 0$. Finally, the anisotropy produced by the disordered magnetic field frozen in the solar stream proposed by one of us [18], is characterized by $m=0$ and $n=1$ for $0 \leqslant P \leqslant P_1$; by $m=1$ and $n=1$ for $P_1 \leqslant P \leqslant P_2$; and by $m=2$ and $n=1$ for $P_2 \leqslant P < \infty$, where P_1 and P_2 are critical values of rigidity. More detailed discussion about the relation of these parameter to particular theories will be published later.

APPENDIX

Expression for the anisotropy.

In general, any anisotropy can be expressed in the form of eq. (2) in any co-ordinate system in momentum space. Among these systems we can choose the most suitable co-ordinate system for the simple representation of the anisotropy. For the case of the extra-terrestrial origin, this is the heliographic co-ordinate system, one axis (p_z') of which is parallel to the heliographic zenith axis and the other two (p_x', p_y') parallel to the heliographic equatorial plane. In this co-ordinate system, momentum $\boldsymbol{p}$ can be expressed in terms of three quantities p, λ_p' and φ_p'. The definition of λ_p' and φ_p' is similar to that of Λ_p and Φ_p for the terrestrial origin (cf. Fig. 1*b*).

Under the same considerations as in the case of the terrestrial origin, we assume the anisotropy can be expressed by the following formula similar to eq. (4), in the p_x', p_y', p_z' co-ordinates,

$$\Delta f(p, \lambda_p', \varphi_p') = \alpha_0' f(p)(p_0/p)^{m'} (\cos \lambda_p')^{n'} \cos(\varphi_p' - \delta') , \tag{25}$$

where δ', the phase angle, is a constant and m' and n' are parameters. In this case, the reference plane of anisotropy is not parallel to the geographic meridian plane but rather to the heliographic meridian plane, and the direction of anisotropy is parallel to the heliographic equatorial plane.

If we transform eq. (25) from the heliographic co-ordinates (p_x', p_y', p_z') to the geographic co-ordinates (p_x, p_y, p_z) defined in Section 3, the transformed representation $\Delta f(p, \lambda_p, \varphi_p)$ for the anisotropy is more complicated than eq. (25). (The definition of λ_p and φ_p is given in Section 3). However, as far as the

[18] K. NAGASHIMA: *Proc. of Moscow Cosmic Ray Conf.*, **4**, 240 (1960).

diurnal variation is concerned, we can take only the terms of $\Delta f(p, \lambda_p, \varphi_p)$ which contain $\cos \varphi_p$ or $\sin \varphi_p$. These terms can be written as follows,

$$\Delta f(p, \lambda_p, \varphi_p) = \alpha_0 f(p)(p_0/p)^m h(\lambda_p) \cos(\varphi_p - \delta) , \tag{26}$$

where $m = m'$.

In eq. (26) δ is the phase angle in the p_x, p_y, p_z co-ordinates and is independent of λ_p. Then, we can define again the reference plane of anisotropy in the p_x, p_y, p_z co-ordinates which includes both the p_z-axis and the direction of anisotropy defined in the p'_x, p'_y, p'_z co-ordinates.

The quantity, h, in eq. (26) is a function of λ_p and depends on $\lambda_p^{d'}$ which is the value of λ_p for the direction of anisotropy defined in the p'_x, p'_y, p'_z co-ordinates. The graphical representation of $h(\lambda_p)$ is shown in Fig. 8 for the

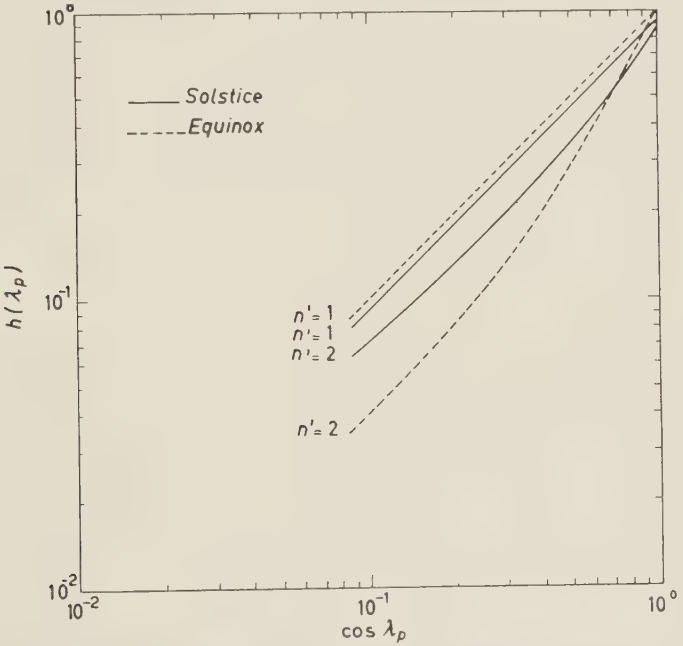

Fig. 8. – Functional dependence of h upon $\cos \lambda_p$. Details are given in the Appendix.

cases in which the reference planes of anisotropy defined in the p'_x, p'_y, p'_z co-ordinates are parallel to the heliographic meridian planes including equinox ($\lambda_p^{d'} = 0°$) and solstice ($\lambda_p^{d'} = \pm 23.5°$), respectively.

As is seen in Fig. 8, $h(\lambda_p)$ is exactly proportional to $(\cos \lambda_p)^{n'(=1)}$ for the case $n' = 1$ and is nearly proportional to $(\cos \lambda_p)^n$ for the case $n' = 2$, hence eq. (26) can be written as follows,

$$\Delta f(p, \lambda_p, \varphi_p) = \alpha_0 f(p)(p_0/p)^m (\cos \lambda_p)^n \cos(\varphi_p - \delta) . \tag{27}$$

From the above considerations, we are able to use the form given by eq. (27) in the p_x, p_y, p_z co-ordinates as long as the anisotropy produced by the extra-terrestrial origin is given by the simple form in the p'_x, p'_y, p'_z co-ordinates, as defined by eq. (25).

As is seen in eq. (25), the anisotropy for the case of $n'=1$ is proportional to $\cos\omega'(=\cos\lambda'_p\cos(\varphi'_p-\delta'))$, where ω' is the angle between a direction (λ'_p, φ'_p) and the direction of anisotropy $(0, \delta')$. Therefore, in such a case, the anisotropy can be expressed by defining only the direction of anisotropy without specifying the reference plane of anisotropy. As discussed above and shown in eq. (27), the transformed representation for such an anisotropy from the p'_x, p'_y, p'_z co-ordinates to the p_x, p_y, p_z co-ordinates is exactly the same as eq. (25), except the difference of the coefficients α'_0 and α_0, which are related mutually by the following equation:

$$\alpha_0=\alpha'_0\cos\lambda_p^{\delta'}, \qquad \text{for} \quad n'=1. \tag{28}$$

In eq. (27), the value of α_0 for the case $n'=1$ and the values of α_0 and n for the case $n'\neq 1$ depend on $\lambda_p^{\delta'}$ defined above, and the anisotropy is a symmetric function of λ_p about the plane of $\lambda_p=0^\circ$. This dependence and symmetry of the anisotropy could be one of the causes for the equinox effect of the diurnal variation, which has been pointed out by SEKIDO and YOSHIDA ([9,20]).

([19]) Y. SEKIDO and S. YOSHIDA: *Journ. Geomag. Geoelectr.*, **2**, 66 (1950).
([20]) S. YOSHIDA: *Nuovo Cimento*, **4**, 1410 (1956).

RIASSUNTO (*)

Formulando una espressione dell'anisotropia dell'intensità dei raggi cosmici primari, si calcola la variazione diurna solare prevista della componente nucleonica della radiazione cosmica al livello del mare a varie latitudini e longitudini geomagnetiche nei casi seguenti: (*a*) l'anisotropia si produce al di fuori del campo magnetico terrestre (origine extraterrestre), e (*b*) l'anisotropia si produce entro il campo magnetico terrestre (origine terrestre). In questo calcolo si tiene conto della differenza di orientazione fra l'asse di rotazione e l'asse del dipolo geomagnetico della terra. Questa espressione dell'anisotropia, Δf, contiene tre parametri m n e P_i. Il parametro m determina la dipendenza di Δf dalla rigidità, nella forma $\Delta f\propto P^{-m}$. Il parametro n determina la dipendenza di Δf dalla direzione nello spazio degli impulsi rispetto al piano parallelo all'equatore geomagnetico o geografico nella forma $\Delta f\propto(\cos\theta)^n$, in cui θ è l'angolo fra quel piano e la direzione suddetta. P_i è un determinato valore della rigidità; per rigidità inferiori a questo valore Δf è nullo. Questa espressione dell'anisotropia può essere facilmente utilizzata per ogni descrizione di un modello di produzione della anisotropia scegliendo opportunamente questi tre parametri. È anche possibile determinare i valori più adatti di questi parametri per confronto fra le variazioni diurne calcolate ed osservate. Il tempo geografico locale della massima intensità presenta una dipendenza dalla longitudine geomagnetica per origine sia terrestre che extraterrestre. D'altra parte l'ampiezza presenta una dipendenza dalle longitudini a latitudini maggiori di 50°, solo per l'origine extraterrestre. A latitudini inferiori a 60° non si ha alcuna differenza significativa fra le variazioni diurne previste per origine terrestre od extraterrestre. Si ottengono i fattori di correzione per l'altitudine per la componente nucleonica. Questi fattori sono quasi indipendenti dalla longitudine geomagnetica della stazione di osservazione.

(*) *Traduzione a cura della Redazione.*

IL NUOVO CIMENTO Vol. XIX, N. 2 16 Gennaio 1961

Dispersion Relation and Analiticity of a Production Amplitude.

G. Mohan

National Physical Laboratory - New Dehli

(ricevuto il 23 Settembre 1960)

Summary. — A dispersion relation and certain analyticity properties of the amplitude for a process like $n+\pi \to n'+\pi'+\pi''$ has been studied on the basis of the Jost-Lehmann-Dyson integral representation of the causal commutator.

1. – Introduction.

Although the dispersion relations for elastic scattering is now well-established theoretically and is in conformity with experiments, a similar development for inelastic scattering has not progressed very far except for processes involving electrons and photons ([1,2]). The difficulty is both, experimental as well as theoretical.

On the theoretical side there appears to be, at first sight, many generalizations possible of the techniques ([3-5]) used in elastic processes, but not all of them are successful. Polkinghorne ([6]) has proposed certain dispersion relations for meson production. Logunov and Todorov ([7]) and Vladimirov and Logunov ([2]) have studied this problem in the spirit of Bogoljubov's method.

([1]) R. Oehme and J. G. Taylor: *Phys. Rev.*, **113**, 371 (1959).

([2]) V. S. Vladimirov and A. A. Logunov: *A proof of some dispersion relations in quantum field theory* (preprint).

([3]) N. N. Bogoljubov, B. V. Medvedev and M. K. Polivanov: *Lecture notes.* translated at the Institute for Advanced Study (Princeton, N. J., 1957).

([4]) H. J. Bremermann, R. Oehme and J. G. Taylor: *Phys. Rev.*, **109**, 2178 (1958).

([5]) H. Lehmann: *Nuovo Cimento*, **14**, 153 (1959).

([6]) J. C. Polkinghorne: *Nuovo Cimento*, **4**, 216 (1956).

([7]) A. A. Logunov and I. T. Todorov: *Nucl. Phys.*, **10**, 552 (1959).

The full solution of this problem will require a better understanding of the three point τ-product. We make use of only the causal commutator to obtain a partial understanding of a dispersion relation and of certain analyticity properties with respect to mass and momentum transfer variables for the pion production amplitude.

In order to avoid complications not connected with the principles of the method employed we shall ignore spin and isotopic spin although the whole development presented here is tuned to the pion-nucleon system. Another simplification is introduced by assuming that no subtraction in the dispersion relation is needed.

2. – Dispersion relation with imaginary mass.

We study the collision of a nucleon and a pion of momenta p and k respectively, resulting into a nucleon and two pions of momenta p', k' and k'' respectively. Assuming invariance under time reversal one may invert the roles of incoming and outgoing particles and consider the transition probability amplitude

$$\langle p_1, k\,(\text{out})\,|\,p', k', k''\,(\text{in})\rangle = 2\pi i\,\delta(p+k-p'-k'-k'')M^{(\text{in})}\,,$$

where

$$(2.1)\qquad M^{(\text{in})} = i\int \mathrm{d}^4x\,\exp\left[\tfrac{1}{2}i(k+k')x\right]\langle p\,|[J(\tfrac{1}{2}x), J(-\tfrac{1}{2}x)]_-|\,p'k''(\text{in})\rangle\,\theta(x)\,.$$

It is not possible to separate $M^{(\text{in})}$ into real absorptive and dispersive parts by the conventional way. This difficulty is removed [8] by working with a slightly different amplitude

$$(2.2)\qquad M = i\int \mathrm{d}^4x\,\exp\left[\tfrac{1}{2}i(k+k')x\right]\langle p\,|[J(\tfrac{1}{2}x), J(-\tfrac{1}{2}x)]_-|\,p'k''(-)\rangle\,\theta(x)\,,$$

where

$$|\,p'k''(-)\rangle = \frac{1}{2i}\{|\,p'k''(\text{in})\rangle - |\,p'k''\,(\text{out})\rangle\}\,.$$

The absorptive part takes the usual form,

$$(2.3)\qquad A = \operatorname{Im} M = \tfrac{1}{2}\int \mathrm{d}^4x\,\exp\left[\tfrac{1}{2}i(k+k')x\right]\langle p\,|[J(\tfrac{1}{2}x), J(-\tfrac{1}{2}x)]_-|\,p'k''(-)\rangle\,,$$

(8) K. Ishida: *Progr. Theor. Phys.*, **22**, 499 (1959).

which can be expressed in terms of a simpler quantity

$$\varphi = \int \mathrm{d}^4x \exp\left[\tfrac{1}{2} i(k + k')x\right] \langle p \,|\, J(\tfrac{1}{2}x) J(-\tfrac{1}{2}x) \,|\, p' k''(-)\rangle = \tag{2.4}$$

$$= (2\pi)^4 \int \langle p \,|\, J(0) \,|\, p + k,\, \alpha\rangle \langle p + k,\, \alpha \,|\, J(0) \,|\, p' k''(-) \quad .$$

There are ten independent scalars formed from the four independent energy-momentum vectors of the initial and final particles. We choose the following set of invariant kinematic parameters (*):

$$\left\{\begin{array}{l} \omega = \dfrac{(k + k')(p + p')}{2\sqrt{(p + p')^2}}\,, \quad \Omega = \dfrac{(k + k')(p - p')}{2\sqrt{-(p - p')^2}}\,, \\ K^2 = (p' + k'')^2\,, \qquad Q^2 = (p - p')^2 = (K' - k)^2\,, \\ \sigma^2 = kk'\,, \qquad m^2 = p^2 = p'^2\,, \qquad \mu^2 = k'^2\,, \\ \zeta = k^2 = k''^2\,. \end{array}\right. \tag{2.5}$$

Here Q and K' represent the 4-vectors $(p - p')$ and $(k' + k'')$ respectively. Notice that among the particle masses the incoming meson mass k^2 and the outgoing meson mass k''^2 will be treated as a variable. The nucleon mass and the outgoing mesons mass k'^2 are fixed at their physical values right from the beginning.

One obtains, from (2.3) and (2.4),

$$A(\omega, \Omega) = \tfrac{1}{2}[\varphi(\omega, \Omega) - \varphi(-\omega, -\Omega)]\,, \tag{2.6}$$

where the kinematic parameters, other than ω and Ω have been suppressed because they take the same value in all the terms. Strictly speaking, φ expressed through the eq. (2.4) does not make sense for non-physical k''^2. A definition for φ is given later from which continuation to non-physical k''^2 is obtained. A similar generalization of M in eq. (2.2) is assumed.

We specialize to the Briet frame of reference O_B characterized by the relation

$$\boldsymbol{p} + \boldsymbol{p}' = 0\,,$$

with the third axis chosen in the direction of $\boldsymbol{p}$.

(*) Instead of σ^2 we shall later use $\tau = k(p - p')/\sqrt{-Q^2}$; note that

$$\sigma^2 = \tfrac{1}{2}(\mu^2 + Q^2) + 2(\tau - \Omega)\sqrt{-Q^2}\,.$$

In this system

$$(2.7) \qquad \tfrac{1}{2}(k+k')x = \omega x_0 + \Omega x_3 - \sqrt{\omega^2 - \tfrac{1}{4}(\zeta + \mu^2 + 2\sigma^2)} - \Omega^2 \cdot (e_1 x_1 + e_2 x_2) ,$$

where $e_1^2 + e_2^2 = 1$. With the usual formulation of microscopic causality it is found that M is an analytic function of $\omega = \omega_1 + i\omega_2$ in a region R_1 defined by

$$\operatorname{Im} \omega > \operatorname{Im} \sqrt{\omega^2 - \tfrac{1}{4}(\zeta + \mu^2 + 2\sigma^2)} - \Omega^2 ,$$

that is, with $\zeta = \zeta_1 + i\zeta_2$,

$$\omega_2 > 0 , \qquad \omega_1^2 > \tfrac{1}{4}(\zeta_1 + \mu^2 + 2\sigma^2 + 4\Omega^2)$$

and

$$2\omega_2 \{\omega_1 - \sqrt{\omega_1^2 - \tfrac{1}{4}(\zeta_1 + \mu^2 + 2\sigma^2 + 4\Omega^2)}\} \leqslant$$
$$\leqslant \tfrac{1}{4}\zeta_2 \leqslant 2\omega_2 \{\omega_1 + \sqrt{\omega_1^2 - \tfrac{1}{4}(\zeta_1 + \mu^2 + 2\sigma^2 + 4\Omega^2)}\} .$$

Choose $\zeta_1 < -\mu^2 - 2\sigma^2 - 4\Omega^2$, $\zeta_2 = 0$. Then M is regular (*) in the entire upper half complex ω-plane. Ignoring the need for substractions we can write

$$(2.8) \qquad M(\omega, \Omega) = \frac{1}{\pi} \int_{\infty}^{\infty} \mathrm{d}\omega' \, \frac{A(\omega, \Omega)}{\omega' - \omega} \qquad \omega_2 > 0 ,$$

$$= \frac{1}{2\pi} \int_{\infty}^{\infty} \mathrm{d}\omega' \left[\frac{\varphi(\omega', \Omega)}{\omega' - \omega} + \frac{\varphi(\omega', -\Omega)}{\omega' + \omega} \right] .$$

This is the desired form of dispersion relation for the non-physical incoming meson mass. Our next objective is to see if one can analytically continue both sides of the above equation on to the physical value.

3. – Analyticity with respect to ζ.

At this stage it is convenient to switch over to the invariant $W^2 = (p+k)^2$ in place of ω. The relation between ω and W^2 is

$$(3.1) \qquad \begin{cases} W^2 = \sqrt{4m^2 - Q^2}\,\omega + \sqrt{-Q^2}\,\Omega + s + \tfrac{1}{2}\zeta , \\ s \;\; = \tfrac{1}{2}(W^2 + m^2 + 2\sigma^2 - \mu^2) . \end{cases}$$

(*) Proper symmetrization with respect to $(e_1, e_2) \to (-e_1, -e_2)$ will be assumed in order to eliminate the branch point at $\omega^2 = \tfrac{1}{4}(\zeta + \mu^2 + 2\sigma^2 + 4\Omega^2)$.

We explore the analytic property of q with respect to ζ. The second factor on the right hand side of equation (2.4) can be analysed as follows:

$$(3.2)\qquad \langle p+k,\ \alpha|J(0)|p'k''(-)\rangle = \frac{1}{2i}\langle p+k,\ \alpha|J(0)\{a^*_{\mathrm{in}}(k'') - a^*_{\mathrm{out}}(k'')\}|p'\rangle =$$

$$= \tfrac{1}{2}(2\pi)^{-\frac{3}{2}}\int \mathrm{d}^4x\, \exp[-ik''x]\langle p+k,\ \alpha|J(0)J(x)|p'\rangle =$$

$$= \tfrac{1}{2}(2\pi)^{\frac{5}{2}}\int_{\alpha'} \langle p+k,\ \alpha|J(0)|p'+k'',\ \alpha'\rangle\langle p'+k'',\ \alpha'|J(0)|p'\rangle\,.$$

Therefore,

$$(3.3)\qquad \varphi = \tfrac{1}{2}(2\pi)^{13/2}\int_{\alpha\alpha'} \langle p|J(0)|p+k,\ \alpha\rangle J(p+k,\alpha;\ p'+k'',\alpha')\langle p'+k'',\alpha'|J(0)|p'\rangle\,,$$

where

$$J(p+k,\ \alpha;\ p'+k'',\ \alpha') = \langle p+k,\ \alpha|J(0)|p'+k'',\ \alpha'\rangle\,.$$

The Jost-Lehmann-Dyson integral representation yields,

$$(3.4)\qquad \varphi = \int_{\alpha\alpha'} J(p+k,\ \alpha;\ p'+k'',\ \alpha')\int \mathrm{d}^4u \int \mathrm{d}^4u' \int \mathrm{d}\varkappa^2 \int \mathrm{d}\varkappa'^2 \cdot$$

$$\cdot \frac{\Phi_1(\alpha,\ p+k,\ u,\ \varkappa)}{\varkappa^2 - (q-u)^2} \cdot \frac{\Phi_2(\alpha',\ p'+k'',\ u',\ \varkappa')}{\varkappa'^2 - (q'-u')^2}\,.$$

where

$$q = \tfrac{1}{2}(k-p)\,, \qquad q' = \tfrac{1}{2}(p'-k'')\,.$$

The support of the integrand is (*)

$$(3.5)\qquad \begin{cases} \left(\dfrac{p-k}{2} - u\right) \varepsilon L_+\,, \quad \left(\dfrac{p'+k''}{2} - u'\right) \varepsilon L_+\,, \\ \varkappa \geqslant \mathrm{Max}\left\{0,\ 3\mu - \sqrt{\left(\dfrac{p+k}{2}+u\right)^2}\,,\ m+\mu - \sqrt{\left(\dfrac{p+k}{2}-u\right)^2}\right\}, \\ \varkappa' \geqslant \mathrm{Max}\left\{0,\ m+\mu - \sqrt{\left(\dfrac{p'+k''}{2}+u'\right)^2}\,,\ 3\mu - \sqrt{\left(\dfrac{p'+k''}{2}-u'\right)^2}\right\}. \end{cases}$$

(*) L_+ represents the forward light cone.

It is important to note at this stage that

$$\Phi(p+k,\ p'+k'',\ u,\ u',\ \varkappa,\ \varkappa') \equiv$$
$$\equiv \int_{\alpha\alpha'} J(p+k,\ \alpha;\ p'+k'',\ \alpha')\,\Phi_1(\alpha,\ p+k,\ u,\ \varkappa)\,\Phi_2(\alpha',\ p'+k'',\ u'\ \varkappa')\ ,$$

depends only on the scalars

$$(p+k)^2 = W^2\,,\quad (p'+k'')^2 = V^2\,,\quad (p+k-p'-k'')^2 = \mu^2\,,\quad (p+k)u\ ,$$
$$(p'+k'')u\,,\quad (p+k)u'\,,\quad (p'+k'')u'\,,\quad uu'\,,\quad u^2\,,\quad u'^2\,,\quad \varkappa \text{ and } \varkappa'\,,$$

and is independent of the momentum transfer parameters Q^2, σ^2, the variable meson mass ζ, and Ω. The dependence on these parameters is only through the denominator of the above integrand.

In order to simplify the problem of finding the minimum of certain expressions which will be obtained presently we will write the 4-vectors u, $(p+k)$, and q in the c.m. system O_C, characterized by $\boldsymbol{p}+\boldsymbol{k}=0$, and u', $(p'+k'')$, q' in a frame of reference O_D characterized by $\boldsymbol{p}^{(\prime)}+\boldsymbol{k}^{(\prime\prime)}=0$. We choose the direction of $\boldsymbol{k}'$ as the Z-axis in either system. The components w_μ of a 4-vector with respect to O_C are related to the components $w_\mu^{(\prime)}$ of the same vector with respect to O_D by the equations

$$w_\mu^{(\prime)} = a_\mu{}^\nu w_\nu\,,$$

where

$$a_\mu{}^\nu = \begin{pmatrix} \dfrac{1}{\sqrt{1-v^2}} & 0 & 0 & \dfrac{v}{\sqrt{1-v^2}} \\ 0 & 1 & 0 & 0 \\ 0 & 0 & 1 & 0 \\ \dfrac{-v}{\sqrt{1-v^2}} & 0 & 0 & \dfrac{1}{\sqrt{1-v^2}} \end{pmatrix}, \tag{3.6}$$

$$r = \frac{p'_3+k''_3}{p'_0+k''_0} = \frac{\sqrt{k'^2_0-\mu^2}}{p'_0+k''_0}\ . \tag{3.7}$$

The transformation matrix is function of W, V and μ only,

$$\begin{cases} k'_0 = \dfrac{k'(p+k)}{W} = \dfrac{W^2+\mu^2-V^2}{2W}\ , \\ p'_0+k''_0 = \dfrac{(p'+k'')(p+k)}{W} = \dfrac{W^2+V^2-\mu^2}{2W}\ . \end{cases} \tag{3.8}$$

It is easily verified that $p_0^{(\prime)}+k_0^{(\prime\prime)}$ also depends only on W, V and μ, further

$$\boldsymbol{p}^{(\prime)}+\boldsymbol{k}^{(\prime\prime)}=0\,.$$

In the following, mixed scalars like $(p+k')\cdot u'$ should be understood to have been written in the form $a_{\mu}{}^{\nu}(p_\nu+k_\nu)u^{(\prime)\mu}$. If polar co-ordinates (r,θ,φ) are introduced for the space components of a 4-vector in the c.m. system then

$$\left\{\begin{aligned} r\sin\theta &= r^{(\prime)}\sin\theta^{(\prime)}\\ \varphi &= \varphi^{(\prime)}\end{aligned}\right. \tag{3.9}$$

because the 1 and 2 components are not altered by the transformation matrix $a_{\mu}{}^{\nu}$. We introduce the polar co-ordinates

$$\begin{aligned} &(U,\theta,\varphi) && \text{for } \boldsymbol{u}\\ &(U^{(\prime)},\theta^{(\prime)},\varphi^{(\prime)}) && \text{for } \boldsymbol{u}^{(\prime)}\\ &(a,\alpha,\beta) && \text{for } \boldsymbol{q}\\ &(a^{(\prime)},\alpha^{(\prime)},\beta^{\prime}) && \text{for } \boldsymbol{q}^{(\prime)}\end{aligned}$$

and note the following invariant expressions for the quantities occurring in the integrand of eq. (10)

$$q_0 = \tfrac{1}{2}(k_0-p_0)=\frac{(k-p)(k'-p)}{2W}=\frac{\zeta-m^2}{2W}\,, \tag{3.10}$$

$$a^2 = \boldsymbol{k}^2=k_0^2-\zeta=\left\{\frac{k(p+k)}{W}\right\}^2-\zeta=\frac{(W^2+m^2-\zeta)^2-4W^2m^2}{4W^2}\,, \tag{3.11}$$

$$q_0^{(\prime)} = \frac{(p^{(\prime)}-k^{(\prime\prime)})(p^{(\prime)}+k^{(\prime\prime)})}{2V}=\frac{m^2-\zeta}{2V}\,, \tag{3.12}$$

$$a^{(\prime)2}=k_0^{(\prime\prime)2}-\zeta=\frac{(V^2+m^2-\zeta)^2-4V^2m^2}{4V^2}\,. \tag{3.13}$$

Turning back to the equation (3.4) we find that the φ, and φ' dependence of $\boldsymbol{\Phi}$ is only through uu' and hence only through

$$u_1u_1^{(\prime)}+u_2u_2^{(\prime)}=UU'\sin\theta\sin\theta'\cos(\varphi-\varphi')\,.$$

Choosing the new variables φ and $\varphi_1=\varphi-\varphi'$ instead of φ and φ' and integ-

rating over φ we obtain

$$(3.14)\quad \varphi = 2\pi\int \mathrm{d}(u_0, u_0^{(\prime)}, U, U^{(\prime)}, \theta, \theta^{(\prime)}, \varphi_1)\, U^2\, U^{(\prime)2} \sin\theta \cdot \sin\theta^{(\prime)} \cdot$$
$$\cdot \frac{\Phi}{AA'} \left\{ \frac{x}{\sqrt{x^2-1}} + \frac{x'}{\sqrt{x'^2-1}} \right\} \frac{1}{xx' + \sqrt{x^2-1}\cdot\sqrt{x'^2-1} - \cos(\varphi_1 + \beta - \beta')} ,$$

where

$$A = 2Ua \sin\theta \sin\alpha , \qquad A' = 2U^{(\prime)} a^{(\prime)} \sin\theta^{(\prime)} \sin\alpha^{(\prime)} = 2U'a' \sin\theta' \sin\alpha' ,$$

$$x = \frac{\varkappa^2 + U^2 + a^2 - (u_0 - q_0)^2 - 2Ua \cos\theta \cos\alpha}{2Ua \sin\theta \sin\alpha} ,$$

$$x' = \frac{\varkappa'^2 + U^{(\prime)2} + a^{(\prime)2} - (u_0^{(\prime)} - q_0^{(\prime)})^2 - 2U^{(\prime)} a^{(\prime)} \cos\theta^{(\prime)} \cos\alpha^{(\prime)}}{2U'a' \sin\theta' \sin\alpha'} .$$

Eq. (3.14) establishes that φ has analytic properties with respect to each of these variables ζ, Q^2, σ^2 and Ω. Our immediate objective is to see if ζ can be analytically continued from the large negative value needed for establishing eq. (2.8) to the physical value. For this we need the minimum values of x and x' in the domain defined by (3.5). The computation goes analogous to the case of elastic meson-nucleon scattering [5] and one finds

$$(3.15)\quad \begin{cases} x_{\min} = \left\{ 1 + \dfrac{1}{a^2 \sin^2\alpha} \cdot \dfrac{(m_1^2 - \zeta)(m_2^2 - m^2)}{W^2 - (m_2 - m_1)^2} \right\}^{\frac{1}{2}} , \\ x'_{\min} = \left\{ 1 + \dfrac{1}{a'^2 \sin^2\alpha'} \cdot \dfrac{(m_1^2 - \zeta)(m_2^2 - m^2)}{W^2 - (m_2 - m_1)^2} \right\}^{\frac{1}{2}} , \end{cases}$$

where $m_2 = m + \mu$ and $m_1 = 3\mu$.

The analytic continuation of φ up to $\zeta = \mu^2$ will be possible provided $(\beta - \beta')$ is so restricted that throughout the range of integration the relationship

$$Y \equiv xx' + \sqrt{(x^2-1)(x'^2-1)} = \cos(\varphi_1 + \beta - \beta')$$

is excluded; which implies, in case $Y_{\min} > 0$, the requirement

$$(3.16)\qquad -Y_{\min} < \cos(\beta - \beta') < Y_{\min} .$$

The above inequality is indeed valid in the entire physical range of all the kinematic parameters. However, the dispersion relation might involve integration over a certain non-physical range also so that the requirement (3.16)

may be fullfilled only by restricting the range of momentum transfer parameters. Thus one concludes that with the inequality (3.16), $q(\zeta)$ is analytic in a certain neighbourhood of the real axis $\frac{1}{4}\ \zeta_2| < \delta$ in the range $\zeta_1 \leqslant \mu^2$ for all ω' [9].

4. – The non-physical region.

The physical region of the ten kinematic parameters (2.5) is the entire range that is reachable by dynamically possible four linearly independent energy momentum vectors of the five particles participating in the collision. The q-function is directly definable in a larger region of these parameters because basically its definition is not linked with the individual particle momenta. For any two energy-momentum vectors P_1 and P_2, in the entire mass spectrum of the nucleon-meson system under consideration, the function q is defined by

$$q = \frac{(2\pi)^{13/2}}{2} \int_{\alpha\alpha'} \langle p\,|J(0)\,|P_1\alpha\rangle\langle P_1\alpha\,|J(0)\,|P_2\alpha'\rangle(P_2\alpha')\,|J(0)\,|p'\rangle\,, \tag{4.1}$$

which depends on the then invariants

$$p^2\,,\quad p'^2\,,\quad P_1^2\,,\quad P_2^2\,,\quad (p-p')^2\,,\quad (P_1-P_2)^2\,,\quad (P_1-p)^2\,,$$
$$(P_2-p')^2\,,\quad (P_1-p)(P_1-P_2)\,,\quad \text{and}\quad \frac{(2P_1-P_2-p)(p-p')}{2\sqrt{-(p-p')^2}}\,.$$

Eq. (4.1) defines q in the entire range of these invariants that is reachable by any physically admissible momenta P_1 and P_2, irrespective of the particle number. In the precedent section we have established analytic continuation in $\zeta = (P_1-p)^2 = (P_2-p')^2$ thereby extending the range of definition of q where only eight of the ten parameters need by reachable by physical P_1 and P_2. We will continue to use the earlier notation, with an exception, for the kinematic parameters, *viz*,

$$\begin{cases} m^2 = p^2 = p'^2\,, \quad W^2 = P_1^2\,, \quad V^2 = P_2^2\,, \quad Q^2 = (p-p')^2\,, \\ \mu^2 = (P_1-P_2)^2\,, \quad \zeta_0 = (P_1-p)^2 = (P_2-p')^2\,, \\ \sigma^2 = (P_1-p)(P_1-P_2)\,, \quad \Omega = \dfrac{(2P_1-P_2-p)(p-p')}{2\sqrt{-(p-p')^2}}\,, \end{cases} \tag{4.2}$$

[9] A. Minguzzi and R. F. Streater: *Nuovo Cimento*, **17**, 946 (1960).

and bear in mind that their region of definition is larger than the « physical region ». In particular, ζ_0 can be analytically continued in the complex plane and assume a general value ζ which cannot be expressed as $(P_1-p)^2$.

Inside the region of definition one necessarily has the condition that the sum of the squares of the 1- and 2-components of any four-vectors, *e.g.*, (P_1-P_2), (P_2-p') and (P_1-p) must be positive semidefinite. Choosing the co-ordinate system O_B we obtain, for any four-vector X, the inequality

$$\left\{\frac{X(p+p')}{\sqrt{(p+p')^2}}\right\}^2-\left\{\frac{X(p-p')}{\sqrt{-(p-p')^2}}\right\}^2-X^2\geq 0\,. \tag{4.3}$$

The following inequalities are obtained by specializing to the above mentioned four vectors for X.

$$\frac{(W^2-V^2-Q^2+2\Omega\sqrt{-Q^2}-3\tau\sqrt{-Q^2})^2}{4m^2-Q^2}\geq(2\Omega-\tau)^2+\mu^2\,, \tag{4.4}$$

$$\frac{(V^2-m^2-\zeta_0+Q^2+2\tau\sqrt{-Q^2}-2Q\sqrt{-Q^2})^2}{4m^2-Q^2}\geq \tag{4.5, ζ_0}$$

$$\geq(2\tau-2\Omega-\sqrt{-Q^2})^2+\zeta_0\,,$$

$$\frac{(W^2-m^2-\zeta_0-\tau\sqrt{-Q^2})^2}{4m^2-Q^2}\geq\tau^2+\zeta_0\,. \tag{4.6, ζ_0}$$

The above inequalities determine the « physical region » if ζ_0 is replaced (*) by μ^2 and if one further imposes the conditions

$$W^2-V^2-Q^2+(2\Omega-3\tau)\sqrt{-Q^2}\geq 0\,, \tag{4.7}$$

$$V^2-m^2-\mu^2+Q^2+2(\tau-\Omega)\sqrt{-Q^2}\geq 0\,, \tag{4.8}$$

$$-Q^2\geq 0\,. \tag{4.9}$$

The region of definition of q is limited by (4.4), (4.5, ζ_0) and (4.6, ζ_0) with any real $\zeta_0\leq\mu^2$. Note that the inequality (4.4), which is independent of ζ_0, limits the « physical region » as well as the region of definition.

In the dispersion relation one integrates over W while other parameters are fixed at their physical values. The validity of (4.8), (4.9), (4.5, μ^2) and (4.4) is given. The range of integration over W is limited by (4.4); the part of this range that violates (4.6, μ^2) or (4.7) is the non-physical region of integration. It is only in this region that (3.16) may be violated unless some restrictions on the fixed parameters is imposed.

(*) The resulting inequalities will be denoted by (4.5, μ^2) and (4.6, μ^2).

The spectrum of W^2 has a discreet line at m^2 followed by a continuum starting at $(m+\mu)^2$. In view of the inequality (4.4) there is a gap in the continuum between

$$\{V^2+Q^2+(3\tau-2\Omega)\sqrt{-Q^2}\}+\sqrt{(4m^2-Q)}\{(2\Omega-\tau)^2+\mu^2\}$$

and

$$\{V^2+Q^2+(3\tau-2\Omega)\sqrt{-Q^2}\}-\sqrt{(4m^2-Q^2)}\{(2\Omega-\tau)^2+\mu^2\}\,.$$

We will obtain the condition that ensures the absence of a non-physical region above this gap. It is also possible to choose V^2 so that the half-width of the gap is wide enough to squeeze out the entire continuum below the gap. Under such circumstances the dispersion relation for physical ζ is very easily established because the entire integration is within the physical range. However the validity of the dispersion relation can certainly be pushed beyond these stringent conditions on the kinematic parameters.

If W^2 lies above the gap (remembering that the inequalities (4.4), (4.5, μ^2) and (4.8) are given to be true), one can establish (4.6, μ^2) provided

$$\{\sqrt{(2\Omega-\tau)^2+\mu^2}+\sqrt{(2\tau-2\Omega-\sqrt{-Q^2})^2+\mu^2}\}^2\geqslant\tau^2+\mu^2\,. \tag{4.10}$$

Note that

$$\tau^2=\{(2\Omega-\tau)+(2\tau-2\Omega-\sqrt{-Q^2})\}^2+2\tau\sqrt{-Q^2}+Q^2\,.$$

A sufficient condition for (4.10) is found, using the elementary property of the sum of two sides of a triangle being larger than the third, *viz.*,

$$\tau\leqslant\frac{3\mu^2-Q^2}{\sqrt{-Q^2}}\,. \tag{4.11}$$

The non-physical spectrum of W^2 is confined entirely below the gap if τ satisfies the above inequality as it ensures (4.6, μ^2) (which is just the condition for the physical region), for the region above the gap. Now to eliminate the non-physical continuum completely we require

$$\Delta V^2+\tau\sqrt{-Q^2}+m^2+\mu^2-\sqrt{(4m^2-Q^2)}\{(2\Omega-\tau)^2+\mu^2\}\leqslant(m+\mu)^2\,, \tag{4.12}$$

where

$$\Delta V^2\equiv V^2-m^2-\mu^2+Q^2+2(\tau-\Omega)\sqrt{-Q^2}>0\,.$$

There remains the contribution from the discreet line $W^2 = m^2$ to the φ function. This can be written in terms of the meson-nucleon coupling constant g and the φ_{el}-function for the elastic meson-nucleon scattering

$$(4.13)\quad \varphi(W^2, V^2, \Omega, \tau, Q^2, \zeta = \mu^2) = \delta(W^2 - m^2) g \varphi_{el}\left(V^2, -\frac{2\tau\sqrt{-Q^2 + \mu^2 - Q^2}}{4}\right) +$$

$$+ \theta\left[W^2 - V^2 - Q^2 - (3\tau - 2\Omega)\sqrt{-Q^2} + \sqrt{(4m^2 - Q^2\{(2\Omega - \tau)^2 + \mu^2\}}\right] \cdot$$

$$\cdot \varphi_1(W^2, V^2, \Omega, \tau, Q^2, \zeta = \mu^2) .$$

In φ_{el}, V takes the role of total energy (in the C.M. system) and

$$-\tfrac{1}{4}(2\tau\sqrt{-Q^2 + \mu^2 + Q^2}) - \Delta^2 ,$$

takes the role of momentum transfer. The latter may be outside the physical range so that an analytic continuation in Δ^2 might be necessary.

5. – Dispersion relation for $\zeta = \mu^2$.

We re-write the eq. (2.8) in terms of W'^2 as the integration variable

$$(5.1)\quad M(\omega, \Omega, \zeta) = \frac{1}{2\pi}\int dW'^2 \left[\frac{\varphi(W'^2\, \Omega, \zeta)}{W'^2 - \sqrt{-Q^2}\,\Omega - s - \tfrac{1}{2}\zeta - \sqrt{4m^2 - Q^2}\,\omega} + \right.$$

$$\left. + \frac{\varphi(W'^2, -\Omega, \zeta)}{W'^2 + \sqrt{-Q^2}\,\Omega - s - \tfrac{1}{2}\zeta + \sqrt{4m^2 - Q^2}\,\omega}\right].$$

The $M(\omega, \Omega, \zeta)$ defined by the eq. (5.1) is an analytic function of ζ in the region

$$R_2: \quad \zeta_1 \leqslant \mu^2 , \qquad \tfrac{1}{2}|\zeta_2| < \mathrm{Min}\{2\delta, 2\omega_2\sqrt{m^2 - \tfrac{1}{4}Q^2}\}$$

and is coincident for $\zeta_1 < -\mu^2 - 2\sigma^2 - 4\Omega^2$, $\zeta_2 = 0$ with the $M(\omega, \Omega, \zeta)$ defined by the eq. (2.2). The latter M is an analytic function of ω and ζ in the region R_1. The limit $\zeta_1 = \mu^2$, $\omega_2 \to 0$, $\zeta_2 \to 0$ can be reached through a finite intersection of R_1 and R_2 if

$$(5.2)\quad \sqrt{m^2 - \tfrac{1}{4}Q^2} > 2\{\omega_1 - \sqrt{\omega_1^2 - \tfrac{1}{4}(2\mu^2 + 2\sigma^2 + 4\Omega^2)}\} .$$

The maximum value of the right hand side in the physical range is

$$\sqrt{2\mu^2 + 2\sigma^2 + 4\Omega^2} ,$$

so that we obtain the inequality

$$(5.3)\qquad \begin{cases} \sqrt{m^2 - \tfrac{1}{4}Q^2} > \sqrt{2(\mu^2 + \sigma^2 + 2\Omega^2)} \\ \text{or} \\ m^2 - \tfrac{1}{4}Q^2 > 3\mu^2 + Q^2 - 4(\Omega - \tau)\sqrt{-Q^2 + 4\Omega^2}\,. \end{cases}$$

Provided the inequality (5.3) is valid, the analytic continuation of both sides of eq. (5.1) to $\zeta = \mu^2$ leads to the dispersion relation of physical amplitude.

* * *

The author is very thankful to the Director, National Physical Laboratory, India, for permission to publish this work.

RIASSUNTO (*)

Si è studiata una relazione di dispersione e alcune proprietà di analiticità della ampiezza del processo $n+\pi \to n'+\pi'+\pi''$ sulla base della rappresentazione integrale del commutatore causale dovuta a Jost-Lehmann-Dyson.

(*) *Traduzione a cura della Redazione.*

IL NUOVO CIMENTO Vol. XIX, N. 2 16 Gennaio 1961

Analytic Properties of Deuteron Photodisintegration Matrix Element for Fixed Energy.

A. Martin

CERN - Geneva

(ricevuto il 27 Settembre 1960)

Résumé. — On étudie les propriétés analytiques de l'élément de matrice non-relativiste de photodésintégration du deutéron pour une énergie fixée, en fonction de l'angle. Le proton et le neutron interagissent par un potential statique qui est une superposition de potentiels de Yukawa. Les complications dues aux spins sont négligées. Le résultat obtenu coïncide avec les prédictions d'une représentation de Mandelstam proposée par De Alfaro et Rossetti à partir des premiers termes du développement de cet élément de matrice, calculé dans une théorie des champs où le deutéron est traité comme une particule élémentaire couplée au neutron et au proton. L'intérêt de cette étude réside dans le fait que d'une part l'une des particules initiales est un état lié et que d'autre part dans la représentation de Mandelstam proposée, les points de départ des coupures sont donnés par des seuils anormaux du type de ceux étudiés par Karplus, Sommerfield et Wichmann. Un résultat analogue, concernant l'analyticité des amplitudes correspondant à une onde partielle donné en fonction de l'énergie a déjà été obtenu par De Alfaro et Rossetti.

1. – Introduction.

De Alfaro and Rossetti [1] have recently studied, in the non-relativistic case, the analytic properties of the partial wave amplitudes for deuteron photodisintegration, under the assumption that the n-p static potential has the form

$$V(r) = \int_{\mu}^{\infty} g(\sigma) \exp[-\sigma r] \, \mathrm{d}\sigma \,. \tag{1}$$

[1] V. De Alfaro and C. Rossetti: preprint, to be published in *Nuovo Cimento*.

On the other hand they study a field theoretical model in which the deuteron is treated as an elementary particle coupled to the neutron and the proton; from the five first perturbation graphs they obtain, using the results of KARPLUS, SOMMERFIELD and WICHMANN [2] a Mandelstam representation with anomalous thresholds. It happens that the predictions of the static model coincide, in the non-relativistic limit, with those obtained by projecting on a partial wave the Mandelstam representation obtained from field theoretical arguments. We think it is worth-while to study more thoroughly the non-relativistic matrix element for two reasons:

i) One of the incoming particles is a bound state and no such case has been investigated up to now.

ii) Anomalous thresholds are present and the proof of the Mandelstam representation to all orders in perturbation theory by EDEN, POLKINGHORNE *et al.* [3] does not include this case.

The present paper deals with analyticity with respect to the angle for fixed energy (*). Our method makes use of two results:

i) The existence of a spectral representation for the deuteron wave function, which was first introduced by the author [1] and independently by BLANCKENBECLER *et al.* [5], under the assumption of a n-p potential of the type (1).

ii) The analytic properties of the T matrix for neutron proton scattering with respect to the angle, *off the energy shell*, for fixed lengths of the initial and final momenta. These properties are very similar to those obtained *on the energy shell* by various authors [6-8], but though they are probably known by all the people working in this field, they have not yet been stated. They are derived in the Appendix.

Our result coincides with the predictions based on the Mandelstam representation obtained by DE ALFARO and ROSSETTI from low order perturbation arguments.

[2] R. KARPLUS, C. SOMMERFIELD and E. WICHMANN: *Phys. Rev.*, **114**, 378 (1959).

[3] J. EDEN: preprint; J. EDEN and J. C. POLKINGHORNE: to be published in the *Proc. of the Ninth Annual Intern. Conf. on High Energy Physics* (Rochester, 1960).

[4] A. MARTIN: *Nuovo Cimento*, **14**, 403 (1959).

[5] R. BLANKENBECLER and Y. NAMBU: to be published.

[6] J. BOWCOCK and A. MARTIN: *Nuovo Cimento*, **14**, 516 (1959).

[7] T. REGGE: *Nuovo Cimento*, **14**, 951 (1959).

[8] R. BLANKENBECLER, M. L. GOLDBERGER, N. N. KHURI and S. B. TREIMAN: *Ann. of Phys.*, **10**, 62 (1960); A. KLEIN: *Journ. Math. Phys.*, **1**, 41 (1960).

2. – The matrix element.

We make the same simplifying assumptions as DE ALFARO and ROSSETTI: the nucleons and the photon have no spin, the deuteron is in an S-state and the n-p potential is a superposition of Yukawa potentials; such a superposition may be written in the form (1) (the reciprocal is not true). Then the photo-disintegration matrix element reads:

$$M(k, q, \cos\theta) = \int \psi_q^*(\boldsymbol{r}) \exp\left[i \frac{\boldsymbol{k}\boldsymbol{r}}{2}\right] \psi_d(\boldsymbol{r})\, \mathrm{d}^3\boldsymbol{r}\,, \tag{2}$$

in co-ordinate space, or

$$M(k, q, \cos\theta) = \int \tilde{\psi}_q^*(\boldsymbol{p})\, \tilde{\psi}_d\left(\boldsymbol{p} - \frac{\boldsymbol{k}}{2}\right) \mathrm{d}^3\boldsymbol{p}\,, \tag{3}$$

in momentum space (2π factors are omitted), where $\boldsymbol{k}$ is the momentum of the incident photon, $\boldsymbol{q}$ is the c.m. momentum of each of the final nucleons, ψ_d the deuteron wave function and ψ_q the wave function of the final state.

We now wish to put in evidence the angular properties of the two quantities entering in the matrix element. It has been shown in [1] and [4] that if the n-p potential has the form (1) the deuteron wave function may be written

$$\psi_d(r) = \frac{1}{N} \frac{\exp[-\alpha r]}{r}\left[1 + \int_\mu^\infty \varrho(\sigma) \exp[-\sigma r]\, \mathrm{d}r\right] \equiv \int_0^\infty \varrho'(\sigma) \frac{\exp[-\sigma r]}{r}\, \mathrm{d}\sigma\,, \tag{4}$$

with

$$\varrho'(\sigma) = \frac{1}{N}\delta(\alpha - \sigma) + \frac{1}{N}\varrho(\sigma - \alpha)\theta(\sigma - \alpha - \mu)\,,$$

and where $\alpha^2 = M|\varepsilon|$, ε binding energy of the deuteron and M mass of the nucleon, so that

$$\tilde{\psi}_d\left(\boldsymbol{p} - \frac{\boldsymbol{k}}{2}\right) = \frac{1}{pk} \int_0^\infty \frac{\varrho'(\sigma)\, \mathrm{d}\sigma}{((p^2 + (k^2/4) + \sigma^2)/kp) - \cos(\boldsymbol{p}\boldsymbol{k})}\,. \tag{5}$$

On the other hand, the wave function of the final state in momentum space may be written

$$\tilde{\psi}_q(\boldsymbol{p}) = \delta(\boldsymbol{p} - \boldsymbol{q}) + \frac{1}{p^2 - q^2 + i\varepsilon} T(\boldsymbol{p}, \boldsymbol{q}, q)\,. \tag{6}$$

$T(\boldsymbol{p}, \boldsymbol{q}, q)$ is the off energy shell scattering matrix given by

$$T(\boldsymbol{p}, \boldsymbol{q}, r) = T(p, q, r, \cos\theta) = \langle \boldsymbol{p} | V | \boldsymbol{q} \rangle + \tag{7}$$
$$+ \int \mathrm{d}^3 p' \langle \boldsymbol{p} | V | \boldsymbol{p}' \rangle \frac{1}{p'^2 - r^2 + i\varepsilon} T(\boldsymbol{p}', \boldsymbol{q}, r) .$$

The analytic properties of $T(\boldsymbol{p}, \boldsymbol{q}, q, \cos\theta)$ with respect to $\cos\theta$, for fixed real p and q are derived in the Appendix under the assumption that V is a superposition of Yukawa potentials:

$$\langle \boldsymbol{p} | V | \boldsymbol{p}' \rangle = \int_{\mu}^{\infty} \frac{w(\sigma)\,\mathrm{d}\sigma}{(\boldsymbol{p} - \boldsymbol{p}')^2 + \sigma^2} . \tag{8}$$

Let us repeat that family (8) is contained in family (1).

The properties are the following:

— T is a holomorphic function of $\cos\theta$ except for a cut on the real axis, from

$$\cos\theta = \frac{\mu^2 + p^2 + q^2}{2pq} \qquad \text{to} \qquad \cos\theta = +\infty ;$$

— the same properties hold for the function which, for physical values of $\cos\theta$, is $\operatorname{Im} T$.

— For strong potentials we were not able to establish the behaviour as $|\cos\theta| \to \infty$. For extreme cases the behaviour is known:

i) $p = q$ REGGE [7] has proven in this case that for potentials $V(r)$ analytic in r for $\operatorname{Re} r > 0$ such that $|V(ir)| < A/r^2$ the T matrix can be bounded as $|\cos\theta| \to \infty$ by some power of $|\cos\theta|$.

ii) $p = \infty$ then $T \equiv 0$.

iii) $p = 0$ then $T =$ constant.

So we believe that nothing really new will happen between these three values of p and that only a finite number of subtractions, less than some fixed number independent of p, is needed in an integral representation of T. With this assumption we can write

$$T(p, q, q, \cos\theta) = \sum_{1}^{n-1} A_i(p, q)(\cos\theta)^i + (\cos\theta)^n \int_{(p^2+q^2+\mu^2)/2pq} \frac{R(u, p, q)\,\mathrm{d}u}{u - \cos\theta} . \tag{9}$$

— For weak potentials, *i.e.* $\int_{\mu}^{\infty} |w(\sigma)|\,\mathrm{d}\sigma$ small enough, $w(\sigma)$ being a sufficiently *smooth* function, satisfying, for instance, some kind of double Lipschitz condition, it is possible to show that at most one subtraction is needed, and that the integral representation of T may be obtained from the behaviour of each term of the Born expansion. Unfortunately, we know that the n-p potential is strong enough to bind a deuteron so that this result is not of much use here.

3. – Analyticity of the matrix element with respect to the angle

Let us first disregard the problem of subtractions and set $n = 0$ in formula (9). We can write

$$M(k, q, \cos\theta) = \frac{1}{qk}\int_0^{\infty} \frac{\varrho'(\sigma)\,\mathrm{d}\sigma}{(q^2 + (k^2/4) + \sigma^2)/qk - \cos\theta} + \tag{10}$$

$$+ \frac{1}{k}\int_0^{\infty} \frac{p\,\mathrm{d}p}{p^2 - q^2 + i\varepsilon} \int_0^{\infty} \mathrm{d}\sigma \int_{(p^2+q^2+\mu^2)/2pq}^{\infty} \mathrm{d}u \int \mathrm{d}\Omega_p \frac{R^*(u, p, q)\,\varrho'(\sigma)}{[(p^2+(k^2/4)+\sigma^2)/pk - \cos(\boldsymbol{kp})][u - \cos(\boldsymbol{pq})]}.$$

Let us now replace the angular integration appearing in the second term by an integral over an auxiliary variable. It can be shown that

$$\int \frac{\mathrm{d}\Omega_2}{[(l^2 + m^2 + \alpha^2)/2lm - \cos\theta_{12}][(l^2 + n^2 + \beta^2)/2ln - \cos\theta_{23}]} = \int_{x_{\min}}^{\infty} \frac{f(x)\,\mathrm{d}x}{x - \cos\theta_{13}}, \tag{11}$$

where $x_{\min}$ is a function of l, m, n, α, β such that

$$x_{\min} \geqslant \frac{m^2 + n^2 + (\alpha + \beta)^2}{2mn}, \qquad \text{for} \qquad 0 \leqslant l \leqslant +\infty;$$

the explicit form of $f(x)$ is given in the Appendix.

Remembering that $\varrho'(\sigma)$ consists of a δ-function plus a function starting at $\sigma = \alpha + \mu$, we perform the angular integration using formula (11). Assuming that no difficulty arises in the remaining integration over the parameters of the integral representations and over p, we finally get:

$$M(k, q, \cos\theta) = \frac{1}{N}\frac{1}{q^2 + (k^2/4) + \alpha^2 - qk\cos\theta} + \int_{((\alpha+\mu)^2+q^2+(k^2/4))/kq}^{\infty} \frac{\mathrm{d}u\,\chi(k, q, u)}{u - \cos\theta}. \tag{12}$$

Let us now compare this formula with the predictions based on field theoretical perturbative arguments. We reproduce here formula (11) of reference [1]).

$$M(q, k, \cos\theta) \equiv F(q, \cos\theta) = \frac{a/4}{q^2+\alpha^2} - \frac{b/2}{\alpha^2+q^2+(k^2/4)-kq\cos\theta} + \tag{13}$$

$$+ 2\int_0^{\infty} \frac{\mathrm{d}q'^2}{q'^2-q^2} \int_{\mu}^{\infty} \frac{\mathrm{d}\sigma(\sigma+\alpha)\, M(\sigma, q'^2)}{(\sigma+\alpha)^2+q^2+(k^2/4)-qk\cos\theta} .$$

If we perform the integral over q'^2 we see that formulae (12) and (13) coincide except that in formula (13) the deuteron pole term $(a/4)/(q^2+\alpha^2)$ is missing. This is not surprising since we have disregarded the problem of subtractions. Now it is very likely that since, in general

$$\lim_{p\to 0} T(p, q, \cos\theta) = \text{const} \neq 0 ,$$

at least one subtraction is needed in representation (9).

Let us now show that formula (14) is not seriously altered when n subtractions are present in representation (9). In this case we have to perform angular integrals of two types:

$$\text{i)} \qquad \int \mathrm{d}\Omega_2 \frac{(\cos\theta_{23})^n}{(A-\cos\theta_{12})(B-\cos\theta_{23})} , \qquad A>1,\ B>1, \tag{14}$$

$$\text{ii)} \qquad \int \mathrm{d}\Omega_2 \frac{\sum_0^{n-1} a_i(\cos\theta_{23})^i}{A-\cos\theta_{12}} = \int \mathrm{d}\Omega_2 \frac{\sum_0^{n-1} b_i P_i(\cos\theta_{23})}{A-\cos\theta_{12}} . \tag{15}$$

Noticing that:

$$\frac{x^n}{B-x} = B^n \left[\frac{1}{B-x} - \frac{1}{B} - \frac{x}{B^2} \cdots - \frac{x^{n-1}}{B^n} \right] , \tag{16}$$

we can reduce integral i) to the angular integral without subtraction (for fixed B and A there is no problem of convergence) and to an integral of the type ii). The integral of the type ii) may be computed; it is just

$$4\pi \sum_0^{n-1} b_i Q_i(A)\, P_i(\cos\theta_{13}) .$$

So, after the angular integration we get an expression

$$\sum_1^{n-1} C_i(A, B)(\cos\theta_{13})^i + \int_{x_{\min}(A\cdot B)} \frac{f(x, A, B)\,\mathrm{d}x}{x-\cos\theta_{13}} . \tag{17}$$

Now it is clear that when one integrates over B, with the convenient weight function, the terms appearing in (17), one gets for each term a divergent result because a factor B^n appears in the right hand side of (16). It turns out that n subtractions have to be made in the integral appearing in (17). Finally one gets the result (12) with n subtractions.

4. – Concluding remarks.

Though the results of the present paper on the analyticity for fixed energy, combined with the results of De Alfaro and Rossetti on partial waves are not sufficient to establish that the non-relativistic photodisintegration matrix element satisfies the Mandelstam representation (13), they are nevertheless very encouraging. In the scattering problem, all the proofs of Mandelstam representation use a combination of the analytic properties for fixed energy and fixed momentum transfer. One may hope to apply the same method here. So, what remains to be done is to derive dispersion relations for fixed momentum transfer. (This momentum transfer has to be defined conveniently). This is being currently investigated now at CERN.

* * *

The author wishes to thank Professors S. Fubini, M. Gourdin and J. Mandelbrojt for very stimulating discussions.

Appendix

A.1. *Angular integrals.* – By means of Feynman parametrization technique one may prove

$$\text{(A.1)}\qquad \int \frac{\mathrm{d}\Omega_2}{(A-\cos\theta_{12})(B-\cos\theta_{23})} =$$

$$= 4\pi \int_1^\infty \frac{\mathrm{d}Z}{\sqrt{Z^2-1}\,[Z\sqrt{A^2-1}\,\sqrt{B^2-1}+AB-\cos\theta_{13}]}, \qquad A>1,\ B>1.$$

So

$$\text{(A.2)}\qquad \int_{A_0}^\infty \int_{B_0}^\infty \int \frac{\mathrm{d}A\,\mathrm{d}B\,\mathrm{d}\Omega_2 f(A)g(B)}{(A-\cos\theta_{12})(B-\cos\theta_{23})} = \int_{C_0}^\infty \frac{\mathrm{d}C\,h(C)}{C-\cos\theta_{13}},$$

with $C_0 = \sqrt{A_0^2-1}\,\sqrt{B_0^2-1}+A_0B_0$.

Further one can prove the following inequality:

$$\int_{C_0}^{\infty} \frac{|h(C)|\,\mathrm{d}c}{C-1} \leqslant 4\pi \int_{A_0}^{\infty} \frac{|f(A)|\,\mathrm{d}A}{A-1} \int_{B_0}^{\infty} \frac{|g(B)|\,\mathrm{d}B}{B-1}. \tag{A.3}$$

Now if

$$A_0 = \frac{l^2+m^2+\alpha^2}{2lm} \qquad \text{and} \qquad B_0 = \frac{l^2+n^2+\beta^2}{2ln},$$

the minimum of C_0 with respect to l for $0 \leqslant l < \infty$ is

$$C_{0\,\min} = \frac{m^2+n^2+(\alpha+\beta)^2}{2mn}.$$

This relation was derived in another way in reference [6].

A.2. *Analytic properties of T off the energy shell for weak potentials.* – Let us first write the n-th term of the Born expansion

$$T_n(\boldsymbol{p},\boldsymbol{q},r) = \tag{A.5}$$

$$= \int \langle \boldsymbol{p}|V|\boldsymbol{k}_1\rangle \frac{1}{k_1^2-r^2+i\varepsilon} \langle \boldsymbol{k}_1|V|\boldsymbol{k}_2\rangle \ldots \frac{1}{k_{n-1}^2-r^2+i\varepsilon} \langle \boldsymbol{k}_{n-1}|V|\boldsymbol{q}\rangle\, \mathrm{d}^3k_1 \ldots \mathrm{d}^3k_{n-1},$$

if V is a superposition of Yukawa potentials, a typical term appearing in $\langle \boldsymbol{k}_i|V|\boldsymbol{k}_{i+1}\rangle$ will be

$$\frac{1}{2k_i k_{i+1}} \frac{1}{(\alpha^2+k_i^2+k_{i+1}^2)/2k_i k_{i+1} - \cos(\boldsymbol{k}_i \boldsymbol{k}_{i+1})}.$$

So, applying formulae (A.1) and (A.4) we can write:

$$T_n(p,q,r) = \int \prod_1^{n-1} \left(\frac{\mathrm{d}k_i}{k_i^2-r^2+i\varepsilon} \right) \int_{C_1(k_1,\ldots k_{n-1},p,q)}^{\infty} \frac{W(C,k_1,k_2\ldots k_{n-1},p,q)\,\mathrm{d}C}{C-\cos\theta},$$

where

$$C_0 \geqslant \frac{n^2\mu^2+p^2+q^2}{2pq},$$

which, if no trouble arises in the radial integrals gives

$$T_n(p,q,r) = \int_{(n^2\mu^2+p^2+q^2)/2pq}^{\infty} \frac{R_n(p,q,r,u)\,\mathrm{d}u}{u-\cos\theta}. \tag{A.6}$$

If the last radial integrals did not contain principal value integrals, it would not be difficult to get, by using inequality (A.3), an upper bound for

$$\int \frac{|R_n(u)|\,\mathrm{d}u}{u-1},$$

and to show that for sufficiently weak potentials $T=\sum T_n$ and $R=\sum R_n$. Unfortunately we have to study more carefully the integration region from $k_i=r-\Delta$ to $k_i=r+\Delta$. A convenient procedure is to write

$$\text{(A.7)}\qquad \frac{1}{k_i^2-r^2}V(\boldsymbol{k}_i,\boldsymbol{k}_{i+1})k_i k_{i+1}\frac{1}{k_{i+1}^2-r^2}=\frac{1}{k_i^2-r^2}r^2V(\hat{\boldsymbol{k}}_i,\hat{\boldsymbol{k}}_{i+1})\frac{1}{k_{i+1}^2-r^2}+$$

$$+\frac{1}{k_i^2-r^2}W(\hat{\boldsymbol{k}}_i,\boldsymbol{k}_{i+1})+\frac{1}{k_{i+1}^2-r^2}W(\boldsymbol{k}_i,\hat{\boldsymbol{k}}_{i+1})+Z(\boldsymbol{k}_i,\boldsymbol{k}_{i+1})\,.$$

where

$$\hat{\boldsymbol{k}}_i=\frac{\boldsymbol{k}_i}{k_i}r\,,$$

then one gets rid of all the singularities. If W, and Z have integral representations in $\cos\theta$ of the same type as V itself, with weight function ϱ such that

$$\int\frac{|\varrho(x)|\,\mathrm{d}x}{x-1}\,,$$

is bounded, one can still get an upper bound for

$$\int\frac{|R_n(u)|\,\mathrm{d}u}{u-1}\,.$$

This is not the case for a pure Yukawa potential corresponding to $w(\sigma)=\delta(\sigma-\mu)$ in

$$V(r)=\int w(\sigma)\frac{\exp[-\sigma r]}{r}\,\mathrm{d}\sigma\,,$$

but it is the case for potentials with a weight function $w(\sigma)$ sufficiently smooth. For instance one can require for $w(\sigma)$ a double Lipschitz condition:

$$\left|\frac{w(\alpha)-w(\beta)}{\alpha-\beta}-\frac{w(\gamma)-w(\delta)}{\gamma-\delta}\right|<A\frac{[|\alpha-\gamma|+|\beta-\delta|][|\alpha-\delta|+|\beta-\gamma|]}{(\alpha+\beta)^2(\gamma+\delta)^2}\,,$$

which, with $w(\infty)=0$ implies

$$\left|\frac{w(\alpha)-w(\beta)}{\alpha-\beta}\right|<\frac{A}{(\alpha+\beta)^2}\qquad\text{and}\qquad|w(\alpha)|<\frac{A}{\alpha}\,.$$

Then one can show that V, W, Z have the desired properties and that

$$T_n = \int_{(n^2\mu^2+p^2+q^2)/2pq} \frac{R_n(p, q, r, u)\,\mathrm{d}u}{u - \cos\theta} \qquad \text{with} \qquad \int \frac{|R_n|\,\mathrm{d}u}{u-1} < \lambda^n A^n ,$$

where λ is some fixed number. Then, for A small enough, the series can be summed and

$$T(\boldsymbol{p}, \boldsymbol{q}, r) = \int_{(\mu^2+p^2+q^2)/2pq}^{\infty} \frac{R(p, q, r, u)\,\mathrm{d}u}{u - \cos\theta} ,$$

with

$$\int_{(\mu^2+p^2+q^2)/2pq} \frac{|R(p, q, r, u)|\,\mathrm{d}u}{u-1} , \tag{A.8}$$

finite.

One can understand why one subtraction is necessary for $p = 0$: as $p \to 0$ the lower limit for u goes to infinity. So it is quite possible that $R(p, q, r, u) \to \infty$ as $p \to 0$, though the integral remains finite. On the other hand, property (A.8) ensures that $\int R(u)\,\mathrm{d}u/(u - \cos\theta)$ exists everywhere outside the cut and goes to zero as $|\cos\theta| \to \infty$ in any direction except the direction of the cut.

It is interesting to note that the case of pure Yukawa potential cannot be treated in this way and that in Regge's proof for $p = q = r$ (7) it is also excluded.

A.3. *Analytic properties for strong potentials.* – There we combine the properties of the terms of the perturbation expansion with general properties of T for potentials decreasing faster than an exponential:

$$T(\boldsymbol{p}, \boldsymbol{q}, r) = \int \exp[-i\boldsymbol{p}\boldsymbol{x}]\, V(\boldsymbol{x})\, G(\boldsymbol{x}, \boldsymbol{x}', r)\, V(\boldsymbol{x}')\, \exp[i\boldsymbol{q}\boldsymbol{x}']\, \mathrm{d}^3\boldsymbol{x}\, \mathrm{d}^3\boldsymbol{x}' , \tag{A.9}$$

where G is the total Green's function which is known to be bounded (9). A sufficient condition for the existence of T is that the integrals at both ends be absolutely convergent. Setting

$$\boldsymbol{p} = \boldsymbol{n}_1 p \cos\alpha\theta + \boldsymbol{n}_2 p \sin\alpha\theta ,$$

$$\boldsymbol{q} = \boldsymbol{n}_1 q \cos(1-\alpha)\theta - \boldsymbol{n}_2 q \sin(1-\alpha)\theta ,$$

with

$$\boldsymbol{n}_1 \perp \boldsymbol{n}_2 \qquad \text{and} \qquad 0 < \alpha < 1 ,$$

(9) A. KLEIN and C. ZEMACH: *Ann. of Phys.*, **7**, 440 (1959).

we get the simultaneous conditions

$$\text{(A.10)} \qquad \begin{cases} \mathrm{sh}^2[\alpha \operatorname{Im}(\theta)] < \dfrac{\mu^2}{p^2}, \\ \mathrm{sh}^2[(1-\alpha) \operatorname{Im}(\theta)] < \dfrac{\mu^2}{q^2}, \end{cases}$$

which define, in the $\cos\theta$ plane two ellipses with foci -1, $+1$. α must be chosen to make the domain as large as possible. This is the case when the two ellipses coincide. Then the semi-major axis is

$$\text{(A.11)} \qquad \sqrt{1+\frac{\mu^2}{p^2}}\sqrt{1+\frac{\mu^2}{q^2}}+\frac{\mu^2}{pq} > \sqrt{1-\frac{\mu^2}{q^2}}.$$

Let us now write

$$\text{(A.12)} \qquad T(\boldsymbol{p},\boldsymbol{q},q) = T_1 + \ldots + T_n + \int T_n(\boldsymbol{p},\boldsymbol{p}',q)\,\frac{1}{p'^2-q^2+i\varepsilon}\,T(\boldsymbol{p}',\boldsymbol{q},q)\,\mathrm{d}^3\boldsymbol{p}',$$

and expand T and T_n under the integral in Legendre polynomials

$$\text{(A.13)} \qquad T_n(\boldsymbol{p},\boldsymbol{p}',q) = \sum B_n P_n(\cos(\boldsymbol{p},\boldsymbol{p}')),$$

$$\text{(A.14)} \qquad T(\boldsymbol{p}',\boldsymbol{q},q) = \sum C_n P_n(\cos(\boldsymbol{p}',\boldsymbol{q})),$$

and

$$\text{(A.15)} \qquad \int \mathrm{d}\Omega_{p'}\,T_n(\boldsymbol{p},\boldsymbol{p}',q)\,T(\boldsymbol{p}',\boldsymbol{q},q) = \sum \frac{4\pi}{2n+1}\,B_n C_n P_n(\cos(\boldsymbol{pq})).$$

Now if (A.13) converges in an ellipse with semi-major axis b and (A.14) in an ellipse with semi-major axis c

$$\limsup_{n\to\infty}(B_n)^{1/n} < \frac{1}{b+\sqrt{b^2-1}},$$

$$\limsup_{n\to\infty}(C_n)^{1/n} < \frac{1}{c+\sqrt{c^2-1}},$$

and expansion (A.15) converges in an ellipse with semi-major axis a where

$$a + \sqrt{a^2-1} = (b+\sqrt{b^2-1})(c+\sqrt{c^2-1}),$$

i.e.

$$a = bc + \sqrt{b^2-1}\,\sqrt{c^2-1},$$

where

$$b = \frac{n^2\mu^2 + p'^2 + p^2}{2pp'},$$

$$c = \sqrt{1+\frac{\mu^2}{p'^2}}\sqrt{1+\frac{\mu^2}{q^2}}+\frac{\mu^2}{p'q},$$

the exact minimum of a with respect to p' is difficult to get but it is clear that

$$a > \sqrt{\left(1 + \frac{n^2\mu^2}{p^2}\right)\left(1 + \frac{\mu^2}{q^2}\right)},$$

so that $T - T_1 - T_2 \ldots T_n$ is holomorphic inside a larger and larger ellipse as $n \to \infty$. This method establishes the analyticity in $\cos\theta$ outside the cut but cannot give any information on the behaviour at infinity.

We add that all the properties we have obtained are valid for Im T where

$$\text{Im } T(\boldsymbol{p}, \boldsymbol{q}, r) = \int \exp[-i\boldsymbol{p}\boldsymbol{x}]\, V(x)\, \text{Im } G(\boldsymbol{x}, \boldsymbol{x}', r)\, V(x')\, \exp[i\boldsymbol{q}\boldsymbol{x}']\, \mathrm{d}^3\boldsymbol{x}\, \mathrm{d}^3\boldsymbol{x}'.$$

RIASSUNTO (*)

Si studiano in funzione dell'angolo le proprietà analitiche dell'elemento di matrice non-relativistica di fotodisintegrazione del deutone per un'energia fissa. Il protone ed il neutrone interagiscono con un potenziale statico che è una sovrapposizione dei potenziali di Yukawa. Si trascurano le complicazioni dovute agli spin. Il risultato ottenuto coincide con le predizioni di una rappresentazione di Mandelstam proposta da De Alfaro e Rossetti a partire dai primi termini dello sviluppo di questo elemento di matrice, calcolato in una teoria di campo in cui il deutone è trattato come una particella elementare accoppiata al neutrone ed al protone. L'interesse di questo studio sta nel fatto che da una parte una delle particelle iniziali è uno stato legato e che d'altra parte nella rappresentazione di Mandelstam proposta, i punti di partenza dei tagli sono dati da alcune soglie anormali del tipo di quelle studiate da Karplus, Sommerfeld e Wichmann. Un risultato analogo, concernente l'analiticità delle ampiezze corrispondenti ad un'onda parziale data in funzione dell'energia è stato già ottenuto da De Alfaro e Rossetti.

(*) *Traduzione a cura della Redazione.*

Connection between Wightman Functions and Green Functions in p-Space.

D. Ruelle

Eidgenössische Technische Hochschule - Zürich

(ricevuto il 10 Ottobre 1960)

Resumé. — Dans le présent travail, après avoir repris l'étude des propriétés d'analyticité de la fonction $\mathscr{W}$ de Wightman dans le cas où le temps seul est variable complexe, nous en déduisons la fonction de Green G, étendant ainsi par une nouvelle méthode les résultats de O. Steinmann relatifs à la fonction à 4 points. La fonction G a pour valeur frontière la transformée de Fourier de la valeur moyenne du vide du produit T des champs et prolonge analytiquement la fonction retardée de L.S.Z. dans l'espace des impulsions. Finalement on établit un ensemble de propriétés qui caractérisent G en ce sens que si G possède ces propriétés, il existe une et une seule fonction $\widetilde{\mathscr{W}}$ possédant les propriétés habituelles et telle que G en dérive.

1. – Introduction. x- and p-spaces.

The Wightman function $\mathscr{W}(z)$, $z = x+iy$ is defined as an analytic continuation of the vacuum expectation value

$$\mathscr{W}(x) = \langle A^{(0)}(x_0) A^{(1)}(x_1) \dots A^{(n)}(x_n) \rangle_0$$

of the local scalar fields $A^{(i)}(x_i)$ [1,2].

The Green function $G(k)$, $k = p+iq$ will be defined as an analytic continuation of the Fourier transform of the vacuum expectation value of a T-pro-

(1) A. S. Wightman: *Phys. Rev.*, **101**, 860 (1956).
(2) D. Hall and A. Wightman: *Mat. Fys. Medd. Dan. Vid. Selsk.*, **31**, no. 5 (1957).

duct [3].

$$G(p) = \mathscr{F}\langle TA^{(0)}A^{(1)} \dots A^{(n)}\rangle_0(p_1, \dots, p_n) .$$

It is convenient to introduce immediately the spaces of variables that will be used in the sequel.

Consider the space R^{n+1} of the independent real variables $t_0, t_1, \dots, t_n$. The quotient of this space by the equivalence relation

$$t_0 - t_1 = t_0' - t_1', \quad t_1 - t_2 = t_1' - t_2', \quad \dots, \quad t_{n-1} - t_n = t_{n-1}' - t_n' \tag{1.1}$$

is a space R^n which will be called (t).

Similarly if $x_0, x_1, \dots, x_n$ or $y_0, y_1, \dots, y_n$ (resp. $z_0, z_1, \dots, z_n$) are sets of independent real (resp. complex) vector variables, the corresponding equivalence relations will yield spaces R^{4n} (resp. C^{4n}) which will be called (x) or (y) (resp. (z)).

If one considers vectors $(z_0^0, \boldsymbol{x}_0)$, $(z_1^0, \boldsymbol{x}_1)$, ..., $(z_n^0, \boldsymbol{x}_n)$ where the first (time) component is allowed to be complex, the other (space) components being real, one obtains in the same way a space $C_n \times R^{3n}$ called $(z^0, \boldsymbol{x})$.

Consider now the space R^{n+1} of the independent real variables $s_0, s_1, \dots, s_n$ The subspace of this space defined by

$$s_0 + s_1 + \dots + s_n = 0 \tag{1.2}$$

is a space R^n which will be called (s).

Similarly if $p_0, p_1, \dots p_n$ or $q_0, q_1, \dots, q_n$ (resp. $k_0, k_1, \dots, k_n$) are sets of independent real (resp. complex) vector variables, the corresponding subspaces are space R^{4n} (resp. C^{4n}) which will be called (p) or (q) (resp. (k)).

If one considers vectors $(k_0^0, \boldsymbol{p}_0)$, $(k_1^0, \boldsymbol{p}_1)$, ..., $(k_n^0, \boldsymbol{p}_n)$ where the first component is allowed to be complex, the other components being real, one obtains in the same way a space $C^n \times R^{3n}$ called $(k^0, \boldsymbol{p})$.

We can now introduce a bilinear form on (t) (s), namely

$$s \cdot t = \sum_{i=0}^{n} s_i \cdot t_i = \sum_{i=1}^{n} s_i (t_i - t_0) . \tag{1.3}$$

Similarly

$$p \cdot x = \sum_{i=0}^{n} p_i \cdot x_i = \sum_{i=1}^{n} p_i (x_i - x_0) , \tag{1.3'}$$

and so on.

---

[3] J. SCHWINGER: *Annual International Conference on High Energy Physics at CERN* (1958).

For integrations over (t), (s); (x), (p), etc., we will use

$$\mathrm{d}t = \mathrm{d}(t_1 - t_0) \ \ldots \ \mathrm{d}(t_n - t_0) \qquad \mathrm{d}s = \mathrm{d}s_1 \ \ldots \ \mathrm{d}s_n \,, \tag{1.4}$$

$$\mathrm{d}x = \mathrm{d}(x_1 - x_0) \ \ldots \ \mathrm{d}(x_n - x_0) \qquad \mathrm{d}p = \mathrm{d}p_1 \ \ldots \ \mathrm{d}p_n \,. \tag{1.4'}$$

In the spaces just introduced, we have of course redundant variables. It is useful to keep them in general for reasons of symmetry. In particular cases however, other variables may be more suitable.

We have introduced above *four*-dimensional vectors for obvious physical reasons. All that will be said can however be easily generalized to $N+1$ dimensional vectors $(x^0, x^1, \ldots, x^n)$ with metric $(x^0)^2 - (x^1)^2 - \ldots - (x^N)^2$, $N \geqslant 1$

2. – The decomposition of (t) and (s) into cones.

Let us consider the set of all planes

$$t_{i'} - t_i = 0 \qquad i, i' = 0, 1, \ldots, n; \ i \neq i' \tag{2.1}$$

in (t). They decompose (t) into a set $\mathscr{T}$ of open convex cones.

In such a cone T, every difference $t_{i'} - t_i$ has a well-defined sign so that we can order the t_i by increasing values into a characteristic sequence $t_{i_0} < t_{i_1} < \ldots < t_{i_n}$.

On the other hand to every sequence $(i_0, i_1, \ldots, i_n)$ there corresponds a permutation π of $\{0, 1, \ldots, n\}$ such that $\pi\,(0, 1, \ldots, n) = (i_0, i_1, \ldots, i_n)$ (and to every permutation corresponds a sequence). There is thus a one-to-one correspondence between $\mathscr{T}$ and the symmetric group $\mathscr{S}_{n+1}$ of permutations of $n+1$ objects, and $\mathscr{T}$ therefore contains $(n+1)!$ cones, each being defined by n relations:

$$t_{i_1} - t_{i_0} > 0 \quad \ldots \quad t_{i_n} - t_{i_{n-1}} > 0 \,.$$

We will often write for convenience

$$T(\pi) = (i_0, i_1, \ldots, i_n) \,. \tag{2.2}$$

The n faces of $T(\pi)$:

$$t_{i_0} = t_{i_1} < t_{i_2} < \ldots < t_{i_n} \,, \quad t_{i_0} < t_{i_1} = t_{i_2} < \ldots < t_{i_n} \,, \quad \ldots, \quad t_{i_0} < t_{i_1} < \ldots < t_{i_{n-1}} = t_{i_n} \,.$$

can then be represented by

$$(i_0 \sim i_1, i_2, \ldots, i_n) \,, \quad (i_0, i_1 \sim i_2, \ldots, i_n) \,, \quad \ldots, \quad (i_0, i_1, \ldots, i_{n-1} \sim i_n) \,, \tag{2.3}$$

where the $\sim$ symbol allows for transposition of the adjacent indices.

The faces of lower dimension are represented with more $\sim$ symbols up to

the vertices:

$$(2.4)\quad (i_0,\ i_1 \sim i_2 \sim \ldots \sim i_n)\,,\quad (i_0 \sim i_1,\ i_2 \sim \ldots \sim i_n)\,,\quad \ldots,\quad (i_0 \sim i_1 \sim \ldots \sim i_{n-1},\ i_n)\,.$$

Each cone (2) can thus be viewed as a formal $n-1$-simplex with n faces (3) and n vertices (4) (this simplex can be realized by cutting T with an appropriate affine plane). The set of all these simplexes together with their faces builds up a « simplicial complex » which is a « triangulation » of a $n-1$-sphere (*e.g.* the sphere $\sum_{i=1}^{n} (t_0 - t_i)^2 = 1$ in (t)).

We go now over to (s) space and consider the set of all planes

$$(2.5)\qquad \sum_{i \in X} s_i = 0\,,\qquad X \subset \{0, 1, \ldots, n\}\,,\qquad X \neq \emptyset\,,\qquad X \neq \{0, 1, \ldots, n\}\,.$$

If X_1 and X_2 are such that $X_2 = \complement X_1$, *i.e.* if they are complementary subsets of $\{0, 1, \ldots, n\}$, the planes $\sum_{i \in X_1} s_i = 0$ and $\sum_{i \in X_2} s_i = 0$ are of course identical.

We will call $\mathscr{S}$ the set of open convex cones into which (s) is decomposed by the planes (5). This set has a less simple geometrical structure than $\mathscr{T}$. For instance a cone $S \in \mathscr{S}$ is not always limited by n planes when $n \geqslant 4$. The situation is illustrated by the case of the cone S for $n = 4$ which is defined by

$$(2.6)\qquad \begin{cases} s_0 + s_2 > 0 & s_0 + s_3 > 0 & s_0 + s_4 > 0\,, \\ s_1 + s_2 > 0 & s_1 + s_3 > 0 & s_1 + s_4 > 0\,. \end{cases}$$

It may be remarked that the subspace of (s) orthogonal to an intersection (different from 0) of planes (1) of (t) is an intersection of planes (5) the converse however is generally not true.

3. – Analyticity of the Wightman function.

The following axioms: Lorentz invariance, existence and uniqueness of the vacuum, stability of the vacuum and local commutativity imply that the Wightman function $\mathscr{W}(z)$ exists, is analytic in $U_\pi \mathscr{R}'_n$ (the union of the permuted extended tubes) (*) and is invariant there under the homogeneous complex Lorentz group.

(*) Let us recall that the tube $\mathscr{R}_n$ is defined by

$$\eta_1^I = y_1 - y_0 \in V_+\,,\qquad \eta_2^I = y_2 - y_1 \in V_+,\ \ldots,\ \eta_n^I = y_n - y_{n-1} \in V_+\,,\quad x \text{ arbitrary};$$

The extended tube is defined by $\mathscr{R}'_n = U_{\Lambda \in L_+(C)} \Lambda \mathscr{R}_n$.

$\mathscr{W}^{\wedge}(z)$ has $(n+1)!$ distribution boundary values $\mathscr{W}^{\wedge\pi}(x)$ (which are assumed to be tempered) when the imaginary part of z tends to zero, z remaining inside some $\pi\mathscr{R}_n$, $\pi \in \gamma_{n+1}$.

Let

$$\zeta_j^\pi = z_{i_j} - z_{i_{j-1}}, \qquad (\zeta_j^\pi = \xi_j^\pi + i\eta_j^\pi), \qquad P_j^\pi = \sum_{k=j}^{n} p_{i_k}, \tag{3.1}$$

with

$$\pi(0, 1, \ldots, n) = (i_0, i_1, \ldots, i_n),$$

then

$$p \cdot x = \sum_{i=0}^{n} p_i \cdot x_i = \sum_{j=1}^{n} P_j^\pi \cdot \xi_j^\pi .$$

If we write

$$\mathscr{W}^{\wedge\pi}(x) = \overline{\mathscr{F}}\, G^\pi(p) = (2\pi)^{-2n} \int \mathrm{d}p \, \exp\left[ip \cdot x\right] G^\pi(p), \tag{3.2}$$

the stability of the vacuum expresses itself by the support condition

$$G^\pi(p) = 0 \quad \text{unless} \quad P_j^\pi \in \overline{V}_+, \qquad j = 1, \ldots, n \tag{3.3}$$

This allows the Fourier transform (2) to be extended to a Laplace transform analytic in $\pi\mathscr{R}_n$ and gives conditions on its behaviour at infinity. We will not however formulate these conditions since it is easier in practical cases to use directly (3.3).

Regarding Lorentz invariance, if space reflections are allowed, $\mathscr{W}^{\wedge}$ is invariant under $L(C)$, if they are rejected, $\mathscr{W}^{\wedge}$ is only invariant under $L_+(C)$, where the complex rotations in $L_+(C)$ have determinant $+1$.

Having introduced the basic properties of the Wightman functions that do not connect several of them (as positive-definiteness of the metric and the asymptotic condition would do) we proceed by studying $\mathscr{W}^{\wedge}$ in the space $(z^0, \boldsymbol{x})$.

The decomposition of the space (y^0) into cones $T(\pi)$ induces a decomposition of $(z^0, \boldsymbol{x})$ into domains $R^{4n} + iT(\pi)$.

If $\pi \in \gamma_{n+1}$, the corresponding permuted tube and permuted extended tube are

$$\pi\mathscr{R}_n = \{z : \pi^{-1}z \in \mathscr{R}_n\}, \qquad \pi\mathscr{R}_n' = \{z : \pi^{-1}z \in \mathscr{R}_n'\}.$$

The real point in $\mathscr{R}_n'$ are the Jost points [1], those in $\pi\mathscr{R}_n'$ the « permuted » Jost points. We do not assume that $\mathscr{W}^{\wedge}(z)$ is uniform in $U\pi\mathscr{R}_n'$ but if x is a Jost point or a permuted Jost point, $\mathscr{W}^{\wedge}(z)$ is holomorphic and uniform in a neighbourhood of x [1,5].

[4] R. Jost: *Helv. Phys. Acta*, **30**, 409 (1957).

[5] D. Kleitman: *Bull. Am. Phys. Soc.*, **5**, 82, 79 (1960).

Since $R^{4n}+iT(\pi)$ is the trace on $(z^0, \boldsymbol{x})$ of $\pi\mathscr{R}_n$, $\mathscr{W}(z^0, \boldsymbol{x})$ is analytic in every $R^{4n}+iT(\pi)$.

Suppose now that $T(\pi')$ and $T(\pi'')$ have a face $(i_0, ..., i_{k-1}\sim i_k, ..., i_n)$ in common. The piece of plane F defined by

$$y^0_{i_0} < ... < y^0_{i_{k-1}} = y^0_{i_k} < ... < y^0_{i_n} \tag{3.4}$$

is then a common boundary of $R^{4n}+iT(\pi')$ and $R^{4n}+iT(\pi'')$.

Let x be a real point in $\pi'\mathscr{R}'_n$ (a permuted Jost point [4]), $\mathscr{W}(z^0, \boldsymbol{x})$ is analytic in a neighbourhood of x, and therefore at some point of F for which $(x_k - x_{k-1})^2 < 0$.

Let now z be any point of F for which $(x_k - x_{k-1}) < 0$. By a very small complex Lorentz transformation, z can be brought either in $\pi'\mathscr{R}_n$ or in $\pi''\mathscr{R}_n$, so that the restrictions of $\mathscr{W}$ to $R^{4n}+iT(\pi')$ and to $R^{4n}+iT(\pi'')$ can both be continued over F at z. These continuations coincide because the set of points of F for which $(x_k - x_{k-1})^2 < 0$ is connected and they coincide at some points of this set.

It is now easy to conclude that $\mathscr{W}$ is analytic at those points of the plane $y^0_k - y^0_{k-1} = 0$ for which $(x_k - x_{k-1})^2 < 0$ and which do not belong to other planes of singularities. The case of these intersections is dealt with by use of the Kantensatz ([6,7]) and we get the following.

THEOREM 1. – *$\mathscr{W}(z^0, \boldsymbol{x})$ can have singularities only if two of its arguments $(z^0_i, \boldsymbol{x}_i)$ and $(z^0_{i'}, \boldsymbol{x}_{i'})$, $i \neq i'$ are such that $y^0_{i'} - y^0_i = 0$ and $x_{i'} - x_i$ is not space-like.*

Let now the function $F(z)$ be invariant under $L^{\uparrow}_+$ and such that $F(z^0, \boldsymbol{x})$ is analytic in the domain $R^{4n}+iT(\pi)$.

We introduce the variables ζ^π_1, ..., ζ^π_n of eq. (4.1) as co-ordinates in (z), writing

$$z = (\zeta^\pi_1, ..., \zeta^\pi_n) = (\zeta^\pi_1, 0, ..., 0) + (0, \zeta^\pi_2, ..., 0) + ... + (0, 0, ..., \zeta^\pi_n) .$$

If $z \in \pi\mathscr{R}_n$, each term in the right-hand side is of the form

$$(0, ..., \zeta_i, ..., 0) = \Lambda^{(i)}(0, ..., \chi_i, ..., 0) ,$$

where $\Lambda^{(i)} \in L^{\uparrow}_+$ and $(0, ..., \chi_i, ..., 0)$ belongs to the boundary of $R^{4n}+iT(\pi)$ in $(z^0, \boldsymbol{x})$, $(0, ..., \zeta_i, ..., 0)$ is thus a limiting point of analyticity points of $\mathscr{W}$ and, by virtue of the tube theorem (*), the same is true for z. Since $\pi\mathscr{R}_n$ is

(*) We need here an unusual form of the tube theorem. That this holds is seen by referring to a proof of it based on the use of the continuity theorem.

([6]) H. BEHNKE and P. THULLEN: *Ergeb. d. Math.*, **3**, no. 3 (Berlin, 1934).

([7]) D. RUELLE: *Helv. Phys. Acta*, **32**, 135 (1959).

an open set, z is a point of analyticity of F and we obtain easily [2] the following

THEOREM 2. – *If the domain of analyticity of $\mathscr{W}(z^0, \boldsymbol{x})$ is as given in Theorem 1 and if $\mathscr{W}(z)$ is invariant under $L^{\uparrow}_{+}$ (resp. $L^{\uparrow}$) $\mathscr{W}(z)$ is analytic in $U\pi R'_n$ and invariant there under $L_+(C)$ (resp. $L(C)$).*

4. – The boundary values of the Wightman function.

We have introduced in the last paragraph the real boundary values $\mathscr{W}^{\pi}(x)$ of $\mathscr{W}(z)$. They may also be defined by

$$\mathscr{W}^{\pi}(x) = \lim_{y^0 \to 0} \mathscr{W}(z^0, \boldsymbol{x}) , \qquad y^0 \in T(\pi) . \tag{4.1}$$

This defines $(n+1)!$ « sheets » along (x) corresponding to the cones $T(\pi) \in \mathscr{T}$.

We divide now each sheet into 2^n oriented « intervals »

$$(\pi, \sigma) = (i_0 \gtrless i_1 \gtrless \ldots \gtrless i_n) \tag{4.2}$$

by giving the differences $x^0_{i_k} - x^0_{i_{k-1}}$ a definite sign so that either $x_{i_{k-1}} < x_{i_k}$ or $x_{i_{k-1}} > x_{i_k}$. σ is thus an arbitrary family of n $>$ or $<$ signs.

Just as the $T(\pi)$, the $(n+1)!\,2^n$ intervals (π, σ) may be viewed as the $(n-1)$-simplexes of a formal complex with faces

$$(i_0 = i_1 \gtrless i_2 \gtrless \ldots \gtrless i_n) , \quad (i_0 \gtrless i_1 = i_2 \gtrless \ldots \gtrless i_n) , \quad \ldots , \quad (i_0 \gtrless i_1 \gtrless \ldots \gtrless i_{n-1} = i_n) \tag{4.3}$$

and vertices

$$(i_0 \gtrless i_1 = i_2 = \ldots = i_n) , \ (i_0 = i_1 \gtrless i_2 = \ldots = i_n) , \ \ldots , \ (i_0 = i_1 = \ldots = i_{n-1} \gtrless i_n), \tag{4.4}$$

where the $=$ sign allows for transposition of the adjacent indices.

A sum of intervals is called a $(n-1)$-cycle when its boundary is zero. We will mostly consider cycles made up of $(n+1)!$ intervals corresponding to the permutations $\pi \in \gamma_{n+1}$.

Let $s(\sigma)$ be the number of $<$ signs in σ, then a necessary and sufficient condition for

$$C = \sum_{\pi \in \gamma_{n+1}} (-)^{s(\sigma_\pi)} (\pi, \sigma_\pi)$$

to be a cycle is that whenever $T(\pi_1)$ and $T(\pi_2)$ differ only by a transposition of consecutive indices, σ_{π_1} and σ_{π_2} may differ only by the sign between these two indices.

Consider now a sequence (*)

$$\varphi_r(x) \in \mathscr{S}_{4n}\,, \qquad r\text{: positive integer} \tag{4.5}$$

chosen once for all and such that $\varphi_r(x) \to \delta(x)$ in $\mathscr{S}'_{4n}$ when $r \to \infty$.

We define $(\pi, \sigma)\mathscr{W} * \varphi_r(x) \in \mathscr{S}'$ to be equal to $\mathscr{W}^{\pi} * \varphi_r(x)$ when the inequalities σ hold, and zero otherwise.

We make then the following assumptions on $\mathscr{W}$ and the sequence φ_r.

ASSUMPTIONS A. – *If* $C = \sum_{\pi} (-)^{s(\sigma_\pi)}(\pi, \sigma_\pi)$ *is a cycle:*

1) $C\mathscr{W} * \varphi_r(x)$ *converges towards a distribution in* $\mathscr{S}'$ *when* $r \to \infty$.

2) $C\mathscr{W}(x) = \lim_{r\to\infty} C\mathscr{W} * \varphi_r(x)$ *is invariant under* $L_+^{\uparrow}$.

The first assumption is less stringent than it would be to require each $(\pi, \sigma)\mathscr{W} * \varphi_r(x)$ to have a limit.

The second one is not unnatural since it can be *proved* for points such that $x_{i'} - x_i \neq 0$ whenever $i' \neq i$. One has just to use Theorem 1 and to notice that the derivatives of $C\mathscr{W}$ with respect to the parameters of the Lorentz group vanish when all x_i are different.

If the assumptions A are fulfilled, we define the vacuum expectation value of the time-ordered product by $\breve{G}(x) = T\mathscr{W}(x)$, where the cycle T is defined by $T = \sum_{\pi} (\pi, >)$. This definition may of course depend upon the sequence φ_r.

5. – Shifting of integral paths and analyticity of the Green function.

Using eq. (3.1), we can write

$$\mathscr{F}[(\pi, \sigma)\mathscr{W} * \varphi_r](p) = (2\pi)^{-2n} \int \mathrm{d}x \exp\left(-i \sum P_j^{\pi} \cdot \xi_j^{\pi}\right)(\pi, \sigma)\mathscr{W} * \varphi_r(x)\,, \tag{5.1}$$

π being held fixed and such that $\pi(0, 1, \ldots, n) = (i_0, i_1, \ldots, i_n)$, let σ' and σ'' differ only by the sign between i_{k-1} and i_k. Clearly then

$$\int \mathrm{d}\xi_k^{\pi} \exp\left[-iP_k^{\pi} \cdot \xi_k^{\pi}\right][(\pi, \sigma')\mathscr{W} * \varphi_r(x) + (\pi, \sigma'')\mathscr{W} * \varphi_r(x)]\,,$$

has the support property $P_k^{\pi} \in \overline{V}_+$.

(*) For a definition of the convolution product $(*)$, of the functionnal space $\mathscr{S}$ and of its dual $\mathscr{S}'$ (space of tempered distributions), see SCHWARTZ [8].

([8]) L. SCHWARTZ: *Théorie des distributions*, t. 2 (Paris, 1951); t. 1, 2ème éd. (Paris, 1957).

Otherwise stated, when P_k^π is restricted to the complementary of $\overline{V}_+$, in particular when $P_k^{\pi 0} < 0$, the formula

$$\mathcal{F}[(\pi, \sigma')\mathcal{W} * \varphi_r](p) = -\mathcal{F}[(\pi, \sigma'')\mathcal{W} * \varphi_r](p) \tag{5.2}$$

allows the path of integration of ξ_k to be « shifted ».

We will apply this result to

$$G_r(p) = (2\pi)^{-2n}\int \mathrm{d}x \exp[-ip\cdot x] T\mathcal{W} * \varphi_r(x) = \sum_\pi \mathcal{F}[(\pi, >)\mathcal{W} * \varphi_r](p). \tag{5.3}$$

Let p^0 belong to some cone S of the family $\mathcal{S}$ into which (p^0) can be divided (see Section 2), the $P_j^{\pi 0}$ then have a definite sign when π and j are fixed.

Shifting the path of integration whenever it is possible in $\mathcal{F}[(\pi, >)\mathcal{W} * \varphi_r](p)$ we get

$$\mathcal{F}[(\pi, >)\mathcal{W} * \varphi_r](p) = (-)^{s(\sigma)}\mathcal{F}[(\pi, \sigma_\pi^S)\mathcal{W} * \varphi_r](p), \qquad p^0 \in S, \tag{5.4}$$

where the support of $(\pi, \sigma_\pi^S)\mathcal{W} * \varphi_r(x)$ is

$$\xi_j^{\pi 0} \leqslant 0 \quad \text{if} \quad P_j^{\pi 0} > 0, \qquad \xi_j^{\pi 0} \geqslant 0 \quad \text{if} \quad P_j^{\pi 0} < 0. \tag{5.5}$$

So, if q is such that $q^0 \in S$ and $\boldsymbol{q} = 0$

$$\exp[q\cdot x](\pi, \sigma_\pi^S)\mathcal{W} * \varphi_r(x) \in \mathcal{S}^*. \tag{5.6}$$

On the other hand, $C^S = \sum_\pi (-)^{s(\pi)}(\pi, \sigma_\pi^S)$ is easily seen to be a cycle and $C^S\mathcal{W}$ is therefore Lorentz-invariant. (5.6) gives then

$$\exp[(\Lambda q)\cdot x] C^S\mathcal{W} \in \mathcal{S}^* \qquad \text{for } \Lambda \in L_+^\uparrow. \tag{5.7}$$

We will now use the following properties [9]:

1) If A is a distribution, the set Γ of all real points q such that $\exp[q\cdot x]A(x) \in \mathcal{S}^*$ is convex.

2) $\mathcal{F}\{\exp[q\cdot x]A\}(p)$ defines a Laplace transform, analytic when the variable $k = p + iq$ is in the tube $R^{4n} + i\,\overset{0}{\Gamma}(\overset{0}{\Gamma}$: the interior of $\Gamma)$.

We will call $\Gamma(S)$ the set Γ corresponding to the distribution $C^S\mathcal{W}$. Using 1) and the invariance of $\Gamma(S)$ under homotheties $s \to \alpha s$ $(\alpha > 0)$, we see that any finite sum of vectors belonging to $\Gamma(S)$ belongs to $\Gamma(S)$.

[9] J. L. Lions: *Suppl. Nuovo Cimento*, **14**, 9 (1959).

Let now $u^\alpha \in V_+$, $\alpha = 1, ..., 4$ and $\sum_{\alpha=1}^{4} u^\alpha = u$, where u is the unit vector along thet ime axis. If $s^\alpha \in S$, the point $q = (\sum_{\alpha=1}^{4} s_0^\alpha u^\alpha, \sum_{\alpha=1}^{4} s_1^\alpha u^\alpha, ..., \sum_{\alpha=1}^{4} s_n^\alpha u^\alpha)$ belongs to $\Gamma(S)$, because we can write $u^\alpha = r^\alpha \Lambda^\alpha u$, $r^\alpha > 0$, $\Lambda^\alpha \in L_+^\uparrow$.

If $s^1 = ... = s^4 = s$, $q = (s, \boldsymbol{o})$. If $s^1, ..., s^4$ are varied over neighbourhoods of s in S, q varies over a neighbourhood of $(s, \boldsymbol{o})$. Since this neighbourhood belongs to $\Gamma(S)$, we have proved that $s \in S$ implies $(s, \boldsymbol{o}) \in \overset{0}{\Gamma}(S)$.

Extending the Fourier transform $G^S(p) = \mathscr{F} C^S \mathscr{W}(p)$ to a Laplace transform $G^S(p + iq)$ analytic in the tube $R^{4n} + i\overset{0}{\Gamma}(S)$ and then restricting to the space $(k^0, \boldsymbol{p})$, we have proved:

1) $G^S(k^0, \boldsymbol{p})$ is analytic in $R^{4n} + iS$ (*i.e.* when $q^0 \in S$).

2) $\lim_{q^0 \to 0, q^0 \in S} G^S(k^0, \boldsymbol{p}) = G(p)$ if $p^0 \in S$.

Let $S_0 \in \mathscr{S}$ be defined by the equations $s_i > 0$, $1 \leqslant i \leqslant n$.

We introduce the retarded cycle R by $R = C^{S_0}$, $R\mathscr{W}$ then reduces to the well-known r function [10] (*) and $\mathscr{F} r(p)$ is analytic if p is a Jost point, *i.e.* if

$$(5.8) \qquad \Big(\sum_{i=1}^{n} \lambda_i p_i\Big)^2 < 0 \quad \text{whenever} \quad \lambda_i \geqslant 0\,, \quad \sum_{i=1}^{n} \lambda_i = 1\,.$$

A set $F \subset (s)$, $F \neq \emptyset$, will be called a face of $S \in \mathscr{S}$ if it is the interior in a subspace $\sum_{i \in X} s_i = 0$ of the intersection of this subspace and the closure $\bar{S}$ of S.

Let now S' and S'' have a face F in common. The piece of plane $R^{4n} + iF$ is then a common boundary of $R^{4n} + iS'$ and $R^{4n} + iS''$.

If a point $k \in R^{4n} + iF$ is such that $\big(\sum_{i \in X} p_i\big)^2 < 0$, it is possible to bring it either in $R^{4n} + i\overset{0}{\Gamma}(S')$ or in $R^{4n} + i\overset{0}{\Gamma}(S'')$ by a very small complex Lorentz transformation. This means that $G^{S'}(k^0, \boldsymbol{p})$ and $G^{S''}(k^0, \boldsymbol{p})$ can both be analytically continued through $R^{4n} + iF$ at k. In order to prove that these continuations agree in the connected set of all points of $R^{4n} + iF$ for which $\big(\sum_{i \in X} p_i\big)^2 < 0$, we will show that they agree at some point of this set.

Let p_J be a Jost point (eq. (5.8)) such that $p_J^0 \in F$ in (p^0). In any real neighbourhood of p_J there exist boundary values of $G^{S'}(k)$ and $G^{S''}(k)$ which coincide with $\mathscr{F} T \mathscr{W} = \mathscr{F} r$ which is analytic in a neighbourhood of p_J. There are thus points of F with $\big(\sum_{i \in X} p_i\big)^2 < 0$ such that $G^{S'}(k)$ and $G^{S''}(k)$ coincide, which proves the announced property.

(*) The connexion with the usual definition of r is given by ref. [11], eq. (3.11).

[10] H. Lehmann, K. Symanzik and W. Zimmermann: *Nuovo Cimento*, **6**, 319 (1957).

[11] N. Nishijima: *Phys. Rev.*, **111**, 995 (1958).

The intersections of several surfaces $\sum_{i\in X} q_i^0 = 0$ are easily dealt with by use of the Kantensatz (6) and we get for the function $G(k)$, whose restriction to $R^{4n} + i\overset{0}{\Gamma}(S)$ is $G^S(k)$, the following

THEOREM 3. – *The function $G(k^0, \boldsymbol{p})$ can have singularities only if $\sum_{i\in X} q_i^0$ vanishes for some $X \subset \{0, 1, ..., n\}$, $X \neq \emptyset$, $X \neq \{0, 1, ..., n\}$ and $\sum_{i\in X} p_i$ is not space-like.*

6. – The multiple commutators.

We will now try to get more information about the connexion between the cones $S \in \mathscr{S}$ in (s) and the corresponding cycles C^S.

Let $\mathscr{B}_n$ be the abelian group generated by the cones $S \in \mathscr{S}$, and let $\mathscr{C}_n$ be the subgroup generated by the cycles C^S in the abelian group of all cycles defined in Section **4**. The mapping $S \to C^S$ extends by linearity to a homomorphism $\mathscr{B}_n \to \mathscr{C}_n$. This homomorphism is obviously onto, but it is not in general an isomorphism. Its kernel $\mathscr{A}_n$ is the set of linear combinations of $S \in \mathscr{S}$ such that the corresponding linear combinations of boundary values of $G(z)$ vanish identically.

We call Steinmann relations the resulting linear relations between the $G^S(p)$.

Let $X = \{i_0, i_1, ..., i_k\} \subset \{0, 1, ..., n\}$. We will call $(s)_X$ the subspace of (s) defined by the relation $\sum_{i\in X} s_i = 0$ in the subspace generated by $s_{i_0}, s_{i_1}, ..., s_{i_k}$. The decomposition of $(s)_X$ into a set $\mathscr{S}_X$ of cones is effected just as in (s) and to these cones we associate cycles C^S for the variables $z_{i_0}, z_{i_1}, ..., z_{i_k}$. We will call $\mathscr{C}_X$ the abelian group generated by the cycles thus formed.

Consider now two cones $S', S'' \in \mathscr{S}$ such that S' and S'' have in common the face F belonging to the plane $\sum_{i\in X} s_i = 0$ so that $\sum_{i\in X} s_i < 0$ in S' and $\sum_{i\in X} s_i > 0$ in S''.

If we write

$$C^{S''} - C^{S'} = \sum_{\pi} [(-)^{s(\sigma'')}(\pi, \sigma_\pi^{S''}) - (-)^{s(\sigma')}(\pi, \sigma_\pi^{S'})] , \tag{6.1}$$

where we have set for simplicity $\sigma' = \sigma_\pi^{S'}$, $\sigma'' = \sigma_\pi^{S''}$, the sum in the right-hand side extends only over those permutations $\pi \in \gamma_{n+1}$ for which

$$\pi(0, 1, ..., n) = (i_0, i_1, ..., i_n) \text{ and } X = \{i_0, ..., i_k\} \text{ or } X = \{i_{n-k}, ..., i_n\}. \tag{6.2}$$

Let $\pi_1 \in \gamma_{k+1}$ and $\pi_2 \in \gamma_{n-k}$ be permutations of X and CX respectively. We may then represent the permutations π of eq. (2) by $\pi_1\pi_2$ or $\pi_2\pi_1$, the

corresponding σ being of the form $\sigma_1 \gtrless \sigma_2$ or $\sigma_2 \gtrless \sigma_1$ respectively, so that

$$(6.3)\qquad \begin{cases} (\pi_1\pi_2,\, \sigma') = (\pi_1\pi_2,\, \sigma_1 > \sigma_2) & (\pi_1\pi_2,\, \sigma'') = (\pi_1\pi_2,\, \sigma_1 < \sigma_2)\,, \\ (\pi_2\pi_1,\, \sigma') = (\pi_2\pi_1,\, \sigma_2 < \sigma_1) & (\pi_2\pi_1,\, \sigma'') = (\pi_2\pi_1,\, \sigma_2 > \sigma_1)\,, \end{cases}$$

σ_1 (resp. σ_2) is determined by the signs of the $\sum_{i\in X_1} s_i$, $X_1 \subset X$, $X_1 \neq \emptyset$, $X_1 \neq X$ (resp. of the $\sum_{i\in X_2} s_i$, $X_2 \subset CX$. $X_2 \neq \emptyset$, $X_2 \neq CX$) in F, which are the same as in S' and S''. Since the sign conditions on the $\sum_{i\in X_1} s_i$ (resp. $\sum_{i\in X_2} s_i$) are compatible, they determine a cone $S_1 \in \mathscr{S}_X$ (resp. $S_2 \in \mathscr{S}_{CX}$) and one may write $\sigma_1 = \sigma_{\pi_1}^{S_1}$ (resp. $\sigma_2 = \sigma_{\pi_2}^{S_2}$) independently of whether $\pi = \pi_1\pi_2$ or $\pi = \pi_2\pi_1$.

Using (6.3), (6.1) can be written

$$(6.4)\qquad \begin{cases} C^{S''} - C^{S'} = \sum_{\pi_1}\sum_{\pi_2} [(-)^{s(\sigma_1>\sigma_2)}(\pi_1\pi_2,\, \sigma_1 > \sigma_2) - (-)^{s(\sigma_1<\sigma_2)}(\pi_1\pi_2,\, \sigma_1 < \sigma_2) + \\ \qquad\qquad + (-)^{s(\sigma_2<\sigma_1)}(\pi_2\pi_1,\, \sigma_2 < \sigma_1) - (-)^{s(\sigma_2>\sigma_1)}(\pi_2\pi_1,\, \sigma_2 > \sigma_1)] \\ \qquad = \sum_{\pi_1} (-)^{s(\sigma_1)} \sum_{\pi_2} (-)^{s(\sigma_2)} [(\pi_1\pi_2,\, \sigma_1 > \sigma_2) + \\ \qquad\qquad + (\pi_1\pi_2,\, \sigma_1 < \sigma_2) - (\pi_2\pi_1,\, \sigma_2 > \sigma_1) - (\pi_2\pi_1,\, \sigma_2 < \sigma_1)]\,. \end{cases}$$

We introduce now the product and the commutator of two cycles C_1 and C_2 when these cycles have no variable in common

$$(6.5)\qquad \begin{cases} C_1 \cdot C_2 = \sum_{\pi_1} (-)^{s(\sigma_1)}(\pi_1,\, \sigma_1) \cdot \sum_{\pi_2} (-)^{s(\sigma_2)}(\pi_2,\, \sigma_2) \\ \qquad\qquad = \sum_{\pi_1} (-)^{s(\sigma_1)} \sum_{\pi_2} (-)^{s(\sigma_2)} [(\pi_1\pi_2,\, \sigma_1 > \sigma_2) + (\pi_1\pi_2,\, \sigma_1 < \sigma_2)]\,, \\ [C_1, C_2] = C_1 \cdot C_2 - C_2 \cdot C_1\,. \end{cases}$$

The commutator of two cycles will be defined to be zero if they have at least one variable in common. We have thus proved the formula

$$(6.6)\qquad C^{S''} - C^{S'} = [C^{S_1}, C^{S_2}]\,.$$

Conversely, if S_1 and S_2 are arbitrary cones of $\mathscr{S}_X$ and $\mathscr{S}_{CX}$ respectively, it is easily seen that there exists at least one couple of cones S', $S'' \in \mathscr{S}$ such that eq. (6.6) holds. This means that the direct sum $\mathscr{C} = \sum_X \mathscr{C}_X$ has the structure of a Lie algebra for commutation.

From the above, it results that the cycle C^S corresponding to any cone $S \in \mathscr{S}$ is equal to the cycle C^{S_0} corresponding to a fixed cone S_0 plus a sum of commutators of cycles with a smaller number of variables.

One may thus reconstruct every cycle in $\mathscr{C}_n$ if one knows one cycle C^S, $S \in \mathscr{S}_X$ for each X. For instance one may take the retarded cycles, obtaining the following

THEOREM 4. – *The abelian group $\mathscr{C}$ generated by the cycles C^S is also generated as a Lie algebra by the retarded cycles R.*

If we restrict to $\mathscr{C}_n$, this means that the abelian group of all linear combinations with integral coefficients of the boundary values $G^S(p)$ of $G(k)$ is identical to the abelian group of the Fourier transforms of all linear combinations with integral coefficients of the vacuum expectation values of multiple commutators of retarded products and fields (each field $A^{(i)}(x_i)$ being used eventually in a R-product, once and only once in each multiple commutator).

7. – Introduction of masses.

When we introduced cycles along the real boundary values of $\mathscr{W}(z)$, we had to cut singularities (at the top of light cones). This difficulty was solved by a regularization process and assumptions about $\mathscr{W}$.

The purpose of this paragraph is to avoid similar troubles with $G(k)$ by introducing a non-zero minimum mass in the theory.

It will also be necessary for the following to introduce the truncated Wightman functions $\widetilde{\mathscr{W}}$ ([12]). No proof will be given here of the properties stated.

Let ϱ_k be the family of all partitions of the set $\{0, 1, ..., n\}$ into $k+1$ subsets: $X_0, X_1, ..., X_k$ and let $\mathscr{W}(z)_{X_j}$ be the Wightman function of the variables z_i such that $i \in X_j$.

We write then the reduction formula

$$\mathscr{W}(z) = \sum_{k=0}^{n} \sum_{\varrho_k} \prod_{j=0}^{k} \widetilde{\mathscr{W}}(z)_{X_j} \tag{7.1}$$

and use it to define the truncated functions $\widetilde{\mathscr{W}}$ recursively on the number of variables.

The function $\widetilde{\mathscr{W}}(z)$ has all mathematical properties described above for $\mathscr{W}(z)$. A Green function can be deduced of it, which also has all the mathematical properties of $G(k)$. *It can be seen that it coincides in fact with $G(k)$.*

We know that the mass operator in Hilbert space has an eigenvalue equal to zero and corresponding to the vacuum. We shall assume that the rest of its spectrum is $\geqslant \mu$, $\mu > 0$.

([12]) R. HAAG: *Phys. Rev.*, **112**, 668 (1958) and *Suppl. Nuovo Cimento*, **14**, 131 (1959).

Let then $V_+^\mu = x: x \in V_+,\ x^2 > \mu^2\}$, x: a vector in Minkowski space. We have the following (see [13])

THEOREM 5. – *Let* $\tilde{\mathscr{W}}^\pi(x) = \tilde{\mathscr{F}}\,\tilde{G}^\pi(p) = (2\pi)^{-2n}\int \mathrm{d}p\, \exp[ipx]\,\tilde{G}^\pi(p)$; $\tilde{G}^\pi(p)$ *then satisfies the support condition* $\tilde{G}^\pi_j(p) = 0$ *unless* $P_j^\pi \in \overline{V}^\mu$, $j = 1, \ldots, n$.

THEOREM 6. – *The function* $G(k^0, \boldsymbol{p})$ *can have singularities only if* $\sum_{i \in X} q_i^0$ *vanishes for some* $X \subset \{0, 1, \ldots, n\}$, $X \neq \emptyset$, $X \neq \{0, 1, \ldots, n\}$ and $\left(\sum_{i \in X} p_i\right)^2 \geqslant \mu^2$.

We gather now the information we have about the functions $\tilde{\mathscr{W}}$ and G.

I. Properties of $\tilde{\mathscr{W}}(z)$.

1) $\tilde{\mathscr{W}}(z)$ *is invariant under* $L_+(C)$ *or* $L(C)$ *according to whether the theory is invariant under* $L_+^\uparrow$ *or* $L^\uparrow$.

2) *The singularities of* $\tilde{\mathscr{W}}(z^0, \boldsymbol{x})$ *are given by the Theorem* 1.

3) $\tilde{\mathscr{W}}(z)$ *has boundary values*

$$\tilde{\mathscr{W}}^\pi(x) = \lim_{y^0 \to 0,\ y^0 \in (\pi)} \tilde{\mathscr{W}}(z^0, \boldsymbol{y})$$

which are tempered distributions.

4) There are conditions on the behaviour of $\tilde{\mathscr{W}}(z)$ at infinity which we replace by the *support conditions of Theorem* 5 *on* $\mathscr{F}\tilde{\mathscr{W}}^\pi(p)$.

From these properties of $\tilde{\mathscr{W}}$, we have derived the following

II. Properties of $G(p)$.

1) $G(k)$ *is invariant under* $L_+(C)$ *or* $L(C)$ *according to wheter the theory is invariant under* $L_+^\uparrow$ *or* $L^\uparrow$.

2) *The singularities of* $G(k^0, \boldsymbol{p})$ *are given by the Theorem* 6.

3) $G(k)$ *has boundary values*

$$G^S(p) = \lim_{q^0 \to 0,\ q^0 \in S} G(k^0, \boldsymbol{p})$$

which are tempered distributions.

4) *These boundary values are subjected to linear conditions: the Steinmann relations* (Section **6**).

5) There are conditions on the behaviour of $G(k)$ at infinity which we replace by the *support conditions on* $\mathscr{F}G^S(x)$ *which follow from eq.* (5.5).

([13]) D. RUELLE: *Thèse* (Bruxelles, 1959).

8. – Products.

In order to show that the information contained in the properties of the $\tilde{\mathscr{W}}$ function has been completely translated into terms of the properties of the G function, we will reconstruct $\tilde{\mathscr{W}}$ (not $\mathscr{W}$!) from G. This paragraph is devoted to an intermediate step in this reconstruction, namely the definition of products.

Since the distributions $G^s(p)$ are subjected to the Steinmann relations, they generate an abelian group which is isomorphic to the group $\mathscr{C}_n$ of cycles introduced in Section 6. For facility, we will in fact identify the two groups and represent the $G^s(p)$ by the corresponding cycles. We will also introduce the commutators by the formula (6.6) and we will be allowed, in computations with multiple commutators, to use the relations

$$(8.1)\qquad [C_1, C_2] = -[C_2, C_1], \qquad [C_1' + C_1'', C_2] = [C_1', C_2] + [C_1'', C_2],$$
$$[C_1, [C_2, C_3]] + [C_2, [C_3, C_1]] + [C_3, [C_1, C_2]] = 0 .$$

Consider now a partition of $\{0, 1, ..., n\}$ into $k+1$ subsets $X_0, X_1, ..., X_k$. If $X_j = \{i_0, i_1, ..., i_{r(j)}\}$, we will write $x_{jj'} = x_{i_{j'}}$ and $p_{jj'} = p_{i_{j'}}$.

We define then

$$\mathrm{d}p_j = \mathrm{d}p_{j1} \ldots \mathrm{d}p_{jr(j)}, \qquad P_j = \sum_{l=j}^{k} \sum_{i \in X_l} p_i .$$

Now,

$$\mathrm{d}p = \mathrm{d}p_0 \cdot \mathrm{d}P_1 \cdot \mathrm{d}p_1 \ldots \mathrm{d}P_k \cdot \mathrm{d}p_k$$

and

$$\sum_{i=0}^{n} p_i \cdot x_i = \sum_{j=1}^{k} P_j (x_{j0} - x_{(j-1)0}) + \sum_{j=0}^{k} \sum_{j'=1}^{r(j)} p_{jj'} (x_{jj'} - x_{j0})$$

so that if

$$\bar{\mathscr{F}}_{X_j} = (2\pi)^{-2r(j)} \int \mathrm{d}p_j \exp\Big[i \sum_{j'=1}^{r(j)} p_{jj'} (x_{jj'} - x_{j0})\Big],$$

we have

$$\bar{\mathscr{F}} = \bar{\mathscr{F}}_{X_0} \bar{\mathscr{F}}_{X_1} \ldots \bar{\mathscr{F}}_{X_k} (2\pi)^{-2k} \int \mathrm{d}P_1 \ldots \mathrm{d}P_k \exp\Big[i \sum_{j=1}^{k} P_j (x_{j0} - x_{(j-1)0}) .$$

Let $C_j \in \mathscr{C}_{X_l}$, we will define products $C_0 \cdot C_1 \ldots C_k$ with the following properties.

III. Properties of the products.

1) *The products are Lorentz-invariant tempered distributions.*
2) *Distributivity*: $C_0 \ldots (C_i' + C_i'') \ldots C_k = C_0 \ldots C_i' \ldots C_k + C_0 \ldots C_i'' \ldots C_k$.

3) $[\overline{\mathscr{F}}_{X_0}\overline{\mathscr{F}}_{X_1}\dots\overline{\mathscr{F}}_{X_k}\, C_0\cdot C_1\dots C_k]\cdot\exp\sum_{j=0}^{k}\sum_{j'=0}^{r(j)} s_{jj'}x^0_{jj'}\in\mathscr{S}^*$
when $C_j = C^{S_j}$, $S_j\in\mathscr{S}_{X_j}$ *and* $\sum_{j'=0}^{r(j)} s_{jj'} = 0$, $(s_{j0}, s_{j1}, \dots s_{jr(j)})\in\overline{S}_j$.

4) *Support properties in* (p):

$$C_0\cdot C_1\dots C_k \text{ vanishes unless } P_j\in\overline{V}^{\mu}_{+},\ 1\leqslant j\leqslant k.$$

5) *The following identity holds*:

$$C_0\dots C_{l-1}\cdot C_l\dots C_k - C_0\dots C_l\cdot C_{l-1}\dots C_k = C_0\dots[C_{l-1}, C_l]\dots C_k\,.$$

This last property allows the definition of multiple commutators of products of cycles, the number of dots $(\cdot)$ plus the number of square brackets ($[\ ]$) being equal to k. This will justify *a posteriori* our use of the symbols $[C_0, C_1\dots C_k]$ and $[C_0\dots C_{k-1}, C_k]$.

Properties III are trivial consequences of Properties II for one single cycle belonging to $\mathscr{C}_n$. We will now define the products recursively on the number of factors and show that III-1)-5) hold at each step.

By definition, let

$$[C_0, C_1\dots C_k] = \sum_{j=1}^{k} C_1\dots C_{j-1}\cdot[C_0, C_j]\cdot C_{j+1}\dots C_k\,. \tag{8.3}$$

First, we show that this expression vanishes unless $P_1^2\geqslant\mu^2$.

By the induction Assumption III-4), $C_1\dots C_{j-1}\cdot[C_0, C_j]\cdot C_{j+1}\dots C_k$ vanishes unless

$$P_2 - P_1\in\overline{V}^{\mu}_{+},\ \dots,\ P_j - P_1\in\overline{V}^{\mu}_{+},\quad P_{j+1}\in\overline{V}^{\mu}_{+},\ \dots,\ P_k\in\overline{V}^{\mu}_{+}\,. \tag{8.4}$$

If $P_k^0<\varepsilon$, $0<\varepsilon<\mu$, the sum in the right-hand side of (8.3) reduces to one term with the support property $P_k - P_1\in\overline{V}^{\mu}_{+}$, so that $[C_0, C_1, \dots, C_k]$ vanishes unless $P_1^0\leqslant -\mu+\varepsilon$.

Similarly, if $P_k^0 - P_1^0<\varepsilon$, $[C_0, C_1, \dots, C_k]$ vanishes unless $P_1^0\geqslant\mu-\varepsilon$. Let now $P_k^0>0$, $P_k^0 - P_1^0>0$, using the induction Assumption III-4), we have

$$C_k\cdot C_1\dots C_{j-1}\cdot[C_0, C_j]\cdot C_{j+1}\dots C_{k-1} = 0\,,\qquad [C_0, C_k]\cdot C_1\dots C_{k-1} = 0\,.$$

Therefore, using III-2)-5),

$$\begin{aligned}[C_0, C_1\dots C_k] &= \sum_{j=1}^{k-1} C_1\dots[C_0, C_j]\dots C_k + C_1\dots C_{k-1}\cdot[C_0, C_k]\\ &= \sum_{j=1}^{k-1}[C_1\dots[C_0, C_j]\dots C_{k-1}, C_k] + [C_1\dots C_{k-1}, [C_0, C_k]]\end{aligned}$$

$$= \sum_{j=1}^{k-1} \Big(\sum_{l=1}^{j-1} C_1 \dots [C_l, C_k] \dots [C_0, C_j] \dots C_{k-1} + C_1 \dots [[C_0, C_j], C_k] \dots C_{k-1} +$$

$$+ \sum_{l=j+1}^{k-1} C_1 \dots [C_0, C_j] \dots [C_l, C_k] \dots C_{k-1} + C_1 \dots [C_j, [C_0, C_k] \dots C_{k-1} ,$$

$$= \sum_{j=1}^{k-1} \Big(\sum_{l=1}^{j-1} C_1 \dots [C_l, C_k] \dots [C_0, C_j] \dots C_{k-1} + C_1 \dots [C_0, [C_j, C_k]] \dots C_{k-1} +$$

$$+ \sum_{l=1}^{k-1} C_1 \dots [C_0, C_j] \dots [C_l, C_k] \dots C_{k-1} \Big)$$

$$= \sum_{l-1}^{k-1} \Big(\sum_{j=1}^{l-1} C_1 \dots [C_0, C_j] \dots [C_l, C_k] \dots C_{k-1} + C_1 \dots [C_0, [C_l, C_k]] \dots C_{k-1} +$$

$$+ \sum_{j=l+1}^{k-1} C_1 \dots [C_l, C_k] \dots [C_0, C_j] \dots C_{k-1} \Big)$$

$$= \sum_{l=1}^{k-1} [C_0, C_1 \dots [C_l, C_k] \dots C_{k-1}] .$$

We have thus proved that $[C_0, C_1, \dots, C_k]$ vanishes unless $P_1^2 \geqslant \mu^2$ when $P_k^0 > 0$, $P_k^0 - P_1^0 > 0$.

As a whole, using the « principe de recollement des morceaux » [8], we have proved that $[C_0, C_1 \dots C_k]$ vanishes when $|P_1^0| < \mu - \varepsilon$, $0 < \varepsilon < \mu$.

Letting ε go to zero and using Lorentz invariance, we see that $[C_0, C_1 \dots C_k]$ vanishes unless $P_1^2 \geqslant \mu^2$.

We define the product $C_0 \cdot C_1 \dots C_k$ to be equal to $[C_0, C_1 \dots C_k]$ when $P_1^0 > -\mu$, and to zero when $P_1^0 < \mu$.

The product may also be defined to be equal to $[C_0 \dots C_{k-1}, C_k]$ when $P_k^0 > -\mu$ and to zero when $P_1^0 < \mu$. The proof of the equivalence of the two definitions is straightforward if one uses the same kind of developments as above.

It remains now to show that the properties III.1-5) III.1), hold. 2), 3), are direct consequences of the corresponding induction assumptions and of the definition of the product.

III.4). The product has been defined so that $P_1 \in \overline{V}_+^\mu$, introducing this into (8.4) one finds $P_j \in \overline{V}_+^\mu$ for $2 \leqslant j \leqslant k$.

III.5). We have

$$[C_0, C_1 \dots C_{l-1} \cdot C_l \dots C_k] = \sum_{j=1}^{l-2} C_1 \dots [C_0, C_j] \dots C_{l-1} \cdot C_l \dots C_k +$$

$$+ C_1 \dots [C_0, C_{l-1}] \cdot C_l \dots C_k + C_1 \dots C_{l-1} \cdot [C_0, C_l] \dots C_k +$$

$$+ \sum_{j=l+1}^{k} C_1 \dots C_{l-1} \cdot C_l \dots [C_0, C_j] \dots C_k ,$$

so that

$$[C_0, C_1 \dots C_{l-1} \cdot C_l \dots C_k] - [C_0, C_1 \dots C_l \cdot C_{l-1} \dots C_k]$$

$$= \sum_{j=1}^{l-2} C_1 \dots [C_0, C_j] \dots [C_{l-1}, C_l] \dots C_k + C_1 \dots [[C_0, C_{l-1}], C_l] \dots C_k +$$

$$+ C_1 \dots [C_{l-1}, [C_0, C_l]] \dots C_k + \sum_{j=l-1}^{k} C_1 \dots [C_{l-1}, C_l] \dots [C_0, C_j] \dots C_k$$

$$= \sum_{j=1}^{l-2} C_1 \dots [C_0, C_j] \dots [C_{l-1}, C_l] \dots C_k + C_1 \dots [C_0, [C_{l-1}, C_l]] \dots C_k +$$

$$+ \sum_{j=l+1}^{k} C_1 \dots [C_{l-1}, C_l] \dots [C_0, C_j] \dots C_k$$

$$= [C_0, C_1 \dots [C_{l-1}, C_l] \dots C_k] .$$

From this equation, the property results, except for

$$C_0 \cdot C_1 \dots C_k - C_1 \cdot C_0 \dots C_k = [C_0, C_1] \dots C_k$$

which is proved by considering the difference

$$[C_0 \cdot C_1 \dots C_{k-1}, C_k] - [C_1 \cdot C_0 \dots C_{k-1}, C_k] .$$

9. – Determination of the Wightman function from the Green function.

We will now prove the following

THEOREM 7. – *If a function $G(k)$ satisfies the conditions* II.1)-5) *of Section* **7**, *it determines uniquely a Wightman function $\tilde{\mathscr{W}}(z)$ from which it derives. $\tilde{\mathscr{W}}(z)$ satisfies the conditions* I.1)-4).

A restriction will be brought to this formulation at the end of the proof.

From $G(k)$ we have already derived the products $C_0 \cdot C_1 \dots C_n$ and proved the properties III.1)-5) starting from II.1)-5).

Let us first consider condition III.3).

Corresponding to the cone $S_j \in \mathscr{S}_{X_j}$ we define the convex closed cone $U(S_j)$:

$$(9.1) \quad U(S_j) = \{(x^0_{j0}, x^0_{1j}, \dots, x^0_{jr(j)}) : \sum_{j'=0}^{r(j)} s_{jj'} x_{jj'} \leqslant 0 \text{ whenever } (s_{j0}, s_{j1}, \dots, s_{jr(j)}) \in \bar{S}_j\}.$$

III.3) implies that $\bar{\mathscr{F}}_{X_0} \bar{\mathscr{F}}_{X_1} \dots \bar{\mathscr{F}}_{X_k} C_0 \cdot C_1 \dots C_n$ decreases faster than exponentially at infinity in the complementary of $U(S_j)$.

But then, it can be shown, using Lorentz invariance, that $\overline{\mathscr{F}}_{X_0}\overline{\mathscr{F}}_{X_1}\ldots\overline{\mathscr{F}}_{X_k}C_0\cdot C_1\ldots C_k$ must actually vanish outside of $U(S_j)$.

So we replace III.3) by

III.3′). *Support properties in* (x): $\overline{\mathscr{F}}_{X_0}\overline{\mathscr{F}}_{X_1}\ldots\overline{\mathscr{F}}_{X_k}C_0\cdot C_1\ldots C_k$ *where* $C_j=C^{S_j}$, $S_j\in\mathscr{S}_{X_j}$, *vanishes unless*

$$(x^0_{j0}, x^0_{j1}, \ldots, x^0_{jr(j)})\in U(S_j)\,, \qquad 0\leqslant j\leqslant k.$$

Consider now the case when $G(k)$ derives from a Wightman function $\tilde{W}(z)$ in the way described in Section 5.

Up to Fourier transformation, the products defined in the last paragraph are then identical with those defined by eq. (6.5) (*). The proof of this statement is easy, it proceeds by induction on the number of factors of the product and is based on the support property $P^\pi_k\in\overline{V}^\mu_+$ of

$$\int \mathrm{d}\xi^\pi_k \exp\,[-iP^\pi_k\cdot\xi^\pi_k](\pi,\sigma')\tilde{W}*\varphi_r(x)+(\pi,\sigma'')\tilde{W}*\varphi_r(x)]\,,$$

when $\pi(0,1,\ldots,n)=(i_0,i_1,\ldots,i_n)$ and σ', σ'' differ only by the sign between i_{k-1} and i_k.

In particular, the boundary values of $\tilde{W}$ are given by

$$\tilde{W}^\pi(x)=\overline{\mathscr{F}}[A^{(i_0)}\cdot A^{(i_1)}\ldots A^{(i_n)}](x)\,, \tag{9.2}$$

where the « cycle » $A^{(i)}$ is C^{S_i}, S_i being the unique « cone » in $\mathscr{S}_{\{i\}}$ ($\mathscr{S}_{\{i\}}$ as well as S_i is of course reduced to a point).

Now, if $G(k)$ satisfies the conditions II.1)-5) but has not been derived from a function $\tilde{W}(z)$, we define a function $\tilde{W}(z)$ from $G(k)$ by equation (9.2).

Properties I.1), 3), 4) are then immediate consequences of III.1), 4). In order to show that I.2) holds too, we refer to the proof of Theorem 1 and see that this holds if

$$\overline{\mathscr{F}}[A^{(i_0)}\ldots A^{(i_{k-1})}\cdot A^{(i_k)}\ldots A^{(i_n)}](x)-\overline{\mathscr{F}}[A^{(i_0)}\ldots A^{(i_k)}\cdot A^{(i_{k-1})}\ldots A^{(i_n)}](x)$$

vanishes when $(x_k-x_{k-1})^2<0$.

To prove this we use first III.5) to write $A^{(i_{k-1})}\cdot A^{(i_k)}-A^{(i_k)}\cdot A^{(i_{k-1})}=[A^{(i_{k-1})}, A^{(i_k)}]$ then (6.6) and III.2) to see that $[A^{(i_{k-1})}, A^{(i_k)}]$ is the difference of two cycles in two variables with supports $x_k-x_{k-1}\in\overline{V}_+$ and $x_{k-1}-x_k\in\overline{V}_+$ respectively, and finally III.3′), 1) to show that these support properties remain in the full products.

(*) The proper extension of eq. (6.5) to products of $k+1$ cycles is immediate. These products are then applied to $\tilde{W}$.

Now that we have constructed a function $\tilde{\mathscr{W}}(z)$ with all the desired properties, it remains just to show that the function $G(k)$ derived from $\tilde{\mathscr{W}}(z)$ by the method of Section 5 is the same as the one from which we have started.

To do this, we will simply show that the products of cycles C^{S_j}, $S_j \in \mathscr{S}_{X_j}$, $\{X_0, X_1, ..., X_k\}$: a partition of $\{0, 1, ..., n\}$, applied to $\tilde{\mathscr{W}}$ are identical, up to Fourier transformation, to the products defined directly from G. This is true indeed for $k = n$ because of our definition of $\tilde{\mathscr{W}}$, and what we want to prove is just that it is also true for $k = 0$.

We use thus recursion on k, k decreasing.

Let

$$\Pi_{1,2} = C^{S_0} \cdot C^{S_1} \dots C^{S_k}$$

be a product according to either definition.

Π_1 and Π_2 satisfy both the same support properties III.3′) in (x).

Now, if $k < n$, there is at least one cycle, say C^{S_j}, in more than one variable. Using (6.6) and III.5), it is possible to transform Π_1 or Π_2 into

$$\tilde{\Pi}_{1,2} = C^{S_0} \dots C^{\tilde{S}_j} \dots C^{S_k}, \qquad \tilde{S}_j \in \mathscr{S}_{X_j}$$

by adding to them a sum of products of $k+2$ factors.

So

$$\Pi_2 - \Pi_1 = \tilde{\Pi}_2 - \tilde{\Pi}_1 .$$

But if $\tilde{S}_j$ is the antipodal of S_j in $(s)_{X_j}$, $U(\tilde{S}_j)$ will also be the antipodal of $U(S_j)$. $\Pi_2 - \Pi_1$ vanishes thus *if the variables* $x_{j_0}, x_{j_1}, ..., x_{j_{r(j)}}$ *are not all equal* and Theorem 7 is proved.

It remains to discuss the restriction brought to Theorem 7 by the fact that

$$\tilde{\mathscr{F}} G^S(x) = C^S \tilde{\mathscr{W}}(x)$$

only when all vectors x_i are different.

This reflects obviously the ambiguity of the definition of $C^S \tilde{\mathscr{W}}(x)$ which involves « cutting singularities ».

Any definition of the $C\tilde{\mathscr{W}}(x)$ involves a choice when some difference $x_{i'} - x_i$ vanishes, but should be such that

1) the identical linear relations between the general cycles C give rise to the same relations between the $C\tilde{\mathscr{W}}(x)$;

2) when C reduces to $A^{(i_0)} \cdot \sigma^{(i_1)} \dots A^{(i_n)}$, $C\tilde{\mathscr{W}}(x)$ should reduce to a boundary value of $\tilde{\mathscr{W}}(z)$.

1) and 2) were achieved here by the trick of regularizing $\tilde{\mathscr{W}}$ before cutting the singularities.

In conclusion and in order to avoid ambiguities it seems preferable to give oneself a function $G(k)$ with properties II.1)-5) rather than a function $\widetilde{W}(k)$ with properties I.1)-4).

* * *

The idea of the present work originated from the Thesis of O. STEINMANN [14] who treated the problem of the connexion between Wightman and Green functions in full details for the four-point function. A later paper of STEINMANN [15] on the same subject treats the general problem of the n-point function with methods and results rather different from what has been done here. A more related treatment is due to H. ARAKI [16]. Most of this work (essentially up to Section 7 incl.) was done in summer 1959 while the author stayed at the E.T.H. as a « chercheur agréé de l'Institut Interuniversitaire des Sciences Nucléaires » (Belgium).

In conclusion, I wish to thank Prof. R. JOST for his kind hospitality at the Institute of Physics of the E.T.H. in Zurich, for an introduction to Axiomatic Field Theory and for interesting discussions on the subject itself. I am also greatly indebted to Dr. O. STEINMANN who made the text of his Thesis available to me at an early stage and with whom I had interesting discussions. I also thank Dr. H. ARAKI for correspondence.

[14] O. STEINMANN: *Helv. Phys. Acta*, **33**, 257 (1960).
[15] O. STEINMANN: *Helv. Phys. Acta*, **33**, 347 (1960).
[16] H. ARAKI: to be published.

RIASSUNTO (*)

Nel presente lavoro, dopo aver ripreso lo studio delle proprietà di analiticità della funzione W di Wightman nel caso in cui il solo tempo sia una variabile complessa, ne deduciamo la funzione G di Green, estendendo altresì con un nuovo metodo i risultati di O. Steinmann relativi alla funzione a 4 punti. La funzione G ha per valore al contorno la trasformata di Fourier del valore medio del vuoto del prodotto T dei campi e prolunga analiticamente la funzione ritardata di L.S.Z. nello spazio degli impulsi. Infine si stabilisce un assieme di proprietà che caratterizzano G nel senso che se G possiede tali proprietà, esiste una ed una sola funzione $\widetilde{W}$ che ha le proprietà solite e tale che ne derivi G.

(*) *Traduzione a cura della Redazione.*

IL NUOVO CIMENTO Vol. XIX, N. 2 16 Gennaio 1961

Renormalization in a Combined Lee-Machida Field Theory.

L. M. Scarfone

Rensselaer Polytechnic Institute - Troy, N. Y.

(ricevuto il 10 Ottobre 1960)

Summary. — The renormalization of a combined Lee-Machida field theory is re-examined. It is shown that the energy of a new V-ghost found in an earlier investigation is sensitive to the renormalization procedure.

1. – Introduction.

In a previous paper (1), an investigation of the physical one particle V-states in a combined Lee-Machida model (2) has shown that there is simultaneously a ghost state in the fermion spectrum with energy greater than the normal V energy as well as a ghost in the boson spectrum for negative values of one of the renormalization constants. The analysis of the physical V-states carried out in I rests upon the coupling constant renormalization adopted in reference (2), namely,

$$f_1 = g_1 Z_1^{-\frac{1}{2}}, \tag{1}$$

$$f_2 = g_2 Z_2^{-\frac{1}{2}}. \tag{2}$$

where g_1 and g_2 are the bare coupling constants for the Lee interaction, $\mathrm{V} \rightleftarrows \mathrm{N} + \theta$, and the Machida interaction, $\theta \rightleftarrows \chi + \bar{\chi}$, respectively. The momentum independent renormalization constants $Z_1^{\frac{1}{2}}$ and $Z_2^{\frac{1}{2}}$ are defined in reference (2) in such a way that Z_1 removes a logarithmic divergence which arises from integration over the meson momentum and Z_2 removes a linear

(1) L. M. Scarfone and W. A. McKinley: *Nuovo Cimento*, **17**, 678 (1960); hereafter referred to as I.

(2) J. S. Goldstein: *Nuovo Cimento*, **9**, 504 (1958).

divergence which arises from integration over the χ-particle momentum. It is characteristic of a non-relativistic theory such as this that these definitions are not sufficient to remove all the divergences. A logarithmic divergence with respect to the χ-particle momentum remains in the theory after renormalization and as a consequence of this it is not possible to go to a point interaction between the θ and χ fields if there is to be a well defined eigenvalue equation for the physical θ-states and χ-$\bar{\chi}$ scattering. The renormalized constants f_1 and f_2 given by (1) and (2), respectively, are to bei dentified with the «physical coupling constants».

The probability, Z_1^{-1}, for finding a bare V in the physical V-state and the probability, Z_2^{-1}, for finding a bare θ in the physical θ-state are connected by the relation (*)

$$Z_1^{-1} = 1 - (f_1^2 Z_2^{-1}/2\Omega) \sum_k F^2(k) D_2^{-2}(k) D_3(k, 0) \omega_k^{-3} , \tag{3}$$

where $F(k)$ represents a cut-off function, $\omega_k = \sqrt{k^2+\mu^2}$, and with the exception, $D_3(k, 0)$, the D-functions are logarithmically divergent with respect to integration over the χ-particle momentum, but are held finite by the above cut-off assumption (**). It is shown in I for the case where there is a ghost state in the boson spectrum, $Z_2^{-1} < 0$, that there is also a ghost in the fermion spectrum even though, $Z_1^{-1} > 1$.

Employing the renormalization (1) and (2), the eigenvalue problem for the sector (V, $N+\theta$, $N+\chi+\bar{\chi}$) can be reduced to the form (**)

$$\omega_0 \left| \left(\frac{1}{f_1^2 Z_2^{-1}} \right) + (1/2\,\Omega) \sum_k \frac{F^2(k) D_1^{-1}(k, \omega_0) D_2^{-1}(k) D_3(k, \omega_0)}{\omega_k^2(\omega_k - \omega_0)} - \right. \tag{4}$$

$$\left. - (1/2\,\Omega) \sum_k \frac{F^2(k) D_2^{-2}(k) D_3(k, 0)}{\omega_k^3} \right| = 0 ,$$

which involves both renormalized coupling constants (f_2 is concealed in the D-functions), the Källén-Pauli energy parameter, ω_0, and Z_2^{-1}; the phase shift expression for elastic N-θ scattering is (**)

$$\operatorname{tg}\delta = \tag{5}$$

$$(f_1^2 Z_2^{-1}/2\Omega\omega_k') \sum_k F^2(k) \omega_k^{-1} D_1^{-1}(k, \omega_k') \delta(\omega_k - \omega_k')$$

$$1 - (f_1^2 Z_2^{-1}/2\Omega) \sum_k F^2(k) \omega_k^{-3} [\omega_k(\omega_k - \omega_k')^{-1} D_1^{-1}(k, \omega_k') D_2^{-1}(k) D_3(k, \omega_k') - D_2^{-2}(k) D_3(k, 0$$

(*) I, eq. (24).
(**) See Appendix of I for properties of the D-functions.
(**) I, eq. (26).
(**) Reference (2), eq. (57).

and this involves the incident 0-energy, $\omega_{\lambda'}$, the renormalized coupling constants and Z_2^{-1}. It is characteristic of the renormalization (1) and (2) that the combination $f_1^2 Z_2^{-1}$ occurs consistently in (3)–(5); therefore it is natural to define this quantity as the renormalized value of g_1^2. The interesting point here is that the energy behavior of the new fermion ghost found in I is sensitive to the definition adopted for the renormalization of g_1.

2. – Reinterpretation of the renormalization.

As suggested above, the combination $f_1^2 Z_2^{-1}$ measures the strength of the Lee interaction in this theory. We define, then, a new renormalized coupling constant, $\tilde{f}_1$, such that

$$\tilde{f}_1 \equiv f_1 Z_2^{-\frac{1}{2}} = g_1 Z_1^{-\frac{1}{2}} Z_2^{-\frac{1}{2}} , \tag{6}$$

with (2) unchanged. Whereas in I, f_1^2 is considered positive, we will now consider that $\tilde{f}_1^2$ is positive. It will be evident that this definition does not alter the chief result of I. Using (6), it is clear that (4) becomes

$$\omega_0[\tilde{f}_1^{-2} + \tilde{H}(\omega_0)] = 0 , \tag{7}$$

where $\tilde{H}(\omega_0)$, representing the integrals in (4), has the following properties (*):

$$\tilde{H}(0) = 0; \qquad \frac{\mathrm{d}\tilde{H}(\omega_0)}{\mathrm{d}\omega_0} > 0; \qquad \lim_{\omega_0 \to -\infty} \tilde{H}(\omega_0) = -\tilde{f}_{c1}^{-2}. \tag{8}$$

Equation (7) represents the eigenvalue problem for the sector mentioned above in terms of ω_0 and $\tilde{f}_1$. The inequality in (8) holds for the physical V domain, $\omega_0 < \mu < 2m$, (m is the mass of the χ-particle) and the elastic N-θ scattering domain, $\mu < \omega_0 < 2m$. Also, we have, expressing (3) in terms of the new constants, the relation

$$Z_1^{-1} = 1 - (\tilde{f}_1^2/\tilde{f}_{c1}^2) . \tag{9}$$

It is shown in I using (3) and (4) that if $Z_2^{-1} < 0$, (boson ghost), then a new V-ghost occurs in the range $0 < \omega_0 < \mu$ with energy greater than the

(*) $\tilde{H} = Z_2 H$ and $\tilde{f}_{c1}^{-2} = Z_2 f_{c1}^{-2}$ where H and the critical constant, f_{c1}, are defined in I by eq. (27) and (8), respectively.

normal V energy. On the other hand, if $Z_2^{-1} > 0$, (no boson ghost), then it is possible to have the Källén-Pauli type ghost.

It follows from equations (7), (8) and (9) that (*A*) if $\tilde{f}_1^2 < \tilde{f}_{c1}^2$ then Z_1^{-1} lies between zero and unity and there is no V-ghost present, (*B*) if $\tilde{f}_1^2 > \tilde{f}_{c1}^2$ then Z_1^{-1} is negative and there is a V-ghost with energy less than the normal V energy as in the ordinary Lee model. The positive character of $\tilde{f}_1^2$ allows in case (*A*) as an examination of (6) will show, (*A*1) both g_1^2 and Z_2^{-1} to be positive (no boson ghost, g_2^2 positive), or (*A*2) both g_1^2 and Z_2^{-1} to be negative (boson ghost, g_2^2 negative). In case (*B*) either (*B*1), g_1^2 is negative or (*B*2), Z_2^{-1} is negative: if g_1^2 is negative then there is only the V-ghost, whereas, if Z_2^{-1} is negative there is a V and a θ-ghost. In all of these cases, f_2^2 is considered positive. The following table summarizes the above possibilities:

Sign character of constants employing new renormalization.

	$\tilde{f}_1^2$	f_2^2	g_1^2	g_2^2	Z_1^{-1}	Z_2^{-1}
A1	+	+	+	+	+	+
A2	+	+			+	−
B1	+	+	−	+	−	+
B2	+	+	+	−	−	−

It is of interest to note in case (*B*2) that the presence of a V and a θ-ghost in the transitions, $V \rightleftarrows N + \theta$ and $\theta \rightleftarrows \chi + \bar{\chi}$, necessitates the hermiticity of the Lee interaction hamiltonian (g_1 real) and the non-hermiticity of the Machida interaction hamiltonian (g_2 pure imaginary). In case (*A*2) the θ-ghost leads to the non-hermiticity of both interaction hamiltonians (g_1 and g_2 pure imaginary) and in case (*B*1) the V-ghost requires a non-hermitian Lee interaction (g_1 pure imaginary).

3. – Conclusions.

It is clear from the above analysis that the new renormalization (6) and (2) still allows the simultaneous presence of a V and θ-ghost in the theory, case (*B*2). Whereas the old renormalization (1) and (2) of I and reference [2] allows the additional V-ghost to have energy greater than the normal V-energy it is characteristic of (6) and (2) that this V-ghost have energy less than the normal

V-energy as in the ordinary Lee model. The reinterpreted renormalization employed here has shifted the energy of the additional V-ghost below the normal V-energy thereby producing a closer correspondence between the ordinary Lee model and the Lee model with pair effects.

* * *

The author would like to express his thanks to Professor W. A. McKinley for helpful discussions.

RIASSUNTO (*)

Si riesamina la rinormalizzazione di una teoria combinata del campo di Lee-Machida. Si mostra che l'energia di un nuovo fantasma V, trovato in una precedente ricerca, risente del procedimento di rinormalizzazione.

(*) *Traduzione a cura della Redazione.*

Experimental Investigation of a Neutral Beam from the CERN 25 GeV Proton Synchrotron (*).

M. Fidecaro, G. Gatti, G. Giacomelli (**), W. A. Love (***), W. C. Middelkoop and T. Yamagata (***)

CERN - Geneva

(ricevuto il 22 Novembre 1960)

Summary. — The spectra of photons from the CERN 25 GeV proton synchrotron using aluminium and beryllium internal targets have been measured at the laboratory angles of 3.2° and 15.9° by means of a lead glass total absorption Čerenkov counter. While at 3.2° the intensity is slightly higher than that predicted by the statistical model with the assumption of isotropy in the c.m.s., at 15.9° it is about an order of magnitude below this prediction. This is interpreted as an indication of anisotropy in c.m.s. The 3.2° beam, at 64 m from the target, has an intensity of about 13600 photons above 1 GeV per cm² when 10^{11} protons impinge on a beryllium target. The number of neutrons was found to be about a factor of 2 below the number of γ-rays of energy larger than 2 GeV. Attenuation measurements of γ-rays and neutrons have been performed in carbon, CH_2 and lead.

Introduction.

There is considerable interest in investigating the neutral beams produced in a high-energy Proton Synchrotron because of the expected large fluxes of high-energy γ-rays, neutrons, antineutrons and K_2^0 [1]. We describe here an

(*) Preliminary results have been presented to the XLVI Congresso della Società Italiana di Fisica, Napoli, 1960.

(**) On leave from the University of Bologna.

(***) National Science Foundation postdoctoral fellow.

(***) Ford Foundation postdoctoral fellow.

[1] G. Salvini and A. Turrin: *The γ-ray beam of the 25 GeV proton-syncrotron. On the experimental use of the γ-rays' relative polarization.* Report I.N.F.N. G 27 (1959). Also a high flux of high-energy neutrinos is produced by the CERN PS. This flux is estimated to be about 10^4 neutrinos of energy above 1 GeV per square centimetre at 50 m from the target for $3 \cdot 10^{11}$ circulating protons.

investigation of the photons which come mainly from the decay of the π^0-mesons.

There are several disadvantages in a photon beam from π^0-decay from a Proton Synchrotron (PS) compared with a bremsstrahlung beam from an Electron Machine (EM):

1) A high number of particles, other than γ-rays (mainly neutrons), are present in a PS neutral beam. In the range of energies of interest (above ~ 1 GeV) the neutrons are about as many as the γ-rays, and although it is easy to get rid of the photons while little affecting the number of neutrons, the converse is not true.

2) The intensity of a usable PS γ-ray beam is several orders of magnitude smaller than that of an EM. The photons are produced in a forward cone whose half angle is about 8° and is thus much larger than that of the photons from a bremsstrahlung beam ($\sim m_e/E$). Therefore a beam must be defined by collimators and the usable intensity is determined by how wide an angular spread of the beam may be tolerated.

3) The energy spectrum of a π^0 decay beam falls off much faster towards high energies than a bremsstrahlung spectrum.

One advantage of the π^0-decay beam over bremsstrahlung lies in the absence of very soft photons so that it is not necessary to harden the beam.

The experimental equipment we have developed for use in conjunction with the γ-ray beam is based on two total absorption lead glass Čerenkov counters [2].

We have developed a γ-ray beam and made a rough determination of the neutron contamination. Attenuation measurements of γ-rays and neutrons were performed mainly for the practical purpose of reducing the contamination of one particle with respect to another.

Finally, we have measured spectra of photons produced at forward angles from Be and Al. Apart from their usefulness in the planning of experiments, these spectra can be, in principle, a test of the statistical model predictions for particle production in nucleon-nucleon collisions, as it has been developed by HAGEDORN, CERULUS, and VON BEHR [3].

It is interesting that our data, combined with other results on charged particle production and backward γ-spectra, strongly suggest a deviation from isotropy in c.m.s. [4].

[2] G. GATTI, G. GIACOMELLI, W. A. LOVE, W. C. MIDDELKOOP and T. YAMAGATA: *A total absorption lead glass Čerenkov counter*, to be published.

[3] R. HAGEDORN: *Nuovo Cimento*, **15**, 434 (1960); F. CERULUS and R. HAGEDORN: *Suppl. Nuovo Cimento*, **9**, 646, 659 (1958); J. VON BEHR and R. HAGEDORN: CERN 60-20 (1960).

[4] See G. COCCONI: *Report at the High-Energy Conference* (Rochester, 1960).

1. – Beam layout.

Fig. 1. shows the layout of the 3.2° (56 mrad) neutral beam. This is the minimum angle at which neutral particles can escape through the thin mylar window (more forward particles pass at a small angle through the 0.2 cm stainless steel vacuum chamber wall where the γ-rays are strongly attenuated).

The beam passes through a defining lead collimator, 1.2 metres long, 3 cm diameter, after which charged particles are swept away by a magnet. A second lead collimator outside the shield wall, 1 m long with an aperture (7.8 cm dia-

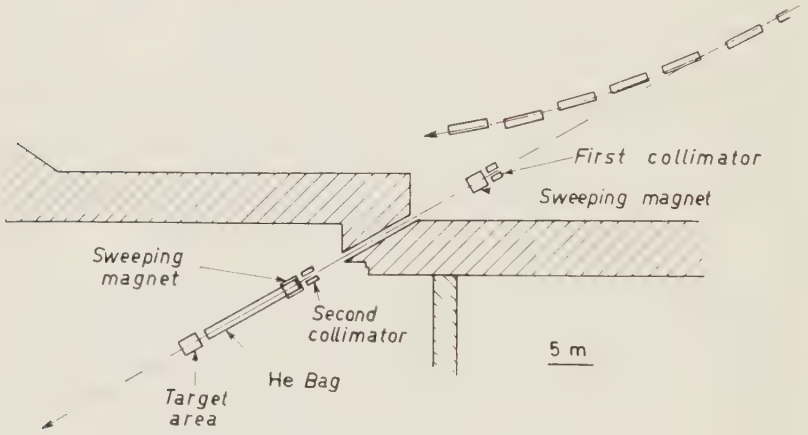

Fig. 1. – Layout of 3.2° neutral beam.

meter) slightly larger than the size of the beam, removes neutral particles scattered by the first collimator at large angles with respect to the 3.2° line. After a second sweeping magnet, a helium atmosphere reduces the number of charged particles produced by the neutral beam.

The beam profile measured with a system of two cylindrical scanning counters, 1 and 2 cm diameter respectively, and 2 cm apart, at 64 m from the internal target, shows an intensity distribution of 6 cm diameter at half height and 9 cm diameter at the base. The intensities at radii larger than 5 cm, do not exceed 3% of the intensities at the centre.

2. – γ-ray investigation.

Fig. 2 shows the photon detection system: γ-rays are converted into electron-positron pairs in a 0.365 cm thick lead plate (1.6×1.6) cm² in area. The pairs traverse counters No. 2 and No. 3 before entering along the axis a Če-

renkov counter where they produce a shower. The anticoincidence counter No. 1 prevents the counting of charged particles. The converter, which defines the solid angle, has an efficiency of 39% for pair creation. The whole system, as used, has an acceptance angle of 10 and is at least 99% efficient in suppressing background from other particles.

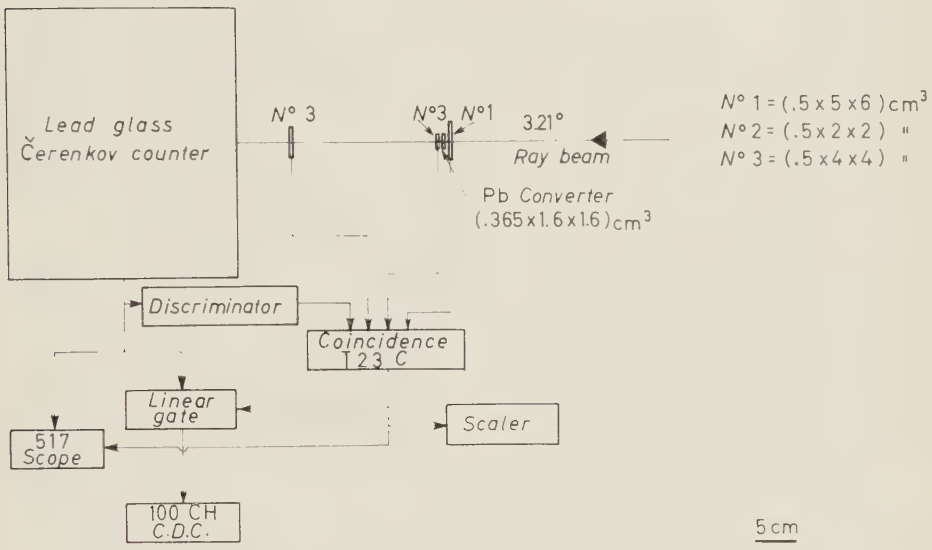

Fig. 2. – Photon detection system with block diagram of the electronics.

The total absorption Čerenkov counter is a cylinder of lead glass, 30 cm long and 35 cm in diameter (respectively 12 and 14 radiation lengths) [2]. The glass is viewed directly by seven RCA 7046 photomultipliers, whose signals are added electronically. The counter itself has 100% efficiency for high-energy γ-rays, and, when used with an arrangement as shown in Fig. 2, it still detects photons with high efficiency, while having a negligible efficiency for any other particle. Its energy resolution improves with increasing energy, and for electrons and photons above 5 GeV, it is better than 10%. The response is linear up to the maximum energy at which it has been tested (14 GeV).

A photon is defined by a coincidence-anticoincidence $\overline{1}23C$. This signal opens a linear gate which allows the pulse from the Čerenkov counter to be recorded on a 100 channel CDC (computing devices of Canada) pulse-height analyser. At the same time the $\overline{1}23C$ rate triggers the sweep of a Tektronix 517 oscilloscope which is photographed. As the recording rate on the film is intrinsically low, practically limited to a single sweep per machine pulse, the information obtained by the film was mainly used as a check on the performance of the kicksorter measurement.

Attenuation measurements of the γ-rays confirmed their identity (see Section 4). The effect of neutrons and other uncharged particles was measured by placing 10 cm of lead in the beam (19 radiation lengths). In this situation

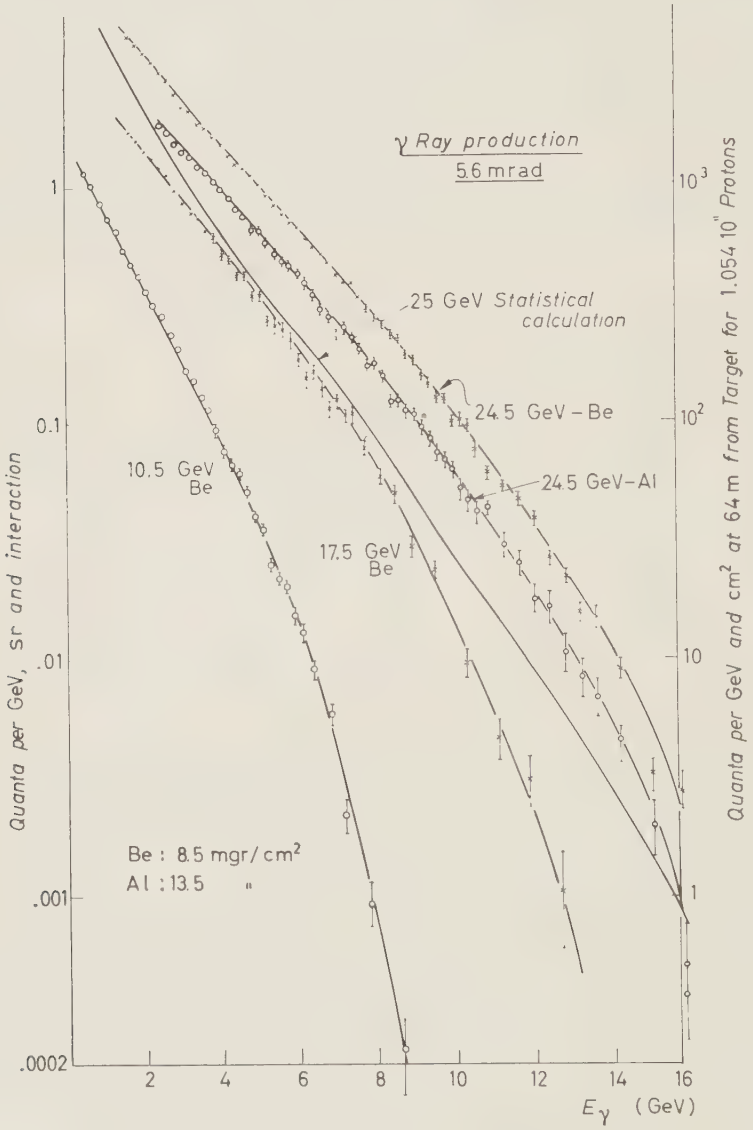

Fig. 3. – γ-ray production at 3.21°.

the counting rate dropped to 0.3%, which yields a correction of about 0.7% to the photon rate. This correction was neglected. We also neglected a 1.5% correction due to randoms. By removing the lead converter we obtained a

counting rate of 5.5% of the normal situation. This rate is interpreted as due to γ-rays converting in the crystals, mountings, etc., between counters No. 1 and No. 2. The intensity has been corrected for this effect. Another correction arises from the long dead-time of the kicksorter. Although the rate was limited to about 100 counts per machine burst of 50 ms duration, a correction of $(10 \div 30)\%$ to the rates was needed.

Fig. 3 shows the results. Errors are standard deviations and include the effect of counting statistics only. The scale at the left gives the number of γ-rays per interaction, corrected for efficiency and absorption, per steradian and GeV interval with the assumption that 50% of the protons interact in the target. Also shown is the prediction of the statistical model. Since the actual number of interactions is poorly known, the measured spectra may easily be shifted by a scale factor of two or more [5].

Practical γ-ray intensities corrected for efficiency in our detecting telescope are shown on the scale at right as γ's per cm^2 and GeV interval at 64 m from the target when a circulating beam of $1.054 \cdot 10^{11}$ protons impinges on an internal target. The scale has an estimated systematic uncertainty of $\pm 15\%$ mainly due to energy scale uncertainty ($\pm 3\%$) and monitor inaccuracy (better than 10%: it was necessary to lower the machine intensity by a factor of 200 for the spectrum measurement). The results on the oscilloscope film agreed within their statistics with the kicksorter spectrum.

Fig. 4 shows a similar measurement at an angle of 15.9° with respect to the internal proton beam.

The main results of these measurements are the following.

1) A beryllium target yields 1.5 times more photons than aluminium over the whole spectrum. While this result is of practical importance, it cannot be regarded as theoretically significant, since the number of protons interacting may well have been different in the two cases due to such effects as multiple scattering loss, etc.

2) The comparison of our data with the predictions of the statistical model, transformed to the laboratory system, shows that while at 3.2° we have more photons than expected, at 15.9° they are about an order of magnitude less. We have to emphasize here that the statistical model gives only the c.m.s. momentum spectra, integrated over angle. The angular distribution is not predicted by the model. To transform the spectra to the laboratory system, the extra hypothesis of isotropy in c.m.s. has been used. It follows that the observed deviations from the theory could be interpreted as an indication of anisotropy in the c.m.s. This result is supported by the data on charged

[5] CERN Proton Synchrotron staff estimates that about 50% of the circulating protons interact in the target.

particle production and backward γ-spectra [1]. Moreover, the predictions refer to a nucleon-nucleon collision, while experimentally we have a nucleon-nucleus collision and thus a large probability for secondary interactions (one radius of the Al nucleus is about 65 g cm^{-2}). This gives an alteration of the momentum

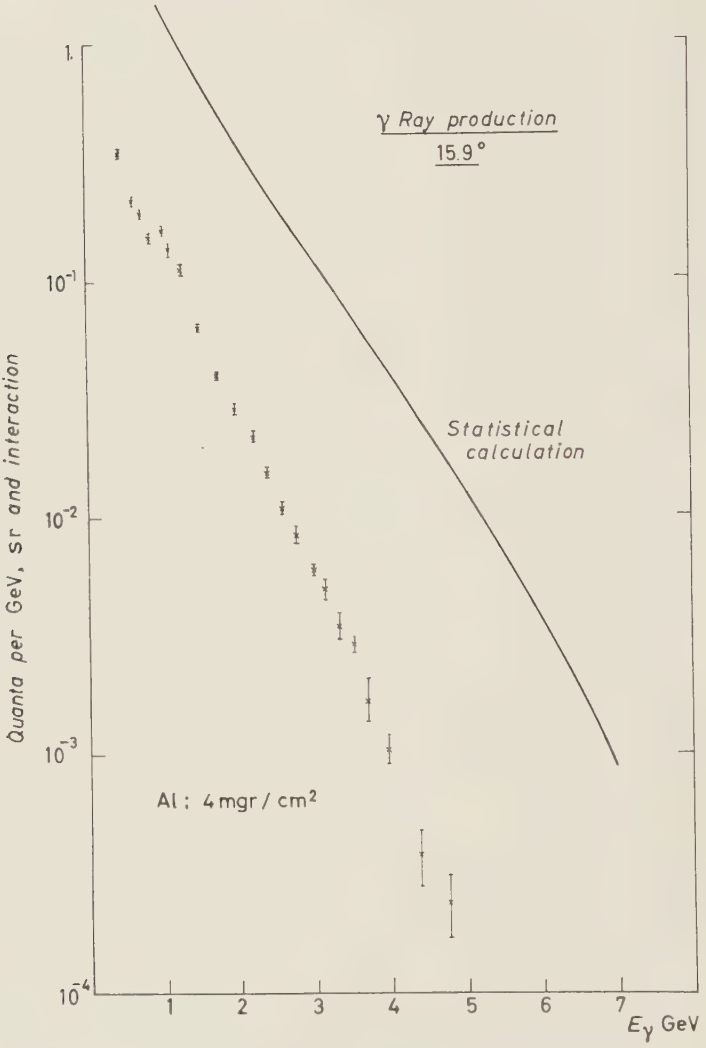

Fig. 4. – γ-ray production at 15.9°.

and angular distribution, decreasing the mean energy of the particles and reducing the forward peaking in the laboratory system [4]. Finally, the Fermi motion of the nucleons in the nucleus has to be taken into consideration.

3) Fig. 2 shows also the spectra obtained at 3.2° when the circulating proton energy was reduced to 10.5 and 17.5 GeV. At these energies the repetition rate may be raised from one pulse every three seconds to one per second and one every two seconds respectively. For some experiments (notably bubble chambers), one may like to increase the repetition rate. Our data show that this would be accompanied by only a small loss in the flux of particles per unit time in the $(1 \div 5)$ GeV region.

4) The total number of γ-rays above 1 GeV obtained by integrating our spectrum, and also from the scanning counter rate, is about 13300 per cm^2 at 64 m from the target per pulse of 10^{11} circulating protons. With the above-mentioned collimators, the total beam flux is $3.8 \cdot 10^5$ photons per pulse of 10^{11} circulating protons ([6]).

3. – Neutron investigation.

Neutrons were measured by detecting the charged particles produced in a light material. From the analysis of some neutron stars in a 1.0 m long propane bubble chamber ([7]), it was evident that neutrons in the GeV region produce charged particles roughly in a 50° forward cone. Thus to have a high efficiency the coincidence counters must subtend a large solid angle.

The apparatus we used consisted of a 25 cm diameter anticoincidence counter, a 10 cm thick (6.5×6.5) cm^2 beryllium converter and three 22 cm diameter counters in coincidence, spaced 6 cm one from the other and all placed on the beam axis. All counters were plastic scintillators 1 cm thick; the last coincidence counter subtended an angle of 58° from the centre of the beryllium converter, in which 20% of the neutrons should interact. 10 cm of Pb in the beam in front of the first sweeping magnet was used to eliminate the photons.

With this arrangement we count the number of neutrons above a certain energy cut-off. Statistical model predictions ([3]) give a neutron spectrum peaked at about 5 GeV with half heights at 2.7 and 8.1 GeV and few neutrons below 1 GeV. This last prediction is partially confirmed by our experiment, since the presence or absence of 8 g/cm^2 polyethylene absorber between the coincidence counters made no difference in the rates. The detector is also sensitive to the antineutrons and K_2^0 which should be present in the beam but these particles are at least an order of magnitude less numerous than the neutrons and their interaction cross-sections not too different, so that we essentially count only neutrons.

([6]) The CERN proton synchrotron is now able to accelerate $3 \cdot 10^{11}$ protons per pulse

([7]) Ecole Polytechnique - Paris, $(1.0 \times 0.5 \times 0.5)$ m^3 propane bubble chamber. We thank the Ecole Polytechnique for having put at our disposal a set of pictures.

Table I shows the number of « neutrons » per steradian and per circulating proton measured at 64 m from the target both for a beryllium and an aluminium target. The numbers have a negligible statistical error and a systematic uncertainty of about $\pm 15\%$ due to uncertainties in efficiencies, extrapolation to zero absorber and calibration of the circulating proton beam monitor. Also shown on the table are the total number of photons and the number of photons above 2 GeV. (The first number has a systematic uncertainty of $\pm 30\%$ due to poor knowledge of the spectrum below 1.5 GeV.) The predictions of the statistical model at 3° shown on the table cannot be compared directly for absolute values with the other numbers, since the measured intensities at 64 m are per *circulating proton* and no correction has been used for loss of particles in air, walls, etc., while predictions are for *interacting proton* at the internal target position ([5]).

TABLE I. – *Measured number of neutrons and of photons per steradian and per circulating proton emitted at* 56 mrad (3.2°). Errors are rough estimated systematic uncertainties. For comparison, the statistical model predictions at 3° per steradian and interaction are also shown.

« Neutrons »		Photons		Photons above 2 GeV		Statistical model	
Be	Al	Be	Al	Be	Al	photons	$n+\bar{n}+K_2^0$
1.66 ± 0.25	1.09 ± 0.16	9.7 ± 3.0	6.4 ± 2.0	3.6 ± 0.5	2.2 ± 0.3	12.51	13.25

From the table the following conclusions can be reached.

a) A beryllium target gives both more neutrons and more photons than an aluminium target.

b) The integrated number of neutrons is considerably smaller than that of the photons. Since it is expected that roughly 5% of the neutrons are in the energy region below 2 GeV, the ratio of photons to neutrons in the high energy region is:

$$\left(\frac{\gamma\text{-rays}}{\text{neutrons}}\right)_{E > 2\ \text{GeV}} = 2.2 \pm 0.5.$$

4. – Attenuation measurements of photons and neutrons.

With the same apparatus used for measuring photons and neutrons, one can measure the attenuation cross-sections of these particles by placing absorbers in the beam.

The relative positioning of the absorber-detector system is very important for the interpretation of the experiment.

For γ-rays the main process contributing to the attenuation is the electron-positron pair creation in the Coulomb field of the nucleus. If the absorber

is relatively thick the probability that these electrons produce by bremsstrahlung lower energy γ-rays becomes appreciable and thus invalidates the measurement in the low-energy region. The contribution of this effect is in practice reduced by the fact that the photon spectrum is essentially exponential so that the number of higher energy photons is small. It is nevertheless desirable to reduce further the effect. This is achieved either by placing the absorber far away from the detector so that reconverted photons, which will be produced at relatively large angles with respect to the natural spread of the beam, have little probability for being counted, or by placing the absorber just in front of the detector so that electrons from showers initiated in the absorber are counted with high probability in the anticoincidence counter in front of the detector. We have used this second arrangement and, in addition, disregarded the measurements for photons of an energy lower than 3 GeV.

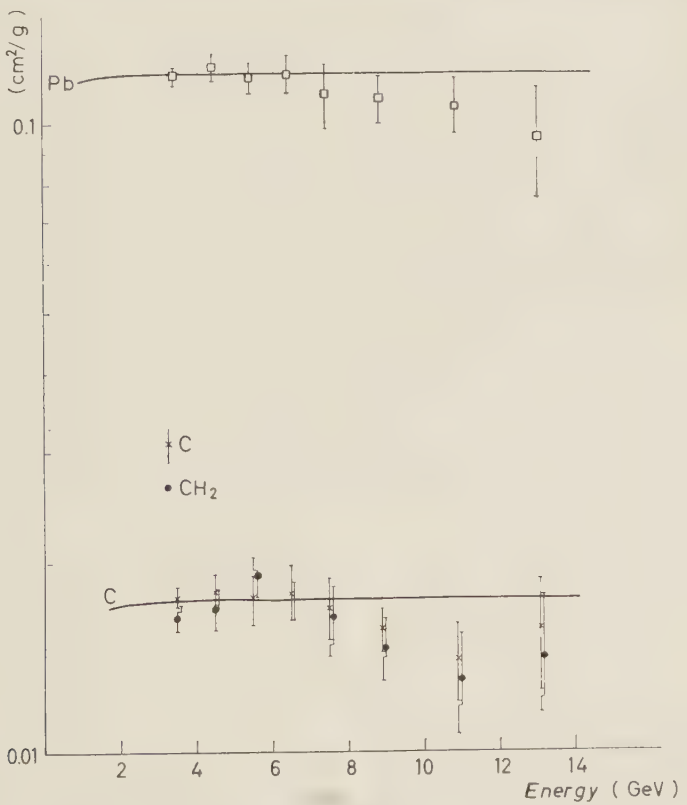

Fig. 5. – Mass absorption coefficient of γ-rays.

Fig. 5 shows the results for the photon attenuation coefficient as function of the incoming γ-ray energy in carbon, polyethylene (CH_2) and lead. Least square fits of exponential absorption curves to the measurements gave reason-

able values of χ^2. Errors shown on the graph are standard deviations and include statistical errors as well as estimated systematic uncertainties. The solid curves shown on Fig. 5 are taken from UCRL 2426 – High energy particle data – Vol. II. They include attenuation due to electron Compton effect, pair production in the field of the nucleus and in the field of the electrons. The agreement with these curves is reasonable considering the large statistical errors and the systematic uncertainty due to the neutrons in the beam.

The complication of regeneration of neutrons of lower energy is present to less extent than with the γ-rays, but we have here the difficulty of not seeing the neutron spectrum. In this case, absorbers were placed far away from the detector in a good geometry arrangement and the extrapolation to the total cross-section was relatively easy. The cross-sections in lead and lithium were measured. In the case of lead, absorbers were placed at two different positions so that we could check that the diffraction pattern follows closely that of a black disc. We obtained a mean free path of (118 ± 2) g cm^2 for lead and (61 ± 5) g/cm^2 for lithium, corresponding to total cross-sections (absorption plus diffraction scattering) of $(2\,910 \pm 50)$ and (190 ± 15) mb respectively. These values are in good agreement with other measurements [8].

We found the ratio of the absorption lengths for neutrons and photons of energy greater than 4 GeV in lithium hydride (in plastic containers) to be 1.50 (the attenuation coefficient for γ-rays in lithium hydride is about 110 g/cm^2). It is thus possible, although costly in photon flux, to increase the ratio of photons to neutrons in our beam.

* * *

It is a pleasure to acknowledge the continuous guidance of Professor G. Bernardini, the assistance of Miss E. Sassi and the skilful help of G. Sicher and B. Smith. We thank the PS machine group for their assistance in the setting up of the experiment, for the alignment of our beams and for the smooth operation of the PS machine.

([8]) J. H. Atkinson: UCRL 8966; A. Ashmore, G. Cocconi, A. N. Diddens and A. M. Wetherell: *Phys. Rev. Lett.*, to be pubblished.

RIASSUNTO

I fotoni prodotti dai protoni di 25 GeV del protosincrotrone del CERN sono stati analizzati con un contatore di Čerenkov ad assorbimento totale ai due angoli di 3.2° e 15.9° (sistema del laboratorio). Mentre a 3.2° l'intensità misurata è lievemente superiore a quella predetta dal modello statistico con l'ipotesi dell'isotropia nel sistema del centro di massa, a 15.9° l'intensità è circa un ordine di grandezza inferiore. Questo risultato viene interpretato come un'indicazione di un'anisotropia nel c.m. A 3.2° e a una distanza di 64 m dal bersaglio (berillio) sono stati misurati 13 600 fotoni al disopra di 1 GeV, per cm^2 e per impulso di 10^{11} protoni. Al di sopra di 2 GeV, i neutroni sono circa la metà dei fotoni. I coefficienti di attenuazione per fotoni e neutroni sono stati misurati in carbonio, paraffina e piombo.

LETTERE ALLA REDAZIONE

(La responsabilità scientifica degli scritti inseriti in questa rubrica è completamente lasciata dalla Direzione del periodico ai singoli autori)

Diffusion of Cobalt and Silver in Ordered and Disordered CuZn.

C. Bassani, P. Camagni and S. Pace

C.N.R.N., Centro di Studi Nucleari, Gruppo di Fisica dei Solidi - Ispra

(ricevuto il 3 Settembre 1960)

The study of atomic diffusion in an ordered alloy has drawn in the past few years the attention of several authors. Its main interest lies in the possibility that the « anomalous » behaviour of diffusion in the ordered lattice may give a tool for checking the proposed mechanisms of atomic migration.

So far, investigation has centered on β-brass, owing to some convenient features of this alloy. Thus, the temperature dependence of Cu and Zn diffusion has been measured systematically by various authors [1,2], in the range where an ordered superlattice is known to occur. Results of a few experiments on the diffusion of impurities in ordered β-brass are reported by the same sources.

The results have already been subjected to a certain amount of speculation [1-4]. However, the lack of systematic data on the diffusion of other atomic species besides Cu and Zn prevented any conclusive remarks to be made. With this in mind, work was undertaken in order to study impurity diffusion in ordered CuZn.

The present is an advance report on the diffusion of Cobalt and Silver in β-brass (47.2 atom. % Zn). The experiments were performed at various temperatures in the range from ~ 700 °C down to ~ 320 °C. The temperature dependence of D_{Co} and D_{Ag} was thus determined in the disordered as well as in the ordered phase of the alloy.

The experimental method was the conventional annealing-sectioning technique, making use of radioactive tracers. Pile-activated isotopes ^{60}Co and ^{110}Ag were deposited electrolitically from suitable baths ($CoSO_4$ or AgCN) onto the end surface of cylindrical β-brass specimens. The samples were polycrystalline with coarse grains, stabilized by heat-treatment at high temperatures. After diffusion, sectioning was performed on a modified precision-lathe; the γ-activity of the slices was counted in a liquid scintillation counter of nearly 4π-geometry.

(1) A. B. Kuper, D. Lazarus, J. R. Manning and C. T. Tomikura: *Phys. Rev.*, **104**, 1536 (1956).

(2) P. Camagni: *Proc. of the 2nd Intern. Conference on Atomic Energy*, P/1365, vol. **20** (Geneva, 1958).

(3) A. B. Lidiard: *Phys. Rev.*, **106**, 823 (1957).

(4) E. W. Elcock and C. W. McCombie: *Phys. Rev.*, **109**, 605 (1958).

The results are illustrated in Fig. 1, where the plots of $\log D$ *vs.* $1/T$ for Ag and Co are shown. The diffusion of the two impurities shows features qualitatively similar to those of self-diffusion:

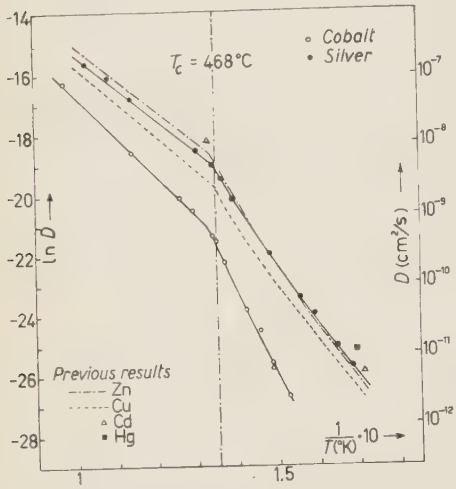

Fig. 1. – Plot of $\log D$ *vs.* $1/T$ for Ag and Co diffusing in ordered or disordered β-brass (47.2 % atom. Zn). [The dotted traces give a comparison with the results of Cu and Zn diffusion, reported in ref.(²)].

a) *In the disordered region* above the transition temperature ($T_c \simeq 468$ °C) D_{Ag} and D_{Co} follow the usual law $D = D_0 \cdot \exp[-Q/RT]$. It is seen that the two $\log D$ plots are linear down to temperatures very near to T_c; the eventual rise of short-range order does not seem to affect diffusion appreciably, in the case of Ag, and only little in the case of Co. This fits well with previous observations on self-diffusion (²).

Values of the heat of activation and frequency factor were determined in this range by least-squares fits; they are given in Table I.

TABLE I. – *Diffusion in disordered β-brass.*

Diffusing element	Q	D_0
Ag	21.90 kcal/g atom.	0.014 cm²/s
Co	26.90 kcal/g atom.	0.047 cm²/s

b) *At the transition temperature*, when long range order begins to set in, the $\log D$ curves drop almost abruptly and assume a complicated behaviour. In the region immediately below T_c, the logarithmic plots do not fit straight lines.

c) *In the ordered region*, the plots still have a finite curvature. However, at low enough temperatures the slope is again practically constant. This would allow an average heat of activation and an average frequency factor to be extrapolated for the ordered range (below ~ 400 °C). However, the above quantities, owing to their definition, would be in no way precise nor meaningful.

The data for the ordered range were then subjected to a more detailed analysis, in order to see if the empirical curves of $D(T)$ can be made to fit some detailed function of σ (long-range order parameter). It was found by means of numerical and graphical interpolations that D_{Ag} and D_{Co} fit satisfactorily relationships such as

$$(1) \qquad \frac{D^{(\mathrm{dis})}}{D^{(\mathrm{ord})}} \simeq \frac{1}{1+\sigma} \exp[\sigma U/kT],$$

where: $D^{(\mathrm{ord})}$ is the experimental value at any temperature in the ordered range, $D^{(\mathrm{dis})}$ is the value the coefficient would have at the same temperature, if it were extrapolated from the known empirical behaviour, characteristic of the disordered range; σ is the degree of long-range order as given by Bethe's 1st order approximation (⁵). U is a constant parameter, which is typical of each diffusing element; in principle, it is the *additional* energy which is required for the activation of an atomic jump when ordering is complete ($\sigma = 1$). It should take into account the disordering effect of the

(⁵) See for instance the results of 1st-order Bethe's theory in: R. H. FOWLER: *Statistical Mechanics*, chap. XXI (Cambridge, 1955).

jump, as well as the difference of vacancy concentration between the ordered and the disordered phase.

Eq. (1) tells us that, in the ordered phase, the anomaly of diffusion can be described in terms of an « additional » free-energy of activation which is linear in σ (apart from the temperature dependence contained in $1/(1+\sigma)$, which is negligible when σ is sufficiently high). It must be noticed that the same conclusion had previously been found to hold for self-diffusion (see ref. [2]).

Best fits of empirical data to relation (1) have been systematically worked out, in order to verify it and to find the good values of U for various atomic species diffusing in ordered β-brass. For Co and Ag, the interpolation was made using the present results; in the same scheme previous data on self-diffusion [2] were interpolated for comparison. The following values have been obtained [*]:

$$U_{Cu} = 5.7 \cdot 10^{-2} \text{ eV/bond},$$
$$U_{Ag} = 6.4 \cdot 10^{-2} \text{ eV/bond},$$
$$U_{Zn} = 7.3 \cdot 10^{-2} \text{ eV/bond},$$
$$U_{Co} = 8.4 \cdot 10^{-2} \text{ eV/bond}.$$

It is thus seen that, on the quantitative side, there are remarkable differences between the behaviour of impurities and self-diffusion, especially for Co. The values of U for the various diffusing elements also deviate, in general, from the value of the « ordering energy », which is known to be $\sim 5.4 \cdot 10^{-2}$ eV/bond for the given alloy [6]: however, the order of magnitude is respected. This fact suggests that the main effect on diffusion comes from a configurational term, namely the energy of ordering of the alloy (or similar « solution terms » in the case of impurities): at the same time, part of the observed differences could be explained by the existence of different concentrations of vacancies on the two sublattices of the ordered alloy.

A detailed discussion of the above results will be given in a separate paper.

(*) It must be noticed that the values of u_{Zn} and u_{Cu} reported in ref. [2] were erroneous, and are to be referred really to one « half-bond ».

(6) C. SYKES and H. WILKINSON: *Journ. Inst. Metals*, **61**, 223 (1937).

IL NUOVO CIMENTO Vol. XIX, N. 2 16 Gennaio 1961

Dispersion Theoretic Approach in Nucleon-Nucleon Scattering.

S. Furuichi and S. Machida

Department of Physics, Rikkyo University - Tokyo

(ricevuto il 15 Novembre 1950)

In the present short note we would like to report briefly a new approach to the dispersion theoretic treatment of the nucleon-nucleon scattering, where the impact parameter will play an important role as it has been shown up in the potential theoretical treatment by Taketani's group in Japan [1]. The detailed discussions will appear soon in the *Progress of Theoretical Physics*.

Assuming the general invariance which has been accepted valid for the strongly interacting particles, one can write down an S-matrix for the elastic nucleon-nucleon scattering with ten independent scalar functions of energy-momentum of nucleons in the initial and final states [2] as follows:

$$(1) \qquad (S-1)_{fi} = i(2\pi)^4\,\delta(p_i + p_i' - p_f - p_f') \sum_{j=1}^{5} I_j \left\{ G_j^{(1)}(s,t,u) + \tau^{(1)}\cdot\tau^{(2)} G_j^{(\tau)}(s,t,u) \right\},$$

$$(2) \qquad s = -(p_i + p_i')^2\,, \qquad t = -(p_i - p_f)^2\,, \qquad u = -(p_i - p_f')^2\,,$$

where p_i, p_i' and p_f, p_f' are energy-momenta of the initial and the final states of nucleons respectively, and I_j's are a set of five independent functions involving spin operators [2,3]. The double dispersion relation [4] or appropriate one-dimensional dispersion relations [2,3] can be applied to the invariant functions G_j's. For example, if we fix the exchanged momentum transfer u, we obtain the following type of dispersion relation, except the contribution from the deuteron pole,

$$(3) \qquad G_j(s,t,u) = \frac{g^2}{\mu^2 - t}\,\delta_{j5} + \frac{1}{\pi}\int_{4m^2}^{\infty} ds' \, \frac{\Phi_1^j(s',u)}{s' - s - i\varepsilon} + \frac{1}{\pi}\int_{4\mu^2}^{\infty} dt' \, \frac{\Phi_3^j(t',u)}{t' - t - i\varepsilon}\,,$$

where g is the renormalized pion-nucleon coupling constant, and m and μ are the nucleon and pion masses respectively. The first term of the right hand side of eq. (3) represents the one-pion exchange contribution (OPEC).

(1) *Prog. Theor. Phys. Suppl.* No. 3, *Nuclear Force* (1956).
(2) M. L. Goldberger, Y. Nambu and R. Oehme: *Ann. of Phys.*, **2**, 226 (1956).
(3) M. Cini, S. Fubini and A. Stanghellini: *Phys. Rev.*, **114**, 1633 (1959).
(4) S. Mandelstam: *Phys. Rev.*, **112**, 1344 (1958).

For energies where inelastic processes are negligible, $\Phi_1^j(s, u)$ may be determined from the unitarity condition of the S-matrix, although kinematical complexity must be overcome. The absorptive parts of the unphysical region $\Phi_3^j(t, u)$ are connected with the absorptive parts of the nucleon-antinucleon process, and we can divide them into the two-pion exchange contribution (TPEC), the three-pion exchange contribution, and so on. The two-pion exchange contribution is calculable, if we adopt the meson theoretical approach, while the theoretical estimation of the more-than-two-pion exchange contributions is almost impossible, because the calculation of the phase volume in such states is very difficult. In order to avoid such a difficulty we had better pick up the physical quantities which are insensitive to the detailed behavior of the heavier intermediate states than the two-pion state.

As is well known, the nucleon-nucleon scattering has been extensively studied by Japanese physicists [1], basing on the potential model. Through their analyses the usefulness of the so-called Taketani methodology [5,1] has been confirmed. Applying Taketani's idea to the phenomenological investigation, Matsumoto and Watari [6,1] showed that the phase shift for the partial wave with a given orbital angular momentum l is dependent only slightly on the behaviour of the potential at distances smaller than one half of the impact parameter b_l

$$b_l = \sqrt{l(l+1)}/k\,, \tag{4}$$

where k is the momentum in the barycentric system. From their results it is seen that taking account of b_l as an index we can separate the phenomena which is insensitive to the detailed behavior of the inner region of the potential, so that the range classification of the potential may be possible.

From the above considerations it could be expected that the division of region depending on the impact parameter may also provide a useful tool in the course of the dispersion theoretical treatment of nucleon-nucleon scattering, although the introduction of the impact parameter is a purely formal procedure. The concept of the impact parameter is implicitly included in the pological consideration given by Chew [7].

If we consider the eigenstates of the total angular momentum, total spin, parity and total iso-spin, evaluation of the imaginary part of the scattering amplitude using the unitarity condition becomes considerably easier and the dispersion relation for each spin state is separated out owing to the conservation law.

For simplicity, we consider the partial wave amplitude $M_l(k^2)$ in the singlet-even state. If we assume the analytical properties of $G_j(s, t, u)$ in the type of the Mandelstam representation, we can derive the following dispersion relation for the $M_l(k^2)$,

$$M_l(k^2) = \frac{1}{\pi}\int_0^\infty \frac{\mathrm{d}k'^2}{k'^2 - k^2 - i\varepsilon}\,\frac{m^2}{(4\pi)^{\frac{3}{2}}}\sqrt{\frac{k'^2}{k'^2+m^2}}\sum_{n=0}^{\infty}\frac{d_l^{l+2n}(k^2, k'^2)}{\sqrt{2l+4n+1}}\,|M_{l\ 2n}(k'^2)|^2 + \tag{5}$$

$$+\, g^2\left\{(\mu^2/2k^2)\,Q_l(1+\mu^2/2k^2) - \delta_{l0}\right\}\sqrt{\pi(2l+1)}/2m^2 + \int_{4\mu^2}^{\infty}\mathrm{d}w\,A(w, k^2)\,Q_l(1+w/2k^2)/k^2\,,$$

(5) M. Taketani, S. Nakamura and M. Sasaki: *Prog. Theor. Phys.*, **6**, 581 (1951).
(6) M. Matsumoto and W. Watari: *Prog. Theor. Phys.*, **11**, 63 (1954).
(7) G. F. Chew: *Phys. Rev.*, **112**, 1380 (1958).

$$(6) \qquad d_l^V(k^2, k'^2) \quad 2\pi \int_{-1}^{1} \mathrm{d}z\, P_l^0(z)\, P_{l'}^0\left(\frac{k^2}{k'^2} z - \frac{k^2}{k'^2}\right),$$

where $A(w, k^2)$ represents the two-pion exchange contribution, three-pion exchange contribution, and so on, and $A(w, k^2)$ is the regular function for $k^2 > -(m^2+3\mu^2)$. The precise verification of eq. (5) will be given in our coming paper. The general features of $Q_l(1+w/2k^2)/2k^2$, where Q_l is the second kind Legendre function, in region $k^2 \geqslant 0$ are represented in Fig. 1.

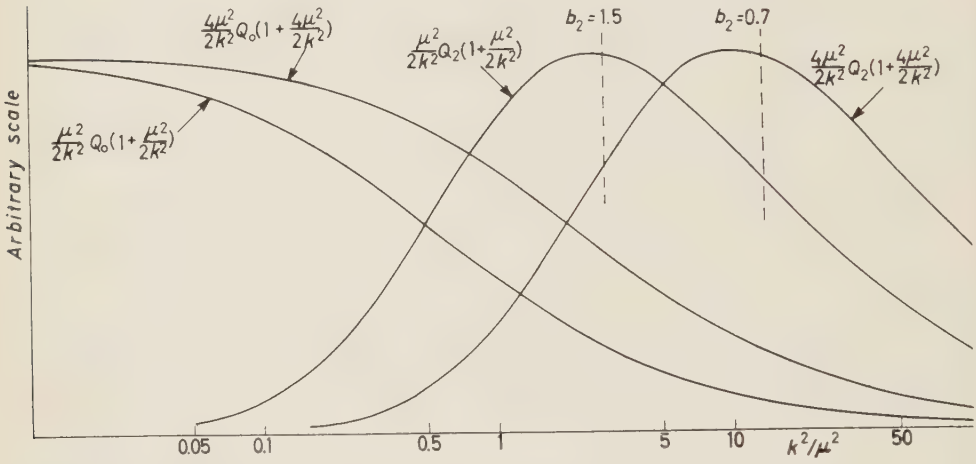

Fig. 1. k^2 dependence of $Q_l(1+w/2k^2)\,w/2k^2$ when we take $w=\mu^2$ and $w=4\mu^2$ respectively.

It should be noted that there may be a region where OPEC is dominant in some sense when l is not zero, while for S-wave amplitude such a region does not exist, if $A(w, k^2)$ is not so singular function. These facts seem to be consistent with the above mentioned classification of the region by the impact parameter. If this is the case, we can put $A(w, k^2)\,Q_l(1+w/2k^2)/k^2 \approx 0$ when b_l is larger than some critical value. Taking into account the analogy with the potential model, we take $1.5\,\mu^{-1}$ as this critical value. In this approximation the only branch point $k^2 = -(\mu^2/4)$ exists on the negative k^2, so that one may solve it easily by making use of the same way as that of the static pion theory given by CHEW and LOW [8]. Thus we obtain

$$(7) \quad (k^{2l+1}/E)\,\mathrm{ctg}\,\delta_l(k^2) = \left[1 - \frac{k^2+(\mu^2/4)}{\pi} P \int_0^\infty \mathrm{d}k'^2\, \frac{B_l(k'^2)}{(k'^2+\mu^2/4)(k'^2-k^2)}\right] \Big/ (E/k^{2l+1})\, B_l(k^2),$$

$$(8) \quad B_l(k^2) = \frac{g^2}{16\pi}\left[Q_l(1+\mu^2/2k^2)(\mu^2/2k^2) - \delta_{l0}\right].$$

[8] G. F. CHEW and F. E. LOW: *Phys. Rev.*, **101**, 1570 (1956).

The calculated (k^5/E) ctg δ_2 is plotted in Fig. 2 as an example, where we take $g^2/4\pi = 14.4$.

In order to cover the lack of the complete experiment in the low energy, the phase shift calculated by HAMADA [9] using the phenomenological potential is also plotted in the corresponding figure as a standard. The mutual deviation of these two phase shifts is rather large even for $b_2 \approx 1.5\ \mu^{-1}$. The appreciable part of this deviation may be provided by the two-pion exchange contribution. On the other hand, it may be unreliable to approximate the high energy part of the integrand of eq. (7) by OPEC only, because the integral of eq. (7) reflects the right hand cuts of the original eq. (5). The latter point can be improved if we introduce $k^{2l+1}/E)$ ctg δ_l at zero momentum as a parameter, $a_l = [(k^{2l+1}/E)\ \mathrm{ctg}\ \delta_l(k^2)]_{k^2=0}$. For the several values of a_2 the phase shifts are also plotted on Fig. 2. It may be pointed out that the variation of a_2, consequently, the variation of phase shift induced by it has the same order of magnitude as the ambiguity of the phase shift due to the inner region effect in the case of the potential theoretical treatment [10]. This fact seems to show that representing the inner region effect by a parameter like a_l is not so implausible.

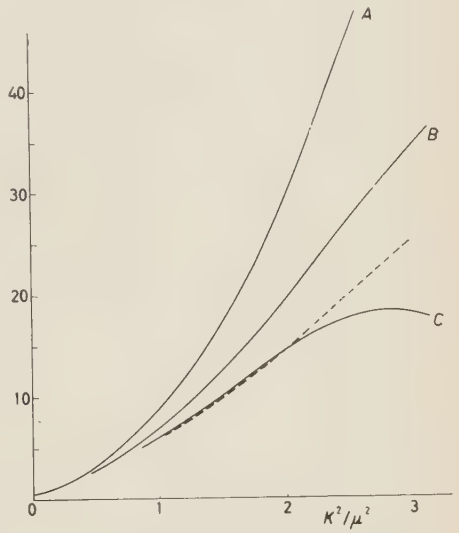

Fig. 2. – (k^5/E) ctg $\delta_2(k^2)$ curve A represents the case given by eq. (7), where the calculated a_2 is 0.519, and curve B and C represent the modified cases when we put $a_2 = 0.5$ and 0.49 respectively. The dashed curve represents (k^5/E) cot δ_2 calculated by HAMADA.

We have assumed the validity of the non-subtracted dispersion relations throughout this article. However, this may largely be masked by the normalization of eq. (7) and the introduction of a_l, though further investigations on this problem should be necessary.

* * *

The authors are indebted to Dr. W. WATARI for his valuable discussions.

[9] T. HAMADA: *Prog. Theor. Phys.*, **24**, 1033 (1960).
[10] W. WATARI: private communication.

IL NUOVO CIMENTO Vol. XIX, N. 2 16 Gennaio 1961

Absorptions in Flight of Σ^- Hyperons in Emulsion Nuclei.

B. D. Jones, B. Sanjeevaiah (*) and J. Zakrzewski (**)

H. H. Wills Physics Laboratory, University of Bristol

and

D. H. Davis

Physics Department, University College London

(ricevuto il 19 Novembre 1960)

1. – Introduction.

K^--meson absorptions in emulsion nuclei are a relatively rich source of $\Sigma^\pm$-hyperons. It may therefore be expected that some of the interaction stars found in following out baryon prongs from such absorptions are caused by $\Sigma^\pm$-hyperons. Σ^--hyperons, when brought to rest, undergo a nuclear capture which, in about 60% of the cases, does not lead to the emission of charged particles [1-3]. However, there is little information concerning $\Sigma^\pm$-hyperon interactions in flight. It is difficult to ascertain the identity of the particles in the case of a disappearance, or a « stop », in flight. An interaction star can be unambiguously identified as being caused by a $\Sigma^\pm$-hyperon only if

i) the $\Sigma^\pm$-hyperon is seen to re-emerge from the star, or

ii) the interaction is exothermic, or

iii) a hyperfragment is emitted from the star or the decay of a free Λ^0-hyperon can be associated with it.

A number of inelastic scatterings of $\Sigma^\pm$-hyperons [4-7] case i), and of exothermic interactions [2-8] case ii), have been reported.

In this communication, an event is described which is interpreted as an absorption in flight of a Σ^--hyperon with

(*) On leave from the University of Mysore, India.

(**) On leave from the University of Warsaw, Poland.

(1) K$^-$ European Collaboration: Part II, *Nuovo Cimento*, **14**, 315 (1959).

(2) M. Nikolić, Y. Eisenberg, W. Koch, M. Schneeberger and H. Winzeler: *Helv. Phys. Acta*, **33**, 221 (1960).

(3) K$^-$ European Collaboration: *Nuovo Cimento*, in press.

(4) W. F. Fry, J. Schneps, G. A. Snow and M. S. Swami: *Phys. Rev.*, **100**, 939 (1955).

(5) H. G. Glasser, N. Seeman and G. A. Snow: *Phys. Rev.*, **107**, 277 (1957).

(6) D. H. Davis, B. D. Jones and J. Zakrzewski: *Nuovo Cimento*, **14**, 265 (1959).

(7) C. M. Garelli, B. Quassiati and M. Vigone: *Nuovo Cimento*, **17**, 786 (1960).

(8) K$^-$ European Collaboration: Part III, *Nuovo Cimento*, **15**, 873 (1960).

the production of a hyperfragment-case iii). To our knowledge, this is the first example of such an interaction to be reported, although emission of hyperfragments from Σ^--hyperons captured at rest has been observed [9]. A previously published [8] exothermic interaction of a Σ-hyperon is also discussed.

2. – Results and discussion.

During a systematic study of two pronged stars produced by K^--mesons captured at rest, an event, which is shown in Photograph 1, has been found (*). The total visible energy in the K^--meson absorption star A is then (88 ± 6) MeV and can be compared with the Q value of 96 MeV for the reaction

$$K^- + p \rightarrow \Sigma^- + \pi^+ .$$

The residual momentum of (280 ± 16) MeV/c is probably taken by the nucleus.

Star A consists of two prongs: track 1 is due to a π^+-meson identified by its decay at rest $\pi^+ \rightarrow \mu^+ \rightarrow e^+$, and track 2 to a particle which, after traversing 2.9 mm, gives rise to a four-pronged interaction star B. Prong 5 of star B is due to a hyperfragment identified by its mesonic decay at rest, star C, after traversing 670 μm. The details of measurements on all prongs from stars A, B and C are displayed in Table I.

The baryon causing the interaction star B can be identified as a $\Sigma^\pm$-hyperon from the observation of the hyperfragment emission, since a strange particle cannot be produced in this case by a non-strange particle. Further, the charge of this hyperon can be inferred as negative from the charge of the accompanying π^+-meson, the probability of two charge exchange processes being negligible [2,10]. The energy of the Σ^--hyperon was estimated from ionization (g) measurements [11] and found to be (53 ± 5) MeV at emission and hence (43 ± 5) MeV at interaction.

TABLE I.

Star	Track No.	Identity	Dip angle (°)	Azimuth angle (°)	Range (μm)
A	1	π^+	15.9 ± 1	0 ± 0.5	19 950
	2	Σ^-	-40 ± 1	150.6 ± 0.5	$\Delta R = 2\,880$
B	3	probably p, d or t	11.5 ± 1	9.8 ± 0.5	360
	4	probably α	37.5 ± 5	110.5 ± 5	5.4 ± 1
	5	$^{4,5}He_\Lambda$	-39 ± 1	220.4 ± 0.5	670
	6	probably α	-31 ± 1	227.9 ± 5	4.1 ± 1
C	7	p	9.6 ± 1	185.2 ± 0.5	437
	8	π^-	0 ± 1	0 ± 0.5	12 460
	9	$^{3,4}He$	—	26 ± 1.2	1.3 ± 0.5

(*) Details of stack exposure and scanning procedure are described in (3).

(9) See *e.g.* G. DASCOLA, C. LAMBORIZIO, S. MORA and T. ORTALI: *Nuovo Cimento*, **16**, 241 (1960).

(10) K^- EUROPEAN COLLABORATION: Part I, *Nuovo Cimento*, **13**, 690 (1959).

(11) P. H. FOWLER and D. H. PERKINS: *Phil. Mag.*, **46**, 587 (1955).

The presence of two short prongs in star B gives the indication that the interaction took place in a light nucleus of the emulsion (C, N, O)([12]). Assuming tentatively the identities of all the prongs it is found from the conservation laws- the direction of the recoil (prong 9) as far as this could be ascertained.

If the recoil is taken to be a ^{3}He or a ^{4}He nucleus, the measured range of 1.3 μm corresponds to that expected from the calculated resultant momen-

TABLE II.

Track No.	Number of δ-rays, having at least 4 grains/650 μm			
		Mean for		
	Measured	Proton	^{4}He	^{7}Li
5	4	0.9 ± 0.1	3.6 ± 0.4	13.5 ± 1.4

that more than one neutron has been emitted. It seems likely that the interaction took place upon an oxygen nucleus (charge conservation) and the possible interaction scheme is then

$$\Sigma^- + {}^{16}\mathrm{O} \rightarrow {}^{4,5}\mathrm{He}_\Lambda + \alpha + \alpha + {}^{1,2,3}\mathrm{H} + \text{neutrons}\,.$$

tum ([13]). The hyperfragment can therefore be interpreted as the decay of $^4\mathrm{He}_\Lambda$ or $^5\mathrm{He}_\Lambda$ according to the scheme

$$^{4,5}\mathrm{He}_\Lambda \rightarrow \pi^- + \mathrm{p} + {}^{3,4}\mathrm{He}\,.$$

The binding energy of the Λ^0-hyperon in these fragments, calculated using the

TABLE III.

Track No.	Identity of the decay products	Momentum MeV/c	Binding energy MeV
7	p	127 ± 7	2.2 ± 1.3 or
8	π^-	90 ± 2	2.3 ± 1.3
9	^{3}He or ^{4}He	43 ± 2	

A δ-ray count was performed on prong 5 and the result compared in Table II with that obtained from measurements on calibration proton tracks. It is seen that the charge of the hyperfragment is very likely to be two. On the assumption that prong 7 is due to a proton, the resultant momentum of the π^--meson (prong 8) and the proton (prong 7) was found to be (43 ± 2) MeV/c and to lie in value of $Q = (37.61 \pm 0.12)$ MeV ([14]) is shown in Table III (calibration procedure is described elsewhere ([15])).

The momentum of the ejected $^{4,5}\mathrm{He}_\Lambda$ is 595 MeV/c or 690 MeV/c respectively, and its direction of flight makes an angle of $31 \pm 1^\circ$ with that of the incident Σ^--hyperon.

([12]) See *e.g.* M. G. K. MENON, H. MUIRHEAD and O. ROCHAT: *Phil. Mag.*, **41**, 583 (1950).

([13]) R. LEVI-SETTI, W. E. SLATER and V. L. TELEGDI: *Suppl. Nuovo Cimento*, **10**, 68 (1958).

([14]) L. W. ALVAREZ: *Report at the Kiev Conference* (1959).

([15]) D. EVANS, B. D. JONES and J. ZAKRZEWSKI: *Phil. Mag.*, **4**, 1255 (1959).

Plate 1. - The K^--meson is captured at rest (star A) to produce a π^+-meson and a Σ^--hyperon. The Σ^--hyperon interacts in flight (star B) with the production of a $^{4,5}He_\Lambda$ hyperfragment which decays at rest (star C) into a π^--meson, a proton and a $^{3,4}He$ recoil (not discernable in the photograph). Track 6 of star B (see Table I) is superimposed on that of the hyperfragment (track 5) and also cannot be distinguished here.

Plate 2. – The K^--meson is captured at rest in a light nucleus (star A) producing a Σ^--hyperon, which interacts in flight (star B). Near the centre of star A, a background track can be seen.

Photograph 2 shows the exothermic interaction in flight of a Σ^--hyperon emitted from a K^--meson absorption at rest, previously reported ([8]). The mass and energy of the interacting Σ-hyperon were found to be respectively (1330 ± 150) MeV and (43 ± 4) MeV. The lengths of prongs from the interaction star B are given in Table IV and the energies are quoted for protons.

TABLE IV.

Track No.	Length (μm)	Energy if proton (MeV)
5	4300	33
6	200	5
7	220	6
8	2700	25
9	460	9
10	100	4

The charge of the hyperon has been deduced as negative from a study of the K^--meson capture, this having been shown to have occurred on a light nucleus ([16]) via either of the reactions:

$$K^- + {}^{16}O \to \Sigma^- + p + p + n + {}^{12}C$$

$$K^- + {}^{14}N \to \Sigma^- + p + p + p + {}^{10}B$$

On consideration of binding energies, the visible energy release in star B is 130 MeV even if all the particles are protons. Furthermore, neutrons must be emitted, and it seems therefore that no Λ^0-hyperon has been emitted from the struck nucleus.

([16]) D. EVANS, B. D. JONES, B. SANJEEVAIAH, J. ZAKRZEWSKI, M. J. BENISTON, V. A. BULL and D. H. DAVIS: *Proc. Roy. Soc.*, in press.

3. – Conclusions.

Two events can be identified as Σ^--hyperon absorptions in flight in the emulsion nuclei. In one of the interactions, the emission of an energetic ${}^{4,5}He_\Lambda$ hyperfragment has been observed In the other, the energy release indicates that the Λ^0-hyperon was trapped in the parent nucleus.

* * *

We are much indebted to Professor C. F. POWELL, F.R.S., for his hospitality and encouragement. We wish to thank Professor E. J. LOFGREN and the Bevatron team for the exposure and Professor G. P. S. OCCHIALINI and the Brussels group for processing the stack. We are very grateful to Dr. P. H. FOWLER, Professor E. H. S. BURHOP and Dr. R. C. KUMAR for many useful discussions.

Acknowledgments are also made to D.S.I.R. for a special development grant to University College London, for research scholarships to B.D.J. and J.Z., and to the Indian Ministry of Education and the University of Mysore for an Overseas Scholarship to B.S.

Our thanks are due to Mr. W. HARBOR for the photographs.

Libri ricevuti.

J. A. Ratcliffe: *Physics of the Upper Atmosphere*, Academic Press, New York and London, 1960; pp. xi-586; $ 14.50.

F. Ajzenberg-Selove: *Nuclear Spectroscopy*; Academic Press Inc., New York, 1960; (Parte A pp. xxi-621; Parte B pp. 625-1147); $ 16 per volume.

H. A. Liebhafsky, H. G. Pfeiffer, E. H. Winslow and P. D. Zemany: *X-Ray absorption and Emission in Analytical Chemistry*; John Wiley and Sons, New York, 1960; pp. x-357; $ 13.50.

R. M. Fano, L. J. Chu and R. B. Adler: *Electromagneti Fields, Energy and Forces*; John Wiley and Sons, New York and London, 1960; pp. xv-520; $ 12.00.

R. M. Fano, L. J. Chu and R. B. Adler: *Electromagnetic Energy Trasmission and Radiation*; John Wiley and Sons, New York and London, 1960; pp. 620.

H. C. Callen: *Thermodynamics*; John Wiley and Sons, New York, 1960; $ 8.75.

M. Burton, J. S. Kirby-Smith and J. L. Magee: *Comparative Effects of Radiation*; John Wiley and Sons, New York, 1960; $ 8.50.

H. C. Corben and P. Stehle: *Classical Mechanics*, ed. II; John Wiley and Sons, New York, 1960; pp. xi-389; $ 12.00.

L. Dresner: *Resonance Absorption in Nuclear Reactors*, Pergamon Press, London, 1960; pp. 131; 40 s.

A. D. Galanin: *Thermal Reactor Theory*; Pergamon Press, London, 1960; pp. 412; Ls. 5.

T. C. Griffith and E. A. Power: *Nuclear Forces and the Few-Nuclear Problem*, vol. I e II; Pergamon Press, London, 1960; pp. 720 complessive; Ls. 10.

L. Landau and E. M. Lifshitz: *Electrodynamics of Continuous Media*; Pergamon Press, London, 1960; pp. 428; 84 s.

W. H. Louisell: *Coupled Mode and Parametric Electronics*; John Wiley and Sons Inc., New York, 1960; $ 11.50.

E. H. Putley: *The Hall Effect and Related Phenomena*; Butterworths, London, 1960; pp. 260; 50 s.

J. C. Slater: *Quantum Theory of Atomic Structure*, vol. II; McGraw Hill House, 1960; pp. 439; Ls. 5.

E. C. G. Sudarshan, J. H. Tinlot and A. C. Melissinos: *Proceedings of the* 1960 *Annual International Conference of High Energy Physics at Rochester*, University of Rochester, New York, 1960; pp. xxv-889.

Studies in Theoretical Physics, Proceedings of the Summer School of Theoretical Physics II, Government of India - Ministry of Scientific Research and Cultural Affairs - New Dehli; Held at Mussorie, 22 May to 18 June 1959 (da p. 341 a 535).

A. Zucker, F. T. Howard and E. C. Halbert: *Reactions Between Complex Nuclei*; John Wiley and Sons Inc., New York, 1960; pp. 313; $ 7.00.

Recensioni.

F. TRICOMI – *Esercizi e Complementi di Analisi Matematica*, Parte Seconda, 3ª ediz.; in 8° di pp. XI-511 con 99 figure. Padova, CEDAM.

Il Prof. TRICOMI è troppo noto fra i nostri maggiori matematici per le sue qualità di espositore chiaro, insieme, e brillante, perchè un suo libro abbia bisogno di commenti in questo senso. Piuttosto nel recensire la terza edizione della Seconda Parte dei *Complementi ed Esercizi* del suo Corso di Analisi Matematica, ci sia lecito fare alcune osservazioni di carattere generale sopra l'insegnamento delle Matematiche nelle nostre Università.

Non si può infatti fare a meno di osservare che giovani laureati in Fisica usciti dalle Università Italiane ignorano o hanno visto appena di sfuggita troppi argomenti di importanza vitale per la loro futura carriera di ricercatori. Chi scrive ricorda per esempio, di essersi laureato nell'Università di Roma vari anni fa senza che nessuno gli avesse parlato di funzioni analitiche o di serie di funzioni ortogonali (inclusa quella di Fourier) o di trasformate integrali, per citare solo alcune lacune fondamentali, salvo brevi cenni che il professore di fisica teorica era costretto ad inserire per rendere comprensibile il suo corso. Ora la situazione sembra alquanto migliorata, ma si ha ancora l'impressione che molto spesso i corsi di matematica siano dedicati più agli argomenti che stanno a cuore all'insegnante, che a quelli che possono essere utili agli alunni. Pur essendo consci della verità del detto (divenuto ormai un luogo comune) che la matematica pura è quella che non è stata ancora applicata, non si deve dimenticare che a molti, anzi alla maggior parte degli studenti, la matematica che essi apprendono all'università, oltre che dar loro una necessaria formazione mentale, deve metterli in grado di risolvere quei problemi che si presentano loro nelle infinite applicazioni alla fisica e ad altre scienze.

Per tal motivo salutiamo con piacere questo libro del Tricomi, il quale, a nostro giudizio, soddisfa alle esigenze del rigore, mentre non perde di vista le finalità applicative di cui abbiamo parlato. Il libro, come dice l'Autore, conduce il lettore fino alla soglia di quella che si suol chiamare « Analisi Superiore », cioè della teoria dell'integrale di Lebesgue, delle funzioni analitiche, della serie di funzioni ortogonali, ecc. Gli argomenti dei Complementi ci sembrano scelti con opportunità al pari degli Esercizi. Si ha l'impressione che molte delle cose contenute nel volume debbano riuscire utili non solo a studenti, ma anche un ricercatore possa ricorrervi almeno per una prima informazione chiara ed autorevole (spesso sufficiente) sopra varie questioni che lo interessano nei suoi lavori.

L. GRATTON

S. E. LIVERHANT – *Elementary introduction to nuclear reactor physics*, XIV+447 pp., J. Wiley and Sons, Inc. (1960).

Questa introduzione alla fisica dei reattori nucleari è più adatta per ingegneri e chimici che non per fisici. Nella successione dei capitoli viene seguito uno schema comune ormai ad altri libri sullo stesso argomento.

Dopo aver discusso la struttura e le proprietà dei nuclei ed introdotto alla teoria delle reazioni nucleari, vengono esaminate più in dettaglio le reazioni prodotte da neutroni. Il capitolo sul processo di fissione lega questa prima parte

di fisica nucleare a quella relativa alla fisica del reattore, dove viene esposta la teoria del rallentamento e della diffusione dei neutroni termici, illustrato il significato dell'equazione di criticità e della equazione che regola il regime transitorio dei reattori nucleari, ed infine affrontato il problema della variazione di reattività durante il funzionamento di un reattore.

Gli ultimi tre capitoli sono un po' a sè, e riguardano l'interazione della radiazione elettromagnetica e delle particelle cariche con la materia, i metodi e gli strumenti per la rivelazione delle particelle e questioni connesse con la fisica sanitaria. Nello spirito del titolo, il libro avrebbe acquistato, a mio giudizio, maggior completezza se fossero stati invece discussi i metodi a più gruppi e più regioni per l'equazione di criticità, le varie approssimazioni per la soluzione delle equazioni esatte del trasporto, onde chiarire meglio i limiti della teoria della diffusione, ed infine il problema dei cicli di combustibile, problema veramente attuale dal punto di vista economico.

Devo però riconoscere che l'esposizione è chiara e ricca di esempi e di grafici. I numerosi esercizi ed una bibliografia aggiornata alla fine di ogni capitolo costituiscono un altro pregio di questo libro.

E. Clementel

A. V. Lebedev e R. M. Fedorova – *A Guide to Mathematical Tables*, Pergamon Press, 1960, pp. XLVI-586; prezzo $ 9.

Il presente volume, traduzione inglese dall'originale russo, pubblicato nel 1956 a cura dell'Accademia delle Scienze dell'URSS, costituisce un ampliamento ed un aggiornamento dell'utilissima opera *An Index of Mathematical Tables* pubblicata nel 1946 a cura di Fletcher, Miller e Rosenhead.

Viene data notizia delle tavole apparse, separatamente o in articoli scientifici, sino a tutto il 1952. Un supplemento al volume, in preparazione, terrà conto del materiale pubblicato dal 1952 al 1958.

I 15 capitoli in cui il volume è suddiviso prendono in considerazione: 1) Potenze, funzioni razionali e algebriche; 2) Funzioni trigonometriche, vari valori connessi con il cerchio e la sfera; 3) Funzioni esponenziali ed iperboliche; 4) Logaritmi; 5) Fattoriali, integrali euleriani e funzioni con essi collegate; 6) Seno, coseno, esponenziale e logaritmo integrali; 7) Integrali di Gauss e funzioni interessanti il calcolo delle probabilità; 8) Integrali e funzioni ellittiche; 9) Funzioni e polinomi di Legendre; 10) Funzioni cilindriche (di Bessel, Neumann, Lommel, Stokes, Kelvin, Airy, Struve) e loro integrali; 11) Funzioni speciali (polinomi di Cebyscev, Jacobi, Bernoulli, Eulero, ..., funzioni di Mathieu, Lamé, Whittaker ...); 12) Radici di equazioni algebriche o trascendenti, funzioni soluzione di certe equazioni differenziali; 13) Valori che intervengono nel calcolo delle differenze finite, somme di serie, prodotti infiniti; 14) Costanti notevoli; 15) Fattori primi, divisori.

Gli elementi fondamentali per la descrizione di una tavola sono di regola così raccolti, da sinistra a destra, su una stessa riga: 1) il numero di cifre decimali o significative; 2) l'intervallo in cui varia l'argomento e le differenze tra i valori d'entrata (passo); 3) un numero che fa riferimento a libri o riviste elencati in serie alla fine del volume e suddivisi corrispondentemente ai capitoli.

L'edizione russa ha termine con un indice degli autori. Nella presente edizione inglese è aggiunta un'appendice di 36 pagine con una traduzione dei titoli dati precedentemente in lingua russa.

L'opera qui recensita non dovrebbe mancare, o nell'originale o nella traduzione, in alcun laboratorio di calcolo, e la presenza in esso di moderne calcola-

trici automatiche non ne riduce l'interesse, per la convenienza di controllare programmi mediante confronto con valori già calcolati.

E. Aparo

D. A. Bell – *Electrical Noise*. Van Nostrand Company, p. 342.

Il libro del Prof. D. A. Bell si distingue dai molti libri recentemente editi a proposito del rumore nei sistemi elettronici per l'aspetto critico-storico della presentazione. L'attenzione è focalizzata sulla fisica relativa alla generazione del rumore nei componenti piuttosto che all'influenza del rumore nei riguardi di specifici problemi di trasmissione dell'informazione.

Il libro è chiarissimo ma di tono decisamente elevato e destinato a ricercatori interessati allo sviluppo di questo campo.

I primi due capitoli richiamano le nozioni di statistica e i metodi matematici usati in seguito.

Nel terzo capitolo vengono discusse criticamente diverse derivazioni del teorema di Nyquist e viene discusso il concetto di grado di libertà di un sistema elettrico, e la distinzione di questo concetto da quello di modi di oscillazioni o gradi di libertà di una forma d'onda in una assegnata banda. In particolare alla fine del capitolo l'Autore con un elegante ragionamento energetico deriva la distribuzione spettrale del rumore dovuto a una resistenza non lineare.

Nel quarto capitolo l'Autore discute nuovamente il rumore termico dal punto di vista della sua generazione microscopica ricollegandolo a problemi di meccanica statistica: questo tipo di attacco prepara la via allo studio di rumore nei sistemi non in equilibrio termodinamico quale il rumore granulare nel diodo in regime di carica spaziale.

I capitoli 5, 6 e 7 sono dedicati al rumore granulare della corrente in diodi rispettivamente con campo accelerato, con campo ritardante, e in regime di carica spaziale.

L'Autore si è occupato particolarmente come ricerca, e il suo libro lo rispecchia, della connessione tra rumore granulare e rumore termico: il suo pensiero che oggi credo sia largamente condiviso, è sintetizzato nella seguente frase: « Le fluttuazioni della corrente possono essere sempre calcolate con un metodo di meccanica statistica: laddove esista una corrente proporzionale alla conduttanza (diodo piano in campo ritardante) la divisione tra rumore termico e rumore granulare è arbitraria dal punto di vista termodinamico; ma in termini di meccanica statistica si può fare una distinzione logica fra fluttuazioni nel numero dei portatori di carica (rumore granulare) e fluttuazioni in velocità (rumore termico) ».

L'ottavo capitolo tratta il rumore nei tubi elettronici amplificatori e nei fototubi moltiplicatori, in particolare il rumore indotto di griglia: la trattazione è basata sull'impiego del teorema di Ramo.

Il nono capitolo tratta del rumore nei tubi a pennello elettronico e negli amplificatori parametrici.

Il decimo capitolo riprende gli argomenti cari all'Autore della generazione del rumore in base al meccanismo fisico della conduzione nei semiconduttori percorsi da corrente: il rumore detto convenzionalmente $1/f$ in base alla sua distribuzione spettrale.

L'Autore presenta una sua teoria che non postula speciali costanti di tempo o meccanismo di intrappolamento dei portatori di carica.

I capitoli successivi 11, 12 e 13 trattano rapidamente problemi particolari quali rumore in film metallici, raddrizzatori, transistors e rivelatori di radiazione, e infine il rumore Barkhausen.

Un breve capitolo è dedicato alle tecniche di misura del rumore.

Ogni capitolo è corredato da una esauriente bibliografia.

Per la completezza, la chiarezza e il vigore l'opera è da consigliarsi a ogni ricercatore che debba risolvere problemi di rumore e a ogni docente che debba criticamente esporre i fondamenti fisici della relative teorie.

E. GATTI

M. DUQUESNE, R. GREGOIRE et M. LEFORT – *Travaux Pratiques de Physique Nucléaire et de Radiochimie*, 324 pp., Masson e Cie. .

Questa raccolta, redatta su invito di F. JOLIOT-CURIE, è destinata agli studenti di fisica e chimica della Facoltà di scienze di Parigi. Il carattere sperimentale del libro mantiene il duplice aspetto fisico e chimico: e ben può affermarsi, per la vastità del materiale pratico trattato, che l'opera interesserà anche il tecnico e l'ingegnere orientati verso attività per le quali siano necessarie chiare nozioni di fisica nucleare.

Il procedimento seguito per la compilazione del libro si basa sulla considerazione di quei procedimenti sperimentali essenziali alla comprensione dei metodi di studio della struttura nucleare. Una breve introduzione teorica richiama le leggi fondamentali necessarie per la comprensione del testo e serve come premessa. L'opera si suddivide in due parti. La prima tratta della rivelazione delle radiazioni e dei metodi impiegati per la misura dell'intensità ed energia dei fotoni, delle particelle e degli elettroni. Una serie di esperienze introduce l'applicazione di questi metodi alla radiochimica.

La seconda parte riguarda i metodi che permettono di studiare i processi di disintegrazione dei nuclei; e ancora l'influenza della disintegrazione radioattiva sull'atomo, l'azione chimica delle radiazioni e l'utilizzazione dei radioisotopi in diversi problemi della chimica. In appendice sono trattati gli effetti biologici delle radiazioni e i problemi connessi con le protezioni.

L'opera, impostata prevalentemente da un punto di vista pratico, non trascura idee e considerazioni che possano servire di guida per una effettiva organizzazione del materiale sperimentale. Riteniamo tuttavia che uno studente o un giovane sperimentatore, ai quali è destinata, dovrebbe penare non poco in tanta messe di notizie e di materiale sperimentale. Una suddivisione della raccolta in più volumi, con carattere specifico ed una fusione più equilibrata tra le considerazioni teoriche e il materiale pratico, permetterebbe a nostro avviso un più adeguato procedimento sperimentale e un'interpretazione corretta dei fatti osservati.

C. MANDUCHI

Direttore responsabile: G. POLVANI Tipografia Compositori - Bologna

Questo Fascicolo è stato licenziato dai torchi il 31-I-1961